STUDIES ON WAVE INTERACTION WITH COMPOSITE BREAKWATER SYSTEM

Thesis
submitted in partial fulfillment of the requirements for the degree of

DOCTOR OF PHILOSOPHY

by

ATHUL KRISHNA K.R.
(177105AM002)

DEPARTMENT OF WATER RESOURCES & OCEAN ENGINEERING
NATIONAL INSTITUTE OF TECHNOLOGY KARNATAKA
SURATHKAL, MANGALORE - 575 025, INDIA

APRIL, 2023

STUDIES ON WAVE INTERACTION WITH COMPOSITE BREAKWATER SYSTEM

Thesis
submitted in partial fulfillment of the requirements for the degree of

DOCTOR OF PHILOSOPHY

by

ATHUL KRISHNA K.R.
(177105AM002)

Under the guidance of

Dr. DEBABRATA KARMAKAR

DEPARTMENT OF WATER RESOURCES & OCEAN ENGINEERING
NATIONAL INSTITUTE OF TECHNOLOGY KARNATAKA
SURATHKAL, MANGALORE - 575 025, INDIA

APRIL, 2023

Dedicated to my loving Grandmother, Father and Sister

DECLARATION

I hereby declare that the Ph.D. Thesis entitled **"Studies on wave interaction with composite breakwater system"** which is being submitted to **National Institute of Technology Karnataka, Surathkal,** for the partial fulfillment of the requirement for the award of degree of **Doctor of Philosophy** in the **Department of Water Resources and Ocean Engineering**, is a bonafide report of the work carried out by me. The material contained in this Ph.D. Thesis has not been submitted to any university or Institution for the award of any degree.

.....

ATHUL KRISHNA K.R. (177105AM002)

Department of Water Resources and Ocean Engineering

National Institute of Technology Karnataka, Surathkal

Place: NITK, SURATHKAL.

Date: 28TH APRIL, 2023

CERTIFICATE

This is to certify that the Ph.D. Thesis entitled **"Studies on wave interaction with composite breakwater system"** submitted by **ATHUL KRISHNA K.R. (177105AM002)**, as the record of the work carried out by him, is accepted as the Ph.D. Thesis submission in partial fulfillment of the requirements for the award of the degree of **Doctor of Philosophy** in the **Department of Water Resources and Ocean Engineering, National Institute of Technology Karnataka, Surathkal**, is a bonafide work carried out by him under my supervision and guidance.

01/05/2023

.....

Dr. DEBABRATA KARMAKAR

Assistant Professor

Department of Water Resources and Ocean Engineering

National Institute of Technology Karnataka, Surathkal

Vanja K 2/5/23

Chairman (DRPC)
Dept. of Water Resources & Ocean Engineering

.....

Chairman - DRPC

Department of Water Resources and Ocean Engineering

National Institute of Technology Karnataka, Surathkal

Dept. of Water Resources & Ocean Engineering
NITK Surathkal

ACKNOWLEDGEMENT

I take this opportunity to express my sincere gratitude and profound thanks to my guide **Dr. D. Karmakar,** Assistant Professor, Department of Water Resources and Ocean Engineering, National Institute of Technology Karnataka for his advice, expert guidance, constant encouragement and reference material provided throughout my research work.

I acknowledge my sincere thanks to **Dr. Pruthviraj U.**, Department of Water Resources and Ocean Engineering and **Dr. B Manu**, Department of Civil Engineering for being the members of Research Progress Assessment Committee (RPAC) and giving valuable suggestions and encouragement at various stages of this work.

I would like to express my sincere gratitude towards **Prof. Amai Mahesha** and **Prof. Amba Shetty,** former Heads of the Department of Water Resources and Ocean Engineering, and **Dr. B.M. Dodamani**, Head of the Department of Water Resources and Ocean Engineering, National Institute of Technology Karnataka, Surathkal for providing necessary facilities and sincere co-operation throughout my stay at the NITK campus. I am very much thankful to **Prof. Carlos Guedes Soares,** President, Centre for Marine Technology and Ocean Engineering (CENTEC), IST Lisbon, Portugal for his valuable advice and suggestion during his visit to NITK Surathkal for India-Portugal Bilateral Technological Cooperation.

I also express my gratitude to my friends, Mr. Ajnas Mohammed, Ms. Aparna Panda, Ms. Aswitha S.K., Mr. Binoy Sebastian, Dr. Dinu Maria Jose, Mr. Hemanth S, Mr. Mansoor C. B, Mr. Parthasarathy K.S., Mr. Ronit Muduli, Mr. Rony J.S., Ms. Shara Mathew Dr. Sreelakshmi S, Mr. Thyaneshwar, Mr. Tom Elias, for the immense support provided during the research period.

My special thanks to Mr. Balakrishna and Mr. Vishwanath Poojary, Asst. Executive Engineer and Mr. Seetharam, Department of Water Resources and Ocean Engineering for their help in all the departmental works. I would also like to thank all the non-teaching staff of the Department of Water Resources and Ocean Engineering, National Institute of Technology Karnataka, Surathkal for their co-operation and help during the project work. I express my heartfelt gratitude to the authors of research articles which have been refereed in preparing this thesis. I also express my gratitude to the reviewers of my research articles for their invaluable suggestions in improving this work. Above all, I thank Lord, the almighty for his grace throughout the research work.

I am very grateful to my family, who provided me with the best education and encouraged me in all my endeavors. Above all, I thank Lord, the almighty, for his grace throughout the research work.

ATHUL KRISHNA K.R. (177105AM002)

ABSTRACT

In the present study, gravity wave dissipation due to the composite breakwater system consisting of porous structure with different configurations of vertical barriers, pile-rock porous structure with vertical barriers, multiple porous structure and barriers, submerged porous plate with bottom-standing and surface piercing porous structure, submerged porous structure with fully-extended barrier and submerged plate, and stratified porous structure backed by stepped obstacle is investigated under the assumption of small amplitude wave theory. The numerical investigation is performed using eigenfunction expansion method and orthogonal mode-coupling relation. The comparative study on specific structural configurations is performed using the physical model test to validate the numerical and experimental investigation. Further, validation of the numerical result is also performed with the results available in the literatures. Darcy's law is incorporated for the flow through porous media and the porosity factor of the structure is introduced using the complex porous effect parameter. The composite breakwater system is studied for various parameters such as relative water depth, porosity of structure and barrier, structural thickness to wavelength ratio, water depth to wavelength ratio, submergence depth of the plate and gap between the structure and barrier.

The study for the wave transformation due to submerged porous plate coupled with porous structure noted that, the wave damping due to the submerged porous plate backed by surface-piercing porous structure is more as compared to the submerged porous plate backed by the bottom-standing porous structure. In addition, the study on the coupled porous structures and submerged plate illustrates that, the increasing width of the fully-extended porous structure improves the performance of the breakwater system. The study on the stratified porous structure with stepped obstacle and porous block illustrates that the presence of the stratified structure decreases wave transmission and efficient wave attenuation can be easily achieved. The wave force acting on stratified structure is noted to be decreased if the structure is combined with wider surface-piercing porous blocks. Further, the presence of stratified porous structure combined with porous block helps in creating a tranquil zone in the leeside of the structure. The proposed study exhibits an informative result for the wave energy attenuation by different configuration of composite breakwater system which can be designed and implemented in coastal and harbour regions for achieving the tranquility.

Keywords: Composite porous structure; Wave dissipation; Multiple porous structure; Stepped seabed; Stratified structure; Submerged plate; Barrier.

NOMENCLATURE

C_m	Coefficient of added mass
C_f	Turbulent resistant coefficient
d	Width of the porous structure
ε_b	Porosity of the barrier
ε_S	Porosity of the structure
f_S	Resistance coefficient of porous structure
f_b	Resistance coefficient of porous barrier
G_b	Porous effect parameter of barrier
g	Acceleration due to gravity
h	Water depth
h_1	Depth of barrier from mean free surface
i	Imaginary number
K_d	Energy dissipation coefficient
k_{jn}	Wave number in x-direction
K_r	Reflection coefficient
K_t	Transmission coefficient
L	Wavelength of incident wave
l	Wave number in z-direction
N	Number of evanescent wave modes
q	Instantaneous Eularian velocity vector
s_s	Reactance coefficient of porous structure
s_b	Reactance coefficient of porous barrier
V	Volume
w	Width between the structure and barrier

ω	Wave frequency
γ_{jn}	Wave number in y-direction
θ	Incident wave angle
ρ	Density of water
ν	Kinematic viscosity
ϕ	Velocity potential
Λ_p	Intrinsic permeability

LIST OF FIGURES

LIST OF TABLES

TABLE OF CONTENTS

CHAPTER 1

GENERAL INTRODUCTION

1.1 PREAMBLE

The shoreline undergoes continuous beach processes such as erosion and accretion due to the corrosion, abrasion, attrition, and hydraulic actions of the sea. Coastal protection plays an important role; if unprecedented gravity waves attack the coast, a huge loss causes to the offshore and coastal facilities. The submerged porous structures are found to be one of the best hard engineering methods to protect the coast from high sea wave actions. The submerged porous breakwaters are also observed as efficient wave energy absorbers with an increased structural life span. Some studies demonstrate, that breakwaters control coastal erosion at a particular location cause erosion on their adjacent coasts (Tsoukala et al., 2015). The particular reason behind the coastal erosion on the adjacent coasts is that breakwaters divert the wave energy from one coast to its adjacent coast, which increases the coastal erosion on the adjacent coasts. Numerous researchers demonstrated that in the locations, where the breakwaters could not able to provide satisfying results, the submerged porous structures are the perfect solutions for controlling coastal erosion from high wave attacks as well as creating a tranquility wave climate at ports and harbours.

The study on composite breakwaters has gained attention in the scientific community in recent years for the protection of shorelines and offshore facilities. The composite breakwater consists of the combination of the structures of different configurations which are capable to resist or dissipate the enormous power of waves. The protection of shorelines and offshore facilities is important for the country's development and progress, as the coastal zones provide a significant role in the country's economy and growth. The conventional hard engineering practices for coastal protection can affect the aesthetical beach profiles. Partial wave transmission is required to take place in order to have the natural beach processes such as erosion and accretion which in turn maintain the beach profile. Several researchers have performed studies on porous structures but submerged porous structures are found to be more suitable for wave energy

absorption. Most of the studies conducted by researchers are on wave reflection and transmission characteristics due to the presence of permeable porous structures such as porous plates, submerged breakwaters, and barriers.

In general, the life of porous structures can be improved by reducing the wave impact on the seaward structural interface (Twu and Chieu, 2000). The vertical permeable structures in various positions such as bottom-standing, surface-piercing, barriers with gaps, and deeply submerged barriers away from the lee side wall are suitable for wave dissipation and wave trapping (Sahoo et al., 2000). The seaward and leeward barriers can work as protective structures for the breakwater in the presence of high wave action. Various studies are conducted on wave trapping by porous structures away from lee side vertical wall and the effect of trapping chamber length is also performed by researchers on considering various structural configurations. The studies are conducted to understand the importance of trapping chamber length. The trapping chamber regions are characterized by minimum wave reflection for a particular interval termed as a resonating trough (Venkateswarlu and Karmakar, 2021). The resonating troughs are considered as an effective design point to attain minimal wave impact on breakwaters.

The submerged porous breakwaters are constructed as compared to conventional breakwaters in dissipating the wave energy where littoral transport is a serious problem (Ming and Chiew, 2000). The submerged breakwaters provide defence by causing high waves to partially reflect, transmit and/or dissipate (Grilli et al., 1994). The submerged breakwaters are used to protect harbour entrances, island states and deltaic coasts, to control wave action at inshore fishing grounds, and to reduce the rate of littoral transport as they allow the waves to get transmitted through the structure. The submerged porous breakwaters are easy to construct and also have less maintenance as compared to the conventional breakwater. Since the structure is porous in nature, the wave force acting on the structure will be less and it will also reduce the effect of wave energy on the leeward side of the structure (Hur and Mizutani, 2003, Johnson, 2006). The significance of the submerged porous structures is studied by various researchers using numerical as well as experimental models. Recently, submerged breakwaters are also implemented in various countries to provide shelter to the mainland from the aggressive action of the gravity waves and to reduce the disturbance in the tranquil conditions (Cho and Kim, 2013, He et al., 2018).

1.1.1 Wave energy dissipation due to porous breakwaters

Coastal protection structures such as breakwaters, groynes, or seawalls, are usually built to guard against erosion. In doing so they harden the coast and reduce its ability to adjust naturally. In the last few decades, there is increased activity in the design and analysis of floating and submerged structures for the protection of the coastline and offshore structures in the harbour region. Various traditional breakwaters are used and proposed by various researchers, but the horizontal breakwaters are less dependent on local seabed geological conditions and are observed more economical in the use of construction materials as compared to traditional breakwaters. Pile-supported submerged horizontal porous plates can be used as an effective breakwater or wave absorber with low transmission and reflection coefficients. Minimum transmission coefficient values are evident along the structure leeward side, and in addition the minimum reflection coefficient plays an important role in reducing seabed scouring and safe vessel navigation in the vicinity of the structure. This type of breakwater has also been proposed as an eco-friendly breakwater for allowing the passage of currents, exchanging waters above and below it, and preventing seawater pollution. Moreover, submerged horizontal porous-plate breakwaters do not hamper the seascape and the hydrodynamic performance of horizontal porous plate breakwaters has aroused considerable interest among researchers and designers.

1.1.2 Wave transformation due to stratified porous structure

The porous structures used in coastal engineering to dissipate the incoming wave energy help in creating a tranquil and safe harbourage. This can be beneficial when vessels are navigating within the harbour adjacent to the structure, as the levels of wave activity will be much less than with a conventional vertical wall structure. In addition, they permit the circulation of water and so assist in the maintenance of the water quality within the harbour. They also help in reducing the wave force impact on the structures. An ideal structure is one which allows less reflection and transmission of incident wave energy, but for a single-layer porous structure, both are simultaneously not possible. A key to this issue may rely on developing a multilayer porous structure. It is known that an incoming wave may partially transmit its wave energy and partially be reflected when encountering interfaces between every two adjoining porous

materials or the interfaces between end materials and water region. A wave that is reflected away from the porous structure, therefore, contains a component that is directly reflected from the first interface the coming wave encounters, and also those components that go back and forth once, twice, or even more than twice between interfaces before they finally leave the structure. All these component waves have phase differences among themselves. Adjusting these phase differences, by adjusting the material thickness, can make their wave amplitude offset themselves. It is important to develop a structure that can damp simultaneously the reflected and transmission waves.

The basic structure is a porous block composed of multiple layers, either horizontally or vertically and each layer consists of different porosities and friction factors with finite thickness. For a horizontally stratified porous structure, stability is achieved due to the use of bigger rocks in the upper porous layer and as a result, both wave reflection and wave force can be reduced considerably. For a vertically stratified porous structure, the breakwater is divided into multiple vertical slices such that the high porosity layer is on the seaward side and that with low porosity on the leeward side.

1.1.3 Wave attenuation due to submerged stepped seabed

In order to understand the behaviour of porous structures, it is critical to consider the field conditions when analysing porous breakwaters. There have been several studies on porous structures that have taken into account flat seabeds, sloping seabeds, undulating seabeds, and stepped bottom topography. The changes in bottom topography are found to have a significant impact on wave transmission and reflection characteristics. In practice, the porous breakwaters are constructed near and far away from the shore and it is very challenging to find uniform/flat seabed for marine engineers. The continental shelves and natural and artificial sand bars are in commonly regarded as elevated impermeable bottoms. The studies performed by researchers observed that, that lower values of friction factor led to oscillation in the reflection coefficient which vanishes for higher values of friction factor. For relatively long waves, the values of the angle of incidence do not affect reflection but for short waves, the higher value of the angle of incidence results in a lower reflection coefficient. The porosity of the structure does not contribute up to a certain range of values of angle of incidence. An increasing number of steps results in a higher reflection coefficient but converges for a sufficiently higher number of steps.

1.2 MOTIVATION

Traditional hard engineering defence structures are ineffective in coastal protection, as well as have a negative impact on the aesthetics of the coast and the economy. When compared to emergent structures, submerged porous structures have shown to absorb more wave energy. The present study is motivated by the benefits of a submerged porous structure. The benefits of submerged porous structures as compared to conventional breakwater are as follows:

- The submerged porous structures promote partial wave transmission to the coast, which is necessary for natural beach processes to occur and maintain the beach profile.
- Submerged structures can protect very large floating structures that are placed in deep water.
- Conventional breakwaters are ineffective in controlling erosion and, in some cases divert wave energy to nearby coasts. Submerged porous structures can control tremendously high wave energy absorption in that location.
- The submerged porous structures can absorb maximum wave energy as the incident wave angle increases and has a lower impact on the marine ecosystem.
- The submerged structures are more environment-friendly, as compared to emergent structures.
- The stability of submerged structures is unaffected by rising sea levels, and increased wave energy absorption is demonstrated by increasing the angle of incidence.
- The smooth movement of the vessels is not hampered by the submerged porous structures.

In light of these findings, submerged coastal protection structures can be considered as a good and effective method of coastal defence.

1.3 AIM AND OBJECTIVES

The present study concentrates on the dissipation of the gravity waves due to the composite breakwater system consisting of porous structures with different configurations of vertical barriers, pile-rock porous structures with vertical barriers, multiple porous structures and

barriers, submerged porous plate with bottom-standing and surface-piercing porous structure, submerged porous structure with fully-extended barrier and submerged plate, and stratified porous structure backed by the stepped seabed. The study aims to analyse suitable composite porous structures with desirable structural porosity, friction factor, structural width, free spacing, and trapping chamber length on wave damping/trapping for wave energy dissipation and protection of the offshore facility.

1.3.1 Objectives of the study

The primary objective of this research is to investigate the hydrodynamic performance of the composite breakwater system to minimize the wave reflection and transmission coefficient and maximize the wave energy damping. In order to achieve the proposed work, the following objective is framed as follows:

- Wave transformation due to porous structures and vertical barriers is analysed
  - ✓ To study the wave interaction with the porous structure/pile-rock porous structure and vertical barrier for different structural configurations such as (i) porous structure and fully-extended barrier, (ii) porous structure with a bottom-standing barrier, (iii) porous structure and surface-piercing barrier.
  - ✓ To analyse the Bragg's scattering due to the wave interaction with the multiple porous structures and vertical barrier of different structural configurations.
- Predict the wave transformation due to submerged plate with porous structures
  - ✓ To examine the performance of submerged porous plate associated with bottom-standing porous structure and surface-piercing porous structure.
  - ✓ To analyse the wave dissipation due to composite breakwater consisting of a fully extended barrier, a submerged horizontal porous plate, and a bottom-standing porous structure.
- The performance of the stratified porous structure in the presence of stepped seabed is analysed
  - ✓ To study the efficiency of stratified porous breakwater system consisting of (i) horizontally stratified porous structure associated with surface-piercing porous structure backed by a stepped seabed and (ii) vertically stratified porous structure associated with surface-piercing porous structure backed by a stepped seabed.

1.3.2 Scope of the work

The porous structures have been extensively tested for wave energy dissipation. A great deal of study has been conducted on composite porous structures to determine their usefulness as a breakwater. The submerged composite porous structure has several advantages, including reduced raw material consumption, reduced mass, accessible transportation, lower production costs, and economy. As a result, the present research work will be promising for wave energy dissipation and, if validated, can be implemented in coastal and harbour locations to produce tranquility. In addition, submerged structures do not detract from the aesthetic appeal of beaches since the structure's porosity allows for partial wave transmission, which is essential for numerous coastal processes maintaining the beach profile. The porous structures are pre-cast, and the in-situ constructions required will be fewer than those needed for the breakwater. As the submerged porous structure has many advantages, the research carried out on the same will be helpful for better coastal protection. Furthermore, the combination of submerged horizontal porous plate and vertical structures can be utilized as an alternative for conventional coastal defence structures like emerged breakwaters, groins, and floating breakwaters.

In the analysis of wave interaction with porous structure, the scope of research activity comprises normalised values and realistic assumptions. Initially, wave damping due to porous structures with vertical barriers is investigated. Further, submerged plate and pile-rock porous structures with various combinations of barriers and submerged structures are considered and analysed for an efficient composite breakwater system. The porous block associated with the porous plate, the composite porous structure consisting of the porous block, plate, and barrier, and the horizontally and vertically stratified porous structure are analysed numerically to determine the wave transformation characteristics. The eigenfunction expansion method and the mode-coupling relation, are used to determine the hydrodynamic coefficients. The wave force on the structure's seaside and lee-side edges are recorded and the results are corroborated using previous analytical, computational, and experimental investigations for specific cases.

1.4 WAVE SCATTERING DUE TO SUBMERGED POROUS STRUCTURES

In recent years, the study on composite breakwaters has gained attention in the scientific community for the protection of shorelines and offshore facilities. The composite breakwater consists of the combination of the structures of different configurations which are capable to resist or dissipate the enormous power of waves. The protection of shorelines and offshore facilities is important for the country’s development and progress as the coastal zones provide

a significant role in the country's economy and growth. The conventional hard engineering techniques used for coastal protection result in an unpleasant aesthetical appearance of beaches. Partial wave transmission is required to take place in order to have the natural beach processes such as erosion and accretion which in turn maintain the beach profile. Several researchers have performed studies on porous structures but submerged porous structures are found to be more suitable for wave energy absorption. Most countries such as Australia, Canada, China, India, Japan, the United States, and European countries adopted permeable structures to protect the mainland that includes coastal cliffs, harbours, wharfs, islands, and beaches (Venkateswarlu and Karmakar, 2019). Most of the studies conducted by researchers are on wave reflection and transmission characteristics due to the presence of permeable porous structures such as porous plates, submerged breakwaters and barriers.

1.4.1 Gravity waves interaction with porous structure

A significant study is performed for porous breakwaters which have the potential to dissipate the incoming waves and these types of structures do not allow the exchange of water between the harbours and the ocean. The porous breakwater is usually implemented in the regions of port and harbour, beaches, and river inlets. The efficiency of these structures is evaluated by determining the wave reflection and transmission coefficients and the hydrodynamic coefficients depend on the structural and wave characteristics such as wavelength, wave period, wave height, and the angle of wave incidence. Various theoretical solutions are derived for the wave reflection and transmission coefficients in the case of the structures having rectangular cross-sections. The wave energy dissipation inside the structure is incorporated using a linearized friction term that includes the friction coefficient which is determined by using Lorentz's conditions (Sollitt and Cross, 1972; Madsen, 1974). In the last few decades, there has been notable progress in the analysis of waves past porous structures. Sollitt and Cross (1972) examined the wave transformation due to the vertical porous structure under the action of incident waves. The study noted wave damping due to the wave-induced flow through the porous structure considering the reactance and resistance due to the porous media. Sulisz (1985) analysed the wave reflection and transmission for the multi-layered trapezoidal breakwater using the Boundary Element Method (BEM) and the study showed better agreement for the wave reflection coefficient with the experimental results. Rojanakamthorn et al. (1989) presented a mathematical model of wave transformation over a submerged permeable breakwater for waves on a permeable seabed using the eigenfunction expansion method. Thereafter, Dalrymple et al. (1991) discussed the wave interaction with the permeable

structure of finite width under oblique wave conditions using the eigenfunction expansion method. The effect of friction coefficient is incorporated and the plane/long wave approximations are discussed to study the wave behaviour with submerged porous structures. Yu and Chwang (1994) reported that the performance of the porous structure under the wave action can be increased by considering the structure of high porosity and less dissipative medium of high structural thickness. Numerous studies on the porous and rigid seabed (Liu and Li, 2013), permeable structure with a leeward wall (Madsen, 1983; Mallayachari and Sundar, 1994; Zhu and Chwang, 2001; Venkateswarlu and Karmakar, 2020) is reported and discussed in the literature.

The submerged porous structures are more effective in the breaking of large waves without disturbing the landward flow of water. Dick and Brebner (1968) studied the performance of solid and permeable submerged breakwaters with rectangular cross sections. The wave transmission is noted to be lower for the submerged porous structure than the solid structure with the increase in the depth of submergence. Losada et al. (1996) analysed the non-breaking regular wave interaction with bottom-standing submerged permeable structures. The influence of various wave characteristics such as structure geometry, angle of incidence, and material properties are analysed and the theoretical study is compared with the available laboratory data. Twu et al. (2001) conducted a numerical investigation on the performance of transmission characteristics of stratified submerged breakwaters. The study concluded that the submerged breakwaters with multi-slices proved to be more effective in reducing the wave transmission coefficient. The effect of porosity on non-breaking surface waves over permeable submerged breakwaters is experimentally investigated by Ting et al. (2004) considering eight model geometries with six different porosities. The wave transformation is noted to have a major impact due to the variation of porosity, and as model height is increased the impact of porosity is observed to be more apparent. The primary harmonic wave energy loss is found to be almost constant for the lower range of porosities, and the wave energy loss is found to decrease for higher porosities. Koley et al. (2015) examined the wave-damping characteristics of bottom-standing and surface-piercing porous structures backed by a solid vertical wall. The suitable arrangements of the rigid wall and partial porous structure of specific configurations are noted to provide long-term and cost-effective solutions for protecting various offshore facilities from wave attacks.

The studies on submerged porous structures with different cross sections are also widely investigated in the existing literature. The trapezoidal cross sections of the breakwater are most commonly used and investigated. Dattatri et al. (1978) experimentally studied the wave

hydrodynamic characteristics of different types of submerged porous structures of various cross-sections. The study observed that the crest width and submergence height of the structure plays an important role in determining the efficiency of the breakwater. Kobayashi and Wurjanto (1989) numerically predicted the monochromatic wave reflection and transmission over a trapezoidal-shaped submerged impermeable breakwater. An equation of wave energy is developed in order to estimate the rate of dissipation of energy due to wave breaking. A mathematical model of wave breaking over a submerged permeable breakwater is developed under the mild-slope assumption by Rojanakamthorn et al. (1990) which is validated on comparing it with the experimental results for trapezoidal and rectangular breakwaters. The numerical study on the transmission characteristics of the submerged breakwater is performed by Rambabu and Mani (2005) to determine the effect of depth of submergence, crest width, and material properties of the breakwater. Chang and Liou (2007) presented the theoretical investigations on a single and a group of trapezoidal submerged breakwaters placed at certain distances. The study noted that the crest width plays a significant role in the design of these structures. Further, the wave motion over a submerged trapezoidal breakwater with a perforated upper layer placed on a sloping bed is examined by Koley et al. (2015) with the structure being placed on a sloping bed. The wave force on the submerged structure is noted to be reduced and the service life of the structure is increased due to the presence of the outer perforated layer. Further, the cost-effective solution for creating a tranquility zone is obtained to protect the offshore facility from extreme climate considering suitable configurations and the location of the submerged structures.

1.4.2 Wave dissipation due to vertical barriers

The wave energy dissipation due to the presence of vertical barriers is widely studied by scientists and researchers. Burke (1964) investigated the wave reflection and transmission characteristics of a submerged plane barrier of finite thickness kept in an infinitely deep fluid. The velocity potential in terms of pressure difference (discontinuity across the barrier) is represented using Green's function and the study is performed using Wiener-Hopf complex Fourier transform method. Mei (1966) studied the initial value problems regarding the scattering and radiation of waves by vertical thin plates in infinitely deep water. The explicit equations for the large-time behaviour of free surface elevation for the rolling plate are derived and the steady state solution is obtained for harmonic point pressure that acts on the free surface close to the vertical barrier. Further, Mei and Black (1969) analysed the scattering of surface waves normally incident on rectangular obstacles kept in a channel having finite water depth. The obstacle considered in the study includes both bottom and surface structures of various

proportions that include surface docks and thin barriers. Tuck (1971) proposed a method for the flow through an impermeable barrier or small aperture. The approximate approximations for the transmission coefficient for specific water wave problems are derived using the matched asymptotic expansion method. Thereafter, significant studies on vertical barriers with gaps (Porter, 1974; Evans, 1976), permeable barriers (Macaskill, 1979), slotted wall barriers (Urashima et al., 1986; Kriebel, 1993), rigid vertical thin barriers (Losada et al., 1992) and wave trapping by vertical barriers (Sahoo et al., 2000) are discussed and reported in detail. Recently, Karmakar and Guedes Soares (2014, 2015) performed studies on wave interaction with vertical barriers. The wave dissipation due to surface-piercing and bottom-standing barriers is analysed using the least-squares approximation considering free, clamped, and moored barrier configuration. In addition, the study on the vertical barriers is extended by Kaligatla et al. (2018) considering seaside seabed variation using the eigenfunction expansion method. The mild-slope equation is considered for analysing the seabed variation which is observed to play a major role in reducing the wave reflection.

In order to protect the offshore structure from high waves, often seawalls are constructed. Kirkgoz (1991) performed studies on the pressure impact of breaking waves on vertical and sloping walls. The impact of pressure and wave forces on sloping wall is higher compared to vertical wall, and for all cases, the maximum impact pressure is observed just below the still water level. Fugazza and Natale (1992) presented a hydraulic design of perforated breakwaters and the design formula for a Jarlan-type breakwater is proposed. The studies showed that a Jarlan-type breakwater having a single chamber is effective for wave reduction. Tsai et al. (2012) studied the wave transformation due to submerged breakwater associated with a seawall. The study reported the wave node or pseudo-node of wave between the seawall and the submerged breakwater influences the mass flux of the breakwater to induce the piling up of water. Further, different types of breakwaters, such as pile-supported oscillating water column-type structures (He and Huang, 2014), floating breakwaters (Karmakar and Sahoo, 2008), slotted barriers (Huang, 2007), submerged plate breakwaters (Liu and Iskandarani, 1991; Patarapanich, 1984), flexible barrier in presence of step-bottom (Behara et al., 2016) and floating structure with submerged breakwater (Gayathri et al., 2021, 2022; Kaligatla et al., 2021) is also considered as an alternative solution to protect the shoreline.

1.4.3 Wave trapping due to pile-rock porous structure

The pile-rock breakwaters are considered to be very suitable for coastal areas with weak geological conditions and severe seabed scour. During construction, the piles penetrate deep

into the seabed which fastens the rock core and provides the structure with strong wave resistance. A significant study on pile rock breakwater along with closely spaced pile breakwaters or slotted/perforated walls is noted and discussed by researchers. Theoretical and experimental studies on wave interaction with closely spaced circular pile rows are studied by Hayashi et al. (1966). The significance of the porous effect parameter in wave dissipation is reported by Chwang (1983). Wave forces and methods for calculating hydrodynamic characteristics including the transmission coefficient for the slotted wall is developed by Kriebel (1992), while theoretical and experimental studies on circular or rectangular piles are presented by Kakuno and Liu (1993). An explicit formula is developed by Yu and Chwang (1994) for wave motion through a porous structure. Mani and Jayakumar (1995) studied the new design of breakwater consisting of a row of closely spaced pipes mounted onto a frame and suspended between the support piles spaced far apart and experimental studies are conducted and also compared with conventionally adopted pile breakwater. Wave transmission through a double-row pile breakwater of closely spaced circular and rectangular piles is studied by Herbich and Douglas (1988) and one or two rows of closely spaced rectangular cylinders by Huang (2007). Liu et al. (2012) analyzed the wave absorption of pile-rock breakwaters and obtained a relationship between the wave transmission, reflection, and dissipation coefficients based on linear potential theory and gave an analytical solution for the wave interaction. Liu and Li (2013) presented a new analytical method without considering the dispersion relation for wave motion through porous media. Li et al. (2017) studied oblique wave scattering by a submerged pile-rock breakwater and closed-form analytical solution based on linear potential theory and matched eigenfunction expansions developed to study the hydrodynamic performance of the breakwater.

In order to improve the life of the porous breakwater, the barrier-rock porous structures are observed to perform significantly. The closed-form solutions for the wave transformations using slotted barriers developed by Suh et al. (2011) show that the inertia term is important for intermediate and deep-water waves so that the solution for the inertial effect gives a better prediction. A similar concept is also applied to deep waters by incorporating other types of vertical slotted barriers including surface-piercing barriers and partially immersed slotted barriers. Karmakar and Guedes Soares (2014, 2015) analysed the wave transformation due to multiple surface-piercing barriers and bottom-standing barriers using the least-squares approximation and found that the free-clamped barrier enhances the energy damping as

compared with the other mooring conditions. The multi-domain boundary element method is employed by Koley et al. (2015) to analyse wave scattering by a submerged porous bar with an impermeable core placed on a sloping bottom. The oblique wave trapping by bottom-standing and surface-piercing porous structures of finite width placed at a finite distance from a vertical rigid wall is studied by considering various aspects of structural configurations. The direct analytical solution is proposed by Venkateswarlu and Karmakar (2020b, 2021) for various types of porous structures. Recently, Krishna et al. (2019) studied submerged porous structure associated with a vertical barrier for wave energy damping which shows that the effect of structural porosity enhances wave energy damping.

1.4.4 Wave interaction with submerged horizontal plate

A significant study on the submerged porous plate as an effective breakwater is performed by various researchers to understand the wave trapping and wave dissipation phenomenon due to the submerged porous plate breakwater. The porous plate breakwaters allow the movement of fluid above and below the structure thus reducing the problem of littoral drift. Patarapanich (1984) performed the long wave approximation for the single submerged plate to analyse the presence of uniform horizontal velocity throughout the water depth where the pressure varies hydrostatically. Later, the study is extended to determine the optimum conditions of the submerged plate for obtaining minimum wave transmission (Patarapanich and Cheong, 1989). Neelamani and Reddy (1992) conducted a detailed experimental study on the performance of a submerged and rigid surface horizontal plate for varying wave steepness and different plate submergence depth in deep water regions. Yueh and Kuo (1993a,b) conducted a numerical and experimental investigation on wave pressure reduction due to a submerged single horizontal plate backed by a vertical wall. The study indicated that for the short-wave period, the pressure reduction by the submerged plate is evident and the optimal submergence depth is obtained for other wave periods. Liu and Li (2011) proposed an alternative analytical solution for the interaction of submerged horizontal porous offshore plate breakwaters using the small amplitude wave theory. The analytical solution obtained is free from determining the complex root of the dispersion relation and is simple to implement for wave interaction with the multi-layered porous submerged plate.

The performance of the submerged porous plate is further extended to dual submerged horizontal plates where instead of using a single horizontal plate, the combinations of rigid and

porous plates and dual porous plates are introduced. The dual submerged plates are more feasible in regions where the sea level variation is more due to tidal range. Wang and Shen (1999) analytically determined the wave hydrodynamic characteristics over a series of submerged horizontal plates using matched eigenfunction expansion method. The study showed that the hydrodynamic coefficients depend mainly on the submergence depth of the top plate, plate length, and relative water depth. Usha and Gayathri (2005) investigated the wave motion over a twin-plate breakwater consisting of a surface plate and submerged plate in terms of water depth, submergence depth of the plate, and width of the plate in wave transformation. Thereafter, Neelamani and Gayathri (2006) conducted experimental studies on the hydrodynamic performance on a surface plate and twin plate barriers for different wave heights and periods and found that the twin plate performance is better in the reduction of transmission characteristics. Wang et al. (2006) performed an experimental investigation on the wave-damping characteristics of the multiple-layer breakwater. The study noted that the wave force on the breakwater is less in the lateral direction which proves to be the best for a structure. Further, Cho and Kim (2008) analysed the interaction of oblique monochromatic waves with horizontal, inclined, and dual porous plates. The wave reflection and transmission characteristics of a two-layer plate breakwater consisting of two submerged horizontal plates placed at a certain distance are performed by Liu et al. (2008).

The studies on submerged horizontal porous plate proved to achieve wave attenuation and also helps in reducing the problem of littoral transport as they permit easy flow of water. The experimental study conducted by Neelamani and Reddy (1992) on the wave hydrodynamic characteristics of a rigidly fixed surface and submerged horizontal plate showed that the transmission coefficient is minimum and the reflection coefficient is maximum when the plate is at still water level. Liu and Li (2011) formulated an alternative analytical solution for water motion over an offshore horizontal plate breakwater and found that the results are acceptable to the previous results obtained by other analytical approaches. Cho and Kim (2013) studied the interaction of incident waves with a submerged horizontal breakwater and noted that the effectiveness of the plate increases as plate width increases and the energy dissipation is higher for large angles of incidence. Later on, an experimental study is carried out by Cho et al. (2013) on the dual porous submerged horizontal breakwater. The study found that there is no significant variation in the performance of the proposed structure when the lower porous plate is added at a gap greater than 10% of water depth. Recently, Mohapatra et al. (2018) presented

an analytical study on the interaction of gravity waves with submerged flexible horizontal plates which suggests that the wave attenuation depends on mooring stiffness and porous effect parameter.

Milgram (1970) introduced the concept of an active wave controller mechanism and thereafter a new concept of a submerged pitching plate as an active wave controller is proposed by Yip et al. (1997) which acts as a self-actuating wave controller when it interacts with the waves. The study noted that the efficiency of the plate depends on its submergence depth as well as dimensions. Karmakar and Guedes Soares (2018) studied the wave motion over a horizontal submerged pitching plate and found that the surface elevation increases with different values of pitching which implies that due to pitching there is an increase in wave energy.

1.4.5 Wave damping by stratified porous structure and change in bottom topography

Significant studies have been carried out on the dissipation characteristics of wave energy by stratified porous structures. Yu et al. (1994) examined the wave motion through a porous structure consisting of two layers and noted that a limiting thickness exists for the structure, beyond which hydrodynamic coefficients remain constant with any further increase in thickness. Later, Twu and Chieu (2000) designed an offshore breakwater having minimal wave reflection and transmission using a complex eigenfunction method. The numerical and experimental study revealed that a multi-layer breakwater can reduce both wave reflection and transmission at narrower width compared to a single-layer porous structure. Thereafter, Twu et al. (2002) studied the wave-damping characteristics of a vertically stratified porous breakwater under oblique wave action. Further, Liu et al. (2007) proposed a two-layer horizontally stratified rock-filled core for a perforated breakwater and studied the effect of the perforated breakwater on wave reflection and wave force impact on the structure. Recently, Venkateswarlu et al. (2020a) studied the oblique wave transformation due to fully-extended two-layered, three-layered, and two-layered submerged horizontally stratified structures using an eigenfunction expansion approach. The study concluded that the increase in porosity of the surface layer and moderate friction factor enhances energy damping. The multiple structures are found to be useful if the structure width is high and for a fixed structural width, separating into several structures helps in achieving high wave damping. Venkateswarlu and Karmakar (2020b) also analysed the oblique wave interaction with multiple horizontally stratified wave absorbers placed away from the vertical wall, permeable wall, and stepped wall. The width of

the rigid step is noted to have the least impact, even though an increase in absorber thickness decreased the magnitude of harmonic oscillation in wave reflection and force.

The seabed on which the breakwaters are constructed is not flat but it is undulating which can influence the hydrodynamic characteristics of the incoming wave. The wave transformation due to variation in seabed characteristics has been studied and reported by various researchers in the literature. Das and Bora (2014) studied the wave reflection by a vertical porous structure placed on a stepped seabed as two separate cases with two and multiple steps. The study reported that lower values of friction factor led to oscillation in the reflection coefficient which vanished for higher values of friction factor but for relatively long waves, the values of the angle of incidence does not affect reflection whereas, for short waves, higher value of angle of incidence resulted in lower reflection coefficient. Afterward, Hu et al. (2019) presented an analytical study for the oblique scattering of monochromatic small amplitude wave trains by a stationary rigid multi-layered object of the rectangular cross-section for a combined floating and bottom-mounted permeable breakwater. Venkateswarlu and Karmakar (2019) studied the wave scattering and wave trapping by the barrier-rock porous structure of different structural configurations placed on an impermeable uniform and step-bottom topography. The study concluded that the length of the trapping chamber is influenced by fluid resonance and the effective configuration of the barrier-rock porous structure is decided by resonating troughs. Venkateswarlu and Karmakar (2020c) studied the significance of seabed characteristics in wave transformation due to the presence of a vertically stratified porous structure. The study noted that the wave energy dissipation increased with the increase in the porosity of the seaward porous layer. The theoretical results are in good agreement with the experimental observations of Twu and Chieu (2000). The study suggested that, for better wave blocking, the porosity of the lee side porous layer can be kept minimal. The performance in wave reflection of the porous structure placed on the stepped seabed is found better compared to that on a uniform and elevated seabed whereas the structure placed on the elevated seabed showed a significant role in wave blocking.

The oblique wave interaction of fully-extended multiple two-layered, three-layered and submerged two-layered porous structures is studied by Venkateswarlu et al. (2020). It is observed that if the structure to be provided has high structural width, then it is effective to provide multiple structures. Barman and Bora (2020) presented study on behaviour of composite porous block placed on a multi-step bottom in a two-layer fluid when wave is

incident on it and this study is beneficial in design of coastal structures. Tabssum et al. (2020) analysed wave interaction with a thick porous breakwater in a two-layer ocean, which is particularly applicable in the continental shelf, having bottom undulation. Venkateswarlu and Karmakar (2020d) examined the wave interaction with multiple porous structures of finite spacing upon elevated seabed in the presence and absence of a leeward wall. The presence of multiple porous blocks with a leeward wall enabled a reduction in wave reflection and force and the 10% - 15% elevated step height enhanced the energy damping.

1.5 CRITICAL REVIEW

The studies on the different configurations of the breakwater are well documented in the literature but the studies on the composite breakwater consisting of a combination of porous structure and different configurations of the vertical barrier are not reported in the literature. So, based on the previous studies, it is observed that limited studies on porous breakwaters combined with vertical barriers are performed. Further, the literature survey suggests that minimal study has been performed on the pile-rock porous structure coupled with different combinations of barriers. So, the hydrodynamic performance of the pile-rock porous structure coupled with vertical barriers has wide application in wave attenuation for the protection of offshore facilities. The study performed by various researchers shows that the existing literature provides very limited information on wave-damping characteristics due to the combination of multiple porous structures. So, a detailed study on the array of porous structures and barriers will provide insight into the wave damping performance and wave scattering effect due to the offshore arrays of composite breakwaters.

The study on the wave attenuation due to stand-alone submerged porous plate and submerged porous structure is available in the existing literature but the dissipation of gravity waves due to the combination of submerged porous plate and porous structures is limited. The aforementioned studies suggest that the installation of the submerged porous plate with the submerged porous structure may help to reinforce the overturning stability of the porous structure. In addition, the wave-absorbing performance of the porous structure may be enhanced as the submerged porous plate may act as a wave absorber (Liu et al., 2007). Thus, from the previous studies, it is observed that the combination of the submerged porous plate and porous structure plays an important role in the dissipation of wave energy and attenuation of wave height in the transmitted region. Finally, the wave dissipating due to the combination

of stratified porous structure in the presence of elevated step seabed is minimal. The presence of an elevated step seabed along with the stratified porous structure is useful in reflecting waves of higher wavelengths. Thus, the stepped seabed on the leeward side in combination with vertical and horizontal stratified porous structure with surface-piercing porous structure is intended to provide an effective solution for the protection of the coastal facility.

1.6 BRIEF OVERVIEW OF THE THESIS

The content of the thesis is organised consisting of seven Chapters depending on the physical problem investigated and the solution approach considered in the problem formulation. The detailed description of the Chapters is as follows:

In Chapter 1, the introduction and motivation for the present study are discussed along with the detailed literature review on wave interaction with submerged porous structures (porous structures, porous plates, and barriers) and changes in bottom topography. The numerical and experimental findings relating to wave-structure interaction problems are discussed. The chapter discusses the aim and objectives derived from the literature along with the scope of the research work. In addition, a brief introduction to the research activity performed in this thesis, the research gap, and a critical review based on the literature review is described.

In Chapter 2, the numerical investigation of gravity wave damping due to the porous structure and the vertical barrier is discussed in detail. Three different cases of vertical barrier configurations such as fully-extended barrier, bottom-standing barrier, and surface-piercing barrier placed in front of the pile-rock porous structure are considered for the investigation. The numerical study is performed using the eigenfunction expansion and the associated orthogonal mode-coupling relations considering the continuity of pressure and velocity for the vertical barrier, seaward, and leeward structural interfaces. The numerical results for the wave reflection, transmission, dissipation coefficient, and force on the front and rear side of the porous structure along with the force on the barrier interface are evaluated for different hydraulic characteristics. The analysis is presented for varying structural porosity, angle of incidence, structural thickness, friction factor, and length between the vertical barrier and porous structure for the three different configurations of the vertical barrier. The numerical work is validated using the experimental results performed in the wave flume.

In Chapter 3, the wave transformation due to arrays of porous structures and barriers is discussed in detail. The eigenfunction expansion technique was adopted along with the mode coupling relation to perform the numerical analysis. The porous blocks associated with

different configurations of barriers are considered for the analysis. The multiple porous blocks associated with barriers, such as fully extended, surface-piercing, and bottom-standing, are analysed. Nine different structural configurations are analysed numerically, and the multiple porous blocks associated with the fully-extended barriers are analysed experimentally to validate the numerical results.

In Chapter 4, the gravity wave dissipation due to submerged porous plate and the porous structure is analysed numerically. Two different configurations of porous structure, such as bottom-standing and surface-piercing porous blocks, are considered for the analysis. The effect of various parameters such as non-dimensional wave number, angle of incidence, porosity, plate length, depth of submergence of the plate, and the non-dimensional gap between the porous block and plate on the hydrodynamic coefficients are discussed in detail. The numerical results of the present study are validated with numerical results obtained by Liu and Li (2011) and Cho and Kim (2013).

In Chapter 5, the numerical investigation of the wave attenuation due to submerged porous structure, plate, and the barrier is presented and analysed. The composite structure is assumed to rest on a flat seabed. The eigenfunction expansion method and the mode-coupling relation are employed to determine the reflection, transmission, and energy dissipation coefficient, and the behaviour of these hydrodynamic coefficients against various parameters such as non-dimensional wave number, porous structure width, the porosity of the structure, angle of incidence, spacing between the plate and porous structures are reported. The numerical results are validated by the theoretical results of Cho and Kim(2013). The wave forces acting on the porous structure and the free surface elevation are also discussed.

In Chapter 6, wave transformation due to stratified porous structure with a stepped seabed is analysed using the eigenfunction expansion method. The horizontally and vertically stratified porous structures associated with a stepped seabed and a surface-piercing porous block are analysed. The study provides insight into the effect of stratification on wave propagation. A comparative study of the reflection coefficient in the case of a single porous structure as in Dalrymple et al. (1991) is presented in the chapter. The effect of multiple porosities, structural width, non-dimensional gap between the porous structure, angle of incidence, and non-dimensional wave number are analysed and reported for the design of an effective composite breakwater system. Finally, Chapter 7 summarises the work performed in the thesis, followed by a discussion of the future research scope. This Chapter also highlights the significant

contributions made in the research work. The brief outline of the thesis is presented as flow chart in Fig. 1.1.

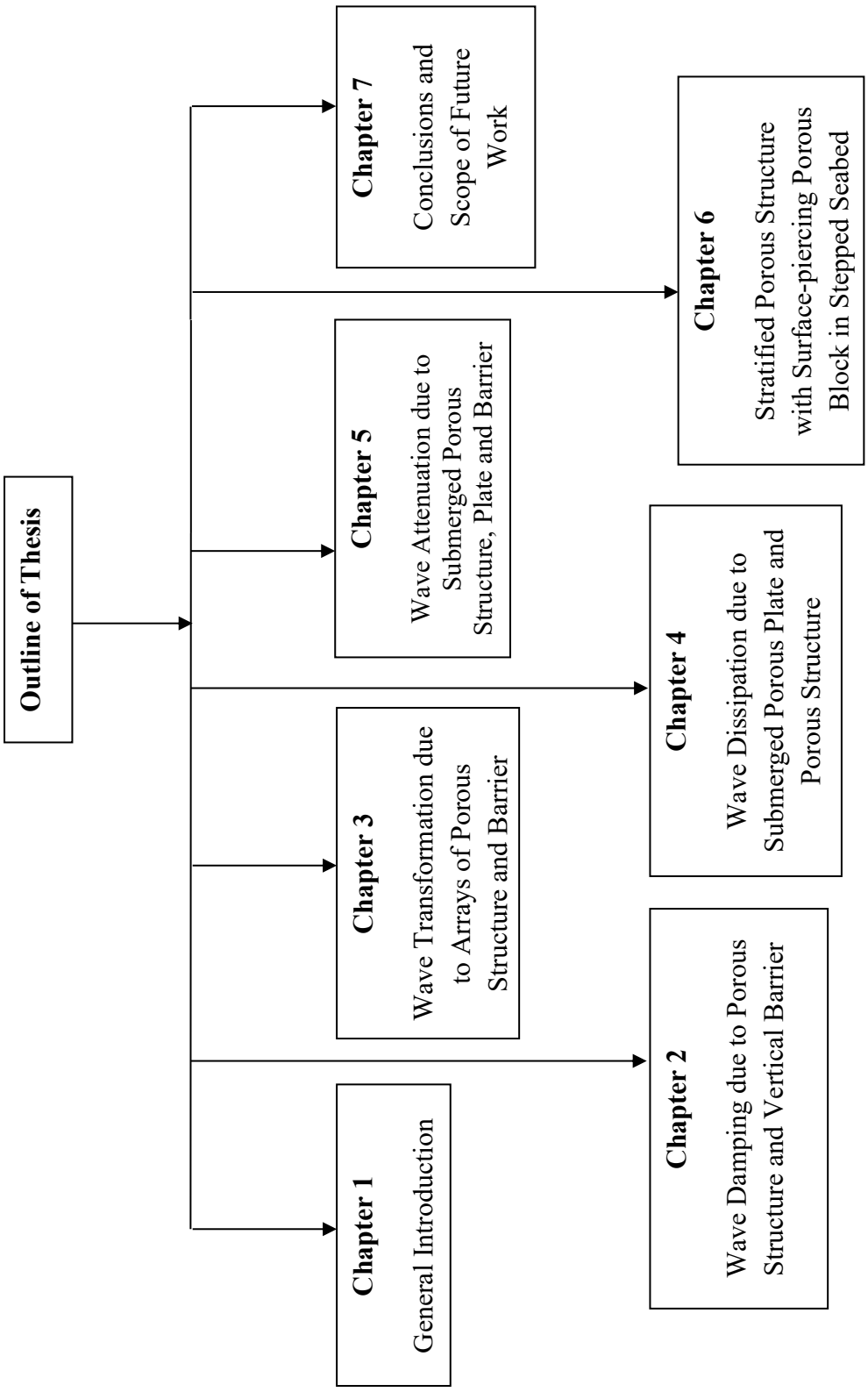

Fig. 1.1: Flow chart of oultline of the thesis.

1.6.1 List of publications in Journals:

1. Sreebhadra, M.N., K.R. Athul Krishna & D. Karmakar, (2022). Wave trapping due to composite pile-rock structure coupled with vertical barrier. Proceedings of the Institution of Mechanical Engineers, Part M: Journal of Engineering for the Maritime Environment, (Scopus indexed Journal), DOI: 10.1177/147509022211127.

2. K.R. Athul Krishna, Abhishek G. Karaseeri & D. Karmakar (2022). Oblique wave propagation through composite permeable porous structures, Marine Systems and Ocean Technology, (Scopus indexed Journal), DOI: 10.1007/s40868-022-00122-1.

3. K.R. Athul Krishna, Khansa Abdullah & D. Karmakar (2023). Dissipation of gravity waves due to submerged porous plate coupled with porous structures, Journal of Offshore Mechanics & Arctic Engineering, 145, 011201-1-13, (Scopus indexed Journal), DOI: 10.1115/1.4055702.

4. K.R. Athul Krishna, Khansa Abdullah & D. Karmakar (2023). Wave energy damping due to coupled porous structure and submerged porous plate, Journal of Marine Science and Application, (Scopus indexed Journal), (Accepted).

5. Ashna Varghese, K.R. Athul Krishna and D. Karmakar (2022). Wave transformation due to stratified porous structure in the presence of stepped obstacle, Marine Systems and Ocean Technology, (Under Review).

1.6.2 List of publications in Book Chapters:

6. K.R. Athul Krishna, V. Venkateshwarlu & D. Karmakar, (2019). Wave transformation due to a submerged porous block associated with a vertical barrier, Proceedings of 10th International Conference on Asian and Pacific Coasts (Springer Nature), 717-724.

1.6.3 List of publications in Conference Proceedings:

7. V. Venkateswarlu, K.R. Athul Krishna and D. Karmakar (2018). Wave force control on seawall using seaside porous blocks. Conference on Next Frontiers in Civil Engineering (NFiCE), IIT Bombay, 30th Nov – 1st December 2018.

8. K.R. Athul Krishna, V. Venkateswarlu & D. Karmakar, (2018). Wave reflection and transmission characteristics due to a piston type porous wave energy converter, Conference on Next Frontiers in Civil Engineering (NFiCE), IIT Bombay, 30th November – 1st December, 2018, 108-109.

9. K.R. Athul Krishna & D. Karmakar (2019). Wave dissipation due to multiple submerged porous blocks associated with vertical barrier, 24th International Conference on Hydraulics, Water Resource and Coastal Engineering (HYDRO), 18th – 20th December, 2019, University College of Engineering, Osmania University, Hyderabad, India.

10. K.R. Athul Krishna & D. Karmakar (2021). Gravity wave dissipation due to multiple porous structures, 25th International Conference on Hydraulics, Water Resources and Coastal Engineering (HYDRO), March 26-28, 2021, NIT Rourkella, Odisha, India.

11. Abhishek G. Karaseeri, K.R. Athul Krishna & D. Karmakar (2021). Wave transformation due to stratified porous structure and vertical barrier, 2nd International Conference on Recent Advances in Fluid and Thermal Sciences (iCRAFT), 19th -21st March 2021, Birla Institute of Technology, Dubai.

1.7 CLOSURE

In this Chapter, the introduction to the interaction of gravity waves with submerged porous structures, porous barriers, and porous plates is presented. The importance and need of the composite porous structure for the protection of offshore facilities are discussed in detail. A detailed literature review of wave-scattering due to various porous structures is incorporated. The effect of submerged porous blocks, porous vertical barriers, porous plates, stratification of porosity, and composite porous structure are reviewed and reported in detail. The critical review and the aim and objectives derived from the research gaps are discussed.

CHAPTER 2

GRAVITY WAVE DAMPING DUE TO POROUS STRUCTURE AND VERTICAL BARRIER

2.1 GENERAL INTRODUCTION

The wave transformation due to pile-rock porous structure in combination with vertical porous barrier is investigated under oblique wave action. The pile-rock breakwaters consists of two rows of closely spaced piles and a rock core between them, and is effective in dissipating wave energy when compared with traditional rigid breakwaters due to its reduced deadweight of construction materials and additional stability. Three different cases of the vertical barrier configurations such as fully-extended barrier, bottom-standing barrier and surface-piercing barrier placed in front of the pile-rock porous structure are considered for the investigation. The numerical study is performed using the eigenfunction expansion and the associated orthogonal mode-coupling relations considering continuity of pressure and velocity for the vertical barrier, seaward and leeward structural interfaces. The Darcy's law is incorporated for the flow through porous media and the porosity factor of the structure is introduced using the complex porous effect parameter. The numerical results for the wave reflection, transmission and dissipation coefficient, wave force on the front and rear side of porous structure along with the wave force on the barrier interface are evaluated for different hydraulic characteristics. The analysis is presented for varying structural porosity, angle of incidence, structural thickness, friction factor, length between vertical barrier and porous structure for the three different configurations of vertical barrier.

2.2 THEORETICAL FORMULATION

The oblique wave interaction with pile-rock porous structure coupled with vertical barrier in a finite water depth h is analysed using the linearized wave theory. The study is performed for three different configurations of vertical barrier associated with pile-rock porous structure. The pile-rock porous structure is considered to be fully-extended and the vertical barrier is considered as fully-extended (Fig. 2.1), bottom-standing (Fig. 2.2) and surface-piercing (Fig. 2.3). The pile-rock porous structure associated with the fully-extended vertical barrier occupies

the region $0 < y < h$ but in the case of bottom-standing barrier, the vertical barrier occupies the region $h_1 < y < h$ and in the case of surface-piercing barrier the vertical barrier occupies the region $0 < y < h_1$. The pile-rock porous structure combined with different barrier configurations is divided into four regions. The region R_1 indicates the incident region, R_2 indicates the region between the vertical barrier and the pile-rock porous structure, R_3 indicates the porous structure region and R_4 indicates the transmitted region. The incident wave is assumed to be obliquely propagating in $x-$ direction with an angle θ. The flow is considered to be time harmonic with angular frequency ω. The velocity potentials in the respective regions are represented in the form of $\phi_j(x,y,z,t) = \mathrm{Re}\left[\phi_j(x,y)\,\mathrm{e}^{\mathrm{i}(lz-\omega t)}\right]$, where $l = \gamma_{10}\sin\theta$ and γ_{10} is the progressive wave number in open water region. The velocity potentials in the respective regions $j = 1,2,3,4$ satisfy the Helmholtz equation given by

$$\frac{\partial^2\phi_j}{\partial x^2} + \frac{\partial^2\phi_j}{\partial y^2} - l^2\phi_j = 0, \text{ for } -\infty < x < \infty, 0 < y < h. \tag{2.1}$$

The linearized free surface boundary condition for the open water and porous structure region is of the form

$$\frac{\partial\phi_j}{\partial y} + K_j\phi_j = 0, \quad \text{on} \quad y = 0, \tag{2.2}$$

where $K_{j=1,2,4} = \dfrac{\omega^2}{g}$ for free surface region and $K_{j=3} = \dfrac{\omega^2}{g}\left(S_s - if_s\right)$ for porous structure region, S_s and f_s are reactance and resistance coefficients of porous structure, g is the acceleration due to gravity and $i = \sqrt{-1}$ is imaginary number. The bottom boundary condition due to the presence of impermeable sea-bed is given by

$$\frac{\partial\phi_j}{\partial y} = 0, \quad \text{on} \quad y = h. \tag{2.3}$$

The propagation of the waves due to the presence of the porous structure suggest the continuity of fluid pressure and velocity across the seaward and leeward structural interfaces. So, the matching condition at each of the structural interface (Isaacson et al., 2000) are given by

$$\frac{\partial\phi_2(x,y)}{\partial x} = \varepsilon_s\frac{\partial\phi_3(x,y)}{\partial x} = i\gamma_{10}G_1\left[\left(S_s - if_s\right)\phi_3(x,y) - \phi_2(x,y)\right] \quad \text{at } x = -b_1, \tag{2.4a}$$

$$\frac{\partial\phi_4(x,y)}{\partial x} = \varepsilon_s\frac{\partial\phi_3(x,y)}{\partial x} = i\gamma_{10}G_2\left[\phi_4(x,y) - \left(S_s - if_s\right)\phi_3(x,y)\right] \quad \text{at } x = -b_2, \tag{2.4b}$$

where ε_s is the breakwater porosity, $G_j, j=1,2$ is the porous effect parameter (Yip and Chwang, 2000) of seaward and leeward vertical pile-rock porous structure respectively of the form

$$G_j = \frac{\varepsilon_j}{\gamma_{10} d_j \left(f_j - iS_j\right)}, \tag{2.5}$$

where $d_j, j=1,2$ is the structural thickness, $\varepsilon_j, j=1,2$ is the porosity, $f_j, j=1,2$ is the resistance and $S_j, j=1,2$ is the reactance of seaward and leeward barriers respectively. In the case of seaward and leeward porous barriers, the reactance $S_j=1, j=1,2$ resistance $f_j=2, j=1,2$ and barrier thickness $d_j/h=0.04$ is kept fixed (Suh et al., 2011; Liu and Li, 2014). The linearized resistance f_s and reactance coefficients S_s (Sollitt and Cross, 1972) due to the presence of porous rock-fill is determined on solving the relation given by

$$S_s = 1 + C_m\left[\frac{1-\varepsilon_s}{\varepsilon_s}\right], \tag{2.6a}$$

$$f_s = \frac{1}{\omega}\left\{\frac{\int_V dV \int_t^{t+T} \varepsilon_s^2 \left(\frac{\nu q^2}{\Lambda_p} + \frac{C_f \varepsilon_s}{\sqrt{\Lambda_p}}|q|^3\right) dt}{\int_V dV \int_t^{t+T} \varepsilon_s q^2 dt}\right\}, \tag{2.6b}$$

where, C_m is coefficient of added mass considered to be very minimal/zero (Sollitt and Cross, 1972), thus $S_s=1$ is kept fixed throughout the study. The Λ_p is the intrinsic permeability, q is the instantaneous Eulerian velocity vector, ν is the kinematic viscosity, V is the volume, C_f is the turbulent resistant coefficient and T is the wave period. The vertical (a) fully-extended barrier, (b) bottom-standing barrier and (c) surface-piercing barrier is placed in front of the pile-rock porous structure. So, the continuity of the velocity and pressure is satisfied for all the three different barrier configurations.

2.2.1 Fully-extended barrier with pile-rock porous structure

The fully-extended barrier (Fig. 2.1a) is considered to be placed at the water depth $0<y<h$. So, the continuity of the velocity and pressure for the fully-extended barrier interface (Krishna et al, 2019) is given by

$$\frac{\partial \phi_1(x,y)}{\partial x} = -i\gamma_{10} G_b \left[\phi_2(x,y) - \phi_1(x,y)\right], \text{ on } x = 0,\ 0 < y < h, \tag{2.7a}$$

$$\frac{\partial \phi_1(x,y)}{\partial x} = \frac{\partial \phi_2(x,y)}{\partial x}, \text{ on } x = 0,\ 0 < y < h. \tag{2.7b}$$

where G_b is the porous effect parameter of the vertical barrier given by

$$G_b = \frac{\varepsilon_b}{\gamma_{10} d_b \left(f_b - iS_b\right)}. \tag{2.7c}$$

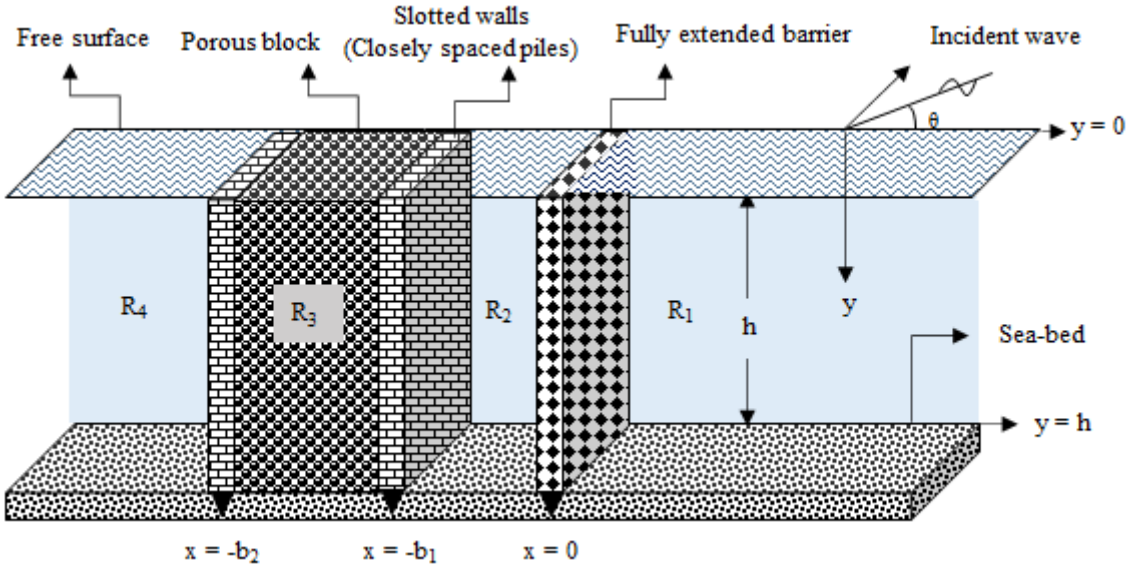

Fig. 2.1(a): Schematic diagram of pile-rock porous structure with fully-extended barrier.

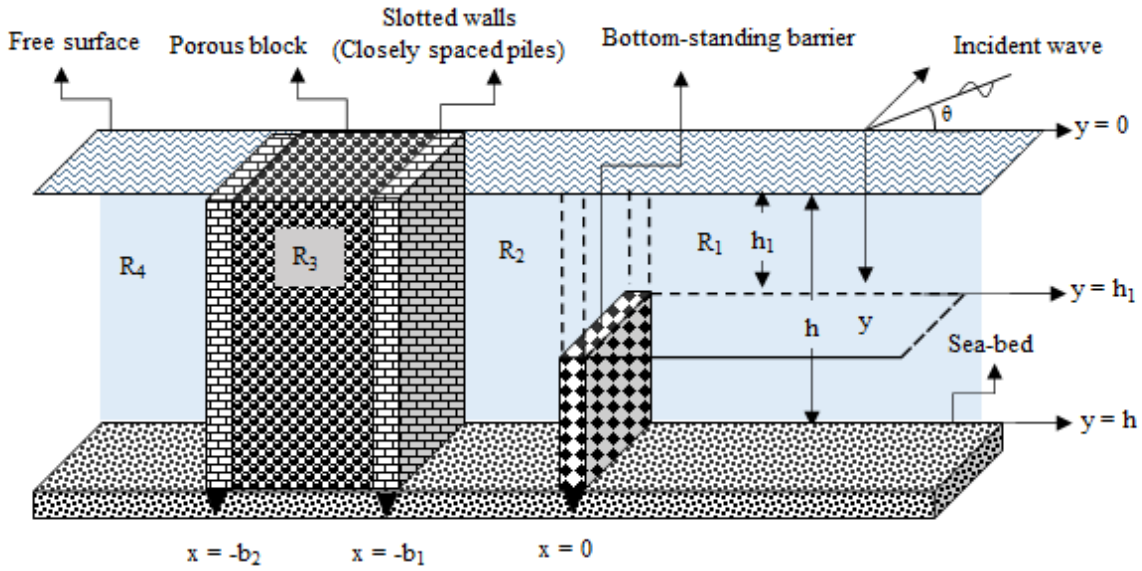

Fig. 2.1(b): Schematic diagram of pile-rock porous structure with bottom-standing barrier.

2.2.2 Bottom-standing barrier with pile-rock porous structure

The bottom-standing barrier (Fig. 2.1b) is placed within $h_1 < y < h$. So, the continuity of velocity and pressure for the bottom-standing barrier interface is given by

$$\phi_1(x,y) = \phi_2(x,y), \text{ on } x = 0,\ 0 < y < h_1, \tag{2.8a}$$

$$\frac{\partial \phi_1(x,y)}{\partial x} = -i\gamma_{10} G_b \left[\phi_2(x,y) - \phi_1(x,y)\right], \text{ on } x = 0,\ h_1 < y < h. \tag{2.8b}$$

2.2.3 Surface-piercing barrier with pile-rock porous structure

The surface-piercing barrier (Fig. 2.1c) is placed within $0 < y < h_1$. So, the continuity of velocity and pressure for the surface-piercing barrier interface is given by

$$\frac{\partial \phi_1(x,y)}{\partial x} = -i\gamma_{10} G_b \left[\phi_2(x,y) - \phi_1(x,y)\right], \text{ on } x = 0,\ 0 < y < h_1, \tag{2.9a}$$

$$\phi_1(x,y) = \phi_2(x,y), \text{ on } x = 0,\ h_1 < y < h. \tag{2.9b}$$

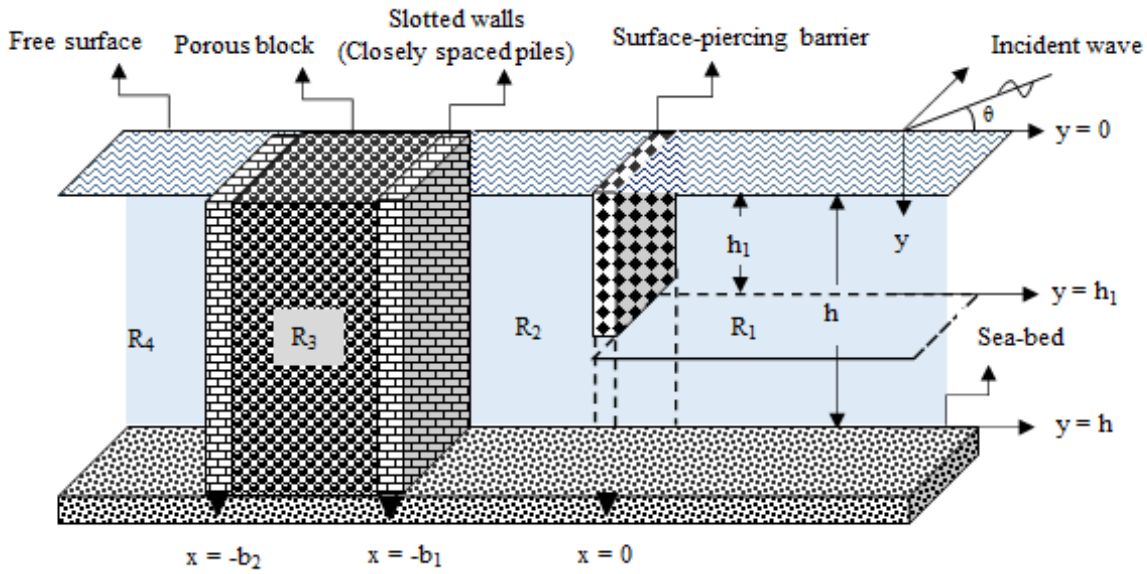

Fig. 2.1(c): Schematic diagram of pile-rock porous structure with surface-piercing barrier.

The wave number in upstream/downstream free surface region γ_{j0} for $j = 1,2,4$ and pile-rock porous structure region γ_{30} satisfies the dispersion relation for finite water depth is given by

$$\omega^2 = \begin{cases} g\gamma_{j0} \tanh \gamma_{j0} h & \text{for} \quad n = 0 \\ -g\gamma_{jn} \tan \gamma_{jn} h & \text{for} \quad n = 1,2,.... \end{cases} \quad \text{for } j = 1,2,4, \tag{2.10a}$$

$$\omega^2 (S_s - if_s) = g\gamma_{3n} \tanh \gamma_{3n} h \quad \text{for} \quad n = 0,1,2,.... \tag{2.10b}$$

where, ω is the wave frequency and g is the acceleration due to gravity. In the far-field region, the radiation conditions in the presence of pile-rock porous structure is given by

$$\phi_j(x,y)=\begin{cases}\left(I_{10}e^{-i\gamma_{10}x}+R_{10}e^{i\gamma_{10}x}\right)f_{10}(y) & \text{as } x\to\ \infty,\\ \left(T_{40}e^{-i\gamma_{40}x}\ \right)f_{40}(y) & \text{as } x\to-\infty,\end{cases} \tag{2.11}$$

where, I_{10}, R_{10} and T_{40} are the complex amplitude of the incident, reflected and transmitted wave energies respectively. However, the incident wave I_{10} is considered to be unity.

2.3 METHOD OF SOLUTION

The pile-rock porous structure combined with different configurations of vertical barrier is examined using the eigenfunction expansion method. The velocity potentials in each of the open water and porous structure regions are given by

$$\phi_1(x,y)=\left(I_{10}e^{-ik_{10}x}+R_{10}e^{ik_{10}x}\right)f_{10}(y)+\sum_{n=1}^{\infty}R_{1n}e^{-\kappa_{1n}x}f_{1n}(y),\quad \text{for}\quad 0<x<\infty, \tag{2.12a}$$

$$\phi_2(x,y)=\left(A_{20}e^{-ik_{20}x}+B_{20}e^{ik_{20}(x+b_1)}\right)f_{20}(y)+\sum_{n=1}^{\infty}\left(A_{2n}e^{\kappa_{2n}x}+B_{2n}e^{-\kappa_{2n}(x+b_1)}\right)f_{2n}(y),\quad \text{for}\quad -b_1<x<0, \tag{2.12b}$$

$$\phi_3=\left(A_{30}e^{-ik_{30}(x+b_1)}+B_{30}e^{ik_{30}(x+b_2)}\right)f_{30}(y)+\sum_{n=1}^{\infty}\left(A_{3n}e^{-i\kappa_{3n}(x+b_1)}+B_{3n}e^{i\kappa_{3n}(x+b_2)}\right)f_{3n}(y),\quad \text{for}\quad -b_2<x<-b_1, \tag{2.12c}$$

$$\phi_4=T_{40}e^{-ik_{40}(x+b_2)}f_{40}(y)+\sum_{n=1}^{\infty}T_{4n}e^{\kappa_{4n}(x+b_2)}f_{4n}(y),\quad \text{for}\quad -\infty<x<-b_2, \tag{2.12d}$$

where, I_{10} is the incident wave, R_{1n}, A_{jn}, B_{jn} and T_{4n} for $n=0,1,2,3,...$ and $j=1,2$ are the unknown constants to be determined, $d=-(b_2-b_1)$ is thickness of the porous structure. The vertical eigenfunctions $f_{jn}(y)$ for the open water and fully extended pile-rock porous structure regions are given by

$$f_{jn}(y)=\frac{\cosh\gamma_{jn}(h-y)}{\cosh\gamma_{jn}h}\ \text{for}\ n=0,1,2,..... \tag{2.13}$$

where γ_{jn} for $j=1,2,3,4$. The eigenvalues satisfy the open water and porous structure dispersion relations given by

$$\omega^2=g\gamma_{jn}\tanh\gamma_{jn}h\quad \text{for}\, j=1,2,4,\ n=0, \tag{2.14a}$$

$$\omega^2(S_s-if_s)=g\gamma_{jn}\tanh\gamma_{jn}h\quad \text{for}\ \ j=3,\ \ n=0,1,2,... \tag{2.14b}$$

with $\gamma_{jn} = i\gamma_{jn}$ for $n = 1,2,3,...$ for open water region. The roots of the dispersion relation for each region $j = 1,2,3,4$ satisfy $\gamma_{jn}^2 = k_{jn}^2 + l^2,\ n = 0$ with $l = \gamma_{10}\sin\theta,\ \theta$ is the angle of incidence, k_{jn} being the component of wave number in $x-$direction and γ_{jn} is the wave number in $y-$direction. In addition, there are purely imaginary roots γ_{jn} with $\gamma_{jn}^2 = \kappa_{jn}^2 - l^2$ for $n = 1,2,3,....$

In Eq. 2.14(a), γ_{10}, γ_{20} and γ_{40} represents the wave number in open water region for progressive waves and γ_{1n}, γ_{2n} and γ_{4n} for $n = 1,2,...$ represents the wave number in the open water region for evanescent wave. In Eq. 2.14(b), $\gamma_{3n}, n = 0,1,2,...$ represents the wave number in pile-rock porous structure region. Eq. 2.14(b) is the dispersion relation for the porous structure region which has infinite number of roots with the associated eigen value. The real part of the complex wave number, specifies the spatial periodicity (Sollitt and Cross, 1972) whereas the imaginary part specifies the decay rate.

The eigenfunctions $f_{jn}(y), j = 1,2,3,4$ satisfy the orthogonality relation of the form

$$\left\langle f_{jn}, f_{jm} \right\rangle_{j=1,2,4} = \begin{cases} 0 & \text{for } m \neq n, \\ C_n' & \text{for } m = n, \end{cases} \text{ and } \left\langle f_{jn}, f_{jm} \right\rangle_{j=3} = \begin{cases} 0 & \text{for } m \neq n, \\ C_n'' & \text{for } m = n, \end{cases} \tag{2.15}$$

with respect to the orthogonal mode-coupling relation defined by

$$\left\langle f_{jm}, f_{jn} \right\rangle_{j=1,2,3,4} = \int_0^h f_{jm}(y) f_{jn}(y) dy, \tag{2.16}$$

where $C_n'\big|_{j=1,2,4} = \left\{ \frac{2\gamma_{jn}h + \sinh 2\gamma_{jn}h}{4\gamma_{jn}\cosh^2 \gamma_{jn}h} \right\}$ and $C_n''\big|_{j=3} = \left\{ \frac{2\gamma_{jn}h + \sinh 2\gamma_{jn}h}{4\gamma_{jn}\cosh^2 \gamma_{jn}h} \right\}$. (2.17)

with $C_n'\big|_{j=1,2,4}$ for $n = 1,2,3,.....$ are obtained by substituting $\gamma_{jn} = i\gamma_{jn}$ in the case of open water region. In the pile-rock porous structure region, the mode-coupling relation (2.16) is employed on velocity potential $\phi_j(x,y)$ and $\phi_{jx}(x,y)$ with the eigenfunction $f_{jm}(y)$ along with continuity of pressure and velocity as in Eq. 2.4(a) across the vertical interface $x = -b_1, 0 < y < h$ to obtain

$$\begin{aligned} \left\langle \phi_j(x,y), f_{jm}(y) \right\rangle &= \int_0^h \phi_j(x,y) f_{jm}(y) dy \\ &= \int_0^h \left\{ (S_s - if_s)\phi_{j+1}(x,y) - \left(\frac{\varepsilon_s}{i\gamma_{10}G_1} \right) \phi_{(j+1)x}(x,y) \right\} f_{jm}(y) dy \end{aligned} \tag{2.18}$$

for $m = 0,1,2,...$ and $j = 2$

$$\left\langle \phi_{jx}(x,y), f_{jm}(y) \right\rangle = \int_0^h \phi_{jx}(x,y) f_{jm}(y)\,dy = \varepsilon_s \int_0^h \phi_{(j+1)x}(x,y) f_{jm}(y)\,dy \quad \text{for } m = 0,1,2,\ldots \text{ and } j = 2 \tag{2.19}$$

Again, the mode-coupling relation (2.16) is employed on velocity potential $\phi_j(x,y)$ and $\phi_{jx}(x,y)$ with the eigenfunction $f_{jm}(y)$ along with continuity of pressure and velocity as in Eq. 2.4(b) across the vertical interface $x = -b_2, 0 < y < h$ to obtain

$$\begin{aligned} \left\langle \phi_{j+1}(x,y), f_{(j+1)m}(y) \right\rangle &= \int_0^h \phi_{j+1}(x,y) f_{(j+1)m}(y)\,dy \\ &= \int_0^h \left\{ \left(\frac{\varepsilon_s}{i\gamma_{40} G_2} \right) \phi_{jx}(x,y) + (S_s - i f_s)\phi_j(x,y) \right\} f_{(j+1)m}(y)\,dy \end{aligned} \quad \text{for } m = 0,1,2,\ldots \text{ and } j = 3. \tag{2.20}$$

$$\left\langle \phi_{(j+1)x}(x,y), f_{(j+1)m}(y) \right\rangle = \int_0^h \phi_{(j+1)x}(x,y) f_{(j+1)m}(y)\,dy = \varepsilon_s \int_0^h \phi_{jx}(x,y) f_{(j+1)m}(y)\,dy \quad \text{for } m = 0,1,2,\ldots \text{ and } j = 3. \tag{2.21}$$

In the next subsection, the method of solution for each of the fully-extended barrier, bottom-standing barrier and surface-piercing barrier configurations are presented and discussed in detail to understand the effect of the wave dissipation due to the presence of the composite breakwater system.

2.3.1 Pile-rock structure with fully-extended barrier

In order to determine the unknown coefficients, the mode-coupling relation (2.16) is employed on the velocity potential $\phi_j(x,y)$ and $\phi_{jx}(x,y)$ with the eigenfunction $f_{jm}(y)$ along with continuity of pressure and velocity as in Eq. 2.7(a,b) across the vertical interface $x = 0, 0 < y < h$ to obtain

$$\left\langle \phi_j(x,y), f_{jm}(y) \right\rangle = \int_0^h \phi_j(x,y) f_{jm}(y)\,dy = \int_0^h \left\{ \phi_{j+1}(x,y) + \left(\frac{1}{i\gamma_{10} G_b} \right) \phi_{jx}(x,y) \right\} f_{jm}(y)\,dy, \quad \text{for } m = 0,1,2,\ldots \text{ and } j = 1. \tag{2.22}$$

$$\left\langle \phi_{jx}(x,y), f_{jm}(y) \right\rangle = \int_0^h \phi_{jx}(x,y) f_{jm}(y)\,dy = \int_0^h \phi_{(j+1)x}(x,y) f_{jm}(y)\,dy, \quad \text{for } m = 0,1,2,\ldots \text{ and } j = 1. \tag{2.23}$$

2.3.1 Pile-rock structure with bottom-standing barrier

In order to determine the unknown coefficients, the mode-coupling relation (2.16) is employed on the velocity potential $\phi_j(x,y)$ and $\phi_{jx}(x,y)$ with the eigenfunction $f_{jm}(y)$ along with continuity of pressure and velocity as in Eq. 8(a,b) across the vertical interface $x=0, 0<y<h$ to obtain

$$\begin{aligned}\left\langle \phi_j(x,y), f_{jm}(y)\right\rangle &= \int_0^h \phi_j(x,y) f_{jm}(y)\,dy = \left\{\int_0^{h_1} + \int_{h_1}^{h}\right\}\phi_j(x,y) f_{jm}(y)\,dy \\ &= \int_0^{h_1} \phi_{j+1}(x,y) f_{jm}(y)\,dy + \int_{h_1}^{h} \phi_j(x,y) f_{jm}(y)\,dy \\ &= \int_0^{h_1} \phi_{j+1}(x,y) f_{jm}(y)\,dy + \int_{h_1}^{h} \left\{\phi_{j+1}(x,y) + \left(\frac{1}{i\gamma_{10}G_b}\right)\phi_{jx}(x,y)\right\} f_{jm}(y)\,dy, \\ &\qquad \text{for } m=0,1,2,\ldots \text{ and } j=1.\end{aligned} \tag{2.24}$$

$$\left\langle \phi_{jx}(x,y), f_{jm}(y)\right\rangle = \int_0^h \phi_{jx}(x,y) f_{jm}(y)\,dy = \int_0^h \phi_{(j+1)x}(x,y) f_{jm}(y)\,dy, \qquad \text{for } m=0,1,2,\ldots \text{ and } j=1. \tag{2.25}$$

2.3.2 Pile-rock structure with surface-piercing barrier

In order to find the unknown coefficients, the mode-coupling relation (2.16) is employed on the velocity potential $\phi_j(x,y)$ and $\phi_{jx}(x,y)$ with the eigenfunction $f_{jm}(y)$ along with continuity of pressure and velocity as in Eq. 2.9(a,b) across the vertical interface $x=0, 0<y<h$ to obtain

$$\begin{aligned}\left\langle \phi_j(x,y), f_{jm}(y)\right\rangle &= \int_0^h \phi_j(x,y) f_{jm}(y)\,dy = \left\{\int_0^{h_1} + \int_{h_1}^{h}\right\}\phi_j(x,y) f_{jm}(y)\,dy \\ &= \int_0^{h_1} \phi_j(x,y) f_{jm}(y)\,dy + \int_{h_1}^{h} \phi_{j+1}(x,y) f_{jm}(y)\,dy \\ &= \int_0^{h_1} \left\{\phi_{j+1}(x,y) + \left(\frac{1}{i\gamma_{10}G_b}\right)\phi_{jx}(x,y)\right\} f_{jm}(y)\,dy + \int_{h_1}^{h} \phi_{j+1}(x,y) f_{jm}(y)\,dy, \\ &\qquad \text{for } m=0,1,2,\ldots \text{ and } j=1.\end{aligned} \tag{2.26}$$

$$\left\langle \phi_{jx}(x,y), f_{jm}(y) \right\rangle = \int_0^h \phi_{jx}(x,y) f_{jm}(y)\,dy = \int_0^h \phi_{(j+1)x}(x,y) f_{jm}(y)\,dy, \quad \text{for } m = 0,1,2,\ldots \text{ and } j = 1. \tag{2.27}$$

The infinite sums presented in the Eqs. (2.18)-(2.21) and Eq. (2.22) - (2.23) for fully-extended barrier, Eq. (2.24) – (2.25) for bottom-standing barrier and Eq. (2.26) – (2.27) for surface-piercing barrier are truncated upto finite M terms to obtain a linear system of $6(M+1)$ algebraic equation for the determination of $6(M+1)$ unknowns and the wave reflection and transmission coefficients due to the presence of pile-rock porous structure and barrier are obtained as

$$K_r = \left| \frac{R_{10}}{I_{10}} \right| \quad \text{and} \quad K_t = \left| \frac{T_{40}}{I_{10}} \right|. \tag{2.28a}$$

Due the existence of porous blocks the energy dissipation in the wave propagation through the porous blocks as in Chwang and Chan (1998) is represented as

$$K_d = 1 - K_r^2 - K_t^2. \tag{2.28b}$$

In the next section, the wave attenuation due to the presence of pile-rock porous structure with bottom standing barrier is examined.

2.3.3 Wave force on barrier and pile-rock porous structure

The wave force impact acting on the vertical barrier K_{fb}, leeward wall of the pile-rock porous structure K_{fs_1} and rearward wall of the pile-rock porous structure K_{fs_2} are given by

$$K_{fb} = \left| \frac{F_b}{2\rho g h I_{10}} \right|, \quad K_{fs_1} = \left| \frac{F_{s_1}}{2\rho g h I_{10}} \right| \text{ and } K_{fs_2} = \left| \frac{F_{s_2}}{2\rho g h I_{10}} \right| \tag{2.29}$$

where $F_{s_1} = i\rho\omega \int_0^h \{\phi_3(x,y) - \phi_2(x,y)\} dy$ at $x = -b_1$, (30a)

$$F_{s_2} = i\rho\omega \int_0^h \{\phi_4(x,y) - \phi_3(x,y)\} dy \quad \text{at} \quad x = -b_2, \tag{30b}$$

and I_{10} is the amplitude of the incident wave potential considered to be unity. In the case of fully-extended, surface-piercing and bottom-standing barrier the wave force on the barrier F_b is given by

$$F_b\big|_{\text{fully-extended}} = i\rho\omega\int_0^h \{\phi_2(x,y)-\phi_1(x,y)\}dy \quad \text{at} \quad x=0, \tag{2.30c}$$

$$F_b\big|_{\text{surface-piercing}} = i\rho\omega\int_0^{h_1} \{\phi_2(x,y)-\phi_1(x,y)\}dy \quad \text{at} \quad x=0, \tag{2.30d}$$

$$F_b\big|_{\text{bottom-standing}} = i\rho\omega\int_{h_1}^h \{\phi_2(x,y)-\phi_1(x,y)\}dy \quad \text{at} \quad x=0. \tag{2.30e}$$

In the next section, the numerical results are obtained for various hydrodynamic parameters and are analysed for different configurations of the barrier with pile-rock porous structure.

2.4 EXPERIMENTAL INVESTIGATION OF COMPOSITE BREAKWATER

The experimental investigation on the wave interaction with porous block and fully-extended vertical barrier is conducted on generating regular waves in wave flume available in the Marine Structures Laboratory of Department of Water Resources and Ocean Engineering, National Institute of Technology Karnataka (NITK), Surathkal, India. The two-dimensional wave flume is having the dimensions of 50 m x 0.74 m x 1.1 m along with 42m long, smooth concrete bottom. The flume consist of 6.3 m long, 1.5 m wide and 1.4 m deep chamber at one end where the bottom hinged flap type wave generator is connected to generate monochromatic wave. Whereas, the other end of the flume consists of the rubble mound spending beach which acts as wave absorber. The wave generator system consists of a bottom-hinged flap, which is moved back and forth by induction motor of 11 kW, 1450 rpm. The induction motor is regulated by Kirloskar made inverter drive of 0-50 Hz which rotate with a speed range of 0-1550 rpm. On changing the frequency through the inverter, the desired wave period is obtained for the propagating waves. The schematic diagram of the experimental setup is presented in Fig. 2.2 and the details of the flume is discussed in Table 2.1.

Table 2.1: Flume details

Total length	50m
Channel length	42m
Width	0.74m
Channel depth	1.1m
Maximum water depth	0.5m
Wave flume type	Two dimensional

Wave Generator	Bottom hinged flap type
Waves generated	Monochromatic type
Wave absorber	Rubble mound spending beach
Range of wave height generation	0.06 m - 0.24 m
Range of wave period generation	1.0 sec to 3.0 sec

2.4.1 Model Scale

The fundamental of all physical modelling is similitude of the model and prototype. The surface tension and the viscous effects are negligible in the prototype, as in the real sea condition the flow will be turbulent. Also, in wave motion the gravity effect is predominant in the prototype. In such conditions Froude similitude is selected. The choice of scale, for the model test is often limited by constraints posed in the available experimental facility. In the present study, similitude is achieved by the method of dimensional analysis. To simulate the field conditions of wave height, period and depth of water by application of Froude's law, a geometrically similar model scale of 1:30 is selected for the present experimental work.

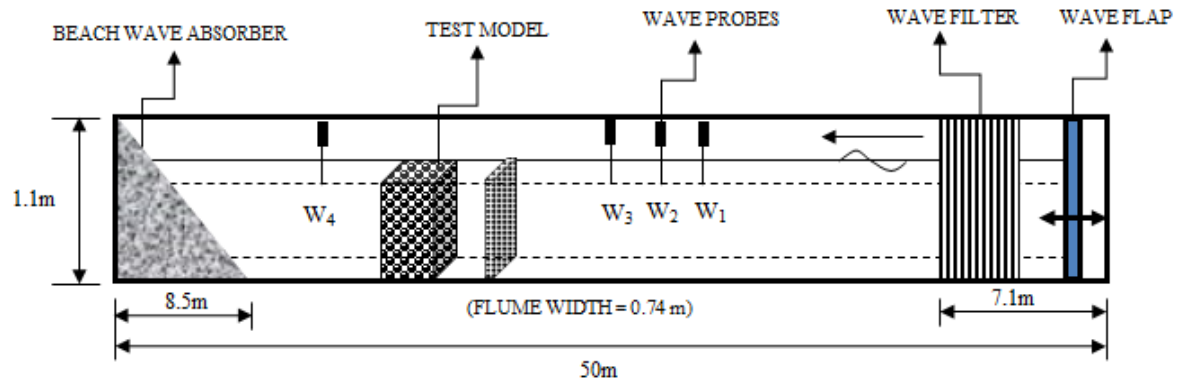

Fig. 2.2: Schematic diagram of experimental setup.

Table 2.2: Selection of the model scale

Scale	H_i (m)		T (sec)	
	1	5.4	8	12
1:10	0.1	0.54	2.53	3.8
1:20	0.05	0.27	1.79	2.68
1:30	**0.033**	**0.18**	**1.46**	**2.19**
1:40	0.025	0.135	1.26	1.9

The breakwater model is tested with the existing facilities in Wave Flume laboratory of Department of Water Resources and Ocean Engineering, NITK, Surathkal. The wave height and wave period of Mangalore coast varies from 1m-5.4m, 8s-12s respectively. In the laboratory regular wave height ranges from 0.06m - 0.24m and wave period ranging from 1s-3s can be generated in a maximum water depth of 0.70m. So, for the studies, a geometrically similar scale (Table 2.2) of 1:30 is selected for the present experimental investigation.

2.4.2 Composite vertical barrier and porous structure

The composite structure is modelled with a 1:30 scale using Froude's similitude criteria. The investigations are conducted for different porosity of the barrier and by varying the wave heights (H) and wave periods (T). The composite breakwater consists of the vertical fully-extended barrier and porous structure, whose dimensions are listed in Table 2.3.

Table 2.3: Structural dimensions of the model

Structural Parameters	Model Dimensions		
	Width (m)	Thickness (m)	Height (m)
Porous Block	0.72 m	0.15 m	0.5 m
Vertical Barrier	0.72 m	0.01 m	0.5 m

2.4.3 Experimental Procedure

The experimental study is conducted for the composite fully-extended barrier and porous structure. The wave flume is calibrated for different water depths to obtain the incident wave heights for different combinations of wave height and wave period. The capacitance type wave probes are installed to measure the water surface elevation and the wave probes are calibrated every time before starting the experiment. The wave height is measured using three probe method as suggested by Isaacson (1991) to calculate the wave reflection. Three probes are installed before the model (in the seaward side) to measure the incident and reflected wave height. The spacing between the probes in the seaward side is adjusted to one-third of the wavelength to ensure accuracy of wave reflections (Goda and Syzuki, 1976; Isaacson, 1991). The transmitted wave heights are recorded from a probe which is placed at a distance L from the model towards the lee side. The list of experimental variables used in the present investigation is presented in Table 2.4 and the experimental set up for the composite breakwater is shown in Fig. 2.3. The accuracy of the experiments are ensured by repeating the cases thrice under the same conditions.

(a) 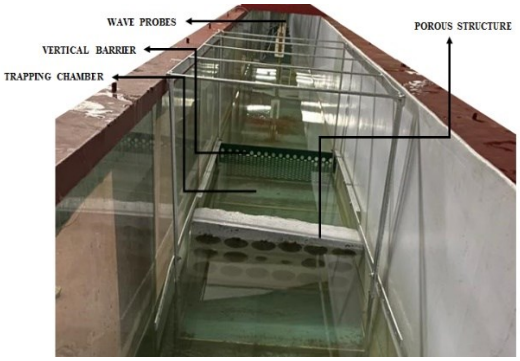

(b) 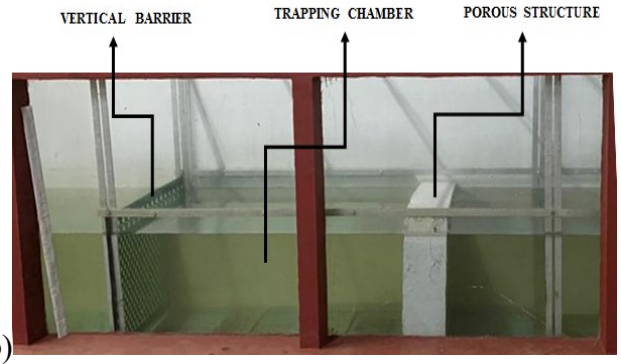

Fig. 2.3: Experimental setup for composite breakwater (a) top view and (b) side view of NITK wave flume.

Table 2.4: Experimental variables

Variables	Expression	Parameter Range
Wave period (s)	T	1.4, 1.6, 1.8, 2.0
Incident wave height (m)	H_i	0.06, 0.08, 0.10, 0.12, 0.14
Water depth (m)	h	0.45
Angle of wave attack	θ	0^0
Incident wave steepness	H_i / gT^2	0.15 – 0.0062

2.4.4 Reflection Transmission and Dissipation Coefficient

The wave reflection coefficient is obtained as the ratio of the reflected wave height and incident wave height represented as

$$K_r = \frac{H_r}{H_i}. \tag{2.31}$$

The reflected wave height (H_r) are obtained by the three-probe method as proposed by Issacson (1991). The wave transmission coefficient is obtained as the ratio of the transmitted wave height and incident wave height given by

$$K_t = \frac{H_t}{H_i}. \tag{2.32}$$

The dissipation coefficient is obtained by considering the energy balance condition as in Eq. (2.28b). In the present study, the experimental investigation is performed to validate the numerical results obtained using the eigenfunction expansion method.

2.5 RESULTS AND DISCUSSION

The numerical investigation on the wave interaction due to pile-rock porous structure coupled with different configurations of the vertical barriers is performed to examine the hydrodynamic

performance of the composite breakwater considering various values of structural porosity ε_s, linearized friction factor f_s angle of incidence θ and water chamber length L/h. The wave reflection coefficient K_r, transmission coefficient K_t, energy dissipation coefficient K_d, wave force impact on the barrier K_{fb}, wave force impact on the leeward pile-rock porous structure K_{fs_1} and wave force impact on the rearward pile-rock porous structure K_{fs_2} are plotted to understand the behaviour of pile-rock porous structure combined with vertical barriers as an effective absorber. The parameters that were kept constant are $\rho = 1000$ kg/m^3, $g = 9.81$ m/s^2 and $S_s = 1$ throughout the computation. Further, it may be noted that for $G_1 = G_2 = 0$ suggests that the porous structure with rigid barrier and for $G_1 = G_2 \to \infty$ suggests that the porous structure without barrier (Liu and Li, 2014). The convergence study in K_r due to the increasing number of evanescent wave modes M is performed for different types of vertical barriers and the results obtained are tabulated in Table 1. It can be observed that, with the increase in the number of evanescent wave modes $M \geq 10$, the convergence in the wave reflection and transmission coefficient is evident.

2.5.1 Validation of Numerical and Experimental Investigation

The comparative study for the wave reflection and transmission coefficient for the wave interaction with porous structure as in Sollitt and Cross (1972) and Darlymple et al. (1991) is performed and validated (Venkateswarlu and Karmakar, 2020). The wave reflection K_r and transmission coefficient K_t are analysed and validated with the analytical results available in the literature for specific configuration.

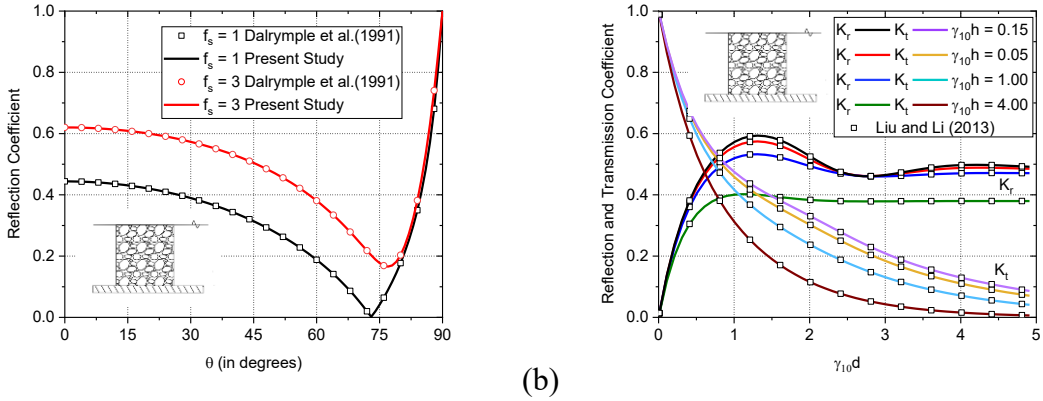

(a) (b)

Fig 2.4: Comparative study for single porous structure with that of (a) Dalrymple et al. (1991) for $\varepsilon_s = 0.4$, $s = 1$, $d/h = 1$ and $\omega^2 h/g = 0.2012$ (b) Liu and Li (2013) for $\varepsilon_s = 0.45$, $s_s = 1$, $f_s = 1.0$ and $f_1 = f_2 = f_b = 2$.

The present study performed using the eigenfunction expansion method is validated with the available numerical results from notable researchers. The K_r versus incidence angle is plotted for varying friction factor f_s and the result obtained is compared with Dalrymple et al. (1991) as shown in Fig 2.4(a). The minimum value of K_r is observed at $\theta = 74^0$ and the K_r value increases with increase in friction factor f_s. The results from Dalrymple et al. (1991) shows that the plane-wave approximation diverges from the full solution in deeper water than the long-wave models and provides a reasonable estimate of the reflection coefficient. Further, in Fig. 2.4(b), the K_r and K_t is plotted against dimensionless structural width $\gamma_{10}d$ for different values of $\gamma_{10}h$ and compared with the results obtained by Liu and Li (2013). The K_r and K_t values tend to decrease with increasing dimensionless structural width $\gamma_{10}d$. In Liu and Li (2013), a new analytical solution which is in agreement with traditional analytical solution and multi-domain BEM solutions has been developed. The comparative study shows that the numerical result obtained using the present approach coincide with the result obtained by Dalrymple et al. (1991) and Liu and Li (2013).

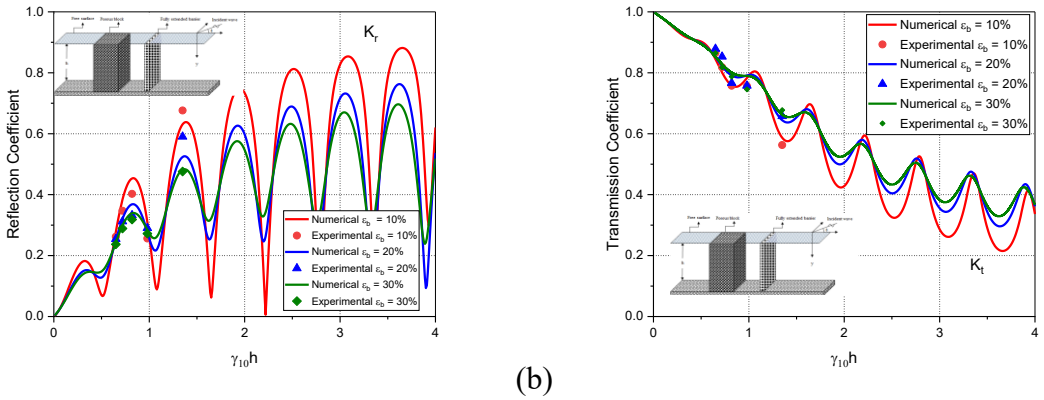

(a) (b)

Fig. 2.5: Validation of (a) K_r and (b) K_t versus $\gamma_{10}h$ using both numerical and experimental study considering $\varepsilon_S = 0.4$, $w/h = 5.53$ and $d/h = 0.33$ for different structural porosity of barrier and normal incident angle.

Table 2.5: Convergence of K_r and K_t for three different types of barrier configuration considering $\theta = 15^0$, $\gamma_{10}h = 1.0$, $\varepsilon_s = 0.6$, $\varepsilon_b = 0.4$, $f_b = 1.0$ and $f_s = 1.0$.

Evanescent wave modes	Pile-rock structure with fully-extended barrier		Pile-rock structure with bottom-standing barrier		Pile-rock structure with surface-piercing barrier	
M	K_r	K_t	K_r	K_t	K_r	K_t
0	0.31089	0.69534	0.44701	0.55704	0.47242	0.54856
1	0.32044	0.69552	0.45276	0.57551	0.47271	0.55313

5	0.32048	0.69568	0.45282	0.57667	0.47404	0.55450
10	0.32054	0.69575	0.45288	0.57693	0.47448	0.55488
15	0.32054	0.69576	0.45288	0.57694	0.47449	0.55498
20	0.32054	0.69576	0.45288	0.57694	0.47449	0.55498

The result obtained using the physical model study is validated with the numerical results obtained for the case of wave interaction with fully-extended porous structure with vertical barrier. The comparative study for the wave reflection and transmission coefficient is performed using both physical model study and numerical model study. In Fig. 2.5(a,b), the wave reflection and transmission coefficient is analysed versus non-dimensional wave number for different porosity of the structure using both numerical and experimental approach. The wave reflection coefficient (Fig. 2.5a) is observed to have multiple minimum with the increase in the non-dimensional wave number. The wave reflection is noted to increase with the increase in $\gamma_{10}h$ and also observed high with the decrease in the porosity of the structure. The experimental results are obtained within $0 \le \gamma_{10}h \le 1.75$ and a close agreement with the numerical and experimental study is noted. Further, the transmission coefficient (Fig. 2.5b) is observed to have oscillating nature with the increase in the non-dimensional wave number $\gamma_{10}h$. The wave transmission coefficient decreases with the decrease in porosity and $\gamma_{10}h$. A close agreement with the numerical and experimental result with the change in the porosity is noted for the wave number within $0 \le \gamma_{10}h \le 1.75$.

2.5.2 Pile-rock porous structure with fully-extended barrier

The wave interaction due to pile-rock porous structure in combination with fully-extended vertical barrier is analysed on studying the wave reflection coefficient K_r, transmission coefficient K_t, dissipation coefficient K_d, wave force impact on the barrier K_{fb}, wave force impact on the leeward pile-rock porous structure K_{fs_1} and wave force impact on the rearward pile-rock porous structure K_{fs_2}. The following parameter $\gamma_{10}h = 1.0$, $f_s = 0.5, f_1 = f_2 = f_b = 2$ and $S_1 = S_2 = S_b = S_s = 1$ is kept fixed throughout the numerical computations unless mentioned.

2.5.2.1 Effect of angle of incidence

The wave reflection K_r, wave transmission K_t and wave energy damping K_d is plotted versus the angle of incidence θ varying the porosity of the structure within $0.2 \le \varepsilon_s \le 0.8$ in Fig. 2.6(a,b). A decreasing pattern in K_r and an increasing trend in K_t (Fig 2.6a) is observed within

$0^0 \leq \theta \leq 65^0$ while an almost constant pattern in K_d (Fig 2.6b) is observed within $0^0 \leq \theta \leq 65^0$. Thereafter, a sudden increase in K_r, reduction in K_t and a drastic reduction in K_d is noted within $85^0 \leq \theta \leq 90^0$. The minimal values in K_r is obtained within $65^0 \leq \theta \leq 80^0$ due to the dominance of standing waves which is known as critical angle where the minimum wave reflection occurs. The reduction in K_r is observed with the increase in the porosity which may be due to the increase in the wave penetration through the pile-rock porous structure causing more interaction between the structure and fluid particles. Further, it is observed that, the K_r is minimum and K_d is maximum for $\varepsilon_S = 0.8$. Thus, the increased porosity can be considered as efficient in wave energy attenuation. It is observed that lower structural porosity shows higher values in K_r and higher structural porosity shows minimal values in K_r which is due to constructive or destructive interference.

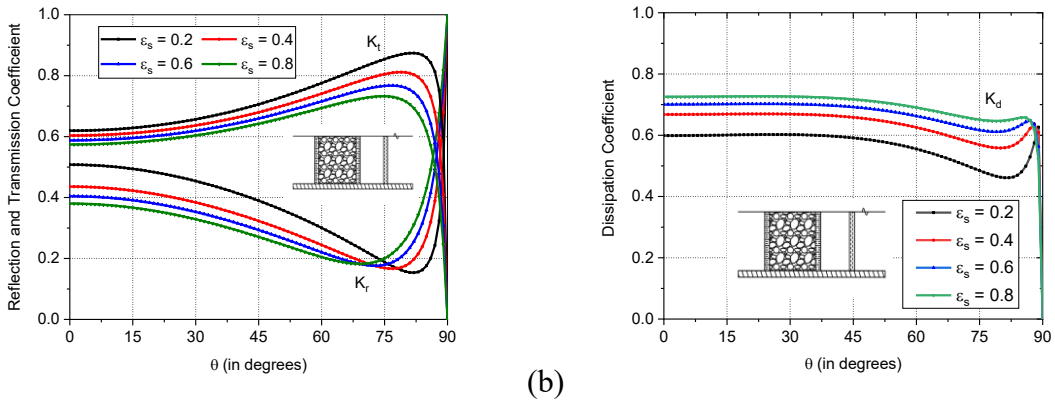

(a) (b)

Fig 2.6: Variation of (a) K_r and K_t (b) K_d versus θ for different values of ε_s considering $\varepsilon_1 = 0.3$, $\varepsilon_2 = 0.1$ and $\varepsilon_b = 0.6$.

2.5.2.2 Effect of dimensionless wavenumber

The effect of K_r (Fig 2.7a) and K_t (Fig 2.7b) versus distance between the pile-rock structure and the vertical barrier L/h with varying dimensionless wave number is analysed to understand the effect of wavelength in the attenuation of wave due to the composite porous structure. The K_r values are noted less for lower values of $\gamma_{10}h$ while the K_t values are observed high for lower values of $\gamma_{10}h$. The increase in L/h shows the periodic crests and troughs in K_r at regular intervals which may be due to the formation of the standing waves at particular intervals where the K_r is minimum. In case of both K_r and K_t, the higher value of

$\gamma_{10}h$ is associated with more closer crests and troughs and higher K_r is observed at each of the harmonic peak due to lesser wavelength. It can be seen that the dimensionless wave number shows significant effect on K_t values for higher $\gamma_{10}h$ showing minimum wave transmission, which is due to the fact that shorter waves can transmit only lesser wave energy onto the rear side of the structure. The values of reflection coefficient K_r decreases as the dimensionless wave number decreases from $\gamma_{10}h = 1.5$ to $\gamma_{10}h = 0.5$. It can be concluded that the waves having higher wavelength has lower reflection characteristic and most of the wave energy gets transmitted.

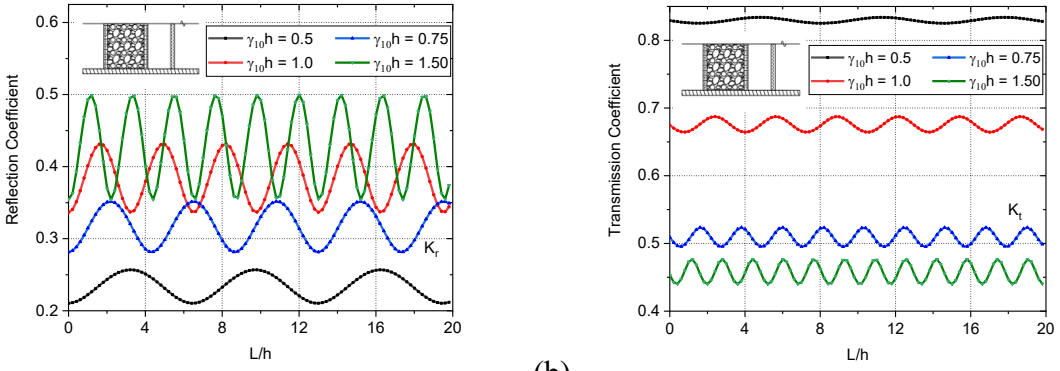

(a) (b)

Fig. 2.7: Variation of (a) K_r and (b) K_t versus L/h for different values of $\gamma_{10}h$ considering $d/h = 1$, $\theta = 15^0$, $\varepsilon_1 = 0.3$, $\varepsilon_2 = 0.1$ and $\varepsilon_b = 0.6$.

2.5.2.3 Effect of structural porosity

The wave reflection, transmission and dissipation coefficients with respect to dimensionless width d/h for variable structural porosity within $0.2 \le \varepsilon_s \le 0.8$ is analysed in Fig. 2.8(a,b) for the case of pile-rock porous structure with fully-extended barrier. A sharp increase in K_r is observed for $0.8 \le d/h \le 1.8$ for all values of structural porosity which further decreases and attains an uniform value due to the seaward constructive or destructive interference as shown in Fig 2.8(a). The K_t shows a reducing trend with increase in structural width as in Fig 2.8(b), while the wave damping shows an oscillating behaviour. Higher wave decay is observed with higher porosity attributed to incident waves passing through the pores. The increase in the structural porosity shows reduction in K_r which may be due to the increase in wave transport through the porous structure enhancing the wave decay. The global minima for K_d is observed

within $0.8 \le d/h \le 1.8$ which may be due to the generation of standing gravity waves due to the interaction between the incident and reflected waves. An almost uniform values in K_r, K_d and a reduction in K_t is observed for $3.0 \le d/h \le 10$ after which designing the breakwater would be uneconomical as its performance is limited. Thus, the optimal values in K_r, K_t and K_d is observed at $d/h = 3$ and can be taken for optimal wave damping for all the cases of porosity within $0.2 \le \varepsilon_s \le 0.8$.

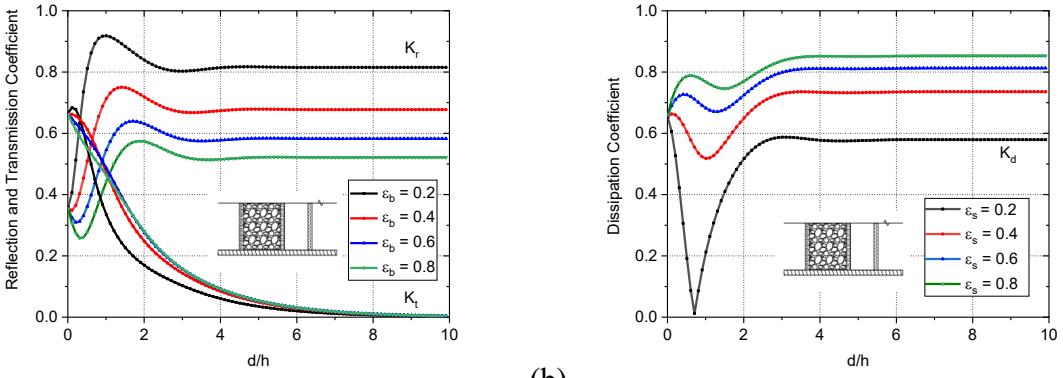

(a) (b)

Fig. 2.8: Variation of (a) K_r and K_t (b) K_d versus d/h for different values of ε_s considering $\theta = 15^0$, $\varepsilon_1 = 0.3$, $\varepsilon_2 = 0.1$ and $\varepsilon_b = 0.6$.

2.5.2.4 Effect of trapping chamber spacing

The wave reflection and transmission coefficient (Fig. 2.9a), dissipation coefficient K_d (Fig 2.9b), the wave forces at front side K_{fs_1} and rear side K_{fs_2} of the structure (Fig 2.9c) and wave force at the barrier K_{fb} (Fig 2.9d) versus the dimensionless water chamber length L/h is plotted for various values of porosities within $0.2 \le \varepsilon_s \le 0.8$. An oscillating trend with periodic crests and trough is observed in all the cases which may be due to the formation of standing waves at particular intervals. It can be seen from Fig 2.9(a) that, the lower values of porosity shows higher values of K_r and K_t. Thus, the higher porosity plays an important role in reducing K_r and K_t and has higher K_d indicating more wave energy dissipation as in Fig 2.9(b). Further, with the increase in L/h the K_{fs_1}, K_{fs_2} and K_{fb} is also seen to undergo oscillating trend.The increase in structural porosity is observed to enhance the wave forces due to large pore spaces. Considering same values for K_{fs_1} and K_{fs_2} with increase in L/h, it is observed that the maximum wave forces on the seaward and leeward interfaces occurs at same

L/h. The harmonic crests in K_{fb} (Fig 2.9d) suggests an optimal wave trapping. In addition, at certain values of L/h, the values of K_{fb} is observed to coincide indicating less effect of porosity at those points.

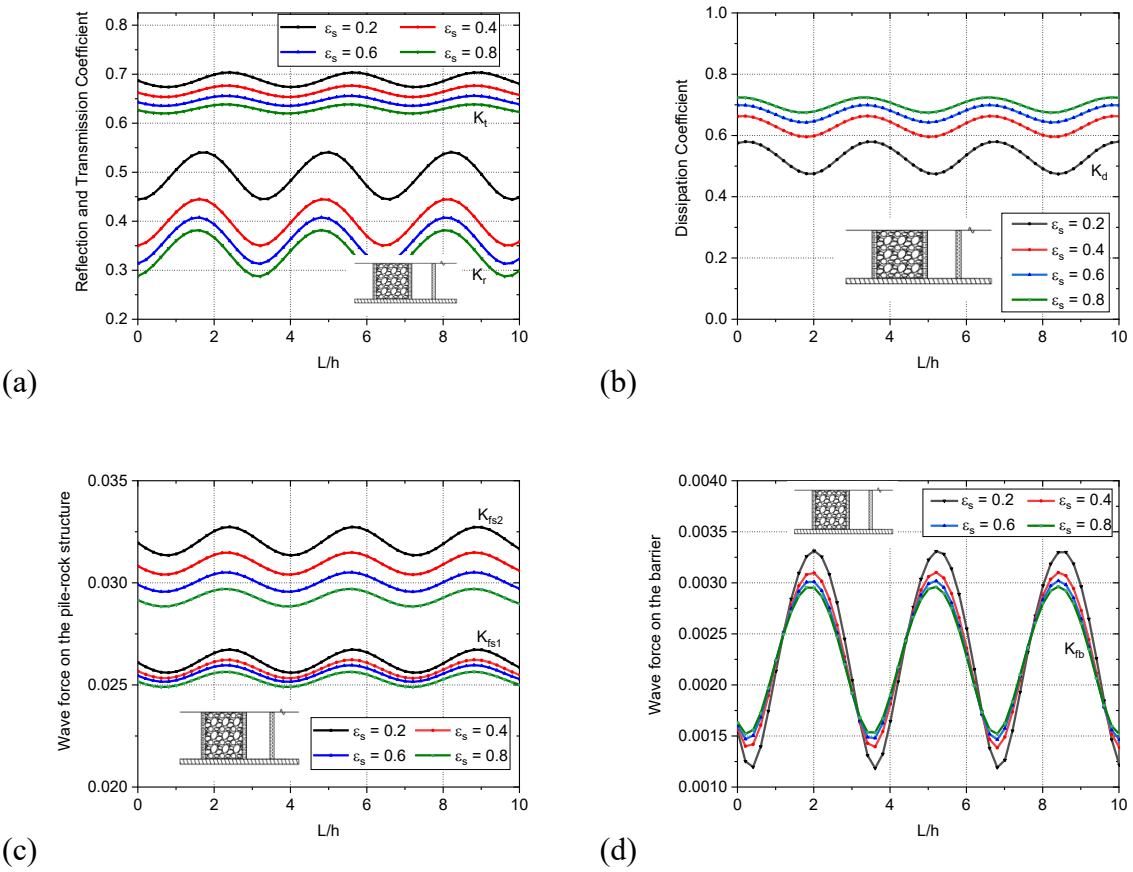

Fig. 2.9: Variation of (a) K_r and K_t (b) K_d (c) K_{fs_1} and K_{fs_2} (d) K_{fb} versus L/h for different values of ε_s considering $d/h = 1$, $\theta = 15^0$, $\varepsilon_1 = 0.3$, $\varepsilon_2 = 0.1$ and $\varepsilon_b = 0.6$.

2.5.2.5 Effect of friction factor

The K_{fs_1} and K_{fs_2} versus dimensionless wave number is obtained by varying friction factor in Fig 2.10(a,b). K_{fs_1} and K_{fs_2} shows an oscillatory trend for $0.1 \le \gamma_{10} h \le 3.5$ with the varying crest at $\gamma_{10} h = 0.8$ and further for higher $\gamma_{10} h$ the wave force coefficient converges for K_{fs_1}, while K_{fs_2} showing a decreasing behaviour. The variation in the wave forces may be due to the wave trapping in the confined region between the pile-rock porous structure and the barrier. The K_{fs_2} value for $f_s = 0.25$ shows the highest values for varying f_s. In the case of $f_s = 0.5$, zero wave

force is noted in the front end for $\gamma_{10}h = 1.8$ while $f_s = 1.0$ shows almost zero wave force for $\gamma_{10}h = 2.1$ at the rear end. Further, K_{fs_1} value increases while K_{fs_2} is observed to decrease with increase in the friction factor. It is observed that only for $f_s = 0.25$, the wave force on the rearward pile-rock structure is more than the leeward side at $\gamma_{10}h = 1.0$ indicating that decreased friction factor value may result in higher forces at the leeward side which is due to the minimum friction offered by the porous structure which further leads to lesser damping of wave energy.

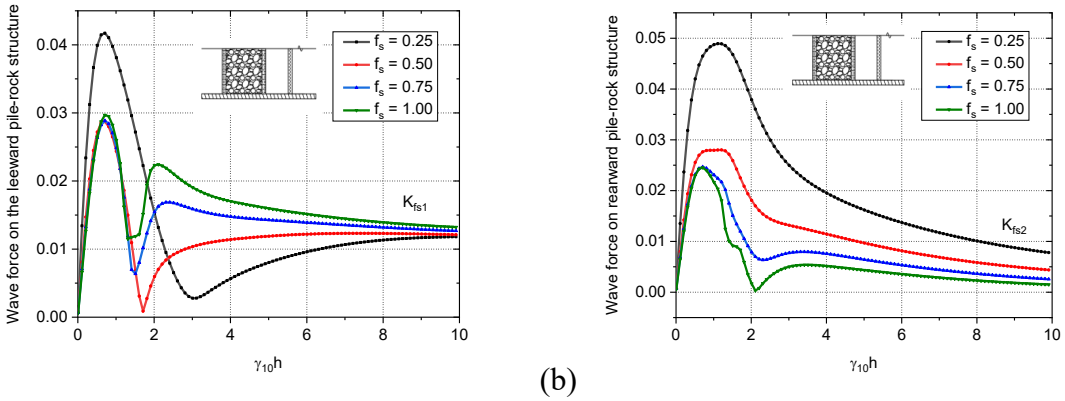

(a) (b)

Fig. 2.10: Variation of (a) K_{fs_1} and (b) K_{fs_2} versus $\gamma_{10}h$ for different values of f_s considering $d/h = 1$, $\theta = 15^0$, $\varepsilon_1 = 0.3$, $\varepsilon_2 = 0.1$ and $\varepsilon_b = \varepsilon_s = 0.6$.

2.5.3 Pile-rock porous structure with bottom-standing barrier

The wave interaction due to pile-rock porous structure combined with bottom-standing barrier is analysed on studying the wave reflection coefficient K_r, transmission coefficient K_t, dissipation coefficient K_d, wave force impact on the barrier K_{fb}, wave force impact on the leeward porous structure K_{fs_1} and wave force impact on the rear wall of porous structure K_{fs_2}.

2.5.3.1 Effect of structural width

The effect of structural width to analyse the hydrodynamic characteristics of wave propagation through pile-rock porous structure along with bottom-standing barrier is presented in Fig. 2.11(a,b) for varying the water chamber length L/h. Fig 2.11(a) shows the effect on the wave reflection, transmission and dissipation coefficients versus structural width, and a resonating trend is noted to be dominating over the range $0.01 \le d/h \le 4.0$. The resonating trend may be due to the wave trapping in the finite spacing between the structure and the vertical barrier

where interaction between the transmitted wave amplitudes from the vertical barrier occurs, and is reflected back by the leeward barrier, which may cause the wave trapping and wave blocking. Similarly, K_{fs_1} (Fig.2.11b) shows resonating trend within $0.01 \le d/h \le 4.0$. The lower values of L/h is observed to have higher wave force on rear side of the structure. Initially the K_{fs_2} (Fig 2.11b) is observed to have higher values within $0.01 \le d/h \le 4.0$ due to minimum structural width which further decreases with the increase in L/h with more dissipation in wave energy. Higher wave force is observed to occur at the leeward side of the structure compared to the rearward side which is due to the wave trapping in the finite spacing between the barrier and the structure. Thus, with the increase in distance between the barrier and the structure from $0 < L/h < 4.0$, the hydrodynamic characteristics and the wave forces show reduced values and lesser resonating trend due to increased spacing between the barrier and the structure leading to lesser trapping of waves.

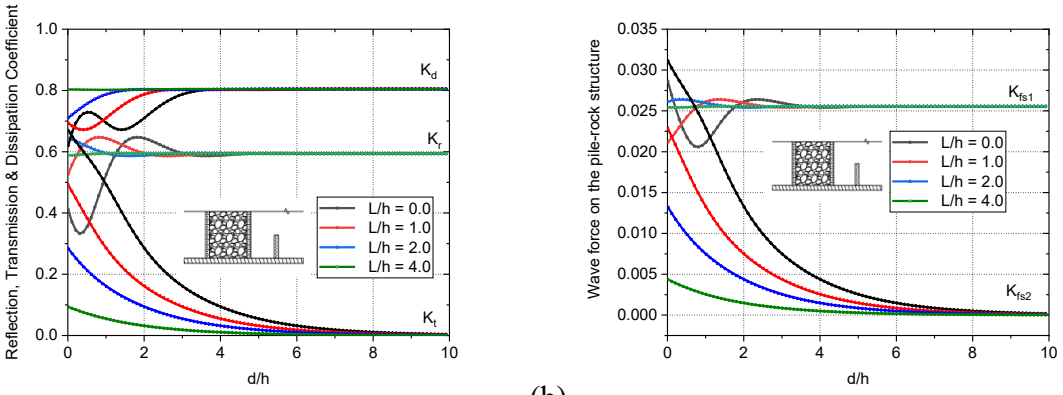

(a) (b)

Fig. 2.11: Variation of (a) K_r, K_t and K_d (b) K_{fs_1} and K_{fs_2} versus d/h for different values of L/h considering $h_1/h = 0.5$, $\theta = 15^0$, $\varepsilon_1 = 0.3$, $\varepsilon_2 = 0.1$ and $\varepsilon_b = \varepsilon_s = 0.6$.

2.5.3.2 Effect of angle of incidence

The wave reflection coefficient K_r and transmission coefficient K_t (Fig. 11a), wave dissipation coefficient K_d (Fig. 2.12b) and wave forces on the front and rear side of the pile-rock porous structure K_{fs_1} and K_{fs_2} (Fig. 2.12c,d) for varying angle of incidence is analysed in the case of pile-rock porous structure combined with bottom-standing vertical barrier for varying friction angle within $0.25 \le f_s \le 1.0$. The K_r shows a decreasing trend while K_t increases within $0^0 \le \theta \le 65^0$ in the case of low friction factor showing less wave reflection thus minimising K_r value due to the formation of standing waves and the critical angle is observed

at $\theta = 74^o$ for $f_s = 0.25$ after which K_t decreases. The decrease in f_s shows the increase in K_d as in Fig. 2.12(b) which may be due to the fact that, the K_r decreases with the increase in friction factor. As shown in Fig. 2.12(b), an uniform values for wave force on front side of the pile-rock structure is observed for $0^0 \le \theta \le 40^0$ and thereafter decreases. The K_{fs_1} for $f_s = 0.5$ shows the minimum value within $0^0 \le \theta \le 80^0$ and $f_s = 0.25$ shows 77% higher wave force on the front side of the structure than $f_s = 0.5$ at $\theta = 0^o$. The K_{fs_2} shows a decreasing trend with higher friction factor offering lower wave force on the rear side of pile-rock porous structure. The K_{fs_2} value for $f_s = 1.0$ shows the minimum value and $f_s = 0.25$ shows 75% higher wave force on rear side of the structure than $f_s = 1.0$ at $\theta = 0^o$.

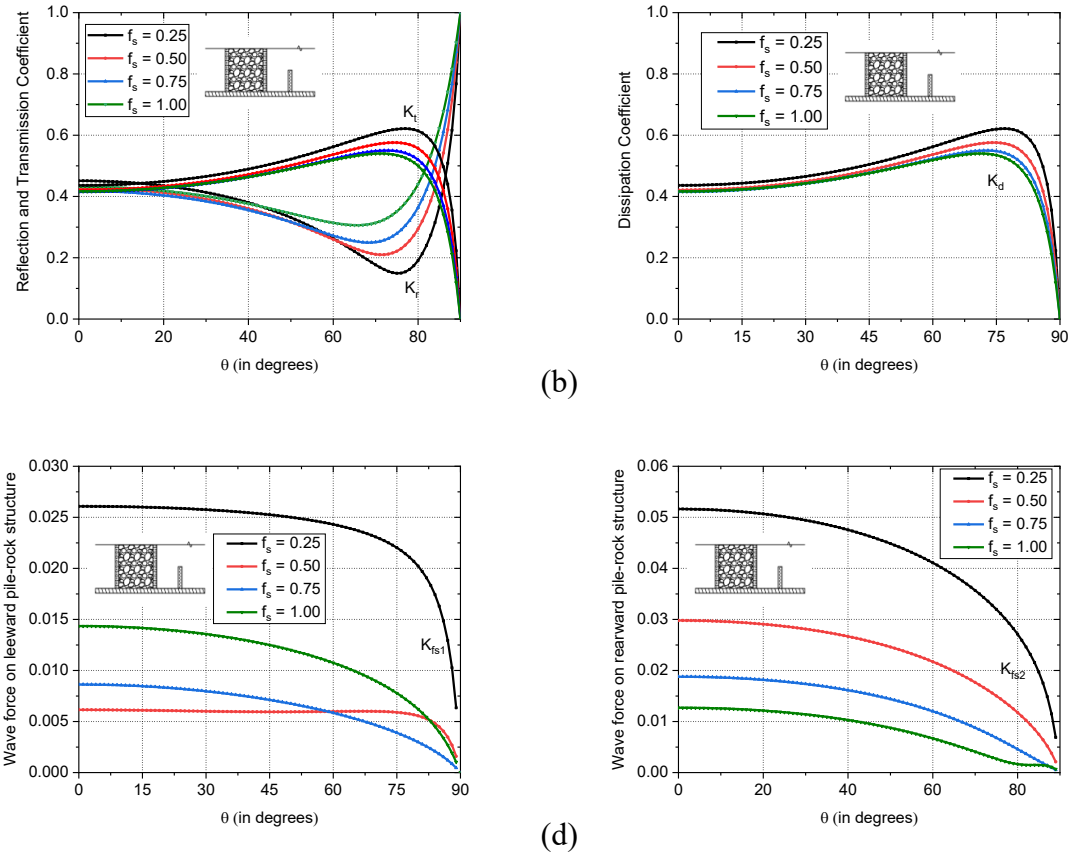

Fig. 2.12: Variation of (a) K_r and K_t (b) K_d (c) K_{fs_1} and (d) K_{fs_2} versus θ for different values of f_s considering $d/h = 1.0$, $\theta = 15^0$, $\varepsilon_1 = 0.3$, $\varepsilon_2 = 0.1$ and $\varepsilon_b = \varepsilon_s = 0.6$.

2.5.3.3 Effect of trapping chamber length

The wave reflection coefficient K_r (Fig. 2.13a) and wave force on the barrier K_{fb} (Fig. 2.13b) versus the dimensionless water chamber length L/h is analysed for various values of incident

angle. An oscillatory pattern is noted for K_r and K_{fb} and it is observed that higher θ values is associated with lower K_r and K_{fb} with wider wave crests and troughs. It is also seen that sharper resonating peaks are present for $\theta = 15^0$ at periodic intervals of L/h in the case of K_{fb} (Fig. 2.13b) and a gradual variation with forward shift is observed due to the presence of the barrier. The lower values of θ is seen to have comparatively larger values of oscillation and the increase in the angle of incidence further vanishes the oscillations and almost uniform values in the K_r is observed for $\theta = 60^0$. Minimal values in K_r and decreased wave force impact with broader peaks are obtained at higher angle of incidence θ which may be due to the formation of standing waves nearing to the critical angle.

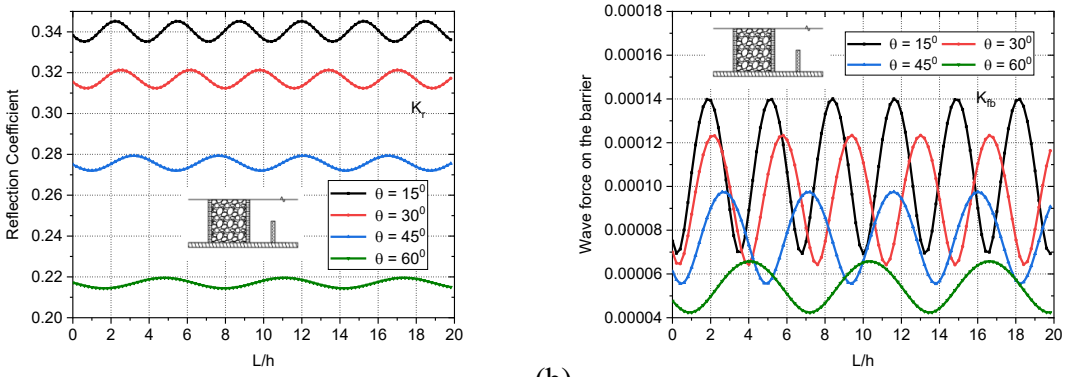

(a) (b)

Fig. 2.13: Variation of (a) K_r (b) K_{fb} versus L/h for different values of θ considering $h_1/h = 0.5$, $f_s = 0.5$, $\varepsilon_1 = 0.3$, $\varepsilon_2 = 0.1$ and $\varepsilon_b = \varepsilon_s = 0.6$.

2.5.3.4 Effect of dimensionless wave number

The effect of dimensionless wave number on the wave force at the seaward and leeward side is studied on varying d/h in Fig. 2.14(a,b). The higher values of $\gamma_{10}h$ reduces K_{fs_1} (Fig 2.14a) and K_{fs_2} (Fig 2.14b) to minimum. The K_{fs_1} shows an oscillatory trend within $0.01 \le d/h \le 2.0$ which may be due to the wave trapping and destructive structural interference in the confined spacing between the barrier and pile-rock porous structure and further increase in dimensionless width has no effect on the wave force values. In the case of lower values of $\gamma_{10}h$, the oscillatory pattern is observed within $0.01 \le d/h \le 4.0$ and a considerable reduction in K_{fs_2} is observed within $0.01 \le d/h \le 4.0$ where higher values in K_{fs_2} is noted. It can be observed that lesser wave force impact on the leeward and rearward side of the structure is

obtained corresponding to higher value of dimensionless wave number and, the wave force on the leeward and rearward side of porous structure decreases from $\gamma_{10}h = 0.5$ to $\gamma_{10}h = 1.5$. Thus, waves having higher wavelength is observed to have more wave force impact on the leeward and rearward side of the porous structure.

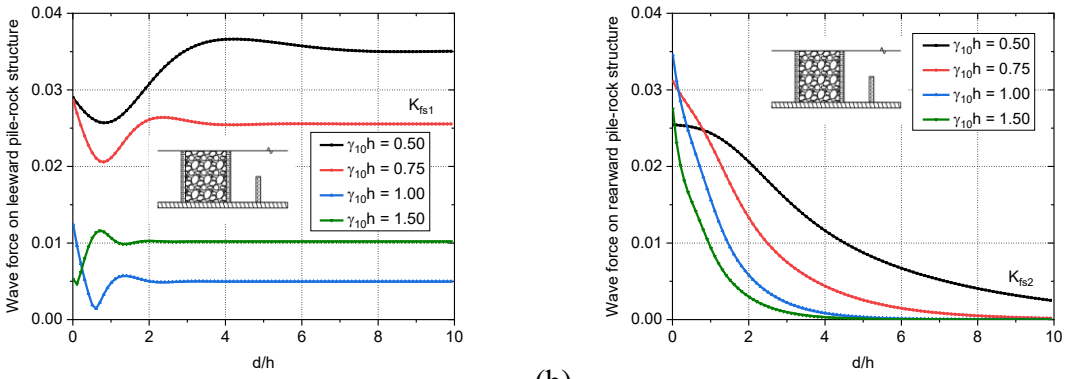

(a) (b)

Fig. 2.14: Variation of (a) K_{fs_1} and (b) K_{fs_2} versus d/h for different values of $\gamma_{10}h$ considering $f_s = 0.5$, $h_1/h = 0.5$, $\theta = 15^0$, $\varepsilon_1 = 0.3$, $\varepsilon_2 = 0.1$ and $\varepsilon_b = \varepsilon_s = 0.6$.

2.5.4 Pile-rock porous structure with surface-piercing barrier

The wave interaction due to pile-rock porous structure combined with surface-piercing barrier is analysed on studying the wave reflection coefficient K_r, transmission coefficient K_t, dissipation coefficient K_d, wave force impact on the barrier K_{fb}, wave force impact on the leeward side of the structure K_{fs_1} and wave force impact on the rear side of the structure K_{fs_2}.

2.5.4.1 Effect of angle of incidence

The K_r and K_t (Fig. 2.15a) and K_d (Fig. 2.15b) for varying dimensionless wave number within $1.0 \le \gamma_{10}h \le 2.5$ is analysed for varying the angle of incidence. The lower values of $\gamma_{10}h$ shows a reducing trend in K_r, increasing trend in K_t and almost a constant pattern of K_d is observed for $\gamma_{10}h = 1.5$ within $0^0 \le \theta \le 85^0$ with the maximum wave damping and then decreases drastically. The K_d values for smaller values of dimensionless wave number shows a varying trend over $78^0 \le \theta \le 88^0$ with resonating peak at $\theta = 80^0$. The critical angle is observed moving towards the left side with increase in $\gamma_{10}h$ and is observed over $70^0 \le \theta \le 78^0$ It is observed that for $\gamma_{10}h = 1.5$, the minimum K_t and maximum K_d (80%) is noted which could be adopted

for better wave attenuation. The critical angle is observed moving towards the left side with increase in $\gamma_{10}h$ and is observed over $70^0 \leq \theta \leq 78^0$, due to the dominance of standing waves over the range. It can be observed that, with the decrease in wavelength of the incident waves, the transmission characteristic of the wave decreases and the dissipation of wave energy is observed to be maximum.

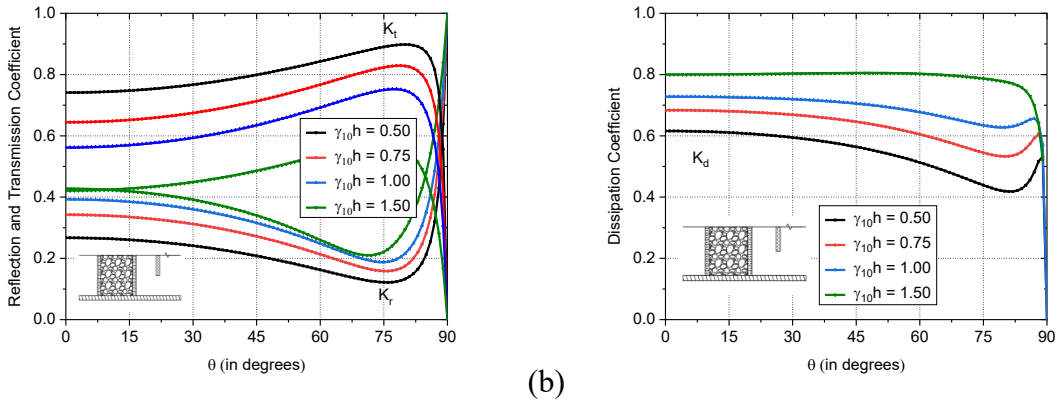

(a) (b)

Fig. 2.15: Variation of (a) K_r and K_t (b) K_d versus θ for different values of $\gamma_{10}h$ considering $h_1/h = 0.5$, $f_s = 0.5$, $\theta = 15^0$, $\varepsilon_1 = 0.3$, $\varepsilon_2 = 0.1$, $\varepsilon_b = 0.4$ and $\varepsilon_s = 0.6$.

2.5.4.2 Effect of structural width

The wave reflection coefficient K_r and transmission coefficient K_t (Fig. 2.16a), energy damping K_d (Fig. 2.16b) and wave force constants are analysed versus the non dimensional width of the porous structure d/h, for varying the dimensionless wave number within $1.0 \leq \gamma_{10}h \leq 1.5$. The values of K_r and K_d shows a fluctuation within $0.01 \leq d/h \leq 4.0$ which may be due to the transmitted waves from the barrier being reflected by the porous structure in the finite spacing and thereafter remains constant. The K_r value is minimum for $\gamma_{10}h = 1.5$ and about 85% wave damping is noted. The K_r values are observed to decrease with increase in dimensionless structural width with a sharp decrease within $0.1 \leq d/h \leq 5.0$. Further, it can be seen that with the increase in the $\gamma_{10}h$, the transmission coefficient decreases and the reflection coefficient increases which may be due to the fact that longer waves with smaller $\gamma_{10}h$ can transmit more wave energy into the leeside of the breakwater. The K_{fs_1} (Fig. 2.16d) and K_{fb} (Fig. 2.16c) shows a fluctuating trend within $0.1 \leq d/h \leq 3.0$ which may be due to the effect of wave trapping inside the porous structure due to width constraint, after which it is uniform

indicating that it has less effect on the structural width after a value of $d/h = 2.0$. The K_{fb} has lesser magnitude (Fig. 2.16c) when compared with K_{fs_1} and K_{fs_2}. The K_{fs_2} with initial higher values within $0.1 \le d/h \le 4.0$ shows a decreasing trend as an outcome of wave energy dissipation through the porous structure with increasing structural width.

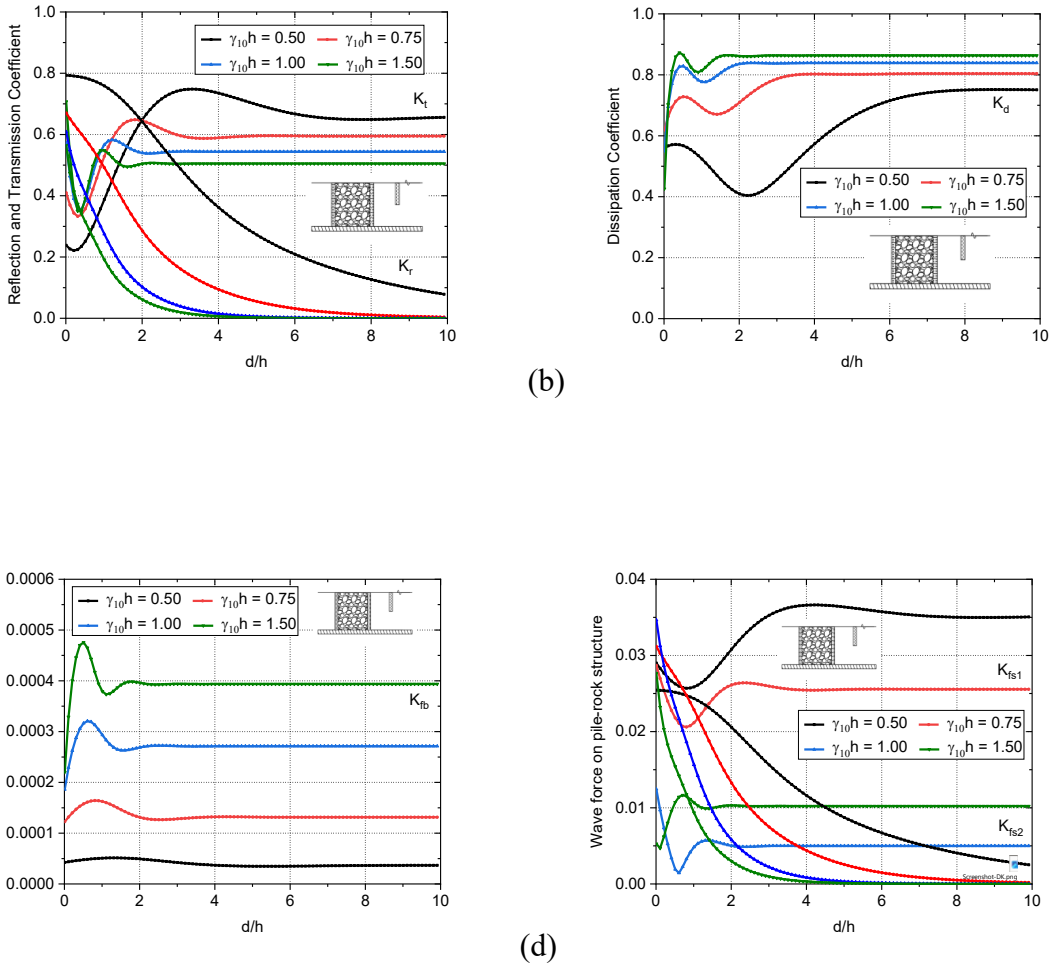

Fig. 2.16: Variation of (a) K_r and K_t (b) K_d (c) K_{fb} (d) K_{fs_1} and K_{fs_2} versus d/h for different values of $\gamma_{10}h$ considering $h_1/h = 0.5$, $f_s = 0.5$, $\theta = 15^0$, $\varepsilon_1 = 0.3$, $\varepsilon_2 = 0.1$ and $\varepsilon_b = \varepsilon_s = 0.6$.

2.5.4.3 Effect of dimensionless wave number

The wave force constants are obtained for varying dimensionless wave number against varying θ in Fig. 2.17(a-c). An uniform values in K_{fs_1} (Fig. 2.17a) is observed within $0^0 \le \theta \le 80^0$ after which there is a drastic reduction in the wave force. The lower wave force on front side of the structural interface is observed for dimensionless wave number $\gamma_{10}h = 1.5$. On the other hand,

for higher dimensionless wave numbers including $\gamma_{10}h = 1.0$ and $\gamma_{10}h = 1.5$, the K_{fs_2} (Fig. 2.17b) values are observed to be higher than K_{fs_1} values. In the case of K_{fs_2} at $\gamma_{10}h = 0.5$ shows minimum value within $0^0 \le \theta \le 47^0$ while $\gamma_{10}h = 1.5$ has minimum value.

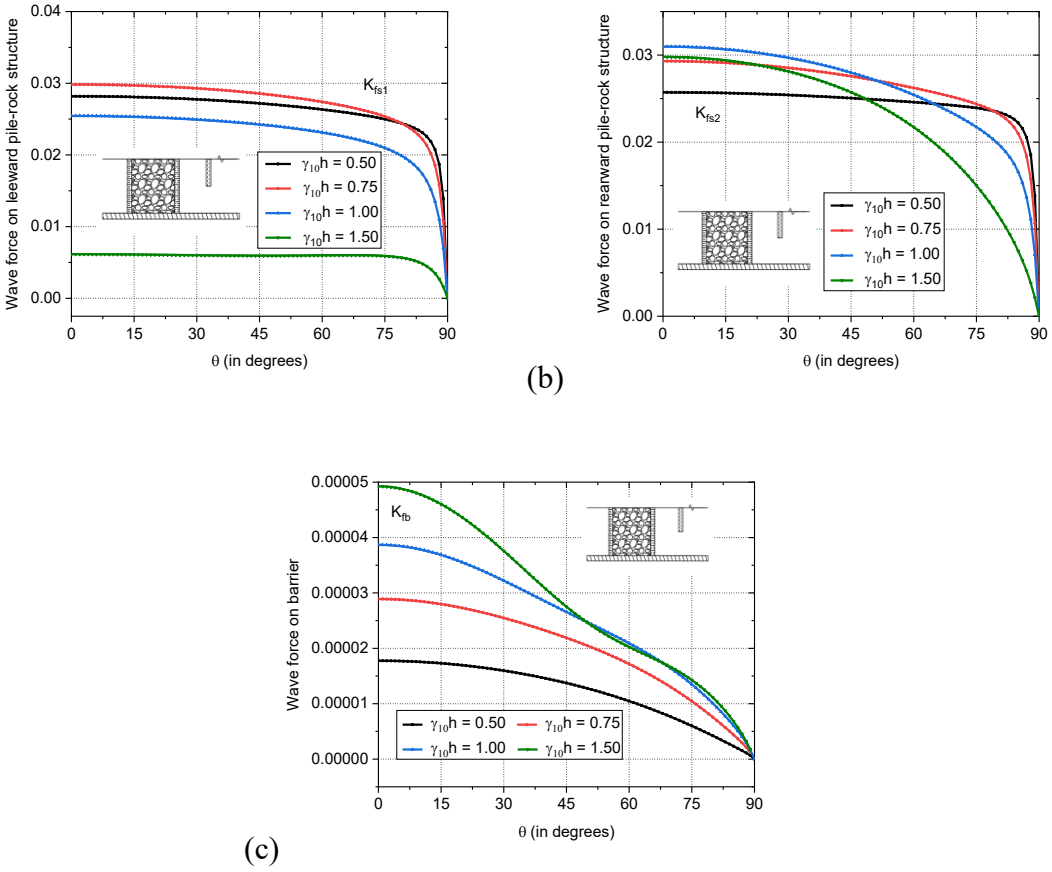

Fig. 2.17: Variation of (a) K_{fs_1}, (b) K_{fs_2} and (c) K_{fb} versus θ for different values of $\gamma_{10}h$ considering $d/h = 1.0$, $h_1/h = 0.5$, $f_s = 0.5$, $\theta = 15^0$, $\varepsilon_1 = 0.3$, $\varepsilon_2 = 0.1$, $\varepsilon_b = 0.4$ and $\varepsilon_s = 0.6$.

The K_{fb} (Fig. 2.17c) shows a decreasing trend with the increase in the angle of incidence and has minimum value corresponding to lower dimensionless wave number $\gamma_{10}h = 0.5$. The K_{fs_2} (Fig. 2.17b) for $\gamma_{10}h = 0.5$ shows uniform value upto $\theta = 85^0$ and is minimum upto $\theta = 47^0$ after which $\gamma_{10}h = 1.5$ takes the minimum value. It is observed that as the dimensionless wavenumber increases from $\gamma_{10}h = 0.5$ to $\gamma_{10}h = 1.5$, the wave force on the structure decreases while that on the barrier increases. Thus, it can be concluded that incident waves having higher wavelength causes more wave force impact on the leeward and rearward side of the pile-rock porous structure while it has lower impact on the surface-piercing barrier.

2.5.5 Comparative study of pile-rock structure with barriers

The comparative study is conducted between the pile-rock porous structures with three different configurations of vertical barrier. The three cases of vertical barriers includes the fully-extended barrier (FEB), bottom-standing barrier (BSB) and surface-piercing barrier (SPB).

2.5.5.1 Wave reflection, transmission and dissipation coefficient

In Fig 2.18(a,b), the reflection, transmission and dissipation coefficients are plotted versus angle of incidence for fully-extended, bottom-standing and surface-piercing barriers and compared with single porous structure without barrier. It is observed that for single porous structure, the K_r shows lesser values while its transmission coefficient is higher of around 32% at $\theta = 0^0$ as in Fig. 2.18(a). More wave damping is evident for pile-rock porous structure with barrier when compared with single porous structure, 35% for surface-piercing and bottom-standing barriers is noted and 30.5% for fully-extended barriers as seen in Fig. 2.18(b). At $\theta = 85^0$ the K_r , K_t and K_d for different vertical barrier configurations is observed to coincide. The critical angle for single porous structure without barrier is observed at $\theta = 62^0$ while for the cases of pile-rock structures with barrier the critical angle is observed within $68^0 \le \theta \le 76^0$.

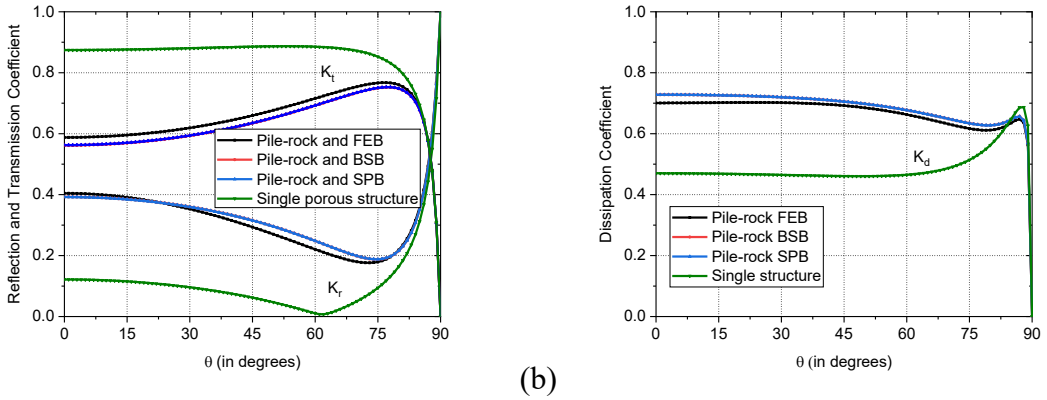

(a) (b)

Fig. 2.18: Variation of (a) K_r and K_t (b) K_d for $\gamma_{10}h = 1.0$ versus θ for different configuration of barriers considering $d/h = 1.0$, $h_1/h = 0.5$, $\theta = 15^0$, $\varepsilon_1 = 0.3$, $\varepsilon_2 = 0.1$ and $\varepsilon_b = \varepsilon_s = 0.6$.

Table 2.6 depicts the comparative study made on the three different cases of vertical barrier for different angle of incidence θ. The values of the reflection and transmission coefficients, K_r

and K_t for the pile-rock porous structure with surface-piercing and bottom-standing barrier is found to be almost similar.

Table 2.6: Reflection and transmission coefficient for different incident wave angle for pile-rock porous structure combined with fully-extended, bottom-standing and surface-piercing barrier.

Incident angle	Pile-rock structure with fully-extended barrier		Pile-rock structure with bottom-standing barrier		Pile-rock structure with surface-piercing barrier	
θ	K_r	K_t	K_r	K_t	K_r	K_t
0^0	0.3772	0.6198	0.4123	0.5861	0.4128	0.5856
15^0	0.3712	0.6280	0.4057	0.5944	0.4068	0.5928
30^0	0.3529	0.6528	0.3853	0.6195	0.3858	0.6190
45^0	0.3223	0.6947	0.3500	0.6629	0.3504	0.6625
60^0	0.2845	0.7525	0.3028	0.7247	0.3029	0.7244
75^0	0.2868	0.8095	0.2871	0.7908	0.2869	0.7906

It is observed from Table 2 that, for pile-rock structure with surface-piercing vertical barrier has the minimum transmission values for a given incident angle, followed by the bottom-standing and the fully-extended barrier. This may be attributed to higher wave energy dissipation observed for pile-rock structure with surface-piercing barrier. In this context, wave energy is dissipated on the free surface at a faster rate as compared to fully-extended or bottom-standing structures.

Table 2.7: Reflection and transmission coefficient for different dimensionless wave number for pile-rock porous structure combined with fully-extended, bottom-standing and surface-piercing barrier.

Wave number	Pile-rock structure with fully-extended barrier		Pile-rock structure with bottom-standing barrier		Pile-rock structure with surface-piercing barrier	
$\gamma_{10}h$	K_r	K_t	K_r	K_t	K_r	K_t
0.1	0.0393	0.9675	0.0536	0.9613	0.0621	0.9496
0.5	0.1654	0.8456	0.2260	0.8113	0.2511	0.7763
1.0	0.2623	0.7074	0.3784	0.6144	0.3848	0.6018
2.0	0.3045	0.4836	0.4175	0.3901	0.4292	0.3770
4.0	0.4681	0.2710	0.5892	0.1570	0.6060	0.1654
6.0	0.6097	0.1616	0.6461	0.0809	0.6340	0.0765

Table 2.7 shows the comparative study of the three different configurations of vertical barriers combined with pile-rock porous structure for different values of dimensionless wave number.

The reflection and transmission coefficients, K_r and K_t is compared and a similar trend is noted for different angle of incidence as seen in Table 2.7. The pile-rock porous structure with surface-piercing vertical barrier is observed to have the least transmission values, followed by the pile-rock porous structure with bottom-standing and the fully-extended barriers for different dimensionless wave numbers. It can be observed that the waves having higher wavelength has lower reflection and maximum transmission in all the three cases considered.

2.5.5.2 Wave force on the structure and barrier

The values of wave force K_{fs_1} (Fig. 2.19a) and K_{fb} (Fig. 2.19b) are plotted against dimensionless wave number varying the non-dimensional wave number. In Fig 2.19(a) the K_{fs_1} shows a sharp increase after reaching maximum at $\gamma_{10}h = 1.0$ and further decreases to zero value at $\gamma_{10}h = 1.7$ unlike single porous structure which shows a slight resonating trend within $0.1 \le \gamma_{10}h \le 4.0$ and further remains constant with increasing dimensionless wave number.

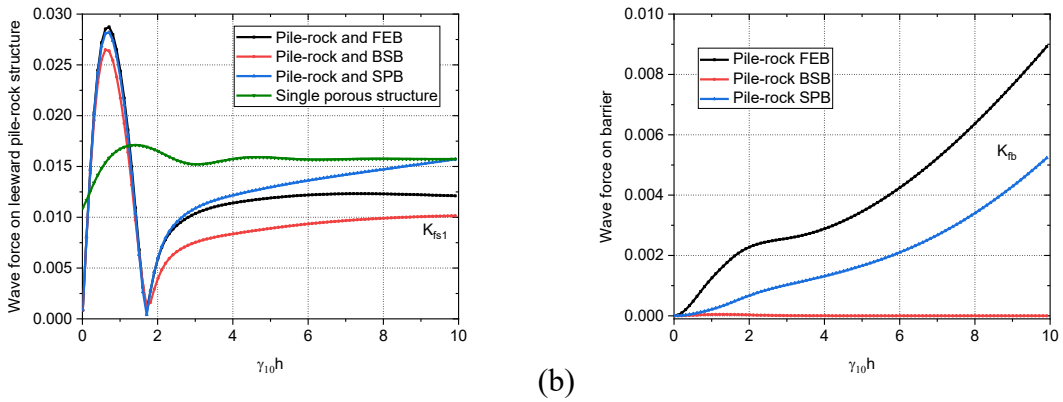

(a) (b)

Fig. 2.19: Variation of (a) K_{fs_1} (b) K_{fb} versus $\gamma_{10}h$ for different configuration of barrier considering $d/h = 1.0$, $h_1/h = 0.5$, $f_b = f_s = 0.5$, $\theta = 15^0$, $\varepsilon_1 = 0.3$, $\varepsilon_2 = 0.1$, $\varepsilon_b = 0.4$ and $\varepsilon_s = 0.6$.

Over the range $1.8 \le \gamma_{10}h \le 8.0$, the single porous structure exhibits higher wave force at front side which is followed by the surface-piercing barrier configuration, the fully-extended barrier and finally the bottom-standing barrier. At $\gamma_{10}h = 1.7$ about 37% higher wave force is exhibited by single porous structure when compared with all other cases of vertical barrier with pile-rock porous structure. The K_{fb} (Fig. 2.19b) is found to increase with increasing dimensionless wave number for fully-extended and bottom-standing barriers but has a negligible value for surface-

piercing barrier. The K_{fb} value is observed around 89% less when compared with fully-extended barrier at $\gamma_{10}h = 10$.

2.5.6 Comparative study for different barrier configurations with porous structure

The comparative study for the wave interaction with the porous structure combined with barrier of three different configurations is performed for various gap between the structure and barrier, width of the structure and angle of incidence. The wave reflection and dissipation coefficient for the three different configurations of the composite breakwater is compared and analysed to understand the effectiveness and importance of the composite breakwater.

In Fig. 2.20(a,b), the wave transformation caused by porous structure in combination with vertical barriers of different configurations is investigated, and a comparative study is conducted for different width of the porous structure. The wave reflection coefficient (Fig. 2.20a) is observed to have oscillatory pattern with the increase in $\gamma_{10}h$ for the case of fully-extended and surface-piercing barrier configurations whereas for bottom-standing barrier combined with porous structure the reflection coefficient remains constant for $\gamma_{10}h > 2$.

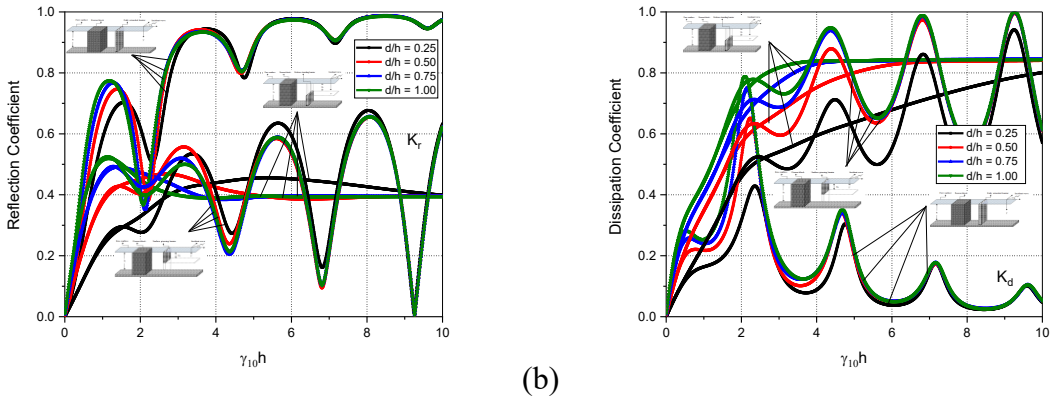

(a) (b)

Fig. 2.20: Variation of (a) K_r (b) K_d versus $\gamma_{10}h$ for different values of d/h considering $\theta = 30^0$, $\varepsilon_b = 0.4$, $\varepsilon_s = 0.4$ and $w/h = 1.5$.

Further, with the increase in the porous structure thickness, more wave reflection is observed and a sharp rise in wave reflection is observed for all the configurations within $0.01 < \gamma_{10}h < 1.5$. The fully-extended barrier configuration is found to reflect more waves, when compared with porous structures associated with bottom-standing and fully-extended barrier configurations. The porous block associated with surface-piercing barrier is observed to have lower values of

wave reflection within $9 < \gamma_{10} h < 10$, and the same structural configuration achieves nearly 100% wave energy damping (Fig. 2.20b) in the same range of $9 < \gamma_{10} h < 10$ for different porous structure thickness. In addition, the porous structure associated with surface-piercing and bottom-standing barrier is observed to reduce the wave reflection by 60% within $9 < \gamma_{10} h < 10$ range. The oscillatory trend in K_r and K_d for fully-extended and surface-piercing barrier could be due to waves being trapped in the gap between the barrier and the porous block. In Fig. 2.21(a,b), the wave reflection and energy damping are analysed for all the three different configurations in the case of various values of non-dimensional gap between the porous structure and barrier. The porous block associated with fully-extended barrier is observed to reflect more waves than other two structural configurations.

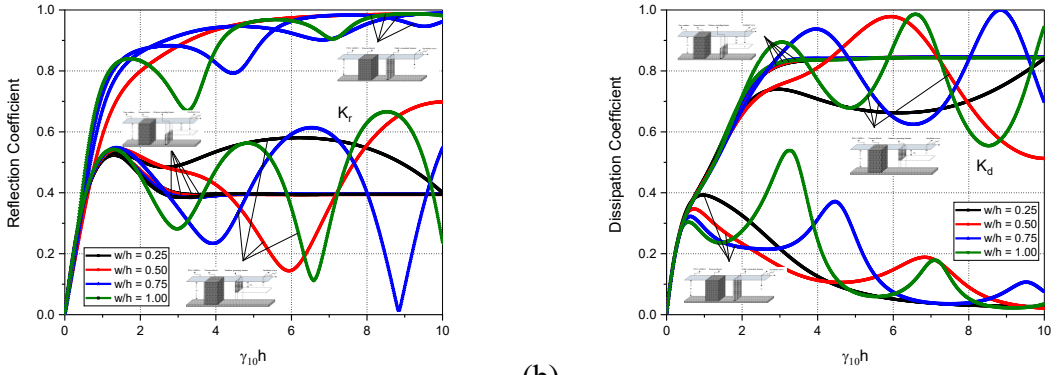

(a) (b)

Fig. 2.21: Variation of (a) K_r (b) K_d versus $\gamma_{10} h$ for different values of w/h considering $\theta = 30^0$, $\varepsilon_b = 0.4$, $\varepsilon_s = 0.4$ and $d/h = 1.0$.

In the case of porous block associated with fully-extended and surface-piercing barrier, the wave reflection coefficient (Fig. 2.21a) is observed to be increasing as the non-dimensional wave number increases whereas for the case of bottom-standing barrier, the K_r is observed to be increasing up to a particular value of $\gamma_{10} h$, and therefter it decreases and remains constant for all the values of w/h. All the configurations of porous structure are found to exhibit a sharp rise in K_d within $0.01 < \gamma_{10} h < 2.0$. In the case of the porous block associated with fully-extended barrier, the wave energy dissipation K_d (Fig. 2.21b) is observed to be decreasing with the increase of $\gamma_{10} h$ whereas the other two configurations exhibit an increasing trend. The porous block associated with surface-piercing barrier exhibits 100% wave energy damping for

the non-dimensional wave number within $9.0 < \gamma_{10} h < 10$. The K_r and K_d is noted to be having periodic maxima and minima with the increase of w/h. Further, as w/h increases, the chances of waves being trapped in confined spaces within the porous structure and barrier increases, which results in the oscillatory trend.

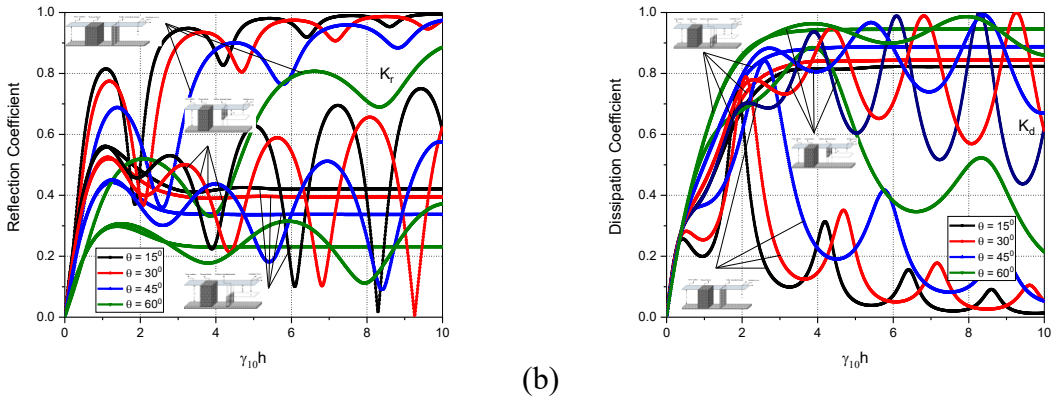

(a) (b)

Fig. 2.22: Variation of (a) K_r (b) K_d versus $\gamma_{10} h$ for different values of θ considering $\varepsilon_b = 0.4$, $\varepsilon_s = 0.4$, $w/h = 1.5$ and $d/h = 1.0$.

In Fig. 2.22(a,b), the comparative study of three different configurations of composite breakwater is presented for various values of incident wave angle θ. It is observed that, as the incident wave angle increases, the wave reflection is observed to get reduced. The porous block associated with fully-extended barrier is found to have maximum reflection when compared with other two configurations. In the case of all the three configurations, the wave reflection coefficient K_r is observed to exhibit a sharp rise within the range of $0.01 < \gamma_{10} h < 1.0$ and thereafter it starts to oscillate. The porous block associated with bottom-standing barrier is found have no oscillatory trend in wave reflection pattern whereas the other two configurations experiences oscillatory trend. The increase in incident wave angle causes reduction in the periodic crests and troughs of K_r and K_d and the porous block associated with surface-piercing barrier is found to exhibit higher wave energy damping and at an incident wave angle of $\theta = 30^0$ the wave energy damping is observed to achieve 100% within $9.0 < \gamma_{10} h < 10$.

2.6 CLOSURE

The wave transformation due to the pile-rock porous structure associated with a vertical permeable barriers of different configurations are examined using the eigenfunction expansion

method and orthogonal mode-coupling relation. The conclusions drawn from the study are as follows:

- The transmission coefficient K_t is noted minimum and the dissipation coefficient K_d is observed maximum for the porosity of the structure $\varepsilon_s = 0.8$, thus increased porosity can be considered as efficient in wave energy attenuation.

- The wave decay due to dimensionless structural width $d/h = 3.0$ is evident for optimal wave damping by pile-rock porous structure with barrier for all the cases of porosity within $0.2 \le \varepsilon_s \le 0.8$.

- The critical angle is noted within $64^0 < \theta < 82^0$, where the minimum reflection is observed with respect to change in the structural porosity $0.2 \le \varepsilon_s \le 0.8$ for fully-extended barrier.

- In case of surface-piercing barrier, around 85% damping and minimum reflection is observed for dimensionless wave number $\gamma_{10}h = 1.0$ on varying the dimensionless structural width.

- In the case of bottom-standing barrier, $f_s = 0.25$ shows minimum reflection and maximum damping of about 95% and thus could be effective for wave attenuation and the critical angle is observed at $\theta = 74^0$ while varying angle of incidence.

- In the case of surface-piercing barrier, it is observed that $\gamma_{10}h = 1.5$ shows minimum K_t and maximum K_d of around 80% and thus could be adopted for better wave attenuation. Also, the wave force on the barrier K_{fb} has lesser magnitude when compared with values of K_{fs_1} and K_{fs_2}.

- The critical angle is observed to be moving towards the left side with increase in $\gamma_{10}h$ and is observed within $70^0 < \theta < 78^0$ for surface-piercing barriers.

- A considerable variation in the amplitude of K_r with larger magnitudes and sharper crest and trough is noted when compared with other cases of periodic values of L/h in the case of fully-extended barrier.

- Higher wave damping is evident for pile-rock porous structure with barrier when compared with that of single porous structure, 35% for surface-piercing and bottom-standing barriers and 30.5% for fully-extended barriers at normal angle of incidence.

CHAPTER 3

WAVE TRANSFORMATION DUE TO ARRAYS OF POROUS STRUCTURE AND BARRIER

3.1 GENERAL INTRODUCTION

The wave scattering due to multiple submerged porous structures associated with porous barriers is analysed based on the small amplitude wave theory. The eigenfunction expansion method is used to ascertain the characteristics of wave transformation caused by the presence of multiple submerged vertical barriers and porous structures while considering the continuity of velocity and pressure at the interfaces of vertical barriers and porous structures. Different combinations of submerged porous structure and barriers are considered for the study. The multiple barriers and porous structure considered in the study are (a) alternate barrier and porous structure, (b) barrier placed within porous structure and (c) porous structure placed within barriers. The orthogonal mode coupling relation is used to determine the hydrodynamic coefficients, such as coefficients of reflection, transmission, and energy dissipation. The porosity of the submerged structure is incorporated using a complex number known as the complex porous effect parameter. The hydrodynamic coefficients are studied for various parameters such as angle of incidence, non-dimensional wave number, the gap between the barrier and porous structure, and non-dimensional structural width. The wave forces on the porous structure and barrier are discussed in detail.

3.2 MATHEMATICAL FORMULATION

The oblique wave scattering due to the porous breakwater system, a combination of multiple porous structures, and different types of porous thin barriers such as fully-extended, surface-piercing, and bottom-standing barriers is analysed mathematically. The porous breakwater is assumed to be submerged in a fluid having depth h. The oblique wave is considered to be propagating in the x-direction. The flow is considered to be harmonic with an angular frequency ω. The velocity potentials in each region are given by the relationship $\phi_j(x,y,z,t) = \mathrm{Re}\left[\phi_j(x,y)\,\mathrm{e}^{\mathrm{i}(lz-\omega t)}\right]$, where l is the wave number in z-direction and is given by $l = \gamma_{10}\sin\theta$ and γ_{10} denotes the open water progressive wave number. The configuration for

alternate barrier and porous structure is having open water region at $j = 1,2,4,5,7$ and porous structure region at $j = 3,6$ whereas the configuration for barrier placed within porous structure the open water region is at $j = 1,3,4,5,7$ and porous structure region at $j = 2,6.$ In addition the configuration for porous structure placed within barriers the open water region is at $j = 1,2,4,6,7$ and porous structure region at $j = 3,5.$ Thus in all the configurations, in both open water region and the porous regions, the velocity potential satisfy the Helmholtz equation given by

$$\frac{\partial^2 \phi_j}{\partial x^2} + \frac{\partial^2 \phi_j}{\partial y^2} - l^2 \phi_j = 0, \text{ for } -\infty < x < \infty, 0 < y < h. \tag{3.1}$$

In the case of the open water region and the porous region, the linearized free surface boundary condition is of the form

$$\frac{\partial \phi_j}{\partial y} + K_j \phi_j = 0, \quad \text{on} \quad y = 0, \tag{3.2}$$

In the case of open water region, $K_j = \frac{\omega^2}{g}$; for porous structure region, $K_j = \frac{\omega^2}{g}\left(s_b + if_b\right)$, where s_b denotes the reactance offered by the porous structure and f_b denotes the resistance provided by the porous structure, g is the acceleration due to gravity and $i = \sqrt{-1}$ denotes the imaginary number.

The seabed is assumed to be impermeable, and the bottom boundary condition for the impermeable seabed is given by

$$\frac{\partial \phi_j}{\partial y} = 0, \quad \text{on} \quad y = h. \tag{3.3}$$

The three different cases such as the combinations of porous structures associated with the fully-extended barrier, bottom-standing barrier, and surface-piercing barrier are considered for the study. The continuity of the velocity and pressure is assumed for all the different barrier configurations.

3.2.1 Multiple fully-extended barrier and porous structure

The multiple fully-extended barrier is assumed to be extending from $0 < y < h.$ At the interface of the fully-extended barrier, the continuity of velocity and pressure is satisfied. The three configurations of the multiple porous structure and barrier considered in the study are (i) alternate fully-extended barrier and porous structure (PS-FEB-1), (ii) barrier placed within

porous structure (PS-FEB-2) and (iii) porous structure placed within barriers (PS-FEB-3). The schematic representation of the three multiple fully-extended barrier and porous structure is presented in Fig. 3.1(a-c).

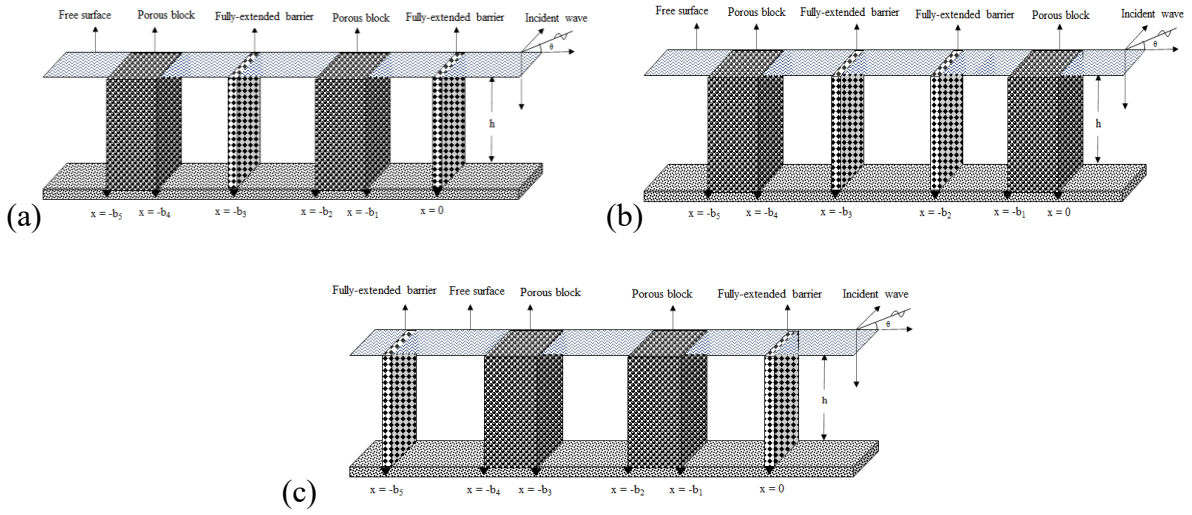

Fig. 3.1: Schematic diagram of (a) PS-FEB-1, (b) PS-FEB-2 and (c) PS-FEB-3 configurations

3.2.1.1 PS-FEB-1 configuration

In the case of PS-FEB-1 configuration (Fig. 3.1a), the fully-extended barrier is placed at the water depth $0 < y < h$ at $x = 0, -b_3$. So, the continuity of the velocity and pressure for the fully-extended barrier interface is given by

$$\frac{\partial \phi_j(x,y)}{\partial x} = -i\gamma_{10} G_b \left[\phi_{j+1}(x,y) - \phi_j(x,y)\right], \text{ on } x = 0,\ j = 1 \text{ and } x = -b_3, j = 4, \quad (3.4a)$$

$$\frac{\partial \phi_j(x,y)}{\partial x} = \frac{\partial \phi_{j+1}(x,y)}{\partial x}, \text{ on } x = 0,\ j = 1 \text{ and } x = -b_3, j = 4, \quad (3.4b)$$

where $G_b = \dfrac{\varepsilon_b}{\gamma_{10} d_b (f_b - i s_b)}$, d_b is the barrier thickness, f_b is the resistance of the barrier, S_b is the reactance coefficient of the barrier, and ε_b is the porosity of the barrier.

The wave propagating due to the presence of the porous structure suggests the continuity of fluid pressure and velocity across the seaward and leeward structural interfaces. So, the matching condition at each of the structural interfaces are given by

$$\frac{\partial \phi_j(x,y)}{\partial x} = \varepsilon_S \frac{\partial \phi_{j+1}(x,y)}{\partial x} \text{ and } \phi_j(x,y) = (s_S + i f_S)\phi_{j+1}(x,y) \quad (3.5a)$$

$$\text{at } x = -b_1, j = 2 \text{ and } x = -b_4, j = 5,$$

$$\frac{\partial \phi_{j+1}(x,y)}{\partial x} = \varepsilon_S \frac{\partial \phi_j(x,y)}{\partial x} \text{ and } \phi_{j+1}(x,y) = (s_S + if_S)\phi_j(x,y) \quad \text{at } x = -b_2, j = 3 \text{ and } x = -b_5, j = 6, \tag{3.5b}$$

where ε_s is the porosity of the structure.

3.2.1.2 PS-FEB-2 configuration

In the case of PS-FEB-2 configuration (Fig. 3.1b), the fully-extended barrier is placed at the water depth $0 < y < h$ at $x = -b_2, -b_3$. So, the continuity of the velocity and pressure for the fully-extended barrier interface is given by

$$\frac{\partial \phi_j(x,y)}{\partial x} = -i\gamma_{10} G_b \left[\phi_{j+1}(x,y) - \phi_j(x,y)\right], \text{ on } x = -b_2, j = 3 \text{ and } x = -b_3, j = 4, \tag{3.6a}$$

$$\frac{\partial \phi_j(x,y)}{\partial x} = \frac{\partial \phi_{j+1}(x,y)}{\partial x}, \text{ on } x = -b_2, j = 3 \text{ and } x = -b_3, j = 4, \tag{3.6b}$$

The wave propagating due to the presence of the porous structure suggests the continuity of fluid pressure and velocity across the seaward and leeward structural interfaces. So, the matching condition at each of the structural interfaces are given by

$$\frac{\partial \phi_j(x,y)}{\partial x} = \varepsilon_S \frac{\partial \phi_{j+1}(x,y)}{\partial x} \text{ and } \phi_j(x,y) = (s_S + if_S)\phi_{j+1}(x,y) \quad \text{at } x = 0, j = 1 \text{ and } x = -b_4, j = 5, \tag{3.7a}$$

$$\frac{\partial \phi_{j+1}(x,y)}{\partial x} = \varepsilon_S \frac{\partial \phi_j(x,y)}{\partial x} \text{ and } \phi_{j+1}(x,y) = (s_S + if_S)\phi_j(x,y) \quad \text{at } x = -b_1, j = 2 \text{ and } x = -b_5, j = 6, \tag{3.7b}$$

3.2.1.3 PS-FEB-3 configuration

In the case of PS-FEB-3 configuration (Fig. 3.1c), the fully-extended barrier is placed at the water depth $0 < y < h$ at $x = 0, -b_5$. So, the continuity of the velocity and pressure for the fully-extended barrier interface is given by

$$\frac{\partial \phi_j(x,y)}{\partial x} = -i\gamma_{10} G_b \left[\phi_{j+1}(x,y) - \phi_j(x,y)\right], \text{ on } x = 0, j = 1 \text{ and } x = -b_5, j = 6, \tag{3.8a}$$

$$\frac{\partial \phi_j(x,y)}{\partial x} = \frac{\partial \phi_{j+1}(x,y)}{\partial x}, \text{ on } x = 0, j = 1 \text{ and } x = -b_5, j = 6, \tag{3.8b}$$

The wave propagating due to the presence of the porous structure suggests that the continuity of fluid pressure and velocity across the seaward and leeward structural interfaces are present.

So, the matching condition at each of the structural interfaces of the porous structure are given by

$$\frac{\partial \phi_j(x,y)}{\partial x} = \varepsilon_S \frac{\partial \phi_{j+1}(x,y)}{\partial x} \quad \text{and} \quad \phi_j(x,y) = (s_S + if_S)\phi_{j+1}(x,y) \quad \text{at } x = -b_1, j = 2 \text{ and } x = -b_3, j = 4, \tag{3.9a}$$

$$\frac{\partial \phi_{j+1}(x,y)}{\partial x} = \varepsilon_S \frac{\partial \phi_j(x,y)}{\partial x} \quad \text{and} \quad \phi_{j+1}(x,y) = (s_S + if_S)\phi_j(x,y) \quad \text{at } x = -b_2, j = 3 \text{ and } x = -b_4, j = 5, \tag{3.9b}$$

3.2.2 Multiple bottom-standing barrier and porous structure

The multiple bottom-standing barrier is assumed to be extending from $h_1 < y < h$. At the interface of the bottom-standing barrier, the continuity of velocity and pressure is satisfied. The three configurations of the multiple porous structure and bottom-standing barrier considered in the study are (i) alternate bottom-standing barrier and porous structure (PS-BSB-1), (ii) bottom-standing barrier placed within porous structure (PS-BSB-2) and (iii) porous structure placed within bottom-standing barriers (PS-BSB-3). The schematic representation of the three multiple bottom-standing barrier and porous structure is presented in Fig. 3.2(a-c).

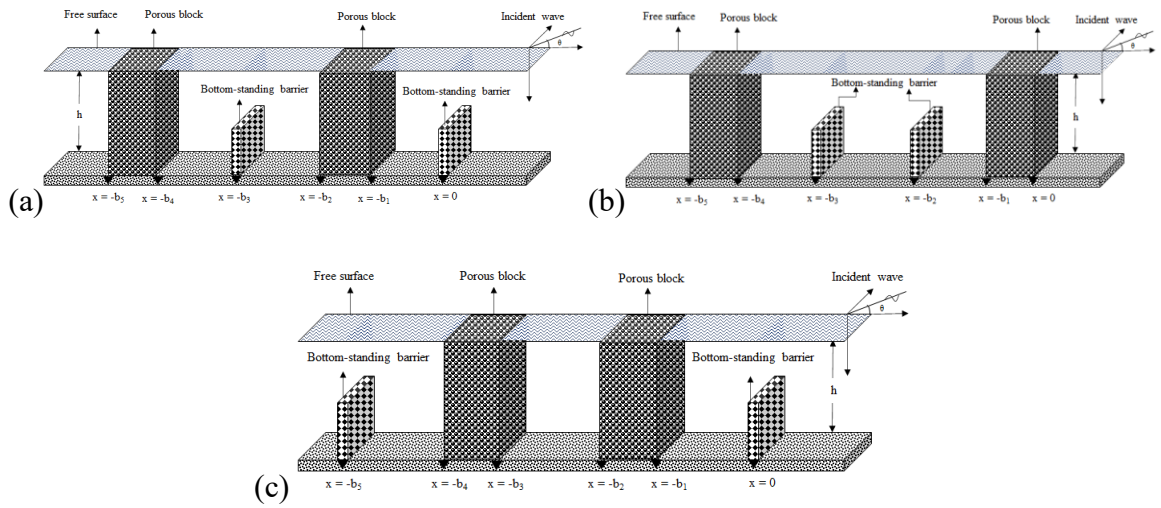

Fig. 3.2: Schematic diagram of (a) PS-BSB-1, (b) PS-BSB-2 and (c) PS-BSB-3 configurations

3.2.2.1 PS-BSB-1 configuration

In the case of PS-BSB-1 configuration (Fig. 3.2a), the bottom-standing barrier is placed at the water depth $h_1 < y < h$ at $x = 0, -b_3$. So, the continuity of the velocity and pressure for the bottom-standing barrier interface is given by

$$\frac{\partial \phi_j(x,y)}{\partial x} = -i\gamma_{10} G_b \left[\phi_{j+1}(x,y) - \phi_j(x,y)\right], \text{ on } x=0,\ j=1 \text{ and } x=-b_3, j=4,\ h_1 < y < h, \tag{3.10a}$$

$$\phi_j(x,y) = \phi_{j+1}(x,y) \text{ and } \frac{\partial \phi_j(x,y)}{\partial x} = \frac{\partial \phi_{j+1}(x,y)}{\partial x}, \quad \text{on } x=0,\ j=1 \text{ and } x=-b_3, j=4,\ 0 < y < h_1, \tag{3.10b}$$

The matching condition at each of the structural interfaces $x=-b_1,-b_2,-b_4,-b_5$ of the porous structure satisfies the boundary condition as in Eq. 3.5(a,b).

3.2.2.2 PS-BSB-2 Configuration

In the case of PS-BSB-2 configuration (Fig. 3.2b), the bottom-standing barrier is placed at the water depth $h_1 < y < h$ at $x=-b_2,-b_3$. So, the continuity of the velocity and pressure for the bottom-standing barrier interface is given by

$$\frac{\partial \phi_j(x,y)}{\partial x} = -i\gamma_{10} G_b \left[\phi_{j+1}(x,y) - \phi_j(x,y)\right], \text{on } x=-b_2,\ j=3 \text{ and } x=-b_3, j=4,\ h_1 < y < h, \tag{3.11a}$$

$$\phi_j(x,y) = \phi_{j+1}(x,y) \text{ and } \frac{\partial \phi_j(x,y)}{\partial x} = \frac{\partial \phi_{j+1}(x,y)}{\partial x}, \quad \text{on } x=-b_2,\ j=3 \text{ and } x=-b_3, j=4, 0 < y < h_1, \tag{3.11b}$$

The matching condition at each of the structural interfaces $x=0,-b_1,-b_4,-b_5$ of the porous structure satisfies the boundary condition as in Eq. 3.7(a,b).

3.2.2.3 PS-BSB-3 Configuration

In the case of PS-BSB-3 configuration (Fig. 3.2c), the bottom-standing barrier is placed at the water depth $h_1 < y < h$ at $x=0,-b_5$. So, the continuity of the velocity and pressure for the bottom-standing barrier interface is given by

$$\frac{\partial \phi_j(x,y)}{\partial x} = -i\gamma_{10} G_b \left[\phi_{j+1}(x,y) - \phi_j(x,y)\right], \text{ on } x=0,\ j=1 \text{ and } x=-b_5, j=6, h_1 < y < h, \tag{3.12a}$$

$$\phi_j(x,y) = \phi_{j+1}(x,y) \text{ and } \frac{\partial \phi_j(x,y)}{\partial x} = \frac{\partial \phi_{j+1}(x,y)}{\partial x}, \quad \text{on } x=0,\ j=1 \text{ and } x=-b_5, j=6,\ 0 < y < h_1, \tag{3.12b}$$

The matching condition at each of the structural interfaces $x=-b_1,-b_2,-b_3,-b_4$ of the porous structure satisfies the boundary condition as in Eq. 3.9(a,b).

3.2.3 Multiple surface-piercing barrier and porous Structure

The multiple surface-piercing barrier is assumed to be extending from $0<y<h_1$. At the interface of the surface-piercing barrier, the continuity of velocity and pressure is satisfied. The three configurations of the multiple porous structure and surface-piercing barrier considered in the study are (i) alternate surface-piercing barrier and porous structure (PS-SPB-1), (ii) surface-piercing barrier placed within porous structure (PS-SPB-2) and (iii) porous structure placed within surface-piercing barriers (PS-SPB-3). The schematic representation of the three multiple surface-piercing barrier and porous structure is presented in Fig. 3.3(a-c).

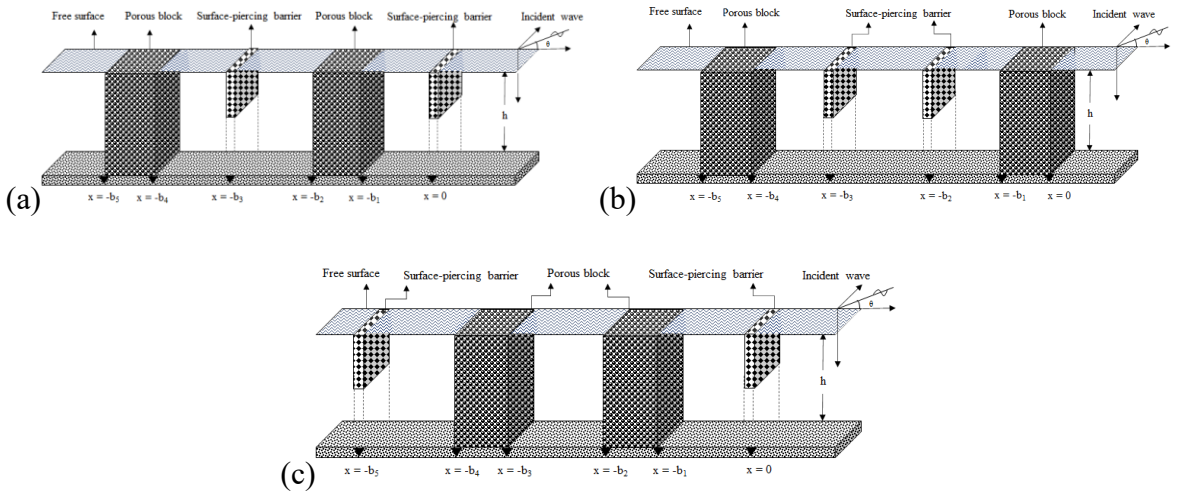

Fig. 3.3: Schematic diagram of (a) PS-SPB-1, (b) PS-SPB-2 and (c) PS-SPB-3 configurations

3.2.3.1 PS-SPB-1 configuration

In the case of PS-SPB-1 configuration (Fig. 3.3a), the surface-piercing barrier is placed at the water depth $0<y<h_1$ at $x=0,-b_3$. So, the continuity of the velocity and pressure for the surface-piercing barrier interface is given by

$$\frac{\partial\phi_j(x,y)}{\partial x}=-i\gamma_{10}G_b\left[\phi_{j+1}(x,y)-\phi_j(x,y)\right],\ \text{on}\ x=0,\ j=1\ \text{and}\ x=-b_3, j=4,\ 0<y<h_1, \tag{3.13a}$$

$$\phi_j(x,y)=\phi_{j+1}(x,y)\ \text{and}\ \frac{\partial\phi_j(x,y)}{\partial x}=\frac{\partial\phi_{j+1}(x,y)}{\partial x},\quad \text{on}\ x=0,\ j=1\ \text{and}\ x=-b_3, j=4,\ h_1<y<h, \tag{3.13b}$$

The matching condition at each of the structural interfaces $x=-b_1,-b_2,-b_4,-b_5$ of the porous structure satisfies the boundary condition as in Eq. 3.5(a,b).

3.2.3.2 PS-SPB-2 configuration

In the case of PS-SPB-2 configuration (Fig. 3.3b), the surface-piercing barrier is placed at the water depth $0<y<h_1$ at $x=-b_2,-b_3$. So, the continuity of the velocity and pressure for the surface-piercing barrier interface is given by

$$\frac{\partial\phi_j(x,y)}{\partial x}=-i\gamma_{10}G_b\left[\phi_{j+1}(x,y)-\phi_j(x,y)\right],\text{on } x=-b_2,\ j=3 \text{ and } x=-b_3,j=4,\ 0<y<h_1, \tag{3.14a}$$

$$\phi_j(x,y)=\phi_{j+1}(x,y) \text{ and } \frac{\partial\phi_j(x,y)}{\partial x}=\frac{\partial\phi_{j+1}(x,y)}{\partial x}, \quad \text{on } x=-b_2,\ j=3 \text{ and } x=-b_3,j=4,h_1<y<h, \tag{3.14b}$$

The matching condition at each of the structural interface $x=0,-b_1,-b_4,-b_5$ of the porous structure satisfies the boundary condition as in Eq. 3.7(a,b).

3.2.3.3 PS-SPB-3 configuration

In the case of PS-SPB-3 configuration, the surface-piercing barrier is placed at the water depth $0<y<h_1$ at $x=0,-b_5$. So, the continuity of the velocity and pressure for the surface-piercing barrier interface is given by

$$\frac{\partial\phi_j(x,y)}{\partial x}=-i\gamma_{10}G_b\left[\phi_{j+1}(x,y)-\phi_j(x,y)\right],\ \text{on } x=0,\ j=1 \text{ and } x=-b_5,j=6,0<y<h_1, \tag{3.15a}$$

$$\phi_j(x,y)=\phi_{j+1}(x,y) \text{ and } \frac{\partial\phi_j(x,y)}{\partial x}=\frac{\partial\phi_{j+1}(x,y)}{\partial x}, \quad \text{on } x=0,\ j=1 \text{ and } x=-b_5,j=6,\ h_1<y<h, \tag{3.15b}$$

The matching condition at each of the structural interface $x=-b_1,-b_2,-b_3,-b_4$ of the porous structure satisfies the boundary condition as in Eq. 3.9(a,b).

The wave number in upstream/downstream free-water region γ_{j0} for alternate barrier and porous structure at $j=1,2,4,5,7$, γ_{j0} for barrier placed within porous structure the open water region at $j=1,3,4,5,7$ and γ_{j0} for porous structure placed within barriers the open water region at $j=1,2,4,6,7$ satisfies the dispersion relation for finite water depth given by

$$\omega^2 = \begin{cases} g\gamma_{j0}\tanh\gamma_{j0}h & \text{for} \quad n=0 \\ -g\gamma_{jn}\tan\gamma_{jn}h & \text{for} \quad n=1,2,.... \end{cases} \tag{3.16a}$$

The wave number in porous structure region γ_{jn} for alternate barrier and porous structure at $j=3,6$, γ_{jn} for barrier placed within porous structure the open water region at $j=2,6.$ and γ_{jn} for porous structure placed within barriers the open water region at $j=3,5.$ satisfies the dispersion relation given by

$$\omega^2(s_s+if_s) = g\gamma_{jn}\tanh\gamma_{jn}h \quad \text{for} \quad n=0,1,2,.... \tag{3.16b}$$

where, ω is the wave frequency and g is the acceleration due to gravity. In the far-field region, the radiation conditions in the presence of porous structure with barrier is given by

$$\phi_j(x,y) = \begin{cases} \left(I_{10}e^{-i\gamma_{10}x} + R_{10}e^{i\gamma_{10}x}\right) f_{10}(y) & \text{as} \quad x \to \infty, \\ \left(T_{70}e^{-i\gamma_{70}x}\right) f_{70}(y) & \text{as} \quad x \to -\infty, \end{cases} \tag{3.17}$$

where, I_{10}, R_{10} and T_{40} are the complex amplitude of the incident, reflected, and transmitted wave energies respectively. However, the incident wave I_{10} is considered to be unity.

3.3 METHOD OF SOLUTION

The multiple porous structures associated with multiple barrier are analysed using the eigenfunction method. The velocity potentials for each of the regions are given

$$\phi_1(x,y) = \left(I_{10}e^{-ik_{10}x} + R_{10}e^{ik_{10}x}\right) f_{10}(y) + \sum_{n=1}^{\infty} R_{1n}e^{-\kappa_{1n}x} f_{1n}(y), \quad \text{for} \quad 0 < x < \infty, \tag{3.18a}$$

$$\phi_2(x,y) = \sum_{n=0}^{\infty}\left(A_{2n}e^{-ik_{2n}x} + B_{2n}e^{ik_{2n}(x+b_1)}\right) f_{2n}(y), \text{ for } -b_1 < x < 0, \tag{3.18b}$$

$$\phi_3(x,y) = \sum_{n=0}^{\infty}\left(A_{3n}e^{-ik_{3n}(x+b_1)} + B_{3n}e^{ik_{3n}(x+b_2)}\right) f_{3n}(y) \quad \text{for} \quad -b_2 < x < -b_1, \tag{3.18c}$$

$$\phi_4(x,y) = \sum_{n=0}^{\infty}\left(A_{4n}e^{-ik_{4n}(x+b_2)} + B_{4n}e^{ik_{4n}(x+b_3)}\right) f_{4n}(y), \quad \text{for} \quad -b_3 < x < -b_2, \tag{3.18d}$$

$$\phi_5(x,y) = \sum_{n=0}^{\infty}\left(A_{5n}e^{-ik_{5n}(x+b_3)} + B_{5n}e^{ik_{5n}(x+b_4)}\right) f_{5n}(y), \text{ for } -b_4 < x < -b_3, \tag{3.18e}$$

$$\phi_6(x,y) = \sum_{n=0}^{\infty}\left(A_{6n}e^{-ik_{6n}(x+b_4)} + B_{6n}e^{ik_{6n}(x+b_5)}\right) f_{6n}(y), \text{ for } -b_5 < x < -b_4, \tag{3.18f}$$

$$\phi_7(x,y) = T_{70}e^{-ik_{70}(x+b_5)} f_{70}(y) + \sum_{n=1}^{\infty} T_{7n}e^{\kappa_{7n}(x+b_5)} f_{7n}(y), \quad \text{for} \quad -\infty < x < -b_5, \tag{3.18g}$$

where, I_{10} is the incident wave, R_{1n}, A_{jn}, B_{jn} and T_{4n} for $n = 0,1,2,3,...$ and $j = 1,2,....6$ are the unknown constants to be determined. The vertical eigenfunctions $f_{jn}(y)$ for the open water and porous structure regions are given by

$$f_{jn}(y) = \frac{\cosh \gamma_{jn}(h-y)}{\cosh \gamma_{jn} h} \text{ for } n = 0,1,2,..... \tag{3.19}$$

where γ_{jn} are the eigenvalues satisfy the open water and porous structure dispersion relations given by

$$\omega^2 = g\gamma_{jn} \tanh \gamma_{jn} h \quad \text{for } n = 0, \tag{3.20a}$$

$$\omega^2 (S_s + if_s) = g\gamma_{jn} \tanh \gamma_{jn} h \quad \text{for } n = 0,1,2,... \tag{3.20b}$$

with $\gamma_{jn} = i\gamma_{jn}$ for $n = 1,2,3,...$ for open water regions. The roots of the dispersion relation for each region satisfy $\gamma_{jn}^2 = k_{jn}^2 + l^2$, $n = 0$ with $l = \gamma_{10} \sin\theta$, θ is the angle of incidence, k_{jn} being the component of wave number in $x-$direction and γ_{jn} is the wave number in $y-$direction. In addition, there are purely imaginary roots γ_{jn} with $\gamma_{jn}^2 = \kappa_{jn}^2 - l^2$ for $n = 1,2,3,....$ The eigenfunctions $f_{jn}(y), j = 1,2,3,4$ satisfy the orthogonality relation of the form

$$\langle f_{jn}, f_{jm} \rangle = \begin{cases} 0 & \text{for } m \neq n, \\ C_n' & \text{for } m = n, \end{cases} \text{ and } \langle f_{jn}, f_{jm} \rangle = \begin{cases} 0 & \text{for } m \neq n, \\ C_n'' & \text{for } m = n, \end{cases} \tag{3.21}$$

with respect to the orthogonal mode-coupling relation defined by

$$\langle f_{jm}, f_{jn} \rangle = \int_0^h f_{jm}(y) f_{jn}(y) dy, \tag{3.22}$$

where $C_n' = \left\{ \frac{2\gamma_{jn} h + \sinh 2\gamma_{jn} h}{4\gamma_{jn} \cosh^2 \gamma_{jn} h} \right\}$ and $C_n'' = \left\{ \frac{2\gamma_{jn} h + \sinh 2\gamma_{jn} h}{4\gamma_{jn} \cosh^2 \gamma_{jn} h} \right\}$. (3.23)

with C_n' for $n = 1,2,3,....$ are obtained by substituting $\gamma_{jn} = i\gamma_{jn}$ in the case of the open water region. In the porous structure region, the mode-coupling relation (3.22) is employed on velocity potential $\phi_j(x,y)$ and $\phi_{jx}(x,y)$ with the eigenfunction $f_{jm}(y)$ along with continuity of pressure and velocity as in Eq. 3.5(a) across the vertical interface to obtain

$$\begin{aligned} \langle \phi_j(x,y), f_{jm}(y) \rangle &= \int_0^h \phi_j(x,y) f_{jm}(y) dy \\ &= \int_0^h (S_s + if_s) \phi_{j+1}(x,y) f_{jm}(y) dy \quad \text{for } m = 0,1,2,... \end{aligned} \tag{3.24}$$

$$\left\langle \phi_{jx}(x,y), f_{jm}(y) \right\rangle = \int_0^h \phi_{jx}(x,y) f_{jm}(y)\,dy = \varepsilon_s \int_0^h \phi_{(j+1)x}(x,y) f_{jm}(y)\,dy \text{ for } m = 0,1,2,.... \quad (3.25)$$

Again, the mode-coupling relation (3.22) is employed on velocity potential $\phi_j(x,y)$ and $\phi_{jx}(x,y)$ with the eigenfunction $f_{jm}(y)$ along with continuity of pressure and velocity as in Eq. 3.5(b) across the vertical interface to obtain

$$\begin{aligned} \left\langle \phi_{j+1}(x,y), f_{(j+1)m}(y) \right\rangle &= \int_0^h \phi_{j+1}(x,y) f_{(j+1)m}(y)\,dy \\ &= \int_0^h (S_s + if_s)\phi_j(x,y) f_{(j+1)m}(y)\,dy \quad \text{for } m = 0,1,2,... \end{aligned} \quad (3.26)$$

$$\left\langle \phi_{(j+1)x}(x,y), f_{(j+1)m}(y) \right\rangle = \int_0^h \phi_{(j+1)x}(x,y) f_{(j+1)m}(y)\,dy = \varepsilon_s \int_0^h \phi_{jx}(x,y) f_{(j+1)m}(y)\,dy \quad \text{for } m = 0,1,2,.... \quad (3.27)$$

The method of solution for the multiple fully-extended barrier, bottom-standing barrier, and surface-piercing barrier configuration is presented in subsections.

3.3.1 Multiple porous structure with fully-extended barrier

In order to determine the unknown coefficients, the mode-coupling relation (Eq. 3.22) is employed on the velocity potential $\phi_j(x,y)$ and $\phi_{jx}(x,y)$ with the eigenfunction $f_{jm}(y)$ along with continuity of pressure and velocity as in Eq. 3.4(a,b) across the vertical interface $x = 0, 0 < y < h$ to obtain

$$\left\langle \phi_j(x,y), f_{jm}(y) \right\rangle = \int_0^h \phi_j(x,y) f_{jm}(y)\,dy = \int_0^h \left\{ \phi_{j+1}(x,y) + \left(\frac{1}{i\gamma_{10} G_b} \right) \phi_{jx}(x,y) \right\} f_{jm}(y)\,dy, \quad \text{for } m = 0,1,2,.... \quad (3.28)$$

$$\left\langle \phi_{jx}(x,y), f_{jm}(y) \right\rangle = \int_0^h \phi_{jx}(x,y) f_{jm}(y)\,dy = \int_0^h \phi_{(j+1)x}(x,y) f_{jm}(y)\,dy, \text{ for } m = 0,1,2,.... \quad (3.29)$$

The infinite sums presented in Eqs. (3.24) -(3.27) along with Eqs. (3.28) -(3.29) are truncated up to finite M terms to obtain a linear system of $12(M+1)$ algebraic equations for the determination of $12(M+1)$ unknowns and the wave reflection and transmission due to the porous structure obtained as

$$K_r = \left| \frac{R_{10}}{I_{10}} \right| \quad \text{and} \quad K_t = \left| \frac{T_{40}}{I_{10}} \right|. \quad (3.30a)$$

Due to the existence of porous blocks, the energy dissipation in the wave propagation through the porous blocks, as in Chwang and Chan (1998), is represented as

$$K_d = 1 - K_r^2 - K_t^2. \tag{3.30b}$$

The wave attenuation due to multiple porous structure with the bottom-standing barrier is examined in the next section.

3.3.2 Multiple porous structure with bottom-standing barrier

In order to find the unknown coefficients, the mode-coupling relation (Eq. 3.22) is employed on the velocity potential $\phi_j(x,y)$ and $\phi_{jx}(x,y)$ with the eigenfunction $f_{jm}(y)$ along with the continuity of pressure and velocity as in Eq. 3.10(a,b) across the vertical interface $x=0, 0<y<h$ to obtain

$$\begin{aligned}\left\langle \phi_j(x,y), f_{jm}(y)\right\rangle &= \int_0^h \phi_j(x,y) f_{jm}(y)\,dy = \left\{\int_0^{h_1} + \int_{h_1}^{h}\right\}\phi_j(x,y) f_{jm}(y)\,dy \\ &= \int_0^d \phi_{j+1}(x,y) f_{jm}(y)\,dy + \int_{h_1}^{h} \phi_j(x,y) f_{jm}(y)\,dy \\ &= \int_0^d \phi_{j+1}(x,y) f_{jm}(y)\,dy + \int_d^h \left\{\phi_{j+1}(x,y) + \left(\frac{1}{i\gamma_{10}G_b}\right)\phi_{jx}(x,y)\right\} f_{jm}(y)\,dy, \\ &\qquad\qquad \text{for } m = 0,1,2,...\end{aligned} \tag{3.31}$$

$$\left\langle \phi_{jx}(x,y), f_{jm}(y)\right\rangle = \int_0^h \phi_{jx}(x,y) f_{jm}(y)\,dy = \int_0^h \phi_{(j+1)x}(x,y) f_{jm}(y)\,dy, \text{ for } m = 0,1,2,.... \tag{3.32}$$

The infinite sums presented in Eqs. (3.24) -(3.27) along with Eqs. (3.31) -(3.32) are truncated up to finite M terms to obtain a linear system of $12(M+1)$ algebraic equations for the determination of $12(M+1)$ unknowns and the wave reflection and transmission due to the porous structure. The wave attenuation due to multiple porous structure with the surface-piercing barrier is examined in the next section.

3.3.3 Multiple porous structure with surface-piercing barrier

In order to find the unknown coefficients, the mode-coupling relation (Eq. 3.22) is employed on the velocity potential $\phi_j(x,y)$ and $\phi_{jx}(x,y)$ with the eigenfunction $f_{jm}(y)$ along with continuity of pressure and velocity as in Eq. 3.13(a,b) across the vertical interface $x=0, 0<y<h$ to obtain

$$\left\langle \phi_j(x,y), f_{jm}(y) \right\rangle = \int_0^h \phi_j(x,y) f_{jm}(y)\,dy = \left\{ \int_0^{h_1} + \int_{h_1}^{h} \right\} \phi_j(x,y) f_{jm}(y)\,dy$$

$$= \int_0^d \phi_j(x,y) f_{jm}(y)\,dy + \int_{h_1}^h \phi_{j+1}(x,y) f_{jm}(y)\,dy$$

$$= \int_0^{h_1} \left\{ \phi_{j+1}(x,y) + \left(\frac{1}{i\gamma_{10} G_b} \right) \phi_{jx}(x,y) \right\} f_{jm}(y)\,dy + \int_{h_1}^h \phi_{j+1}(x,y) f_{jm}(y)\,dy,$$

$$\text{for } m = 0,1,2,... \tag{3.33}$$

$$\left\langle \phi_{jx}(x,y), f_{jm}(y) \right\rangle = \int_0^h \phi_{jx}(x,y) f_{jm}(y)\,dy = \int_0^h \phi_{(j+1)x}(x,y) f_{jm}(y)\,dy, \text{ for } m = 0,1,2,.... \tag{3.34}$$

The infinite sums presented in the Eqs. (3.24)-(3.27) along with Eqs. (3.33)-(3.34) are truncated up to finite M terms to obtain a linear system of $12(M+1)$ algebraic equations for the determination of $12(M+1)$ unknowns and the wave reflection and transmission due to the porous structure.

3.4 RESULTS AND DISCUSSION

The wave interaction with multiple porous structures with the fully-extended, bottom-standing, and surface-piercing barriers is analysed considering three different configurations such as (i) alternate porous structure and barrier, (ii) barrier placed between porous structure and (iii) porous structure placed between barriers. The numerical results are obtained for the variation of the reflection, transmission, and wave energy dissipation coefficients to understand the effect of wave attenuation due to the multiple composite structures.

Table 3.1: Different configurations of multiple porous structure and vertical barrier

Multiple porous structures (PS) and fully-extended barrier (FEB)	Alternate PS and FEB (PS-FEB-1)	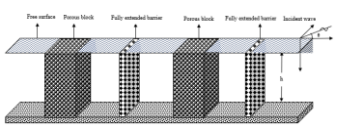
	FEB placed within PS (PS-FEB-2)	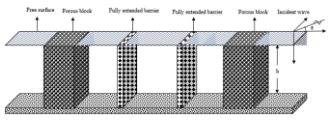

	PS placed within FEB (PS-FEB-3)	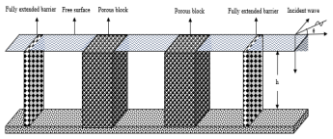
Multiple porous structures (PS) and bottom-standing barrier (BSB)	Alternate PS and BSB (PS-BSB-1)	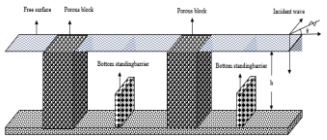
	BSB placed within PS (PS-BSB-2)	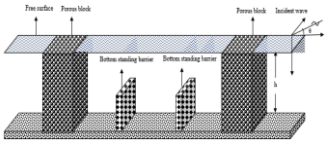
	PS placed within BSB (PS-BSB-3)	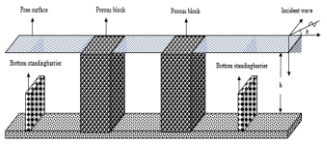
Multiple porous structures (PS) and surface-piercing barrier (SPB)	Alternate PS and SPB (PS-SPB-1)	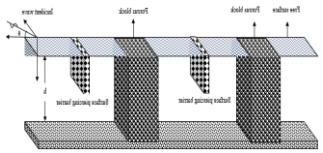
	SPB placed within PS (PS-SPB-2)	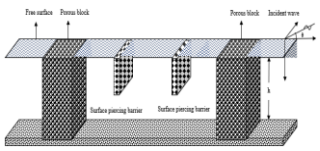
	PS placed within SPB (PS-SPB-3)	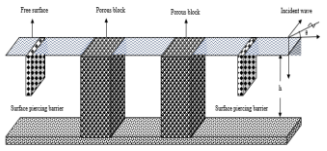

3.4.1 Validation of numerical results

The comparative study for the wave reflection and transmission coefficient for the wave interaction with porous structure as in Sollitt and Cross (1972) and Darlymple et al. (1991) is performed and validated (Venkateswarlu and Karmakar, 2020). The wave reflection K_r and transmission coefficient K_t are analysed and validated with the analytical results available in the literature for specific configuration. In Fig. 3.4(a), the K_r and K_t for a rectangular porous structure with finite thickness is compared with Sollitt and Cross (1972) and Sulisz (1985)

considering $\varepsilon_s = 0.4$ and $f = 0.5$. The present study shows a good agreement with Sollitt and Cross (1972). The wave reflection coefficient is observed to be increasing within $0.01 < \gamma_{10}h < 1.5$ and thereafter decreases. On the other hand, the transmission coefficient decreases with the increase in $\gamma_{10}h$.

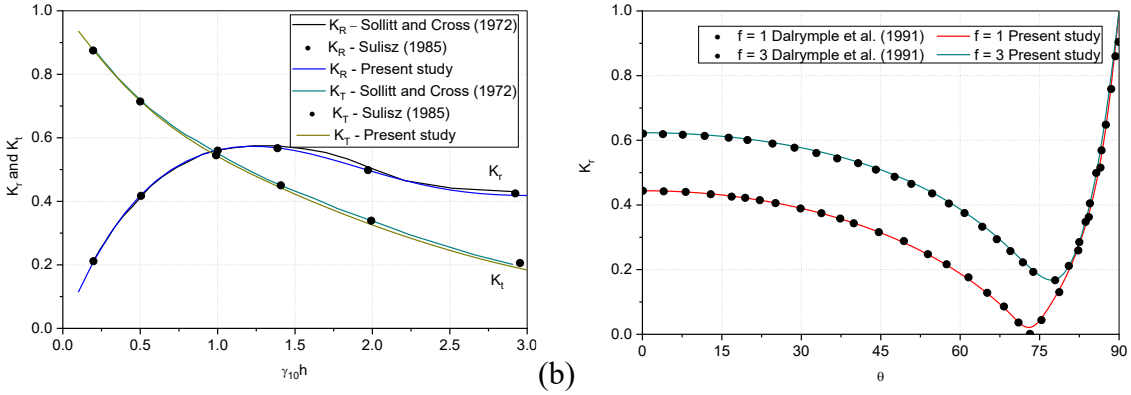

Fig. 3.4: Comparative study of (a) K_r and K_t versus $\gamma_{10}h$ due to porous structure with $\varepsilon_s = 0.4$ and $f = 0.5$ (Sollitt and Cross, 1972), (b) K_r due to porous structure with $d/h = 1$ and $\omega^2 h/g = 0.2012$ (Dalrymple et al., 1991).

In Fig. 3.4(b), the variation of K_r versus θ is obtained with the change in the friction factor varying within $1 \le f \le 3$ for rectangular porous structure as in Dalrymple et al. (1991). The numerical result is observed to converges with Dalrymple et al. (1991) and good agreement is achieved. The wave reflection is observed to be minimum for $65^0 < \theta < 80^0$ and then approaches to one as θ approaches to 90^0.

3.4.2 Alternate porous structure and barrier

The multiple porous structures associated with alternate porous barriers (PS-FEB-1, PS-BSB-1 and PS-SPB-1) are analysed due to the variation in wave reflection coefficient, transmission coefficient and wave energy dissipation coefficient by changing the porosity of porous block ε_2 within $0.2 < \varepsilon_2 < 0.8$, non-dimensional wave number $\gamma_{10}h$ within $0.5 < \gamma_{10}h < 1.5$ and the non-dimensional gap between porous block and barrier w/h within $0.25 < w/h < 1.0$.

3.4.2.1 Porous structure with fully-extended barrier (PS-FEB-1)

In Fig. 3.5(a,b), the variation of hydrodynamic coefficients K_r, K_t and K_d are plotted against non-dimensional wave number $\gamma_{10}h$. The reflection coefficient K_r (Fig. 3.5a) is observed to

exhibits a reduction of 73.42% when the gap between porous structure and barrier w/h varies within $0.25 < w/h < 1.0$, and the transmission coefficient is observed to increase with the increase in the gap between porous structure and barrier w/h. The increased variation attributes to the gap between porous structure and the barrier, wherein the waves are trapped resulting in decreased wave reflection coefficient. In Fig. 3.5(b), as the gap between porous structure and barrier w/h increases, an increasing trend of wave energy dissipation is observed. The increasing trend K_d could be due to the trapping of waves within the porous structure and barrier.

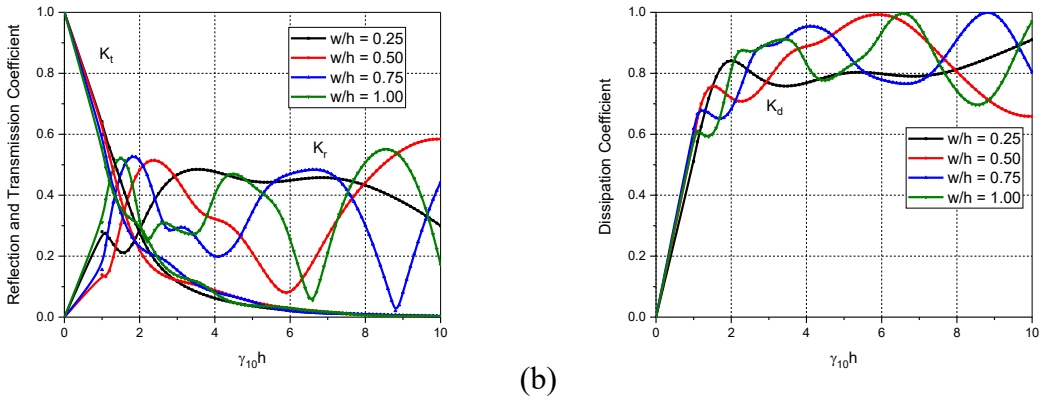

(a) (b)

Fig. 3.5: Variation of (a) K_r, K_t and (b) K_d versus $\gamma_{10}h$ for different values of gap between porous structure and barrier w/h considering $\varepsilon_1 = 0.5$, $\varepsilon_2 = 0.5$, $s_1 = s_2 = 1$, $f_1 = f_2 = 0.5$, $d/h = 0.5$ and $\theta = 30^0$.

In Fig. 3.6(a,b), the K_r, K_t and K_d versus d/L is plotted for various porosity ε_2 of the structure. The study found that the K_r decreases with the increase in ε_2, except for 80% porosity of porous block. In Fig.3.6(a), periodic maxima and minima is observed in K_r and for $2 < d/L < 3$, the higher values of K_r is achieved for all the porosity values, and 32% reduction in K_r is observed for $\varepsilon_2 = 0.8$ when compared to $\varepsilon_2 = 0.2$. Further, the K_t is found to be increasing with the increase in the porosity ε_2 of the structure. In Fig. 3.6(b), almost full wave energy dissipation is achieved by the structure with 60% porosity of the structure within $0.5 < d/L < 1.0$ and 40% porosity of block within $2.0 < d/L < 2.25$. As d/L increases, an increasing trend in wave reflection K_r, and wave energy dissipation K_d is observed which could be due to the effect of the increased surface area of the porous structure.

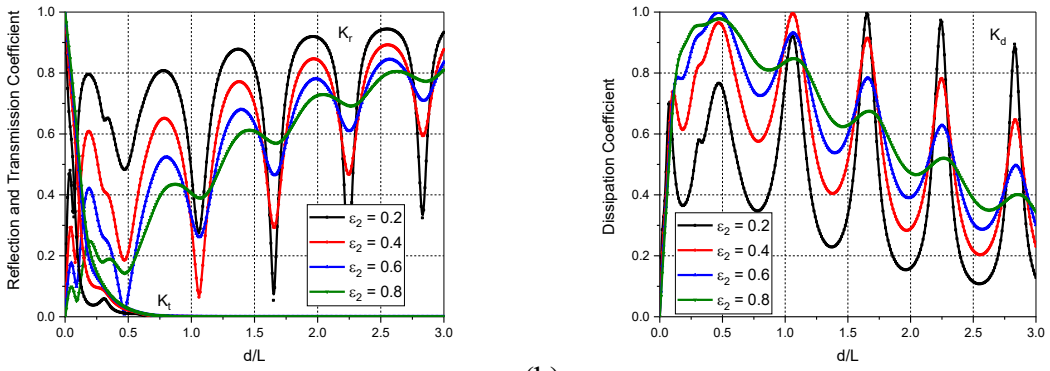

(a) (b)

Fig 3.6: Variation of (a) K_r, K_t and (b) K_d versus d/L for different values of ε_2, considering $\varepsilon_1 = 0.5$, $s_1 = s_2 = 1$, $f_1 = f_2 = 0.5$, $d/h = 0.5$, $w/h = 0.5$, and $\theta = 30^0$.

3.4.2.2 Porous structure with bottom-standing barrier (PS-BSB-1)

In Fig. 3.7(a,b), the variation of K_r, K_t and K_d versus $\gamma_{10}h$ is analysed for different values of gap between porous structure and barrier w/h. A sharp rise in the value of K_r, is observed within $0.01 < \gamma_{10}h < 0.5$ and thereafter, within $0.5 < \gamma_{10}h < 2.5$, the K_r, value reaches the maximum, and then it decreases. It is observed that maximum wave reflection K_r, occurs at $\gamma_{10}h = 2.3$ for $w/h = 0.75$.

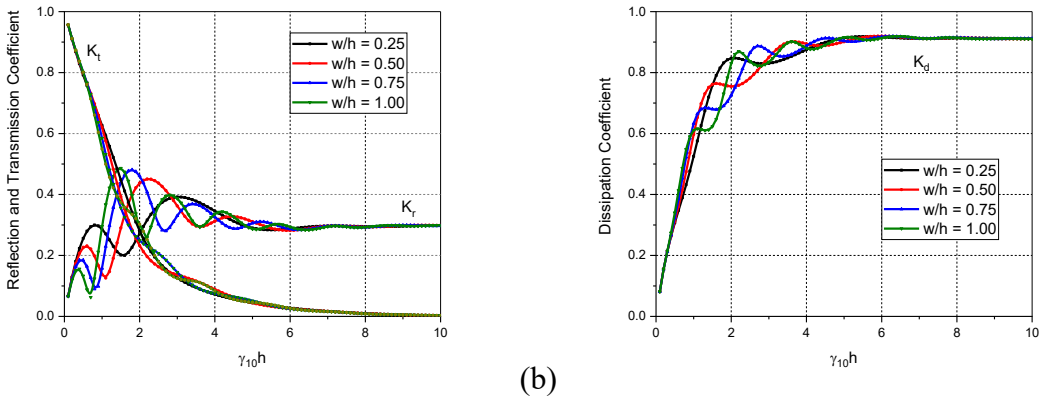

(a) (b)

Fig. 3.7: Variation of (a) K_r, K_t and (b) K_d versus $\gamma_{10}h$ for different values of gap between porous structure and barrier w/h considering $\varepsilon_1 = 0.5$, $\varepsilon_2 = 0.5$, $s_1 = s_2 = 1$, $f_1 = f_2 = 0.5$, $d/h = 0.5$ and $\theta = 30^0$.

A similar trend in the wave reflection curve is observed with changing gap between porous structure and barrier, and it is observed that a reduction of 29% in K_r for $w/h = 0.25$, 55%

reduction in K_r, for $w/h=0.5$, and 77% reduction in K_r for $w/h=0.75$ when compared to $w/h=0.25$. The wave transmission coefficient K_t (Fig. 3.7a) decreases with the increase in the non-dimensional wave number $\gamma_{10}h$ and with an increase in the gap between porous structure and barrier, the change in K_t is found to be not so significant as observed in the case of K_r. The variation in K_r and K_t due to the increase in w/h may be due to the increased energy dissipation K_d as observed in Fig. 3.7(b). As the gap between porous structure and barrier increases the K_d is observed to be increasing.The higher wave energy dissipation is observed for higher w/h.

In Fig. 3.8(a,b), the variation of K_r, K_t and K_d versus θ are analysed for various non-dimensional wave numbers $\gamma_{10}h$. The wave reflection K_r is observed to be increasing with the increase of non-dimensional wave number $\gamma_{10}h$ and incident wave angle θ, and the percentage change in K_r is found to be less compared to that of wave transmission K_t.

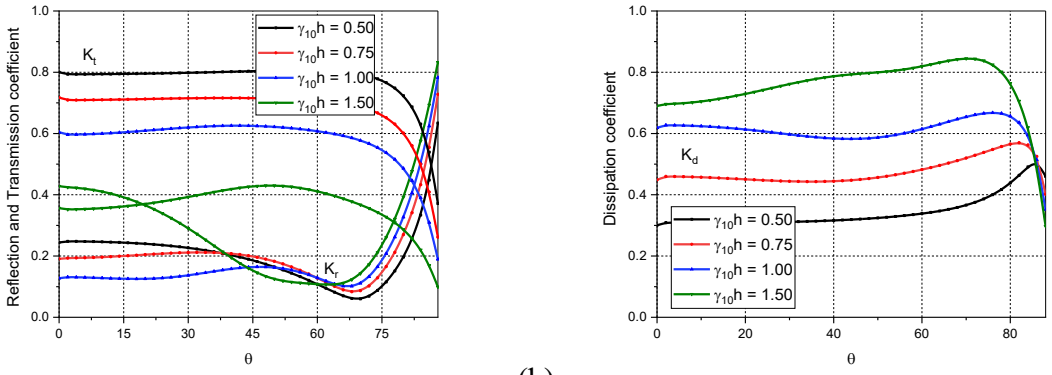

(a) (b)

Fig. 3.8: Variation of (a) K_r, K_t and (b) K_d versus θ for different values of $\gamma_{10}h$, considering $\varepsilon_1=\varepsilon_2=0.5$, $s_1=s_2=1$, $f_1=f_2=0.5$, $d/h=0.5$ and $w/h=0.5$.

The minimum wave reflection is observed for all the values of $\gamma_{10}h$ when the incident wave angle is within $60^0<\theta<80^0$, and hence the critical angle is observed within $60^0<\theta<80^0$. The study noted that, with the increase of $\gamma_{10}h$, 50% reduction in the value of wave transmission K_t (Fig. 3.8a) is observed for $\gamma_{10}h=1.5$ when compared with $\gamma_{10}h=0.5$ at $\theta=60^0$, and when the incident angle approaches 90^0, K_t is reduced to a minimum. The wave energy dissipation

(Fig. 3.8b) is observed to be increasing with the increase in $\gamma_{10}h$, and for all the values of $\gamma_{10}h$, the highest wave energy dissipation is observed when the incident wave angle lies in the range $70^0 < \theta < 80^0$. This may be due to the increased fluid-structure interaction that has taken place inside the porous structure.

3.4.2.3 Porous structure with surface-piercing barrier (PS-SPB-1)

In Fig. 3.9(a,b), the wave reflection, transmission, and energy dissipation coefficients are analysed for various non-dimensional gap between the porous structure and barrier w/h and plotted against the non-dimensional width of the porous structure d/L. As the width of the porous block increases, an increasing trend in wave reflection is observed, and higher wave reflection is observed when $2.5 < d/L < 3$. The periodic local maxima and minima are observed in the wave reflection, which may be due to the destructive interference. The wave transmission K_t is observed to exhibit a lesser effect with the change in the non-dimensional width of the porous block.

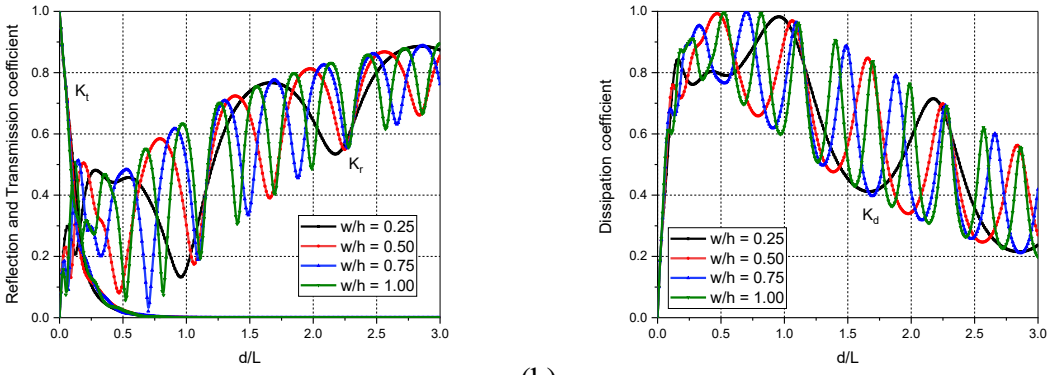

(a) (b)

Fig. 3.9: Variation of (a) K_r, K_t and (b) K_d versus d/L for different values of w/h, considering $\varepsilon_1 = \varepsilon_2 = 0.5$, $s_1 = s_2 = 1$, $f_1 = f_2 = 0.5$ and $\theta = 30^0$.

Further, as the non-dimensional gap w/h increases, the percentage change in wave transmission is observed to be less significant. The wave transmission (Fig. 3.9a) is observed to be decreasing with the increase in d/L and the effect of non-dimensional gap of the structure is observed to be very less on K_t. The wave energy damping K_d (Fig. 3.9b) is observed to be decreasing with the increase of d/L and the periodic local minima and maxima are also observed for all the values of w/h. The increase in d/L results in enhanced fluid-structure interaction, which will result in increased wave energy damping.

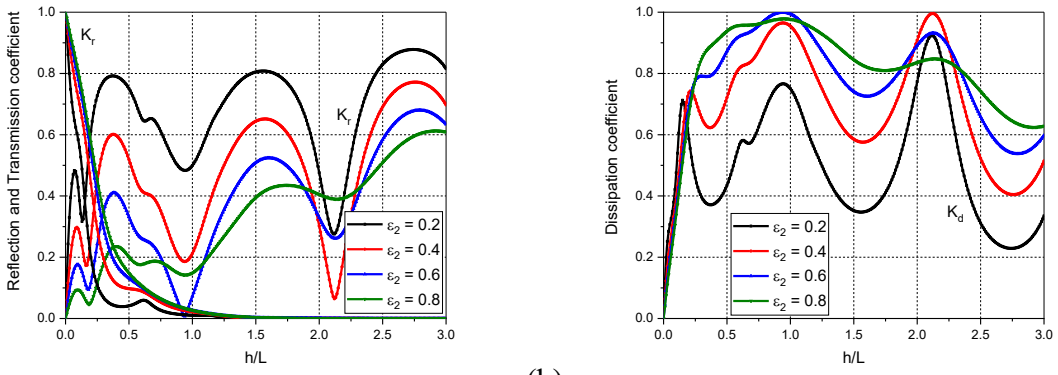

(a) (b)

Fig. 3.10: Variation of (a) K_r, K_t and (b) K_d versus h/L for different values of ε_2, considering $\varepsilon_1 = 0.5$, $s_1 = s_2 = 1$, $f_1 = f_2 = 0.5$, $d/h = 0.5$, $w/h = 0.5$ and $\theta = 30^0$.

In Fig. 3.10(a,b), the wave reflection K_r, transmission K_t and energy damping K_d coefficients are analysed for varying structural porosity. The periodic local maxima and minima are observed for K_r (Fig. 3.10a) with the increase of h/L. As the porosity of the structure increases, the wave reflection reduces, and wave transmission increases. Also, as the structure's height increases, a decreasing wave transmission and an increasing wave reflection are observed. The higher wave reflection is observed for $2.5 < h/L < 3.0$. The porous structure with 40% and 60% porosity exhibits complete wave energy dissipation when h/L is within $0.75 < h/L < 1.25$ and $2 < h/L < 2.5$ respectively. The wave reflection and wave energy dissipation (Fig. 3.10b) are observed to be resonating, and it may be due to the trapped waves in the confined spaces between the porous structure and porous barriers.

3.4.3 Barrier placed within porous structure

The multiple porous barriers placed within porous structures (PS-FEB-2, PS-BSB-2 and PS-SPB-2) are analysed to understand the effect of wave dissipation due to the multiple structures. The variation of wave reflection coefficient, transmission coefficient and wave energy dissipation coefficient is analysed by changing the porosity of porous block ε_2 within $0.2 < \varepsilon_2 < 0.8$, non-dimensional wave number $\gamma_{10}h$ within $0.5 < \gamma_{10}h < 1.5$ and the non-dimensional gap between porous block and barrier w/h within $0.25 < w/h < 1.0$.

3.4.3.1 Porous structure with fully-extended barrier (PS-FEB-2)

In Fig. 3.11(a,b), the effect of structure porosity ε_2 on wave reflection K_r, transmission K_t and energy dissipation coefficient K_d are analysed against $\gamma_{10}h$. A resonating trend in wave

reflection (Fig. 3.13a) is observed with the increase of $\gamma_{10}h$. The increase in ε_2 causes a reduction in wave reflection K_r, and an increase in wave transmission K_t. The effect of wave trapping is observed which shows resonating effect in the wave reflection pattern. The 87% wave energy dissipation (Fig. 3.11b) is observed for the structure with 20% porosity ε_2. The wave transmission K_t is reduced with the increase of non-dimensional wave number $\gamma_{10}h$. In addition, the higher wave transmission is observed when comparatively longer waves approach the porous system. The wave energy dissipation K_d is observed to resonate with the increase of non-dimensional wave number $\gamma_{10}h$, and higher wave energy dissipation is achieved for longer waves than shorter waves. Further, higher wave energy dissipation is observed within $2.0 < \gamma_{10}h < 3.0$.

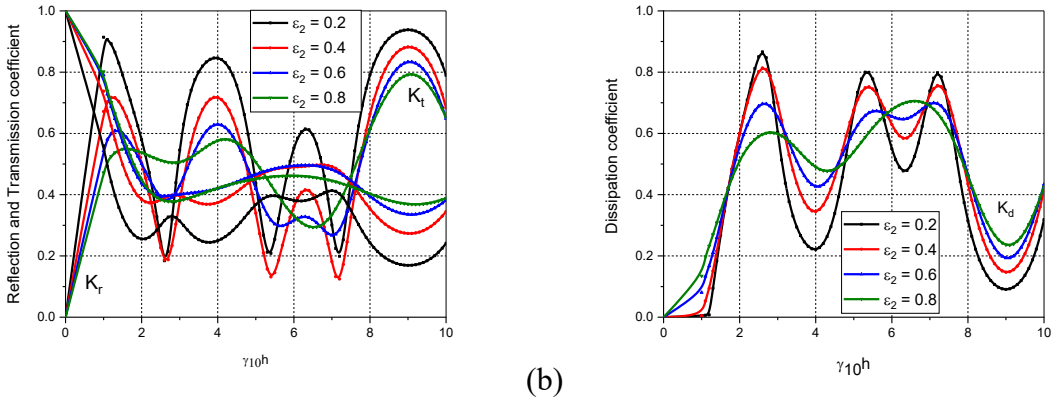

(a) (b)

Fig. 3.11: Variation of (a) K_r, K_t and (b) K_d versus $\gamma_{10}h$ for different values of structural porosity ε_2 considering $\varepsilon_1 = 0.5$, $s_1 = s_2 = 1$, $f_1 = f_2 = 0.5$, and $d/h = 0.5$ and $\theta = 30^0$.

In Fig. 3.12(a,b), the reflection K_r, transmission K_t and energy dissipation coefficient K_d are analysed for various non-dimensional wave number against the incident wave angle θ. The increase in $\gamma_{10}h$ and incident wave angle θ is found to enhance the wave reflection (Fig. 3.12a). The minimum wave reflection is observed to occur at an angle within $60^0 < \theta < 80^0$ for all the non-dimensional numbers. The minimum value in the reflection coefficient at particular angle of incidence can be referred as critical angle and is very helpful in designing coastal defense structures. The wave transmission is observed to be decreasing with the increase of non-dimensional wave number, and the study shows that the long waves are transmitted more through the multiple porous structure systems than short waves. In Fig. 3.12(b), as the incident wave angle increases, a comparatively higher wave energy dissipation is noted, and it reduces when the incident wave angle approaches $\theta = 90^0$. The multiple porous systems is found to be

dissipating the short waves effectively and higher wave energy dissipation is achieved for the waves with $\gamma_{10}h = 1.5$ at an angle within $60^0 < \theta < 80^0$.

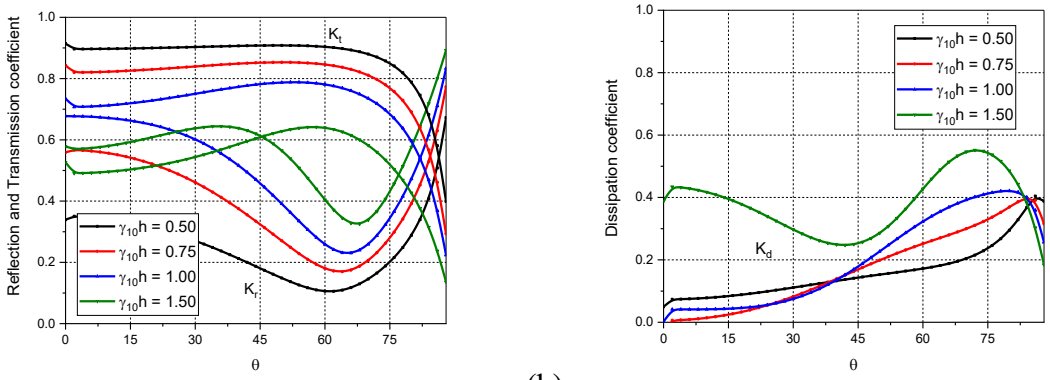

(a) (b)

Fig. 3.12: Variation of (a) K_r, K_t and (b) K_d versus θ for different values of $\gamma_{10}h$ considering $\varepsilon_1 = \varepsilon_2 = 0.5$, $s_1 = s_2 = 1$, $f_1 = f_2 = 0.5$, $d/h = 0.5$ and $w/h = 0.5$.

3.4.3.2 Porous structure with bottom-standing barrier (PS-BSB-2)

In Fig. 3.13(a,b), the wave transmission due to the multiple porous blocks associated with the bottom standing barrier is analysed and the effect of the porosity of the structure is plotted against the non-dimensional wave number $\gamma_{10}h$. It is observed that, the increase in porosity of the structure reduces the wave reflection (Fig. 3.13a).

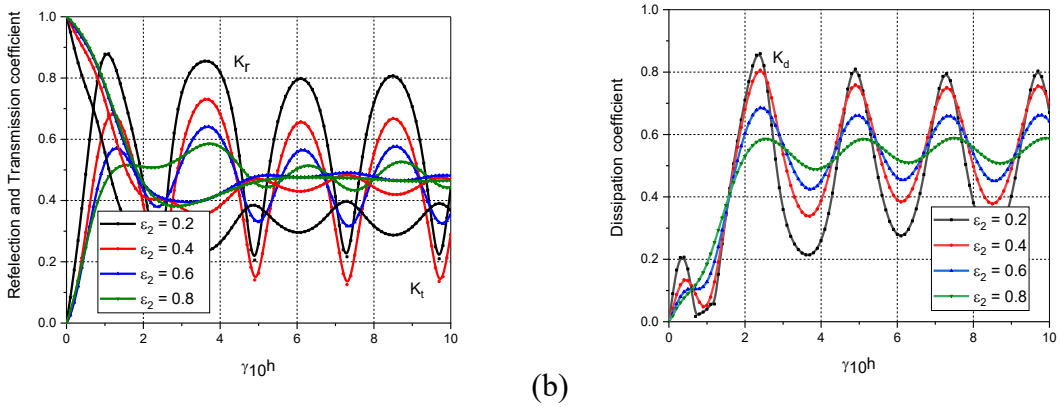

(a) (b)

Fig. 3.13: Variation of (a) K_r, K_t and (b) K_d versus $\gamma_{10}h$ for different values of ε_2 considering $\varepsilon_1 = 0.5$, $s_1 = s_2 = 1$, $f_1 = f_2 = 0.5$, $d/h = 0.5$ and $w/h = 0.5$.

The highest wave reflection is observed within $0.01 < \gamma_{10}h < 2$. In the range $0.01 < \gamma_{10}h < 2$, 52% reduction in wave reflection is observed for $\varepsilon_2 = 0.8$ when compared to the porosity

$\varepsilon_2 = 0.2$. The porosity also enhances wave transmission through the structure. With the increase of porosity of structure within $0.2 < \varepsilon_2 < 0.8$, the local minima in wave transmission are found to be diminishing. The porous structure with porosity $\varepsilon_2 = 0.2$ has higher wave energy dissipation (Fig. 3.13b) that dissipates almost 85% of the incoming wave energy. Higher wave energy damping is observed for longer waves compared to shorter waves.

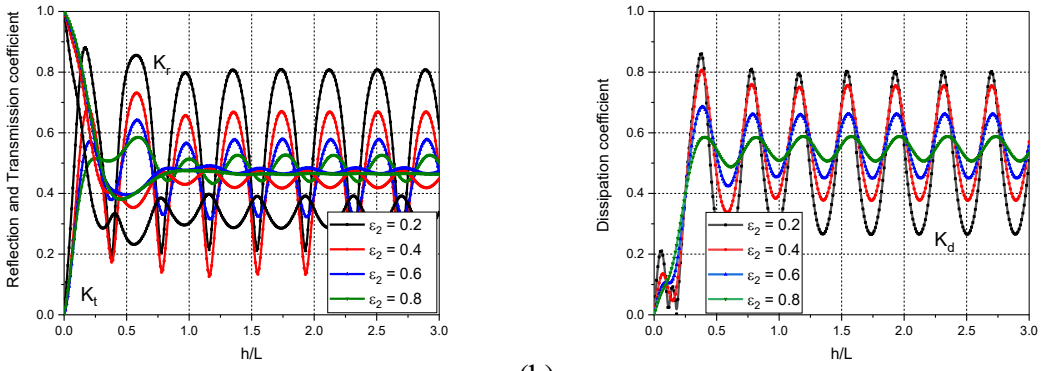

(a) (b)

Fig. 3.14: Variation of (a) K_r, K_t and (b) K_d versus h/L for different values of ε_2, considering $\varepsilon_1 = 0.5, s_1 = s_2 = 1, f_1 = f_2 = 0.5, w/h = 0.5, d/h = 0.5$ and $\theta = 30^0$.

In Fig. 3.14(a,b), the variation of wave reflection, transmission coefficient and wave energy dissipation coefficient due to the change in porosity of ε_2 is analysed against the non-dimensional height of the porous structure h/L. As h/L increases, the periodic maxima and minima of wave reflection are observed and the increased porosity imparts increased wave transmission through the porous structure and hence causes a reduction in wave reflection K_r (Fig. 3.14a). The non-dimensional height of the structure within $0.01 < h/L < 0.75$ shows higher K_r for all the values of porosity ε_2, thereafter, the wave reflection is found to be resonating and exhibits the same value of K_r. As ε_2 increases to 80%, the local minima and maxima of wave transmission K_t is found to be diminishing. In Fig. 3.14(b), the higher values of wave energy dissipation K_d are observed for lower values of porosity ε_2 within $0.01 < h/L < 0.5$; thereafter, it shows a resonating trend with the same local maxima and minima values. The wave trapping inside the confined regions of the porous system could be the reason for the resonance.

3.4.3.3 Porous structure with surface-piercing barrier (PS-SPB-2)

In Fig. 3.15(a,b), the wave reflection K_r, transmission K_t and wave energy dissipation K_d due to the multiple porous structure associated with the surface piercing barrier is analysed for various non-dimensional gap between the structure and barrier against the non-dimensional wave number $\gamma_{10}h$. The wave reflection (Fig. 3.15a) reduces with the increase in the gap between the structure and barrier and on the other hand the transmission coefficient increases slightly with the increase in the gap between the structure and barrier. The wave reflection coefficient shows the resonating pattern with the increase of $\gamma_{10}h$. A sharp rise in K_r is observed in the range $0.01 < \gamma_{10}h < 6.0$ and thereafter it reduces and starts to resonate. Higher wave reflection is observed in the range of $8.0 < \gamma_{10}h < 10.0$; which shows that waves with small wavelengths get reflected more by the breakwater system than that with higher wavelengths. In Fig. 3.17(b), the gap beween the structure and barrier $w/h = 0.75$ exhibits a higher percentage of wave energy dissipation.

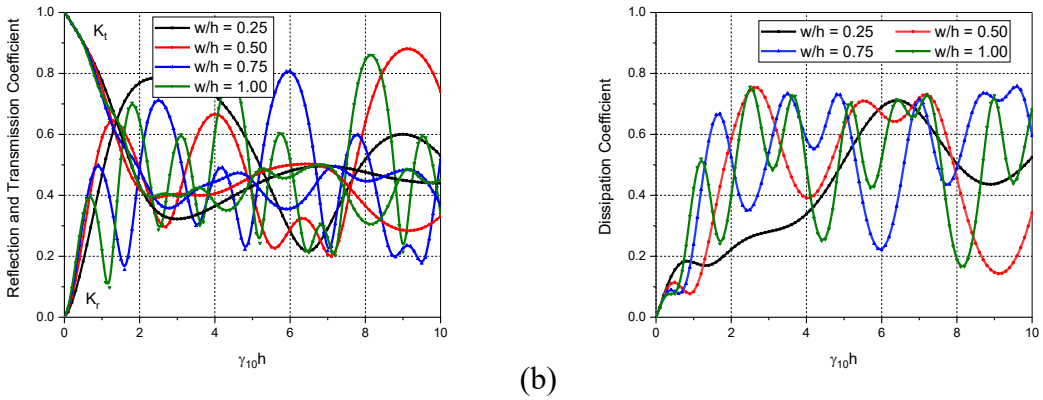

(a) (b)

Fig. 3.15: Variation of (a) K_r, K_t and (b) K_d versus $\gamma_{10}h$ for different values of w/h considering $\varepsilon_1 = \varepsilon_2 = 0.5$, $s_1 = s_2 = 1$, $f_1 = f_2 = 0.5$, $d/h = 0.5$ and $\theta = 30^0$.

In Fig. 3.16(a,b), the variation of wave reflection K_r, transmission K_t and wave energy dissipation K_d is analysed for various porosity of structure and plotted against h/L. The increase in the porosity allows more waves to transmit through the porous structure, and hence the wave reflection K_r (Fig. 3.16a) gets reduced. Higher wave reflection is observed within $2.5 < h/L < 3.0$ for all values ε_2. As the height of the structure increases, a reduction in wave transmission is observed.

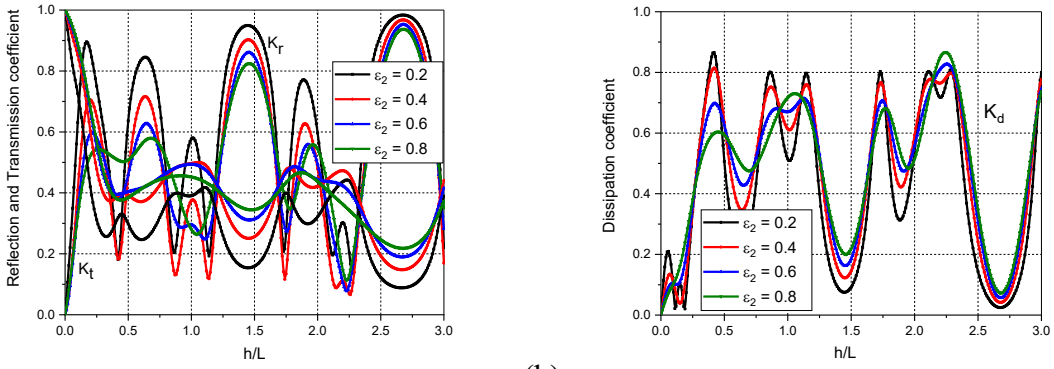

(a) (b)

Fig. 3.16: Variation of (a) K_r, K_t and (b) K_d versus h/L for different values of ε_2, considering $\varepsilon_1 = 0.5, s_1 = s_2 = 1,\ f_1 = f_2 = 0.5,\ w/h = 0.5,\ d/h = 0.5$ and $\theta = 30^0$.

Further, as the porosity of the structure increases, the percentage change in wave transmission is observed to be notable. The structure having 20% and 80% porosity achieved 86% of wave energy dissipation within $0.01 < h/L < 0.5$ and $2.0 < h/L < 2.5$ respectively. As h/L increases, the resonating trend in the wave reflection, transmission, and wave energy dissipation (Fig. 3.16b) coefficients is noted which could be due to the presence of multiple chambers inside the porous breakwater system that catches and traps the waves inside the confined spaces present in the system.

3.4.4 Porous structure placed within barrier

The multiple porous structures placed within porous barriers (PS-FEB-3, PS-BSB-3 and PS-SPB-3) are analysed. The variation of wave reflection coefficient, transmission coefficient and wave energy dissipation coefficient is analysed by changing the porosity of porous block ε_2 within $0.2 < \varepsilon_2 < 0.8$, non-dimensional wave number $\gamma_{10}h$ within $0.5 < \gamma_{10}h < 1.5$ and the non-dimensional gap between porous block and barrier w/h within $0.25 < w/h < 1.0$.

3.4.4.1 Porous structure with fully-extended barrier (PS-FEB-3)

Fig. 3.17(a,b) shows the wave reflection K_r, transmission K_t and energy dissipation coefficient K_d due to the presence of porous structure for different values of porosity of the structure against non-dimensional wave number. It is observed that the K_r (Fig. 3.17a) and K_d (Fig. 3.17b) shows a resonating trend which may be due to the presence of trapping chambers.

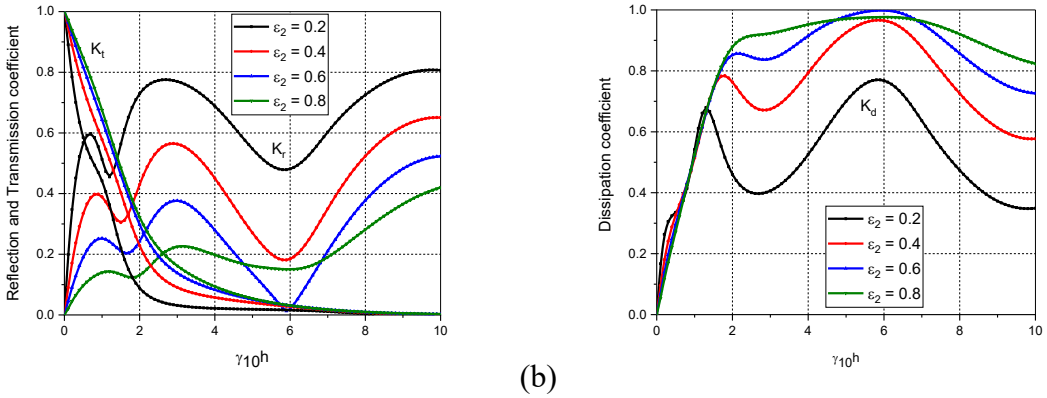

(a) (b)

Fig. 3.17: Variation of (a) K_r, K_t and (b) K_d versus $\gamma_{10}h$ for different values of porosity of structure ε_2 considering $\varepsilon_1 = 0.5$, $s_1 = s_2 = 1$, $f_1 = f_2 = 0.5$, $w/h = 0.5$, $d/h = 0.5$ and $\theta = 30^0$.

The K_t value shows a sharp decreasing trend within $0 \le \gamma_{10}h \le 3$. Further K_t shows relatively constant trend with an increase in dimensionless wave number. In addition, with the increase in porosity, the wave reflection decreases, and transmission increases while more incident wave energy is dissipated. Also, the resonating trend in K_d decreases with an increase in porosity. An increase of 29% in wave damping (Fig. 3.17b) is observed when porosity is varied within $0.2 < \varepsilon_2 < 0.8$. A sharp increase in wave energy damping is observed for all the porosity values within $0.01 \le \gamma_{10}h \le 2$ which shows that longer waves tend to penetrate the porous structure than shorter waves which causes a sudden increase in wave-structure interaction that results in increased wave energy damping. Also, higher wave energy damping is achieved by all the porosity values within $5 \le \gamma_{10}h \le 7$.

Fig. 3.18(a,b) presents the behavior of porous structure in terms of reflection K_r, transmission K_t and dissipation K_d coefficient against the dimensionless height of the structure for varying porosity. In Fig. 3.18(a), it is observed that the wave reflection has a resonating trend within $0 \le h/L \le 3.0$ which is due to constructive and destructive interferences. The resonating troughs are particularly useful in designing the optimum structure height to achieve the least reflection. The minimum reflection is observed for h/L values of 0.8 and 2.13. The wave transmission shows a sharp decline up to a structure height half of the incident wavelength. In addition, with the increase in height of structure, the transmission is negligible. The resonating behaviour is also observed in the case of K_d (Fig. 3.18b) where maximum dissipation is

achieved for h/L values with the least reflection. Further, wave reflection increases and transmission decreases with an increase in porosity. The wave reflection is found to be maximum for $h/L = 2.75$. In the case of change in porosity from 80% to 20%, the K_r shows 40% increase and the energy dissipation is observed to increase for 80% structural porosity.

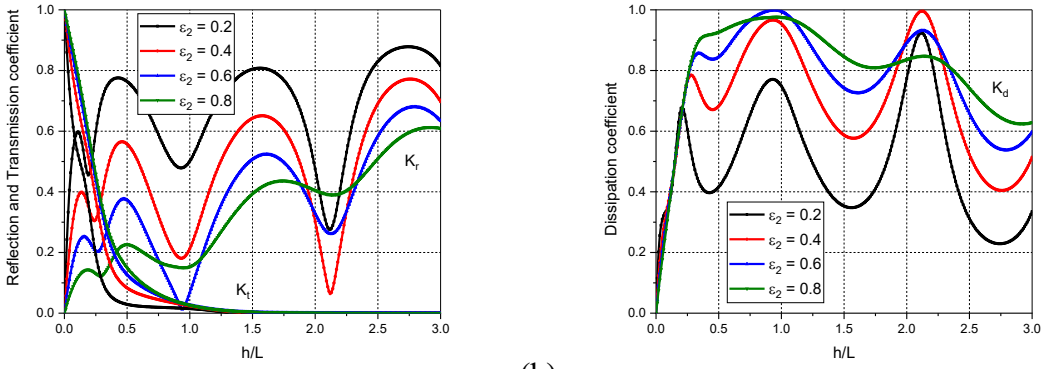

(a) (b)

Fig. 3.18: Variation of (a) K_r, K_t and (b) K_d versus h/L for different values of ε_2, considering $\varepsilon_1 = 0.5$, $s_1 = s_2 = 1$, $f_1 = f_2 = 0.5$, $d/h = 0.5$, $w/h = 0.5$, and $\theta = 30^0$.

3.4.4.2 Porous structure with bottom-standing barriers (PS-BSB-3)

In Fig. 3.19(a,b), the reflection K_r, transmission K_t and dissipation coefficients K_d are plotted against non-dimensional wave number $\gamma_{10}h$ for different structural porosity.

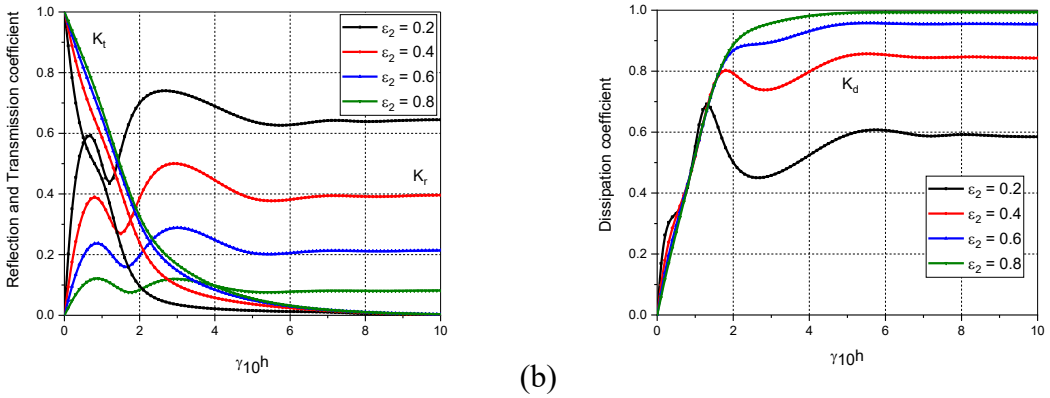

(a) (b)

Fig. 3.19: Variation of (a) K_r, K_t and (b) K_d versus $\gamma_{10}h$ for different values of porosity of structure ε_2 considering $\varepsilon_1 = 0.5$, $s_1 = s_2 = 1$, $f_1 = f_2 = 0.5$, $w/h = 0.5$, $d/h = 0.5$ and $\theta = 30^0$.

The K_r and K_d (Fig. 3.19a) shows a slight resonating trend within $0 \le \gamma_{10} h \le 5$, and thereafter it can be observed that the dimensionless wave number has not much effect on the structural porosity and attains a constant value which may be due to seaward constructive or destructive interference. The K_t tends to decrease sharply within $0 \le \gamma_{10} h \le 5$ and shows a percentage decrease of 84% while there is a percentage increase of 67%, with an increase in porosity values from 20% to 60%. The wave energy dissipation (Fig. 3.19b) exhibits a sharp rise for all the porosity values within $0.01 \le \gamma_{10} h \le 2.0$. This demonstrates that longer waves tend to enter porous structures more readily than shorter waves.

In Fig. 3.20(a,b), the wave reflection K_r, transmission K_t, and the wave energy dissipation K_d is plotted versus the dimensionless structural height h/L for different values of structural porosity ε_2. The K_r (Fig. 3.20a) and K_d (Fig. 3.20b) shows a resonating trend within $0 \le h/L \le 1.0$, which may be due to the wave trapping inside the porous structure. As h/L increases, the wave transmission is observed to be decreasing and comparatively higher wave transmission is observed with the rise in the structure porosity. The increased transmission coefficient as seen in Fig. 3.20(a) attributes to the presence of voids that enhance the structural porosity. A dimensionless wave height value of $h/L = 1.2$ can be considered as optimum value for design beyond which there is no much effect on the hydrodynamic coefficients. A higher porosity value is observed to reduce the wave reflection and increase the wave damping (Fig. 3.20b). The resonating trend is minimal for a porosity value of 80% and is found to have around 95% wave energy dissipation within $1.0 \le h/L \le 3.0$.

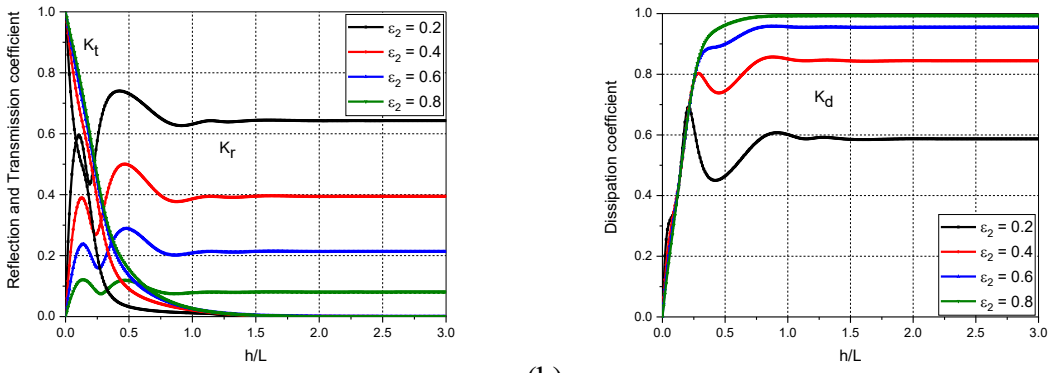

(a) (b)

Fig. 3.20: Variation of (a) K_r, K_t and (b) K_d versus h/L for different values of ε_2, considering $\gamma_{10} h = 1$, $\varepsilon_1 = 0.5$, $s_1 = s_2 = 1$, $f_1 = f_2 = 0.5$, $d/h = 0.5$, $w/h = 0.5$ and $\theta = 30^0$.

3.4.4.3 Porous structure with surface-piercing barrier (PS-SPB-3)

In Fig. 3.21(a,b), the change in hydrodynamic coefficients due to the variation in non-porosity of the barrier ε_1 are analysed and plotted against the non-dimensional width of the structure d/L. It is observed that the K_r (Fig. 3.21a) is increased with the increase in d/L. As porosity of the barrier ε_1 increases, the resonance also increased, which may be due to the increased wave trapping in the gaps between porous structure and barriers. The increase in the width of the porous structure does not allow much waves to pass through it, which may be due to the increase in the width of the structure causing higher reflection of waves and allows only less incident waves to pass through the system. Also, with the increase in the porosity of the barrier, the percentage change in wave transmission K_t is observed to be negligible. Thus, in Fig. 3.21(b), the wave energy dissipation is observed to be less with the increase of d/L and it is recommended that the optimum value of porosity of the barrier should be adopted on analysing the wave reflection pattern.

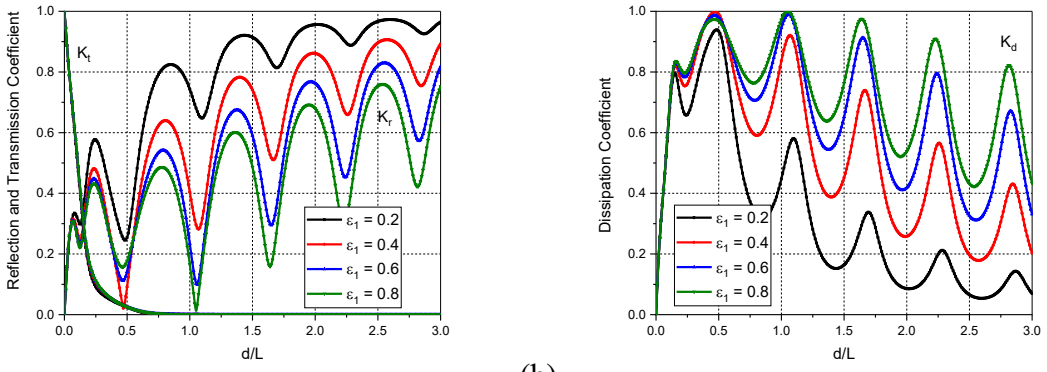

(a) (b)

Fig 3.21: Variation of (a) K_r, K_t and (b) K_d versus d/L for different values of ε_1, considering $\varepsilon_2 = 0.5$, $s_1 = s_2 = 1$, $f_1 = f_2 = 0.5$, $w/h = 0.5$ and $\theta = 30^0$.

In Fig. 3.22(a,b), the wave transformation due to multiple porous blocks structure associated with porous barrier is analysed and the variation of the wave reflection, transmission and energy dissipation coefficient are plotted against d/L. In Fig. 3.22(a), the increase in d/L is observed to be causing the resonating trend in wave reflection. The higher values of angle of incidence causes a reduction of K_r. The wave transmission is found to be decreasing with the rise of d/L. Almost complete wave energy damping K_d (Fig. 3.22b) is achieved by the multiple porous breakwater system at $\theta = 60^0$ and $0.75 < d/L < 1.25$.

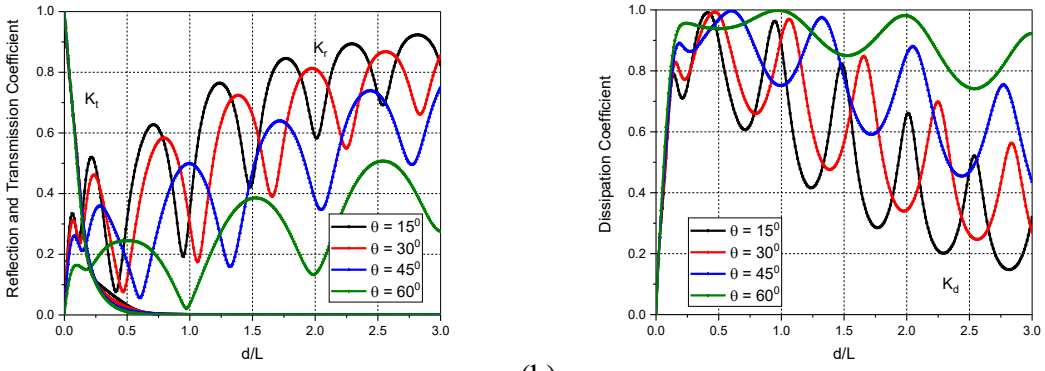

(a) (b)

Fig 3.22: Variation of (a) K_r, K_t and (b) K_d versus d/L for different values of θ, considering $\varepsilon_1 = \varepsilon_2 = 0.5$, $s_1 = s_2 = 1$, $f_1 = f_2 = 0.5$ and $w/h = 0.5$.

3.5 CLOSURE

The wave transformation due to the multiple submerged porous structures associated with different barrier configurations such as fully extended-barriers, bottom-standing barriers, and surface-piercing barriers are analysed for different position of structure and barrier. The conclusions drawn from the study are as follows:

- In all the configurations of PS-FEB, PS-BSB and PS-SPB, the increase in the porosity ε_2 of the structure is observed to be causing a reduction in the wave reflection.

- The increase in porosity of the structure ε_2 causes an increase in wave transmission coefficient K_t for all the configurations of alternate porous structure and barrier.

- The multiple porous PS-FEB and PS-SPB yielded almost 100% of wave energy dissipation K_d for the value of porosity of structure $\varepsilon_2 = 0.6$ at $\gamma_{10}h = 6.0$, whereas the multiple PS-BSB yielded 100% of wave energy dissipation K_d for the value of 80% porosity of the structure.

- A resonating trend of K_r is observed with the increase of non-dimensional wave number $\gamma_{10}h$. All configurations of PS-FEB, PS-BSB and PS-SPB shows the critical angle in which the minimum wave reflection K_r is observed to be occurring within $60^0 < \theta < 80^0$.

- The multiple PS-FEB and PS-FEB are found to be almost similar when analysed for various porosity of the structure ε_2, incident angles θ and non-dimensional gap between the structures w/h.

- The confined spacing between the porous structure and the barriers are observed to be causing the resonance in wave reflection for all configurations of multiple porous structures and barriers.

- The variation of hydrodynamic coefficients is found to be almost similar for the configurations associated with PS-FEB and PS-SPB when the effect of ε_2, $\gamma_{10}h$, w/h and θ is considered.

CHAPTER 4

GRAVITY WAVE DISSIPATION DUE TO SUBMERGED POROUS PLATE AND POROUS STRUCTURE

4.1 GENERAL INTRODUCTION

The study on the wave attenuation due to stand alone submerged porous plate and submerged porous structure is studied by researchers but the studies on the dissipation of gravity waves due to the combination of submerged porous plate and porous structures are limited. The aforementioned studies suggest that, the installation of the submerged porous plate with the submerged porous structure may help to reinforce the overturning stability of the porous structure. In addition, the wave absorbing performance of the porous structure may be enhanced as the submerged porous plate may act as wave absorber (Liu et al., 2007). Thus, from the previous studies, it is observed that the combination of the submerged porous plate and porous structure plays an important role in the dissipation of wave energy and attenuation of wave height in the transmitted region. The present study deals with the interaction of gravity waves with the different combinations of submerged horizontal porous plate with bottom-standing and surface-piercing porous structure. The numerical solution is developed using matched eigenfunction expansion method and orthogonal mode-coupling relation. Further the continuity of velocity and pressure at the structure interface is employed to analyse the effectiveness of the composite breakwater system.

4.2 MATHEMATICAL FORMULATION

The wave propagation through submerged porous structures in finite water depth is examined under the assumption of linearized wave theory for two different configurations of composite breakwater. A train of small amplitude waves propagate in the negative $x-$ direction and are obliquely incident upon a breakwater system. A three-dimensional coordinate system is considered in the analysis with $x-z$ being horizontal plane and $y-$axis being vertically downward positive. The porous structures used in the study are submerged horizontal porous plate of negligible thickness (Liu and Li, 2011) combined with bottom-standing submerged porous structure (Fig. 1a) and surface-piercing porous structure (Fig. 1b). The floating plate is considered to be thin and is assumed to be very small in comparison with the water depth and incident wavelength (Liu and Li, 2011). The fluid domain is divided into upstream open water

region at $0 < x < \infty,\ 0 < y < h$ as region 1, fluid domain above the plate at $-a_1 < x < 0,\ 0 < y < h_1$ as region 2, fluid domain beneath the plate at $-a_1 < x < 0,\ h_1 < y < h$ as region 3, fluid domain between the plate and porous structure at $-a_2 < x < -a_1,\ 0 < y < h$ as region 4 and downstream open water region at $-\infty < x < -a_3,\ 0 < y < h$ as region 7. The fluid domain above the bottom-standing porous structure at $-a_3 < x < -a_2,\ 0 < y < h_1$ is taken as region 5 (Fig. 4.1a) and for the bottom-standing porous structure region at $-a_3 < x < -a_2,\ h_1 < y < h$ is taken as region 6 (Fig. 4.1a). Further, for the surface-piercing porous structure region at $-a_3 < x < -a_2,\ 0 < y < h_1$ is taken as region 5 (Fig. 4.1b) and fluid domain below the surface-piercing porous structure at $-a_3 < x < -a_2,\ h_1 < y < h$ is taken as region 6 (Fig. 4.1b).

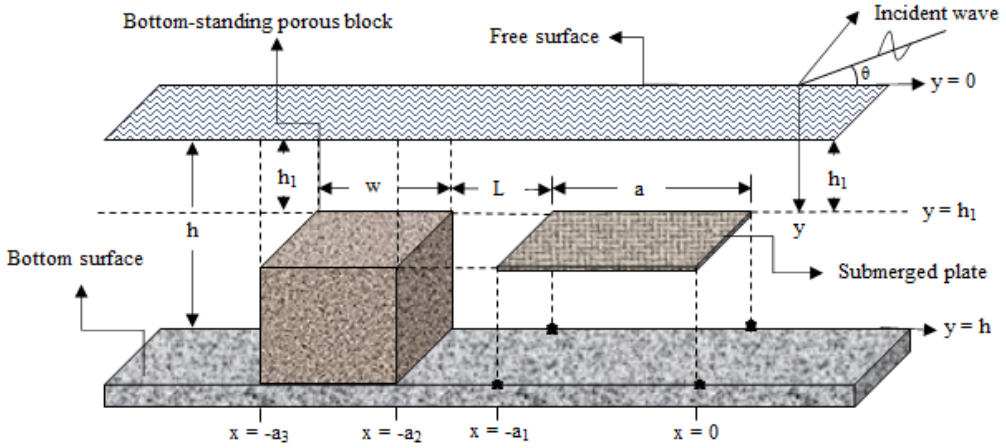

(a)

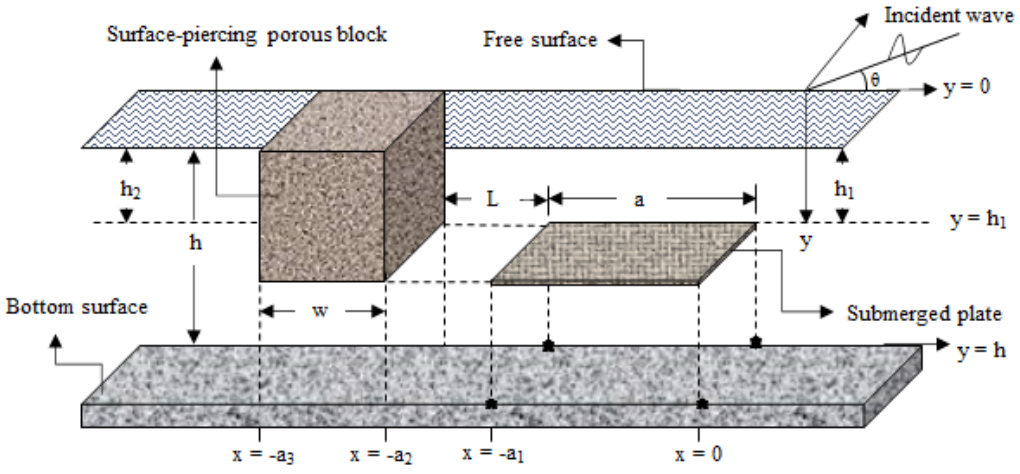

(b)

Fig. 4.1: Schematic diagram for a submerged porous plate backed by (a) bottom-standing porous structure and (b) surface-piercing porous structure.

The velocity potential $\Phi_j(x,y,z,t)$ is time harmonic in frequency and harmonic with wavenumber l and is given by $\Phi_j(x,y,z,t) = \mathrm{Re}\left\{\phi_j(x,y)e^{-ilz-i\omega t}\right\}$ and free surface deflection is given by $\zeta_j(x,z,t) = \mathrm{Re}\left\{\eta_j(x)e^{-ilz-i\omega t}\right\}$ where Re represents the real part and $l = \gamma_{10}\sin\theta$ represents the progressive wave mode, θ is the angle of incidence and γ_{10} is the progressive wave number in y direction. The spatial velocity potential $\phi_j(x,y,z)$ satisfies the Helmholtz equation given by

$$\frac{\partial^2\phi_j}{\partial x^2} + \frac{\partial^2\phi_j}{\partial y^2} - l^2\phi_j = 0 \quad \text{for } 0 < y < h. \tag{4.1}$$

The seabed is assumed to be flat and impermeable, so the no flow condition is given by

$$\frac{\partial\phi_j(x,y)}{\partial y} = 0 \quad \text{at } y = h \quad \text{for} \quad j = 1,2,...,7. \tag{4.2}$$

The linearized free surface boundary condition in open water region is given by

$$\frac{\partial\phi_j(x,y)}{\partial y} + \frac{\omega^2}{g}\phi_j(x,y) = 0 \quad \text{at } y = 0 \quad \text{for } j = 1,2,4,7. \tag{4.3}$$

The linearized boundary condition for the bottom-standing porous region is given by

$$\frac{\partial\phi_j(x,y)}{\partial y} + \frac{\omega^2(s_2 + if_2)}{g}\phi_j(x,y) = 0 \quad \text{at } h_1 < y < h \quad \text{for } j = 6. \tag{4.4a}$$

where s_2 is the inertia coefficient and f_2 is the friction coefficient for bottom-standing porous structure. The linearized boundary condition for the surface-piercing porous structure is given by the relation

$$\frac{\partial\phi_j(x,y)}{\partial y} + \frac{\omega^2(s_2 + if_2)}{g}\phi_j(x,y) = 0 \quad \text{at} \quad 0 < y < h_1 \quad \text{for } j = 5, \tag{4.4b}$$

where s_3 is the inertia coefficient and f_3 is the friction coefficient for surface-piercing porous structure. The linearized boundary condition for the porous plate at the interface is given by

$$\frac{\partial\phi_2}{\partial x} = \frac{\partial\phi_3}{\partial x} = i\gamma_{10}G_p(\phi_3 - \phi_2) \quad \text{for } y = h_1, \tag{4.5}$$

where $G_p = \dfrac{\rho b\omega}{\mu}$ is the porous effect parameter, ρ is the density of the structure, b is the material constant of dimension l and μ is the dynamic viscosity constant. In the case of submerged porous plate, the material used is considered to be having fine pores which allows the fluid to pass through the porous plate and obeys Darcy's law. The edge condition at the interface $y = h_1$ for the bottom-standing porous structure is given by

$$\phi_5 = (s_2 + if_2)\phi_6 \text{ and } \frac{\partial \phi_5}{\partial y} = \varepsilon_2 \frac{\partial \phi_6}{\partial y}, \tag{4.6}$$

Further, the edge condition for the surface-piercing porous structure at $y = h_1$ is given by

$$(s_2 + if_2)\phi_5 = \phi_6 \text{ and } \varepsilon_2 \frac{\partial \phi_5}{\partial y} = \frac{\partial \phi_6}{\partial y}, \tag{4.7}$$

where ε_2 is the porosity of bottom-standing porous structure and surface-piercing porous structure. The continuity of dynamic pressure and mass flux along the horizontal *x*-direction of fluid and porous plate interfaces is given by

$$\phi_1(x,y) = \phi_j(x,y) \text{ and } \phi_{1x}(x,y) = \phi_{jx}(x,y) \text{ for } j = 2,3 \text{ at } x = 0, \tag{4.8a}$$

$$\phi_4(x,y) = \phi_j(x,y) \text{ and } \phi_{4x}(x,y) = \phi_{jx}(x,y) \text{ for } j = 2,3 \text{ at } x = -a_1. \tag{4.8b}$$

4.2.1 Bottom-standing porous structure

In the case of bottom-standing porous structure, the continuity of dynamic pressure and mass flux at the interfaces is given by

$$\phi_4(x,y) = \phi_5(x,y) \text{ and } \phi_{4x}(x,y) = \phi_{5x}(x,y) \text{ at } x = -a_2, \tag{4.9a}$$

$$\phi_4(x,y) = (s_2 + if_2)\phi_6(x,y) \text{ and } \phi_{4x}(x,y) = \varepsilon_2\phi_{6x}(x,y) \text{ at } x = -a_2, \tag{4.9b}$$

$$\phi_7(x,y) = \phi_5(x,y) \text{ and } \phi_{7x}(x,y) = \phi_{5x}(x,y) \text{ at } x = -a_3, \tag{4.9c}$$

$$\phi_7(x,y) = (s_2 + if_2)\phi_6(x,y) \text{ and } \phi_{7x}(x,y) = \varepsilon_2\phi_{6x}(x,y) \text{ at } x = -a_3. \tag{4.9d}$$

4.2.2 Surface-piercing porous structure

Further, in the case of surface-piercing porous structure, at the interface of fluid and the porous structure, the continuity of dynamic pressure and mass flux at the interfaces is given by

$$\phi_4(x,y) = (s_2 + if_2)\phi_5(x,y) \text{ and } \phi_{4x}(x,y) = \varepsilon_2\phi_{5x}(x,y) \text{ at } x = -a_2, \tag{4.10a}$$

$$\phi_4(x,y) = \phi_6(x,y) \text{ and } \phi_{4x}(x,y) = \phi_{6x}(x,y) \text{ at } x = -a_2, \tag{4.10b}$$

$$\phi_7(x,y) = (s_2 + if_2)\phi_5(x,y) \text{ and } \phi_{7x}(x,y) = \varepsilon_2\phi_{5x}(x,y) \text{ at } x = -a_3, \tag{4.10c}$$

$$\phi_7(x,y) = \phi_6(x,y) \text{ and } \phi_{7x}(x,y) = \phi_{6x}(x,y) \text{ at } x = -a_3. \tag{4.10d}$$

The wave number in upstream/downstream free-water region γ_{jn} for $j = 1,4,7$ and the bottom-standing porous structure region γ_{6n} satisfies the dispersion relation for finite water depth is given by

$$\omega^2 = \begin{cases} g\gamma_{j0}\tanh\gamma_{j0}h & \text{for } n = 0 \\ -g\gamma_{jn}\tan\gamma_{jn}h & \text{for } n = 1,2,.... \end{cases} \text{ for } j = 1,4,7 \tag{4.11a}$$

$$\omega^2(s_2 + if_2) = g\gamma_{6n}\tanh\gamma_{6n}h \quad \text{for} \quad n = 0,1,2,.... \tag{4.11b}$$

Similarly, the wave number in upstream/downstream free-water region γ_{jn} for $j=1,4,7$ and the surface-piercing porous structure region γ_{5n} satisfies the dispersion relation for finite water depth is given by

$$\omega^2 = \begin{cases} g\gamma_{j0}\tanh\gamma_{j0}h & \text{for} \quad n=0 \\ -g\gamma_{jn}\tan\gamma_{jn}h & \text{for} \quad n=1,2,.... \end{cases} \quad \text{for} \quad j=1,4,7 \tag{4.11c}$$

$$\omega^2(s_2+if_2) = g\gamma_{5n}\tanh\gamma_{5n}h \quad \text{for} \quad n=0,1,2,.... \tag{4.11d}$$

where, ω is the wave frequency and g is the acceleration due to gravity. In the far-field region, the radiation conditions in the presence of porous structure with submerged plate is given by

$$\phi_j(x,y) = \begin{cases} \left(I_{10}e^{-i\gamma_{10}x} + R_{10}e^{i\gamma_{10}x}\right) f_{10}(y) & \text{as} \quad x \to \infty, \\ \left(T_{70}e^{-i\gamma_{30}x}\right) f_{70}(y) & \text{as} \quad x \to -\infty, \end{cases} \tag{4.12}$$

where, I_{10}, R_{10} and T_{70} are the complex amplitude of the incident, reflected and transmitted wave energies respectively. However, the incident wave I_{10} is considered to be unity.

4.3 METHOD OF SOLUTION

The wave interaction with submerged plate with different combinations of submerged porous structures is analysed to understand the wave dissipation and hydrodynamic performance of the composite breakwater. The velocity potentials $\phi_j(x,y)$ in each of the respective regions for the two different configurations satisfying the governing equation (1) along with the boundary conditions are of the form

$$\phi_1(x,y) = (I_{10}e^{-ik_{10}x} + R_{10}e^{ik_{10}x})f_{10}(y) + \sum_{n=1}^{\infty} R_{1n}e^{-k_{1n}x} f_{1n}(y) \quad \text{for} \quad 0<x<\infty,\ 0<y<h, \tag{4.13a}$$

$$\phi_2(x,y) = \sum_{n=0}^{\infty} \left\{ A_{2n}\frac{\cos k_{2n}x}{\cos k_{2n}a_1} + B_{2n}\frac{\sin k_{2n}x}{\sin k_{2n}a_1} \right\} f_{2n}(y) \quad \text{for} \quad -a_1<x<0,\ 0<y<h_1, \tag{4.13b}$$

$$\phi_3(x,y) = \sum_{n=0}^{\infty} \left\{ A_{2n}\frac{\cos k_{2n}x}{\cos k_{2n}a_1} + B_{2n}\frac{\sin k_{2n}x}{\sin k_{2n}a_1} \right\} f_{3n}(y) \quad \text{for} \quad -a_1<x<0,\ h_1<y<h, \tag{4.13c}$$

$$\phi_4(x,y) = \left\{ A_{40}e^{-ik_{40}(x+a_1)} + B_{40}e^{ik_{40}(x+a_2)} \right\} f_{40}(y) + \sum_{n=1}^{\infty} \left\{ A_{4n}e^{k_{4n}(x+a_1)} + B_{4n}e^{-k_{4n}(x+a_2)} \right\} f_{4n}(y) \quad \text{for} \quad -a_2<x<-a_1,\ 0<y<h, \tag{4.13d}$$

$$\phi_5(x,y) = \sum_{n=0}^{\infty} \left\{ A_{5n}e^{-ik_{5n}(x+a_2)} + B_{5n}e^{ik_{5n}(x+a_3)} \right\} f_{5n}(y) \quad \text{for} \quad -a_3<x<-a_2,\ 0<y<h_1, \tag{4.13e}$$

$$\phi_6(x,y)=\sum_{n=0}^{\infty}\left\{A_{5n}e^{-ik_{5n}(x+a_2)}+B_{5n}e^{ik_{5n}(x+a_3)}\right\}f_{6n}(y)\ \text{ for }\ -a_3<x<-a_2,\ h_1<y<h, \tag{4.13f}$$

$$\phi_7(x,y)=T_{70}e^{-ik_{70}(x+a_3)}f_{70}(y)+\sum_{n=1}^{\infty}T_{7n}e^{k_{7n}(x+a_3)}f_{7n}(y)\ \text{ for }\ -\infty<x<-a_3,\ 0<y<h. \tag{4.13g}$$

where I_{10} is the incident wave which is considered as unity and $R_{1n}, A_{2n}, B_{2n}, A_{4n}, B_{4n}, A_{5n}, B_{5n}$ and T_{7n} for $n=0,1,2...$ are the unknowns to be determined. The eigen functions $f_{jn}(y)$'s for the open water regions for $j=1,4,7$ is given by

$$f_{jn}(y)=\frac{\cosh\gamma_{jn}(h-y)}{\cosh\gamma_{jn}h}\ \text{ for }\ n=0\ \text{ and }\ f_{jn}(y)=\frac{\cos\gamma_{jn}(h-y)}{\cos\gamma_{jn}h}\quad \text{for } n=1,2,3..., \tag{4.14}$$

where γ_{jn} for $j=1,4,7$, $n=0$ are eigen values and satisfies the dispersion relation

$$\omega^2=g\gamma_{jn}\tanh\gamma_{jn}h\ \text{ for } n=0, \tag{4.15}$$

satisfying $\gamma_{jn}{}^2=k_{jn}{}^2+l^2$, where γ_{jn} is the wave number in y – direction, k_{jn} is the wave number in x – direction and $l=\gamma_{10}\sin\theta$ is the wave number in the z – direction. The eigenfunctions $f_{jn}(y)$'s for the submerged porous plate region $j=2$ and 3 and $n=0,1,2...$ is given by

$$f_{2n}(y)=\sinh\gamma_{2n}(h-h_1)\left\{g\gamma_{2n}\cosh\gamma_{2n}y-\omega^2\sinh\gamma_{2n}y\right\}, \tag{4.16a}$$

$$f_{3n}(y)=-\left\{g\gamma_{2n}\sinh\gamma_{2n}h_1-\omega^2\cosh\gamma_{2n}h_1\right\}\cosh\gamma_{2n}(h-y), \tag{4.16b}$$

where γ_{2n} is the eigenvalue and satisfies the dispersion relation is of the form given by

$$\gamma_{2n}\sinh\gamma_{2n}(h-h_1)\left\{g\gamma_{2n}\sinh\gamma_{2n}h_1-\omega^2\cosh\gamma_{2n}h_1\right\}-ik_{10}G_p\left\{\omega^2\cosh\gamma_{2n}h-g\gamma_{2n}\sinh\gamma_{2n}h\right\}=0, \tag{4.17}$$

for $n=0,1,2...$ The eigenfunctions $f_{jn}(y)$'s for the bottom-standing submerged porous structure region $j=5,6,\ n=0,1,2...$ is given by

$$f_{5n}(y)=\left\{\frac{\cosh\gamma_{5n}(h-y)-F_n\sinh\gamma_{5n}(h-y)}{\cosh\gamma_{5n}h-F_n\sinh\gamma_{5n}h}\right\}, \tag{4.18a}$$

$$f_{6n}(y)=\left\{\frac{1-F_n\tanh\gamma_{5n}(h-h_1)}{(s_2+if_2)(\cosh\gamma_{5n}h-F_n\sinh\gamma_{5n}h)}\right\}\cosh\gamma_{5n}(h-y), \tag{4.18b}$$

where $$F_n = \frac{\{(s_2 + if_2) - \varepsilon_2\}\tanh\gamma_{5n}(h-h_1)}{\{(s_2+if_2)-\varepsilon_2\tanh^2\gamma_{5n}(h-h_1)\}}, \tag{4.19}$$

ε_2 is the porosity of the permeable material, s_2 is an inertial coefficient and f_2 is a linearized friction coefficient. The eigen value γ_{5n} satisfies the dispersion relation

$$\omega^2 - g\gamma_{5n}\tanh\gamma_{5n}h - F_n(\omega^2\tanh\gamma_{5n}h - \gamma_{5n}g) = 0, \quad \text{for } n = 0,1,2\ldots. \tag{4.20}$$

Proceeding in a similar way, the eigenfunction $f_{jn}(y)$'s for the surface-piercing porous structure region $j = 5,6,\ n = 0,1,2\ldots$ is given by

$$f_{5n}(y) = \left\{\frac{\cosh\gamma_{5n}(h-y) - G_n\sinh\gamma_{5n}(h-y)}{\cosh\gamma_{5n}h - G_n\sinh\gamma_{5n}h}\right\}, \tag{4.21a}$$

$$f_{6n}(y) = \left\{\frac{(s_2+if_2)(1-G_n\tanh\gamma_{5n}(h-h_1))}{(\cosh\gamma_{5n}h - G_n\sinh\gamma_{5n}h)}\right\}\cosh\gamma_{5n}(h-y) \tag{4.21b}$$

where $$G_n = \frac{\{\varepsilon_2 - (s_2+if_2)\}\tanh\gamma_{5n}(h-h_1)}{\{\varepsilon_2 - (s_2+if_2)\tanh^2\gamma_{5n}(h-h_1)\}}, \tag{4.22}$$

ε_2 is the porosity of the permeable material, s_2 is an inertial coefficient and f_2 is a linearized friction coefficient with γ_{5n} satisfies the dispersion relation is of the form

$$\omega^2(s_2+if_2) - g\gamma_{5n}\tanh\gamma_{5n}h - G_n\left\{\omega^2(s_2+if_2)\tanh\gamma_{5n}h - \gamma_{5n}g\right\} = 0, \tag{4.23}$$

for $n = 0,1,2\ldots$ The eigenfunction $f_{jn}(y)$ in the open water region $j = 1,4,7$ satisfy the orthogonality relation given by

$$\left\langle f_{jm}, f_{jn}\right\rangle_{j=1,4,7} = \begin{cases} 0 & \text{for } m \neq n, \\ \mathrm{C}_n & \text{for } m = n, \end{cases} \tag{4.24}$$

with respect to the orthogonal mode-coupling relation defined by

$$\left\langle f_{jm}, f_{jn}\right\rangle_{j=1,4,7} = \int_0^h f_{jm}(y)f_{jn}(y)dy, \tag{4.25}$$

where $C_n = \left\{\frac{2\gamma_{jn}h + \sinh 2\gamma_{jn}h}{4\gamma_{jn}\cosh^2\gamma_{jn}h}\right\}$ for $n = 0$ with C_n for $n = 1,2,3,\ldots$ are obtained by substituting $\gamma_{jn} = i\gamma_{jn}$.

The orthogonal mode-couplingrelation as in Eq. (4.25) is employed on $\phi_j(x,y)$ and $\phi_{jx}(x,y)$ with the eigenfunction $f_{jm}(y)$ along with continuity of velocity and pressure as in Eq. 4.8(a) across the vertical interface $x=0, 0<y<h$ to obtain

$$\begin{aligned}\left\langle \phi_j(x,y), f_{jm}(y)\right\rangle_{j=1} &= \int_0^h \phi_j(x,y) f_{jm}(y)\,dy \\ &= \int_0^{h_1} \phi_{j+1}(x,y) f_{jm}(y)\,dy + \int_{h_1}^h \phi_{j+2}(x,y) f_{jm}(y)\,dy \text{ for } m=0,1,2,...,\end{aligned} \tag{4.26a}$$

$$\begin{aligned}\left\langle \phi_{jx}(x,y), f_{jm}(y)\right\rangle_{j=1} &= \int_0^h \phi_{jx}(x,y) f_{jm}(y)\,dy \\ &= \int_0^{h_1} \phi_{(j+1)x}(x,y) f_{jm}(y)\,dy + \int_{h_1}^h \phi_{(j+2)x}(x,y) f_{jm}(y)\,dy \text{ for } m=0,1,2,...,\end{aligned} \tag{4.26b}$$

Again, orthogonal mode coupling relation as in Eq. (4.25) is employed on $\phi_j(x,y)$ and $\phi_{jx}(x,y)$ with the eigenfunction $f_{jm}(y)$ along with continuity of velocity and pressure as in Eq. 4.8(b) across the vertical interface $x=-a_1, 0<y<h$ to obtain

$$\begin{aligned}\left\langle \phi_j(x,y), f_{jm}(y)\right\rangle_{j=4} &= \int_0^h \phi_j(x,y) f_{jm}(y)\,dy \\ &= \int_0^{h_1} \phi_{j-2}(x,y) f_{jm}(y)\,dy + \int_{h_1}^h \phi_{j-1}(x,y) f_{jm}(y)\,dy \text{ for } m=0,1,2,...,\end{aligned} \tag{4.27a}$$

$$\begin{aligned}\left\langle \phi_{jx}(x,y), f_{jm}(y)\right\rangle_{j=4} &= \int_0^h \phi_{jx}(x,y) f_{jm}(y)\,dy \\ &= \int_0^{h_1} \phi_{(j-2)x}(x,y) f_{jm}(y)\,dy + \int_{h_1}^h \phi_{(j-1)x}(x,y) f_{jm}(y)\,dy \text{ for } m=0,1,2,...,\end{aligned} \tag{4.27b}$$

4.3.1 Bottom-standing porous structure

In the case of bottom-standing porous structure, the orthogonal mode coupling relation as in Eq. (4.25) is employed on $\phi_j(x,y)$ and $\phi_{jx}(x,y)$ with the eigenfunction $f_{jm}(y)$ along with continuity of velocity and pressure as in Eq. 4.9(a,b) across the vertical interface $x=-a_2, 0<y<h$ to obtain

$$\begin{aligned}\left\langle \phi_j(x,y), f_{jm}(y)\right\rangle_{j=4} &= \int_0^h \phi_j(x,y) f_{jm}(y)\,dy \\ &= \int_0^{h_1} \phi_{j+1}(x,y) f_{jm}(y)\,dy + (s_2+if_2)\int_{h_1}^h \phi_{j+2}(x,y) f_{jm}(y)\,dy \text{ for } m=0,1,2,...,\end{aligned} \tag{4.28a}$$

$$\begin{aligned}\left\langle \phi_{jx}(x,y), f_{jm}(y)\right\rangle_{j=4} &= \int_0^h \phi_{jx}(x,y) f_{jm}(y)\,dy \\ &= \int_0^{h_1} \phi_{(j+1)x}(x,y) f_{jm}(y)\,dy + \varepsilon_2\int_{h_1}^h \phi_{(j+2)x}(x,y) f_{jm}(y)\,dy \text{ for } m=0,1,2,...,\end{aligned} \tag{4.28b}$$

Again, orthogonal mode coupling relation as in Eq. (4.25) is employed on $\phi_j(x,y)$ and $\phi_{jx}(x,y)$ with the eigenfunction $f_{jm}(y)$ along with continuity of velocity and pressure as in Eq. 4.9(c,d) across the vertical interface $x=-a_3, 0<y<h$ to obtain

$$\begin{aligned}\left\langle \phi_j(x,y), f_{jm}(y)\right\rangle_{j=7} &= \int_0^h \phi_j(x,y) f_{jm}(y)\,dy \\ &= \int_0^{h_1} \phi_{j-2}(x,y) f_{jm}(y)\,dy + (s_2+if_2)\int_{h_1}^h \phi_{j-1}(x,y) f_{jm}(y)\,dy \text{ for } m=0,1,2,...,\end{aligned} \tag{4.29a}$$

$$\begin{aligned}\left\langle \phi_{jx}(x,y), f_{jm}(y)\right\rangle_{j=7} &= \int_0^h \phi_{jx}(x,y) f_{jm}(y)\,dy \\ &= \int_0^{h_1} \phi_{(j-2)x}(x,y) f_{jm}(y)\,dy + \varepsilon_2\int_{h_1}^h \phi_{(j-1)x}(x,y) f_{jm}(y)\,dy \text{ for } m=0,1,2,...,\end{aligned} \tag{4.29b}$$

The infinite sums presented in the Eqs. (4.26a,b)-(4.27a,b) and Eq. (4.28a,b)-(4.29a,b) are truncated upto finite M terms to obtain a linear system of $8(M+1)$ algebraic equation for the determination of $8(M+1)$ unknowns and the wave reflection and transmission due to the combined submerged plate and bottom-standing porous structure are obtained as

$$K_r = \left|\frac{R_{10}}{I_{10}}\right| \quad \text{and} \quad K_t = \left|\frac{T_{70}}{I_{10}}\right|. \tag{4.30a}$$

Due the existence of porous blocks the energy dissipation in the wave propagation through the porous blocks as in Chwang and Chan (1998) is represented as

$$K_d = 1 - K_r^2 - K_t^2. \tag{4.30b}$$

4.3.2 Surface-piercing porous structure

In the case of surface-piercing porous structure, the orthogonal mode-coupling relation as in Eq. (4.25) is employed on $\phi_j(x,y)$ and $\phi_{jx}(x,y)$ with the eigenfunction $f_{jm}(y)$ along with continuity of velocity and pressure as in Eq. 4.10(a,b) across the vertical interface $x=-a_2, 0<y<h$ to obtain

$$\begin{aligned}\left\langle \phi_j(x,y), f_{jm}(y)\right\rangle_{j=4} &= \int_0^h \phi_j(x,y) f_{jm}(y)\,dy \\ &= (s_2+if_2)\int_0^{h_1}\phi_{j+1}(x,y) f_{jm}(y)\,dy + \int_{h_1}^h \phi_{j+2}(x,y) f_{jm}(y)\,dy \text{ for } m=0,1,2,...,\end{aligned} \tag{4.31a}$$

$$\begin{aligned}\left\langle \phi_{jx}(x,y), f_{jm}(y)\right\rangle_{j=4} &= \int_0^h \phi_{jx}(x,y) f_{jm}(y)\,dy \\ &= \varepsilon_2\int_0^{h_1}\phi_{(j+1)x}(x,y) f_{jm}(y)\,dy + \int_{h_1}^h \phi_{(j+2)x}(x,y) f_{jm}(y)\,dy \text{ for } m=0,1,2,...,\end{aligned} \tag{4.31b}$$

Again, orthogonal mode-coupling relation as in Eq. (4.25) is employed on $\phi_j(x,y)$ and $\phi_{jx}(x,y)$ with the eigenfunction $f_{jm}(y)$ along with continuity of velocity and pressure as in Eq. 4.10(c,d) across the vertical interface $x=-a_3, 0<y<h$ to obtain

$$\begin{aligned}\left\langle \phi_j(x,y), f_{jm}(y)\right\rangle_{j=7} &= \int_0^h \phi_j(x,y) f_{jm}(y)\,dy \\ &= (s_2+if_2)\int_0^{h_1}\phi_{j-2}(x,y) f_{jm}(y)\,dy + \int_{h_1}^h \phi_{j-1}(x,y) f_{jm}(y)\,dy \text{ for } m=0,1,2,...,\end{aligned} \tag{4.32a}$$

$$\begin{aligned}\left\langle \phi_{jx}(x,y), f_{jm}(y)\right\rangle_{j=7} &= \int_0^h \phi_{jx}(x,y) f_{jm}(y)\,dy \\ &= \varepsilon_2\int_0^{h_1}\phi_{(j-2)x}(x,y) f_{jm}(y)\,dy + \int_{h_1}^h \phi_{(j-1)x}(x,y) f_{jm}(y)\,dy \text{ for } m=0,1,2,...,\end{aligned} \tag{4.32b}$$

The infinite sums presented in the Eqs. (4.26a,b)-(4.27a,b) and Eq. (4.31a,b)-(4.32a,b) are truncated upto finite M terms to obtain a linear system of $8(M+1)$ algebraic equation for the determination of $8(M+1)$ unknowns and the wave reflection and transmission due to the combined submerged plate and surface-piercing porous structure are obtained as in Eq. 4.30(a,b).

4.3.3 Wave force on the porous structure

The wave force acting at the front and back of the bottom-standing and surface-piercing porous structure is given by

$$K_{fs_1} = \frac{F_{front}}{2\rho g I_{10} h} \quad \text{and} \quad K_{fs_2} = \frac{F_{back}}{2\rho g I_{10} h}, \tag{4.33a}$$

where $F_{front} = i\rho\omega\int_{h_1}^{h}(\phi_6 - \phi_4)dy$ at $x = -a_2$ for bottom-standing porous structure. (4.33b)

$F_{back} = i\rho\omega\int_{h_1}^{h}(\phi_6 - \phi_7)dy$ at $x = -a_3$ for bottom-standing porous structure. (4.33c)

$F_{front} = i\rho\omega\int_{0}^{h_1}(\phi_5 - \phi_4)dy$ at $x = -a_2$ for surface-piercing porous structure. (4.33d)

$F_{back} = i\rho\omega\int_{0}^{h_1}(\phi_5 - \phi_7)dy$ at $x = -a_3$ for surface-piercing porous structure. (4.33e)

4.3.4 Surface displacement

The surface defection $\eta_j(x)$ is given by

$$\eta_j(x) = \left(-\frac{1}{i\omega}\right)\phi_{jy}(x) \text{ on } y = 0 \quad \text{for } j = 1, 4, 7. \tag{4.34}$$

4.4 RESULTS AND DISCUSSION

The numerical investigation for the two different configurations of porous structures combined with submerged plate is conducted to determine the wave transformation characteristics considering various values of porosity of the submerged porous structure, angle of incidence θ, submergence depth of plate h_1 / h and plate length a / h. The wave reflection coefficient K_r, transmission coefficient K_t, energy dissipation K_d, wave force on the front side of porous structure K_{fs_1} and back side of porous structure K_{fs_2} along with surface displacements $\eta_j(x)$ are plotted to examine the efficiency of these configurations. The parameters that are kept constant during the numerical modelling are $\rho = 1025$ kg/m^3 and $g = 9.8$ m/s^2.

4.4.1 Validation of the Numerical Model

In Fig. 4.2, the numerical results obtained for a single submerged horizontal porous plate is validated with the result obtained by Liu and Li (2011) and Cho and Kim (2013). The reflection coefficient K_r is plotted against the non-dimensional wave number $\gamma_{10}h$ for a submerged

porous plate considering $h_1 / h = 0.2$ and $a / h = 1.0$ is compared with the theoretical results of Liu and Li (2011). It is observed that an acceptable comparison of the result is obtained for the wave interaction with submerged porous plate. Further, the transmission coefficient K_t is compared with the results as in Cho and Kim (2013) and the comparison between the result is noted to be acceptable. The experimental results of Cho and Kim (2013) support the findings of the systematic parametric study, which shows that there is an optimal porosity near $\varepsilon_1 = 0.1$ and an optimal submergence depth within $0.05 < h_1 / h < 0.1$. The study noted that as the porosity exceeds $\varepsilon_1 = 0.1$, then the performance decreases. Further, as the plate width increases, the performance improves, especially in the long-wave regime. In the context of linear potential theory, Liu and Li (2011) given an alternative analytical solution for water wave problems that does not require the complex roots of the wave dispersion relation and the identical results are obtained after the convergence test with the right number of evanescent waves.

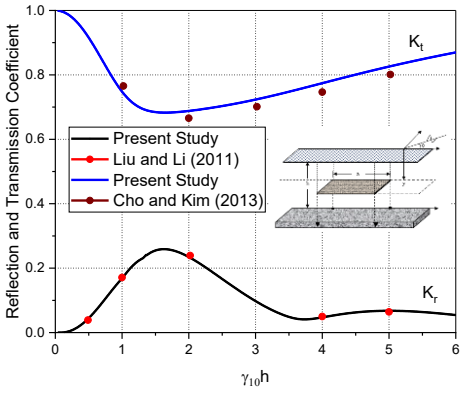

Fig. 4.2: Comparative study on K_r and K_t due to submerged porous plate with Liu and Li (2011) and Cho and Kim (2013).

The K_r and K_t for the submerged porous plate as in Liu and Li (2011) and Cho and Kim (2013) compared with the present study is presented in Table 4.1. The comparative study for the reflection coefficient shows that the numerical result obtained using the present approach coincide with the result obtained by Liu and Li (2011). The K_r is noted to be maximum within $1.2 < \gamma_{10} h < 1.6$ and thereafter decreases and approaches to minimum. Further, a good agreement of the numerical result as in the present study with Cho and Kim (2013). An opposite trend in the transmission coefficient is noted within $1.2 < \gamma_{10} h < 1.6$.

Table 4.1: Comparison of K_r and K_t for wave interaction with submerged porous plate.

Wave number	Submerged porous plate Liu and Li, (2011) and Cho and Kim, (2013)		Submerged porous plate (Present Method)	
$\gamma_{10}h$	K_r	K_t	K_r	K_t
1.0	0.17102	0.76541	0.16821	0.75276
2.0	0.23912	0.65541	0.23461	0.66802
3.0	0.09624	0.70125	0.09777	0.71333
4.0	0.04988	0.74641	0.04715	0.75420
5.0	0.06416	0.80115	0.06766	0.81574

The convergence study in K_r and K_t due to the increasing number of evanescent wave modes M is performed for submerged porous plate combined with bottom-standing and surface-piercing structure. The numerical results obtained are tabulated in Table 4.2. It can be observed that with the increase in the number of evanescent wave modes $M \geq 10,$ the convergence in the wave reflection and transmission coefficient is evident.

Table 4.2: Convergence of K_r and K_t for submerged porous plate combined with bottom-standing and surface-piercing structure considering $\gamma_{10}h = 3.0,\ \varepsilon_2 = 0.4$ and $\theta = 30^0.$

Evanescent wave modes	Submerged porous plate with bottom-standing structure		Submerged porous plate with surface-piercing structure	
M	K_r	K_t	K_r	K_t
0	0.18621	0.72836	0.95892	0.11694
1	0.18947	0.72932	0.95948	0.11860
5	0.19463	0.73068	0.96036	0.12037
10	0.19833	0.73672	0.96531	0.12232
15	0.19845	0.73646	0.96555	0.12266

4.4.2 Submerged porous plate backed by a bottom-standing porous structure

In this section, the wave attenuation due to a submerged horizontal plate and a bottom-standing porous structure is studied and the wave reflection, transmission and dissipation coefficients

along with the wave force on the structure is analysed to understand the effectiveness of the combined structure.

4.4.2.1 Wave reflection, transmission and dissipation coefficient

The wave transformation due to the submerged porous plate backed by a bottom-standing porous structure is analysed and the hydrodynamic performance of the composite breakwater are discussed considering the effect of structural porosity, submergence depth of horizontal porous plate, angle of incidence, plate length, width of bottom standing submerged porous structure and distance between porous plate and bottom-standing porous structure.

4.4.2.1.1 Effect of structural porosity of the submerged structure

The structural porosity plays a major role in the wave reflection, transmission and wave energy damping. In most of the cases, as the porosity of the structure increases, a decreasing trend in wave reflection is observed which may be due to the enhanced wave transmission that results due to the increased porosity.

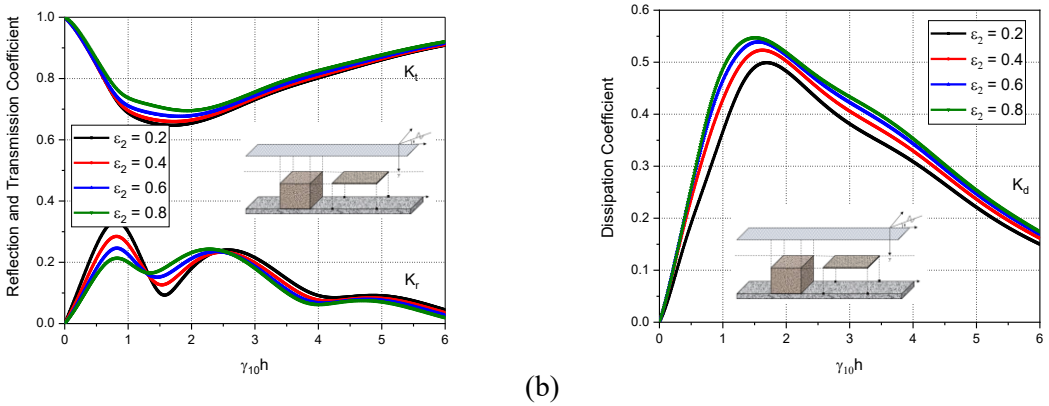

(a) (b)

Fig. 4.3: Variation in (a) K_r and K_t and (b) K_d versus $\gamma_{10}h$ for different values of porosity considering $h_1/h = 0$ and $\theta = 30^0$.

In Fig. 4.3(a,b), the structural porosity is varied within $0.2 < \varepsilon_2 < 0.8$ for the determination of K_r, K_t and K_d against the non-dimensional wave number $\gamma_{10}h$ considering $h_1/h = 0$ and $\theta = 30^0$. It is observed that, as the wave number increases, K_r shows an oscillating pattern up to $\gamma_{10}h = 2.5$ and then K_r decreases. There is a sudden increase in K_r within $0.01 < \gamma_{10}h < 0.75$ for all values of porosity within $0.2 < \varepsilon_2 < 0.8$. It is also noted that with the increase in porosity,

the K_r decreases (Fig. 4.3a). An opposite trend is observed in the case of transmission coefficient K_t as it increases with increase in structural porosity. This may be due to the fact that, as the porosity increases, more water is allowed to pass through the structure hence decreasing the reflection and increasing the transmission. Similarly, there is a sharp reduction in the K_r value within $0.01 < \gamma_{10}h < 0.75$ for all values of porosity within $0.2 < \varepsilon_2 < 0.8$. Also, an increase in K_t can be observed after $\gamma_{10}h = 2$ (Fig. 4.3a). The decrease in the K_r due to increase in porosity may be due to increase in energy dissipation K_d as seen in Fig. 4.3(b). A decreasing trend in wave reflection is observed as the structure's porosity increases, which could be due to the increased wave transmission caused by the increased porosity.

4.4.2.1.2 Effect of submergence depth of horizontal porous plate

The depth of submergence of porous plate demonstrates a reasonable effect in the pattern of wave reflection, transmission and dissipation of wave energy. As the depth of submergence of plate increases, the wave reflection may get reduce as it enhances more waves to pass through the gap that creates on the upper and lower sides of the porous plates.

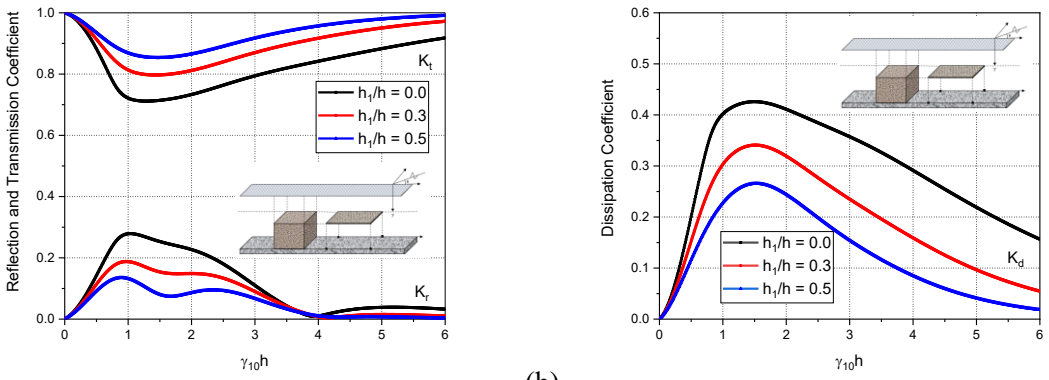

(a) (b)

Fig. 4.4: Variation in (a) K_r and K_t and (b) K_d versus $\gamma_{10}h$ for different values of submergence depth considering $\theta = 30^0$ and $\varepsilon_2 = 0.3$.

In Fig. 4.4(a,b), the reflection, transmission and dissipation coefficients are plotted against the non-dimensional wave number $\gamma_{10}h$ for different values of submergence depth h_1 / h considering angle of incidence $\theta = 30^0$ and structural porosity $\varepsilon_2 = 0.3$. It is noted that as the submerged depth increases the K_r value decreases (Fig. 4.4a), but the transmission coefficient is increasing for higher values of submergence. As wavenumber increases, reflection

coefficient increases up to $\gamma_{10}h=1$ and then decreases. On the other hand, K_t decreases up to $\gamma_{10}h=1.25$ and then beyond that value K_t increase. This suggests that with the increase in the non-dimensional wave number $\gamma_{10}h$, the wavelength of the incident wave decreases and as a result, wave reflection decreases as the plate submergence depth increases. Further, the wave dissipation (Fig. 4.4b) decreases as the plate submergence depth increases, which may be due to the passage of more waves above and below the plate.

4.4.2.1.3 Effect of angle of incidence

The angle of wave incidence on a coastal structure is critical because it influences wave energy dissipation. The wave reflection from the porous structure increases as the incident wave angle increases, whereas the wave transmission decreases as the incident wave angle increases. In Fig. 4.5(a,b), the reflection, transmission and dissipation coefficients are plotted against the angle of incidence θ for different porosity ranging within $0.2<\varepsilon_2<0.8$.

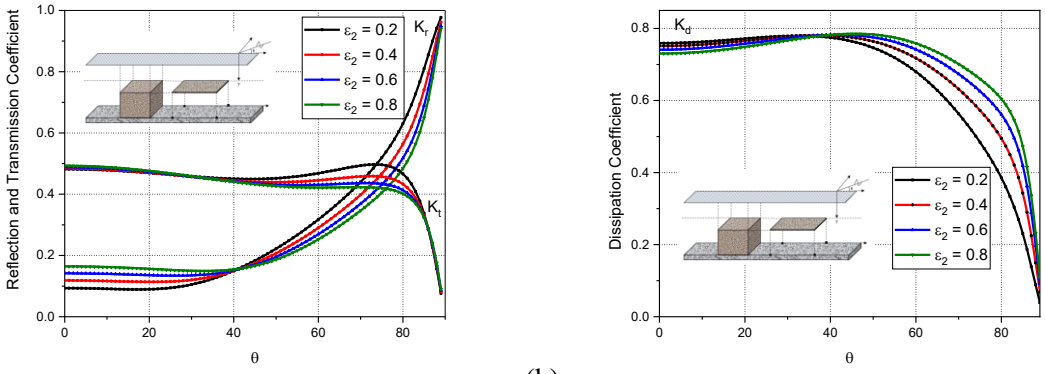

(a) (b)

Fig. 4.5: Variation in (a) K_r and K_t and (c) K_d versus θ for different values of porosity considering $a/h=2.0$ and $h_1/h=0.$

In Fig. 4.5(a), it is observed that reflection coefficient is constant up to an angle of incidence of 40^0 and then it increases up to 90^0. It is also seen that the K_r value slightly higher for higher porosity up to 40^0. After 40^0, K_r decreases as structural porosity increases. A sudden transformation of K_t (Fig.4.5a) is noticed at $\theta=78^0$ for different porosities. The maximum value of K_t is observed at $\theta=78^0$ for structural porosity $\varepsilon_2=0.2$. This angle is called the critical angle which is the same for all the porosities. In Fig. 4.5(b), it is evident that the wave energy dissipation K_d is higher for $\theta<40^0$ and then it starts decreasing beyond $\theta=40^0$. The

wave reflection is observed to be decreasing with the increase of porosity of the structure and it may be due to the enhanced wave structure interaction that resulted from the presence of more pore spaces inside the structure.

4.4.2.1.4 Effect of plate length

The plate length is observed to influence the wave energy dissipation. In general, the plate with longer dimensions is observed to be dissipating wave energy efficiently than small plates. Fig. 4.6(a,b) shows the reflection, transmission and dissipation coefficient against non-dimensional wave number $\gamma_{10}h$ for various values of plate length a/h considering structural porosity $\varepsilon_2 = 0.3$ and angle of incidence $\theta = 30^0$. In Fig. 4.6(a), high oscillating pattern is observed in case of reflection coefficient within $0.3 < \gamma_{10}h < 6$ for all values of plate length within $2.0 < a/h < 3.5$. It is evident from Fig. 4.6(a) that there is a decrease in K_t as the plate length increases. However, K_t value decreases within $0.01 < \gamma_{10}h < 1$ for all values of plate length within $2.0 < a/h < 3.5$ and then increases beyond $\gamma_{10}h = 1$. The energy dissipation increases as the plate length increases (Fig. 4.6b). This could be due to the dissipation of more wave energy along the length of the plate, with only a small amount reaching the leeward side. With an increase in plate length, the incoming waves exposed to greater surface area can result in higher wave energy dissipation.

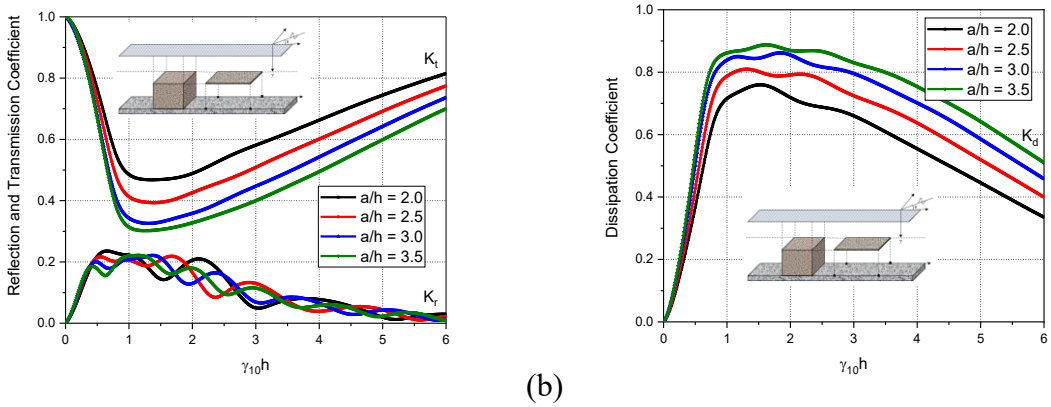

(a) (b)

Fig. 4.6: Variation in (a) K_r and K_t and (c) K_d versus $\gamma_{10}h$ for different values of plate length considering $\theta = 30^0$, $\varepsilon_2 = 0.3$ and $h_1/h = 0$.

4.4.2.1.5 Effect of width of submerged porous structure

The wave transformation caused by a porous structure is found to be strongly influenced by the structure's broadness, as changes in width or thickness directly affect the number of pores

that can fit inside the structure. Fig. 4.7(a,b) shows the K_r, K_t and K_d against width of the bottom standing porous structure w/h for various values angle of incidence within $0^0 < \theta < 60^0$. In Fig. 4.7(a), it is observed that a resonating trend is shown by reflection coefficient as the width of the structure increases. It is evident that K_r increases as the angle of incidence increases. As the width of the bottom standing porous structure w/h increases, the resonating crest and trough decreases. This may be because most of the wave energy gets trapped within the porous structure. The transmission coefficient K_t (Fig. 4.7a) decreases as the width of the structure w/h increases. It is also observed that there is a slight decrease in the K_t value as the angle of incidence increases. Further, from Fig. 4.7(b), it can be understood that the dissipation coefficient K_d increases as w/h increases. And we can also observe that the energy dissipation is slightly higher for $\theta = 45^0$. The trapping of wave energy within the porous structure could explain the resonating trend in wave reflection. The wave transmission is observed to decrease as the width of the structure increases. This could be because as the width of the structure increases, more pore spaces are created inside the structure, allowing more waves to pass through the structure easily.

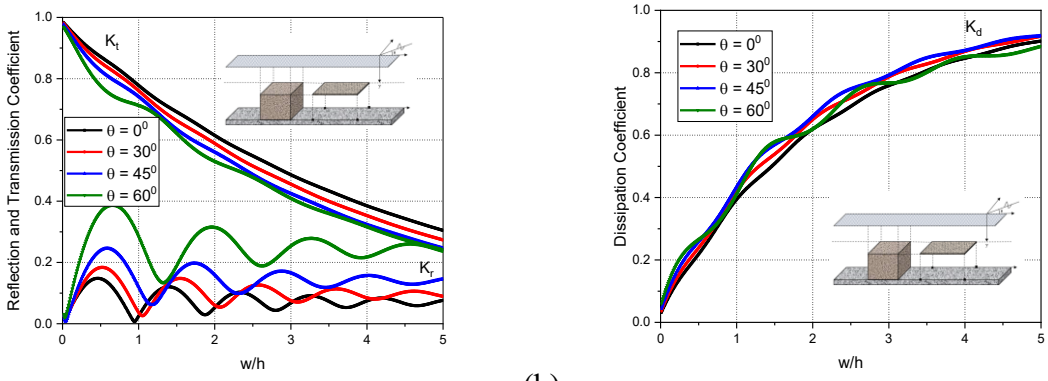

(a) (b)

Fig. 4.7: Variation in (a) K_r and K_t and (c) K_d versus w/h for different values of angle of incidence considering $\varepsilon_2 = 0.3$ and $h_1/h = 0$.

4.4.2.1.6 Effect of distance between porous plate and bottom-standing porous structure

In the case of multiple porous structures as breakwater, the gap between them is extremely useful in dissipating wave energy. The space between these structures can act as a captive area for incident waves, resulting in increased wave structure interaction and efficient wave energy damping. In Fig. 4.8(a,b), the hydrodynamic coefficients K_r, K_t and K_d are plotted against

the distance between the horizontal plate and submerged porous structure L/h for different values of structural porosity within $0.2 < \varepsilon_2 < 0.8$. In Fig. 4.8(a), a resonating trend is observed in K_r as L/h increases. The local maxima in the reflection coefficient K_r may be due to the constructive interference of the incident and reflected waves and the local minima in the reflection coefficient K_r may be due to the destructive interferences of incident and reflected waves. Similar resonating trend is observed in case of K_t (Fig. 4.8a). This may be mainly because of the wave trapping between the confined spacing between the submerged porous plate and bottom standing porous structure. The minimum resonating trough of K_r is obtained for $\varepsilon_2 = 0.6$ and the minimum resonating trough for K_t is obtained for $\varepsilon_2 = 0.2$. The oscillating trend repeats after every L/h ratio of 3.5. Further, the oscillating trend is noted in wave dissipation (Fig. 4.8b) which may be due to the trapping of waves between the confined spacing between the submerged porous plate and bottom-standing porous structure.

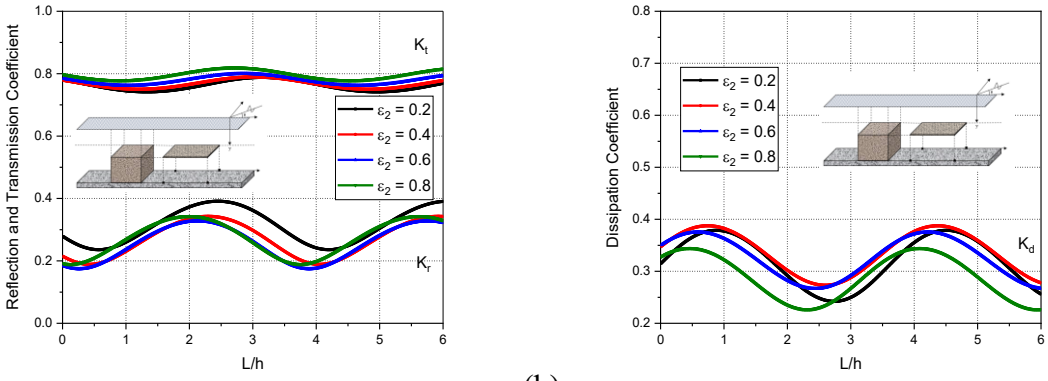

(a) (b)

Fig. 4.8: Variation in (a) K_r and K_t and (c) K_d versus L/h for different values of structural porosity considering $\theta = 30^0$ and $h_1/h = 0$.

4.4.2.2 Wave force on the structure

The wave forces acting on the front and back side of the porous structure is analysed and the effect of porosity, submergence depth of horizontal porous plate, angle of incidence, plate length, width of bottom standing submerged porous structure, distance between submerged plate and bottom-standing structure are investigated.

4.4.2.2.1 Effect of submergence depth of horizontal porous plate

The wave force shows reasonable effect with the increase in the depth of submergence of porous plates. As the depth of submergence of the plate increases, the wave reflection may

decrease as the wave interaction with the submerged porous plate improves, resulting in higher wave forces. Fig.4.9(a,b) shows the wave force on the front K_{fs_1} and back K_{fs_2} of the bottom standing submerged porous structure plotted against the non-dimensional wave number $\gamma_{10}h$ for various values of submergence depth of plate h_1/h. In Fig. 4.9(a,b), it is evident that the wave force on the front and back of the structure increases with increase in the submergence depth. This is because as the submergence depth of plate increases, more amount of wave energy will be allowed to pass above and below the plate hence the wave force on the structure increases. It is also observed that the wave force at the front of the structure is slightly higher than the wave force at the back of the structure. The increase in wave force as the depth of submergence of the plate increases could be due to the fact that as the depth of submergence increases, more of the wave passes through the gap present in the below and above regions of the plate, causing increased wave interaction with the pores.

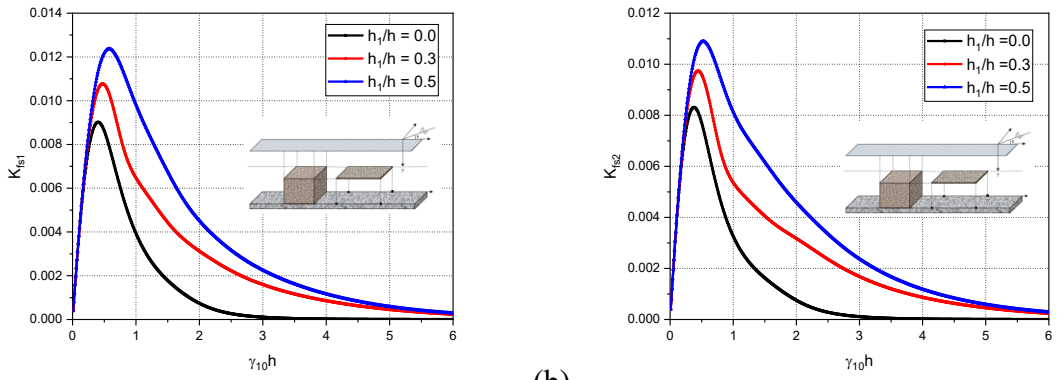

(a) (b)

Fig. 4.9: Variation in (a) K_{fs_1} and (b) K_{fs_2} versus $\gamma_{10}h$ for different values of submergence depth considering $\theta = 30^0$ and $\varepsilon_2 = 0.3$.

4.4.2.2.2 Effect of width of bottom standing submerged porous structure

The width of the porous structure can have a significant impact on the wave forces acting on the structure. The width of the porous structure can affect the wave forces as it can incorporate more void spaces inside and also provide a large surface area for the waves to interact. The wave force on the front K_{fs_1} and back K_{fs_2} of the bottom standing submerged porous structure are plotted against the width of the bottom standing porous structure w/h in Fig. 4.10(a,b) for different values of structural porosity varying within $0.2 < \varepsilon_2 < 0.8$. In Fig. 4.10(a), it is observed that the wave force of the front of the structure K_{fs_1} first decreases and then increases to a peak value and then again decreases. The resonating nature gradually subsides as the width

of the submerged porous structure increases. This may be because of the wave trapping between the plate and the porous structure. Greater the structural width lesser will be the wave force.

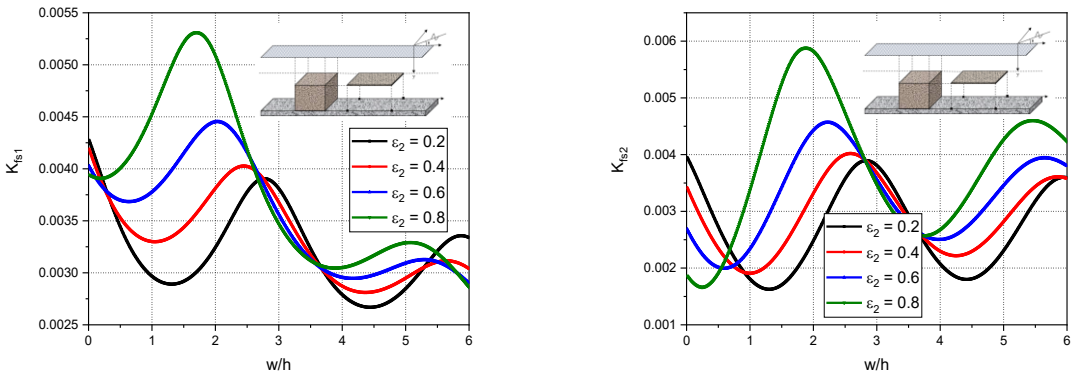

(a) (b)

Fig. 4.10: Variation in (a) K_{fs_1} and (b) K_{fs_2} versus w/h for different values of structural porosity considering $\theta = 30^0$ and $h_1/h = 0$.

In Fig. 4.10(b), the wave force on the back of the structure K_{fs_2} shows an oscillating pattern. It is seen that the K_{fs_2} increases as structural porosity increases. The maxima and minima of K_{fs_2} gradually reduces as the structural width increases. This may be due to the energy dissipation within the submerged porous structure. The oscillating trend in K_{fs_1} may be due to the wave trapping between the plate and the porous structure.

4.4.2.3 Surface displacement

The effect of angle of incidence on the surface displacement is analysed and the change in surface displacement in the incident and transmitted regions are discussed.

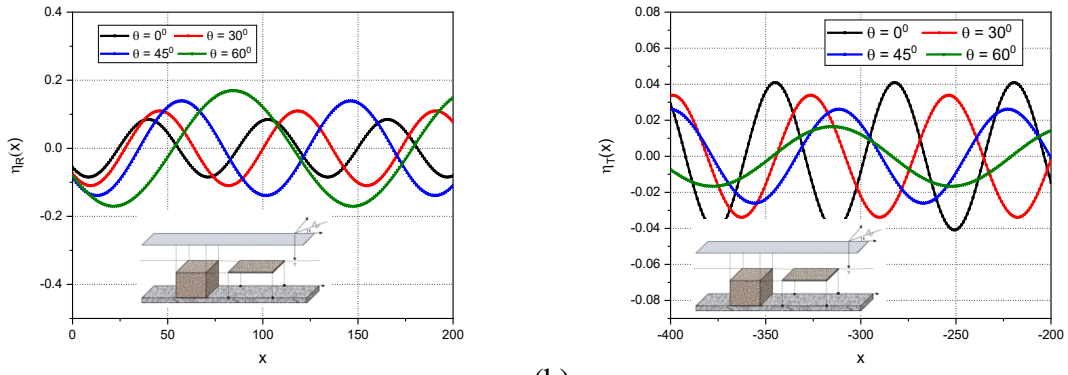

(a) (b)

Fig. 4.11: Variation in (a) $\eta_I(x)$ and (b) $\eta_T(x)$ versus x for different values of angle of incidence considering $\varepsilon_2 = 0.3$, $h_1/h = 0$ and $a/h = 2.0$.

In Fig. 4.11(a,b), the surface displacement in the incident $\eta_I(x)$ and transmitted $\eta_T(x)$ region is plotted against the distance x for various values of angle of incidence θ. In Fig. 4.11(a), it is observed that with the increase in the angle of incidence the surface elevation in the incident region increases due to which there is a shift in the phase of the incident waves. On the other hand, in Fig. 4.11(b), the surface deflection is noted lower than that of incident wave region. Further, as the angle of incidence increases, a reduction in the surface displacement in the transmitted region is observed.

4.4.3 Submerged porous plate backed by a surface-piercing porous structure

In the present section, the wave attenuation due to a submerged horizontal plate backed by a surface-piercing porous structure is performed and the detailed analysis on the hydrodynamic characteristics along with the wave force on the structure and the surface displacement in the incident and transmitted region due to the presence of the composite structure is presented.

4.4.3.1 Reflection, Transmission and Dissipation Coefficient

The wave reflection, transmission and dissipation coefficient are analysed considering the effect of structural porosity, submergence depth of horizontal porous plate, angle of incidence, plate length, width of bottom standing submerged porous structure and distance between porous plate and surface-piercing porous structure.

4.4.3.1.1 Effect of structural porosity of surface piercing porous structure

The porosity of structure is an important parameter that is considered for the designing of a breakwater system. In Fig. 4.12(a,b), the wave hydrodynamic coefficients K_r, K_t and K_d are plotted against the non-dimensional wave number $\gamma_{10}h$ for different values of structural porosity. In Fig. 4.12(a), it is observed that the K_r decreases as porosity increases within $0.2 < \varepsilon_2 < 0.8$. Further, the transmission coefficient K_t (Fig. 4.12a) initially decreases then increases and then again decreases within $0.01 < \gamma_{10}h < 1$ for all values of structural porosity. It is evident that transmission coefficient is higher for higher structural porosity. The increase in wave reflection could be due to the fact that as porosity increases, more waves are transmitted to the leeward side, reducing the reflection coefficient. In Fig. 12(b), the dissipation coefficient K_d increases within $0.01 < \gamma_{10}h < 1$ and then decreases for porosity within $0.2 < \varepsilon_2 < 0.8$. Furthermore, higher structural porosity results in the greatest dissipation of wave energy which

may be due to the enhanced wave structure interaction that result from the higher number of pore spaces inside the structure.

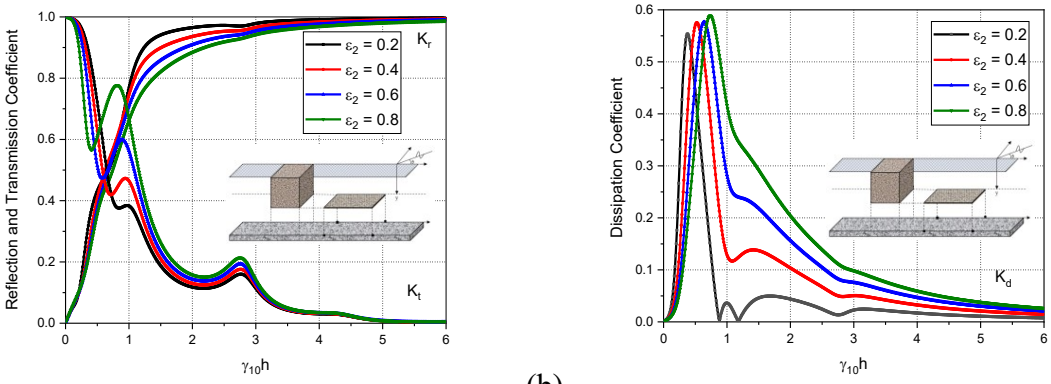

(a) (b)

Fig. 4.12: Variation in (a) K_r and K_t and (b) K_d versus $\gamma_{10}h$ for different values of structural porosity considering $\theta = 30^0$ and $h_1 / h = 0$.

4.4.3.1.2 Effect of submergence depth of horizontal porous plate

Fig. 4.13(a,b) shows the reflection K_r, transmission K_t and dissipation coefficients K_d plotted against the width of surface piercing porous structure w/h for different values of submergence depth of plate h_1 / h.

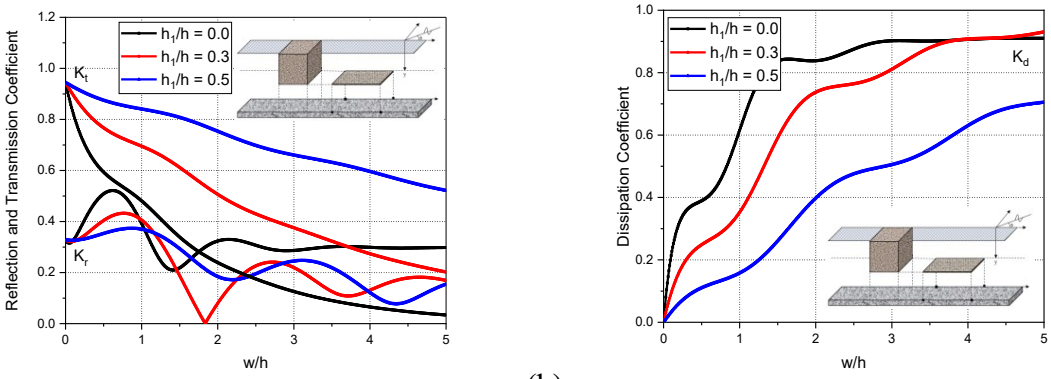

(a) (b)

Fig. 4.13: Variation in (a) K_r and K_t and (b) K_d versus w/h for different values of submergence depth of plate h_1 / h considering $\varepsilon_2 = 0.3$ and $\theta = 30^0$.

In Fig. 4.13(a), it is observed that K_r decreases as the submergence depth h_1 / h increases. This may be due to the fact that, as h_1 / h increases, more waves can pass above and below the plate which reduces the reflection. It is seen that K_r shows a resonating pattern initially which

gradually diminishes as the width of the structure increases. For $h_1/h=0$, K_r becomes constant beyond $w/h=3$. On the other hand, the K_t increases as h_1/h increases. It is also observed that K_t decreases as the width of the structure increases. The wave energy dissipation is maximum when the plate is kept on the water surface level ($h_1/h=0$). As the plate submergence h_1/h increases, K_d decreases (Fig. 4.13b). This could be due to the fact that as the submergence depth increases, more water can pass through the gap, increasing the transmission rate, but when the plate is kept closer to the water surface, wave transmission through the gap between plate and water surface decreases, resulting in higher energy damping due to the vigorous agitation of water particles at the wave entry point.

4.4.3.1.3 Effect of angle of incidence

In Fig. 4.14(a,b), the reflection K_r, transmission K_t and dissipation coefficients K_d are plotted against the angle of incidence θ for different values of structural porosity within $0.2<\varepsilon_2<0.8$. In Fig. 4.14(a), it is observed that the reflection coefficient is almost constant up to $\theta=40^0$ and then increases. It is also seen that K_r decreases as the porosity increases up to $\theta=40^0$ and then remains almost uniform for all values of porosity. It is observed that K_t (Fig. 4.14a) decreases as angle of incidence increases. This may be because at lower incident angles the waves pass easily when compared to higher incident angles. The transmission coefficient K_t increases as the structural porosity increases.

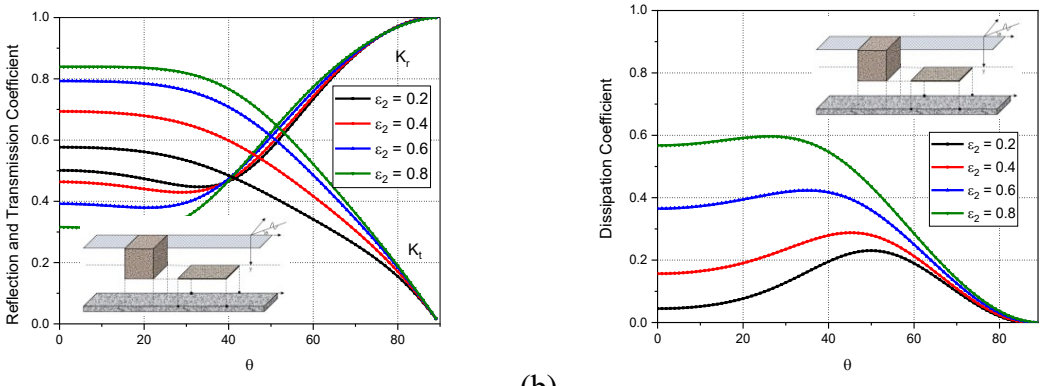

(a) (b)

Fig. 4.14: Variation in (a) K_r and K_t and (b) K_d versus θ for different values of structural porosity considering $h_1/h=0$ and $\theta=30^0$.

In Fig. 4.14(b), it is observed that the wave energy dissipation K_d first increases and then decreases as the angle of incidence θ increases. For $\varepsilon_2=0.2$, K_d increases up to $\theta=45^0$ and

then decreases. This may be because beyond $\theta = 45^0$, the only a small number of waves may be transmitted and majority of waves may be reflected. As result, the energy dissipation decreases. The study noted that, as the angle of incidence exceeds $\theta = 70^0$, the wave reflection is observed to be converging to the higher values for all the cases of porosity. The minimum wave reflection is observed in the range of $20^0 < \theta < 40^0$. The minimum wave reflection which is also the critical angle is important in terms of designing a coastal defence structure. In addition, the transmission is higher for high structural porosity attributed to increased number of pore spaces inside the structure.

4.4.3.1.4 Effect of width of surface-piercing porous structure

Fig. 4.15(a,b) shows the reflection K_r, transmission K_t and dissipation K_d coefficients plotted against the width of the surface piercing porous structure w/h for different values of angle of incidence θ. In Fig. 4.15(a), it is observed that as the width of the porous structure increases, K_r first decreases up to $w/h = 0.4$ and then increases up to $w/h = 2.5$ after which K_r remains constant. Further, the K_t decreases as the width of the structure increases. The dissipation coefficient K_d (Fig. 4.15b) as w/h increases and then remains constant after a certain width. This could be due to the fact that, as the width is reduced, the reflection coefficient is less and the transmission coefficient is higher. The reflection of the wave increases with the width of the structure up to a certain point, then remains constant as the wave energy dissipates with the width of the structure.

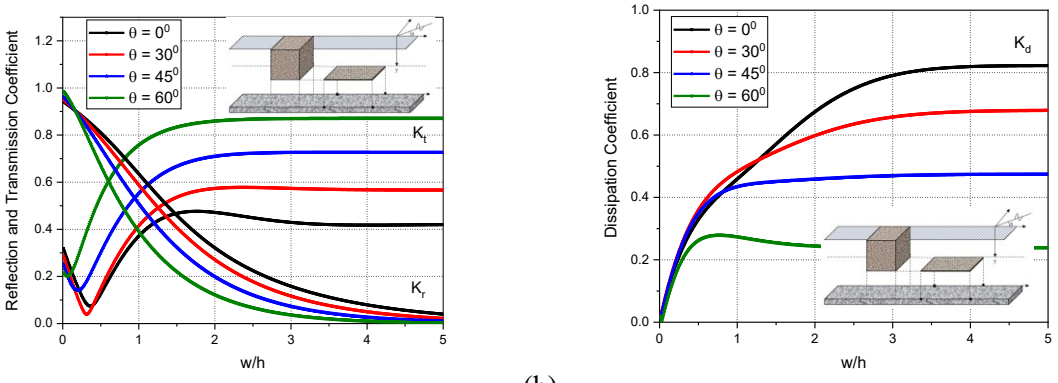

(a) (b)

Fig. 4.15: Variation in (a) K_r and K_t and (b) K_d versus w/h for different values of angle of incidence θ considering $\varepsilon_2 = 0.3$ and $h_1/h = 0$.

4.4.3.1.5 Effect of distance between the submerged plate and surface-piercing structure

In Fig. 4.16(a,b), the reflection K_r, transmission K_t and dissipation K_d coefficients are plotted against the distance between the submerged porous plate and surface-piercing porous structure L/h for different values of angle of incidence θ. In Fig. 4.16(a), it is observed that the K_r value shows a resonating trend as L/h increases. The reason for the resonating trend may be the constructive and destructive interferences due to the incident and reflected waves. It is also seen the reflection coefficient is higher for higher angle of incidence. The K_t shows an oscillating pattern as L/h increases. The local maxima and minima reduce as the angle of incidence increases. This could be due to incident waves being trapped between the submerged porous plate and the surface piercing porous structure in a confined region. Further, a similar oscillating trend as K_d (Fig. 4.16b) is observed with the increasing in L/h.

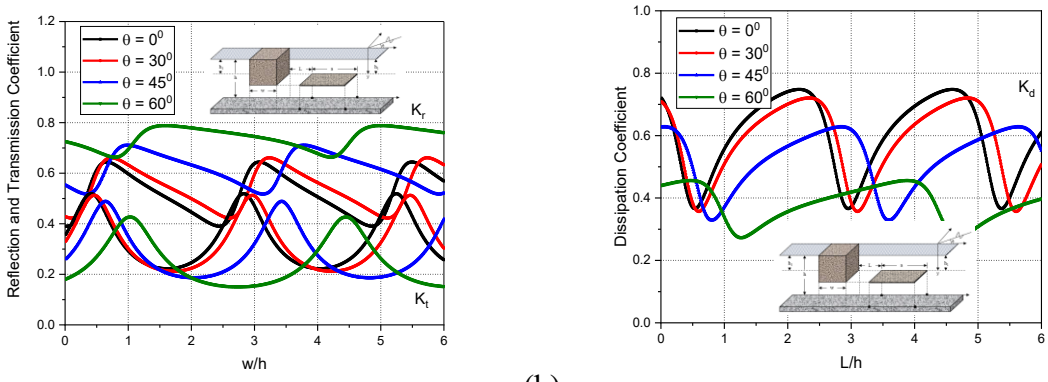

(a) (b)

Fig. 4.16: Variation in (a) K_r and K_t and (b) K_d versus L/h for different values of angle of incidence θ considering $\varepsilon_2 = 0.3$ and $h_1/h = 0$.

4.4.3.2 Wave force on the structure

The wave force on the front and the back side of the surface-piercing porous structure is analysed for the effect of structural porosity, submergence depth of plate, angle of incidence, plate length and width of the porous structure.

4.4.3.2.1 Effect of submergence depth of horizontal porous plate

The wave force on the front K_{fs_1} and back K_{fs_2} of the surface-piercing submerged porous structure is plotted against the non-dimensional wave number $\gamma_{10}h$ (Fig. 4.17a,b) for various

values of submergence depth of plate h_1 / h. The waves with shorter wavelengths are observed to impart lesser wave force on the surface piercing submerged porous structure in both front and back sides. In Fig. 4.17(a), it is observed that the wave force on the front of the porous structure K_{fs_1} decreases with increase in submergence depth h_1 / h. This could be due to the fact that, as h_1 / h increases, the wave energy dissipation by the plate increases, so only a small portion of the wave reaches the porous structure, reducing the impact. In Fig. 4.17(b), it is evident that the wave force on the back of the porous structure K_{fs_2} is less than the wave force on the front of the porous structure K_{fs_1}.

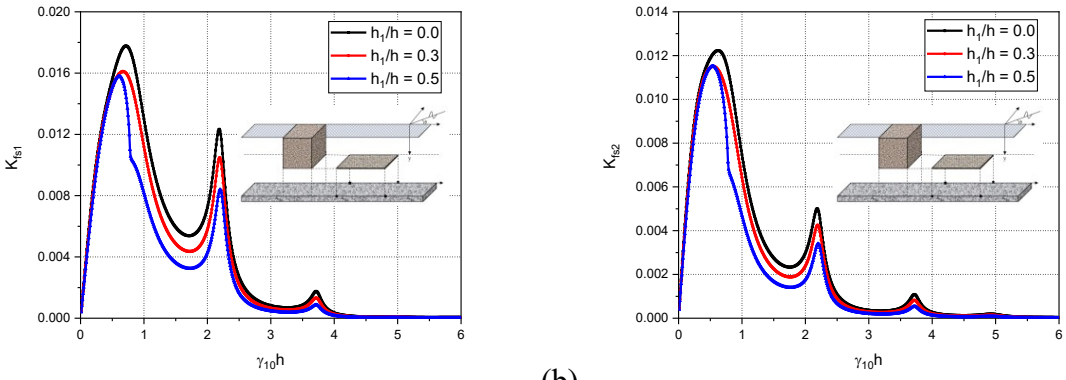

(a) (b)

Fig. 4.17: Variation in (a) K_{fs_1} and (b) K_{fs_2} versus $\gamma_{10}h$ for different values of submergence depth h_1 / h considering $\varepsilon_2 = 0.3$ and $a / h = 2.0$.

4.4.3.2.2 Effect of width of surface-piercing porous structure

The increase in the width of porous block influence the wave energy damping which further make an impact on wave force on the structure. The wave force on the front K_{fs_1} and back K_{fs_2} of the surface-piercing submerged porous structure plotted against the width of the surface piercing porous structure w / h (Fig. 4.18a,b) for different values of structural porosity. In Fig. 18(a), the wave force on the front of the porous structure K_{fs_1} shows a similar trend and it is also seen that K_{fs_1} decreases as porosity increases. In Fig. 4.18(b), it is observed that for $\varepsilon_2 = 0.2,$ the wave force increases after a certain width of the surface-piercing porous structure. As the width of porous block increases, the wave forces acting on the front and back side of the porous block is observed to be increasing which may be due to the enhanced wave-porous block interaction resulting in the increased number of pore spaces.

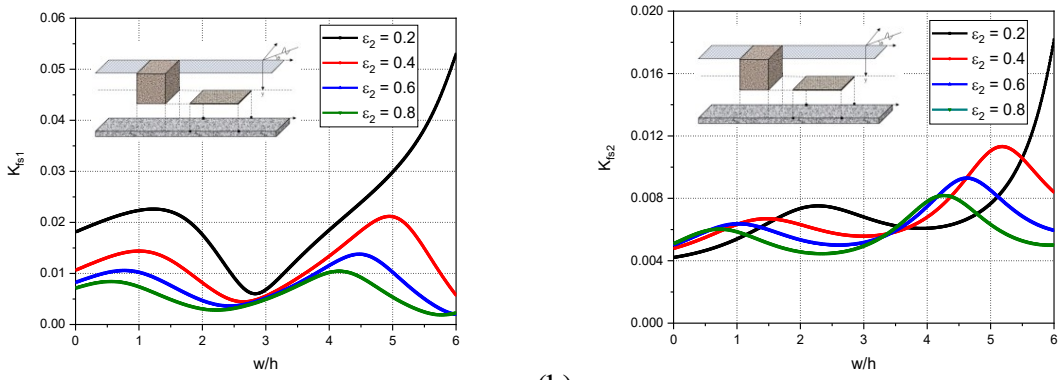

(a) (b)

Fig. 4.18: Variation in (a) K_{fs_1} and (b) K_{fs_2} versus w/h for different values of structural porosity considering $h_1/h = 0$ and $a/h = 2.0$.

4.4.3.3 Surface displacement

The wave surface displacement in the incident region $\eta_1(x)$ (Fig. 4.19a) and in the transmitted region $\eta_T(x)$ (Fig. 4.19b) is plotted against the distance x for different values of angle of incidence θ. In Fig. 4.19(a), it is observed that the surface displacement $\eta_I(x)$ increases as the angle of incidence θ increases in the incident region and a phase change in incident angle is observed.

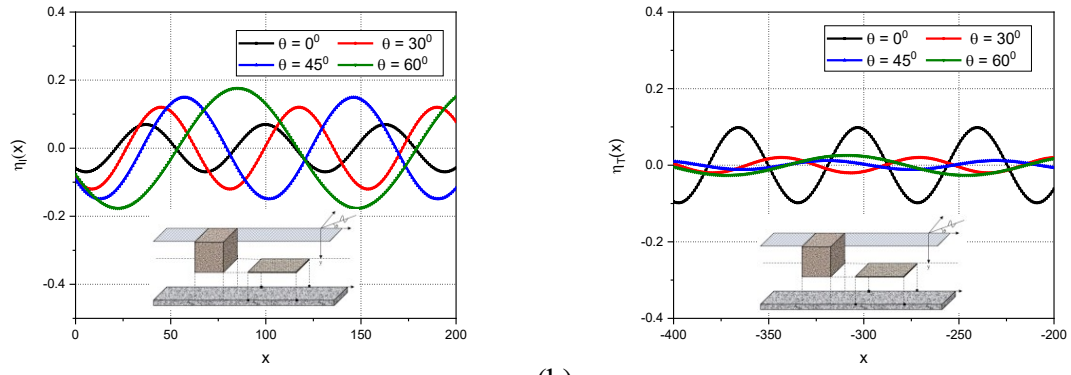

(a) (b)

Fig. 4.19: Variation in (a) $\eta_I(x)$ and (b) $\eta_T(x)$ versus x for different values of angle of incidence considering $\varepsilon_2 = 0.3$ and $h_1/h = 0$ and $a/h = 2.0$.

On the other hand, the surface deflection $\eta_T(x)$ decreases as the angle of incidence θ increases in the transmitted region. It is also observed that the surface deflection in the transmitted region $\eta_T(x)$ is lower than that of the incident region. As the incident wave angle increases, the surface deflection is observed to be reduced in the transmitted region and an almost 160% reduction in

surface displacement is achieved in the transmitted region. The reduction in the surface displacement could be due to the fact that, the incident wave crests being parallel to the structure, causes the wave energy to strike with the high force and resulting in wave energy damping.

4.5 CLOSURE

The wave energy dissipation due to submerged porous structures combined with submerged porous plate are examined to understand the effect of wave transformation. The study is carried out for two configurations consisting of a submerged porous plate backed by a bottom-standing porous structure and submerged porous plate backed by a surface-piercing porous structure. The reflection, transmission and dissipation coefficients, wave force on the structure and surface deflection are examined for the two different configurations of porous structures. The conclusions drawn from the present study are as follows:

- The submerged porous plate backed by a bottom-standing porous structure is noted to have 10% increase in energy damping as the structural porosity is varied within $0.2 < \varepsilon_2 < 0.8$. On the other hand, 7.5% increase in energy damping is noted as structural porosity of surface-piercing porous structure varied within $0.2 < \varepsilon_2 < 0.8$. Further, the wave force impact is lesser for higher structural porosity.
- The wave energy dissipation is noted higher for both structural configurations combined with submerged plate. The wave force on the bottom-standing porous structure is found to be less for $h_1 / h = 0$ and the most effective results are obtained when the porous plate is kept on the water surface level. However, the wave force on the surface-piercing porous structure is higher in the case of $h_1 / h = 0$.
- The higher values of angle of incidence show lesser wave transmission. The wave force impact on the bottom-standing porous structure and the surface elevation in the transmitted region decreases as the angle of incidence increases. Further, the wave energy dissipation is observed higher for lower angle of incidence for surface-piercing porous structure along with submerged plate breakwater and the surface deflection in the transmitted region is lower for higher angle of incidence.
- The hydrodynamic performance is found better for larger plate lengths. However, it is observed that the wave force impact on the plate is higher for larger plate length thus

reducing the wave force impact on the bottom-standing submerged porous structure. Whereas the larger plate length is noted to dissipate more wave energy and the wave force on the surface-piercing porous structure decreases as the plate length increases.

- The width of the bottom-standing structure plays a major role in reducing the wave impact on the structure. The lesser wave force is noted for higher width of the porous structure. On the other hand, the dissipation coefficient attains a constant value after a certain width of the surface-piercing porous structure.

CHAPTER 5

WAVE ATTENUATION DUE TO SUBMERGED POROUS STRUCTURE, PLATE AND BARRIER

5.1 GENERAL INTRODUCTION

The present study examines the hydrodynamic performance of the wave interaction with a composite breakwater consisting of submerged porous structure, submerged horizontal porous plate and vertical porous barrier using linear potential theory. Analytical solutions are obtained using matched eigenfunction expansion method and mode coupling relations are used in solving the interaction of water waves with composite breakwater. The reflection, transmission, energy loss coefficient, wave force acting on the breakwater and surface deflections are examined in detail with changing the porosity of the structure, porosity of plate, submergence depth, inertia factor and wave angle of incidence. Numerical results shows that the breakwater with low plate porosity is effective in reducing the transmission. The study found that when the submerged structure porosity increases, there is more wave structure interaction and thus energy dissipation is maximum. In addition, wave forces acting on the plate and barrier decreases with increase in the plate porosity. Further, the surface deflection in the transmitted region is found to be less compared to that of incident region thus making the breakwater effective in protecting the coastal regions.

5.2 MATHEMATICAL FORMULATION

The interaction of monochromatic oblique incident waves with a submerged porous structure, submerged horizontal porous plate and fully-extended vertical porous barrier (Fig. 5.1) is analysed using the small amplitude wave theory. The x -axis is chosen along the free surface, and the y -axis is chosen vertically upwards. The wave is considered to be propagating at water depth h and the submergence depth of porous structure and plate is represented as h_1 whereas the width of the submerged porous structure is taken w. The vertical barrier is located at $x=-a_4$ from the origin at $x=0.$ The fluid is assumed to be inviscid, incompressible and the motion is irrotational. The velocity potential and the surface deflection is represented as

$\phi(x,y,z,t)=\mathrm{Re}\left\{\phi_j(x,y)e^{i(lz-\omega t)}\right\}$ and $\zeta_j(x,z,t)=\mathrm{Re}\left\{\eta_j(x)e^{i(lz-\omega t)}\right\}$ where Re illustrates the real part with $l=\ l=\gamma_{10}\sin\theta$ and γ_{10} is the progressive wave number in y direction, θ is the angle of incidence and ω is the wave frequency.

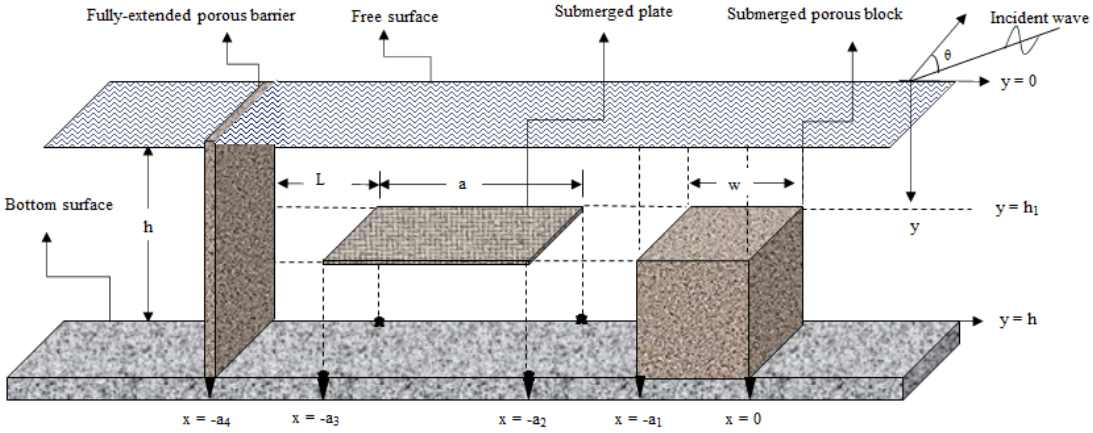

Fig. 5.1: Schematic diagram for composite porous structure

The fluid domain is divided into eight regions such as upstream open water region $I_1\equiv\left(0<x<\infty,0<y<h\right)$, region above porous block $I_2\equiv\left(-a_1<x<0,0<y<h_1\right)$, submerged porous block region $I_3\equiv\left(-a_1<x<0,h_1<y<h\right)$, open water region between submerged porous block and submerged plate $I_4\equiv\left(-a_2<x<-a_1,0<y<h\right)$, open water region above submerged plate $I_5\equiv\left(-a_3<x<-a_2,0<y<h_1\right)$, region below submerged plate $I_6\equiv\left(-a_3<x<-a_2,h_1<y<h\right)$, open water region between submerged porous plate and barrier $I_7\equiv\left(-a_4<x<-a_3,0<y<h\right)$, and downstream open water region $I_8\equiv\left(-\infty<x<-a_4,0<y<h\right)$. The velocity potential in each of the fluid region satisfies the Helmholtz equation is given by

$$\frac{\partial^2\phi_j}{\partial x^2}+\frac{\partial^2\phi_j}{\partial y^2}-l^2\phi_j=0,\ \text{for}\ j=1,2,....,8. \tag{5.1}$$

The bottom boundary condition is given by

$$\frac{\partial\phi_j}{\partial y}=0,\ \text{at}\ y=h\ \text{for}\ j=1,4,6,7,8. \tag{5.2}$$

The linear free surface boundary condition in each region is given by

$$\frac{\partial\phi_j}{\partial y}+\kappa\phi_j=0,\quad \text{on}\ y=0\ \text{for}\ j=1,4,7,8. \tag{5.3}$$

where $\kappa = \omega^2 / g$ for $j = 1,4,7,8$ in the case of open water region and g is the acceleration due to gravity. The linearized free surface condition in porous structure region for the bottom-standing porous structure is given by

$$\frac{\partial \phi_j(x,y)}{\partial y} + \frac{\omega^2 (s_1 + if_1)}{g} \phi_j(x,y) = 0 \quad \text{at} \quad h_1 < y < h \quad \text{for } j = 3, \tag{5.4a}$$

where s_1 is the inertia coefficient and f_1 is the friction coefficient for bottom-standing porous structure. The linearized boundary condition for the porous plate at the interface is given by

$$\frac{\partial \phi_5}{\partial y} = \frac{\partial \phi_6}{\partial y} = i\gamma_{10} G_p (\phi_6 - \phi_5) \quad \text{for } y = h_1, \tag{5.4b}$$

where γ_{10} is the incident wave number, G_p is the porous effect parameter of thin permeable plate. It may me noted that for $|G_p| = 0$, the porous plate reduces to an impermeable plate whereas for $|G_p| \to \infty$, the plate becomes transparent. The boundary condition at the interface $y = h_1$ for the bottom-standing porous structure is given by

$$\phi_2 = (s_1 + if_1)\phi_3 \quad \text{and} \quad \frac{\partial \phi_2}{\partial y} = \varepsilon_1 \frac{\partial \phi_3}{\partial y}. \tag{5.5}$$

The continuity of velocity and pressure at the edge $x = 0, -a_1$ is given by

$$\phi_2(x,y) = \begin{cases} \phi_1(x,y)\big|_{x=0} \\ \phi_4(x,y)\big|_{x=-a_1} \end{cases} \quad \text{and} \quad \phi_{2x}(x,y) = \begin{cases} \phi_{1x}(x,y)\big|_{x=0} \\ \phi_{4x}(x,y)\big|_{x=-a_1} \end{cases} \quad \text{for } 0 < y < h_1, \tag{5.6a}$$

$$(s_1 + if_1)\phi_3(x,y) = \begin{cases} \phi_1(x,y)\big|_{x=0} \\ \phi_4(x,y)\big|_{x=-a_1} \end{cases} \quad \text{and} \quad \varepsilon_1 \phi_{3x}(x,y) = \begin{cases} \phi_{1x}(x,y)\big|_{x=0} \\ \phi_{4x}(x,y)\big|_{x=-a_1} \end{cases} \quad \text{for } h_1 < y < h, \tag{5.6b}$$

Further, at the edge $x = -a_j, j = 2,3$ of the fluid and porous plate interfaces, the continuity of velocity and pressure is given by

$$\phi_5(x,y) = \begin{cases} \phi_4(x,y)\big|_{x=-a_2} \\ \phi_7(x,y)\big|_{x=-a_3} \end{cases} \quad \text{and} \quad \phi_{5x}(x,y) = \begin{cases} \phi_{4x}(x,y)\big|_{x=-a_2} \\ \phi_{7x}(x,y)\big|_{x=-a_3} \end{cases} \quad \text{for } 0 < y < h_1, \tag{5.7a}$$

$$\phi_6(x,y) = \begin{cases} \phi_4(x,y)\big|_{x=-a_2} \\ \phi_7(x,y)\big|_{x=-a_3} \end{cases} \quad \text{and} \quad \phi_{6x}(x,y) = \begin{cases} \phi_{4x}(x,y)\big|_{x=-a_2} \\ \phi_{7x}(x,y)\big|_{x=-a_3} \end{cases} \quad \text{for } h_1 < y < h, \tag{5.7b}$$

In addition, at the edge $x = -a_j, j = 4$ of the fully-extended porous barrier, the continuity of velocity and pressure is given by

$\phi_7(x,y)=\phi_8(x,y)$ and $\phi_{7x}(x,y)=\phi_{8x}(x,y)=i\gamma_{70}G_b\left\{\phi_8(x,y)-\phi_7(x,y)\right\}$ for $0<y<h$, (5.8)

where $G_b=\varepsilon_3/\{k_{40}d(s_3+if_3)\}$ is the porous effect parameter of porous barrier (Yu and Chwang, 1994), ε_3 is the porosity, d is the thickness, s_3 is the inertia, f_3 is the friction factor due to the presence of vertical barrier.

The wave number in upstream/downstream free-water region γ_{jn} for $j=1,4,7,8$ and the bottom-standing porous structure region γ_{2n} satisfies the dispersion relation for finite water depth is given by

$$\omega^2=\begin{cases} g\gamma_{j0}\tanh\gamma_{j0}h & \text{for} \quad n=0 \\ -g\gamma_{jn}\tan\gamma_{jn}h & \text{for} \quad n=1,2,.... \end{cases} \quad \text{for} \quad j=1,4,7,8 \tag{5.9a}$$

$$\omega^2-g\gamma_{2n}\tanh\gamma_{2n}h-F_n(\omega^2\tanh\gamma_{2n}h-\gamma_{2n}g)=0, \quad \text{for} \quad n=0,1,2,.... \tag{5.9b}$$

where $F_n=\dfrac{\left\{(s_1+if_1)-\varepsilon_1\right\}\tanh\gamma_{2n}(h-h_1)}{\left\{(s_1+if_1)-\varepsilon_1\tanh^2\gamma_{2n}(h-h_1)\right\}}$, ω is the wave frequency and g is the acceleration due to gravity. Further, the wave number γ_{5n} within $-a_2<x<-a_3, 0<y<h$ satisfies the dispersion relation of the form for $n=0,1,2...$ given by

$$\gamma_{5n}\sinh\gamma_{5n}(h-h_1)\left\{g\gamma_{5n}\sinh\gamma_{5n}h_1-\omega^2\cosh\gamma_{5n}h_1\right\}-ik_{10}G_p\left\{\omega^2\cosh\gamma_{5n}h-g\gamma_{5n}\sinh\gamma_{5n}h\right\}=0. \tag{5.10}$$

In the far-field region, the radiation conditions in the presence of porous structure with barrier is given by

$$\phi_j(x,y)=\begin{cases} \left(I_{10}e^{-i\gamma_{10}x}+R_{10}e^{i\gamma_{10}x}\right)f_{10}(y) & \text{as} \quad x\to\ \infty, \\ \left(T_{80}e^{-i\gamma_{90}x}\ \right)f_{80}(y) & \text{as} \quad x\to-\infty, \end{cases} \tag{5.11}$$

where, I_{10}, R_{10} and T_{40} are the complex amplitude of the incident, reflected and transmitted wave energies respectively. However, the incident wave I_{10} is considered to be unity.

5.3 METHOD OF SOLUTION

The matched eigenfunction expansion method is adopted for the numerical analysis of wave interaction with the bottom-standing porous structure away from the submerged horizontal porous plate and vertical barrier. The velocity potentials in each of the region is given by

$$\phi_1(x,y)=(I_{10}e^{-ik_{10}x}+R_{10}e^{ik_{10}x})f_{10}(y)+\sum_{n=1}^{\infty}R_{1n}e^{-k_{1n}x}f_{1n}(y) \quad \text{for} \quad 0<x<\infty,\ 0<y<h, \tag{5.12a}$$

$$\phi_2(x,y)=\sum_{n=0}^{\infty}\left\{A_{2n}e^{-ik_{2n}x}+B_{2n}e^{ik_{2n}(x+a_1)}\right\}f_{2n}(y)\ \text{ for } -a_1<x<0,\ 0<y<h_1, \tag{5.12b}$$

$$\phi_3(x,y)=\sum_{n=0}^{\infty}\left\{A_{2n}e^{-ik_{2n}x}+B_{2n}e^{ik_{2n}(x+a_1)}\right\}f_{3n}(y)\ \text{ for } -a_1<x<0,\ h_1<y<h, \tag{5.12c}$$

$$\phi_4(x,y)=(A_{40}e^{-ik_{40}(x+a_1)}+B_{40}e^{ik_{40}(x+a_2)})f_{40}(y)+\sum_{n=1}^{\infty}\left\{A_{4n}e^{k_{4n}(x+a_1)}+B_{4n}e^{-k_{4n}(x+a_2)}\right\}f_{4n}(y) \tag{5.12d}$$
$$\text{for } -a_2<x<-a_1,\ 0<y<h,$$

$$\phi_5(x,y)=\sum_{n=0}^{\infty}\left\{A_{5n}\frac{\cos k_{5n}x}{\cos k_{5n}a_2}+B_{5n}\frac{\sin k_{5n}x}{\sin k_{5n}a_3}\right\}f_{5n}(y)\quad \text{for } -a_3<x<-a_2,\ 0<y<h_1, \tag{5.12e}$$

$$\phi_6(x,y)=\sum_{n=0}^{\infty}\left\{A_{5n}\frac{\cos k_{5n}x}{\cos k_{5n}a_2}+B_{5n}\frac{\sin k_{5n}x}{\sin k_{5n}a_3}\right\}f_{6n}(y)\ \text{ for } -a_3<x<-a_2,\ h_1<y<h, \tag{5.12f}$$

$$\phi_7(x,y)=(A_{70}e^{-ik_{70}(x+a_3)}+B_{70}e^{ik_{70}(x+a_4)})f_{70}(y)+\sum_{n=1}^{\infty}\left\{A_{7n}e^{k_{7n}(x+a_3)}+B_{7n}e^{-k_{7n}(x+a_4)}\right\}f_{7n}(y) \tag{5.12g}$$
$$\text{for } -a_4<x<-a_3,\ 0<y<h,$$

$$\phi_8(x,y)=T_{80}e^{-ik_{90}(x+a_5)}f_{80}(y)+\sum_{n=1}^{\infty}T_{8n}e^{k_{9n}(x+a_5)}f_{8n}(y)\ \text{ for } -\infty<x<-a_4,\ 0<y<h, \tag{5.12h}$$

where I_{10} is the incident wave amplitude taken as unity and $R_{1n}, A_{2n}, B_{2n}, A_{4n}, B_{4n}$, $A_{5n}, B_{5n}, A_{7n}, B_{7n}$ and T_{8n} for $n=0,1,2...$ the unknown constants are to be determined. The eigen functions $f_{jn}(y)$'s for the open water regions for $j=1,4,7,8$ are given by

$$f_{jn}(y)=\frac{\cosh\gamma_{jn}(h-y)}{\cosh\gamma_{jn}h}\ \text{ for } n=0 \text{ and } f_{jn}(y)=\frac{\cos\gamma_{jn}(h-y)}{\cos\gamma_{jn}h}\ \text{ for } n=1,2,3... \tag{5.13}$$

where γ_{jn} for $j=1,4,7,8$ are the eigen values and will satisfy the open water dispersion relation as in Eq. 9(a) satisfying ${\gamma_{jn}}^2={k_{jn}}^2+l^2$, where γ_{jn} is the wave number in y – direction, k_{jn} is the wave number in x – direction and $l=\gamma_{10}\sin\theta$ is the wave number in the z – direction. The eigenfunctions $f_{jn}(y)$ for $j=2,3$ for the bottom-standing submerged porous structure region is given by

$$f_{2n}(y)=\left\{\frac{\cosh\gamma_{2n}(h-y)-F_n\sinh\gamma_{2n}(h-y)}{\cosh\gamma_{2n}h-F_n\sinh\gamma_{2n}h}\right\}, \tag{5.14}$$

$$f_{3n}(y)=\left\{\frac{1-F_n\tanh\gamma_{2n}(h-h_1)}{(s_1+if_1)(\cosh\gamma_{2n}h-F_n\sinh\gamma_{2n}h)}\right\}\cosh\gamma_{2n}(h-y), \tag{5.15}$$

where $$F_n = \frac{\{(s_1 + if_1) - \varepsilon_1\}\tanh\gamma_{2n}(h-h_1)}{\{(s_1 + if_1) - \varepsilon_1\tanh^2\gamma_{2n}(h-h_1)\}} \tag{5.16}$$

ε_1 is the porosity, s_1 is inertial parameter and f_1 is the friction coefficient of the bottom standing porous structure where γ_{2n} satisfies the dispersion relation as in Eq. 5.9(b). The eigenfunctions $f_{jn}(y)$'s for the submerged porous plate region $j = 5$ and 6 is given by

$$f_{5n}(y) = \sinh\gamma_{5n}(h-h_1)\{g\gamma_{5n}\cosh\gamma_{5n}y - \omega^2\sinh\gamma_{5n}y\}, \tag{5.17a}$$

$$f_{6n}(y) = -\{g\gamma_{5n}\sinh\gamma_{5n}h_1 - \omega^2\cosh\gamma_{5n}h_1\}\cosh\gamma_{5n}(h-y), \tag{5.17b}$$

where γ_{5n} is the eigen value satisfies the dispersion relation as in Eq. (5.10).

The eigenfunction $f_{jn}(y)$ in the open water region $j = 1, 4, 7, 8$ satisfy the orthogonality relation given by

$$\langle f_{jm}, f_{jn}\rangle_{j=1,4,7,9} = \begin{cases} 0 & \text{for } m \neq n, \\ \mathrm{C}_n & \text{for } m = n, \end{cases} \tag{5.18}$$

with respect to the orthogonal mode-coupling relation defined by

$$\langle f_{jm}, f_{jn}\rangle_{j=1,4,7,9} = \int_0^h f_{jm}(y) f_{jn}(y)dy, \tag{5.19}$$

where $C_n = \left\{\frac{2\gamma_{jn}h + \sinh 2\gamma_{jn}h}{4\gamma_{jn}\cosh^2\gamma_{jn}h}\right\}$ for $n = 0$ with C_n for $n = 1, 2, 3, \ldots$ are obtained by substituting $\gamma_{jn} = i\gamma_{jn}$. In order to determine the unknown coefficients, the orthogonal mode coupling relation as in Eq. (5.19) is employed on $\phi_j(x, y)$ and $\phi_{jx}(x, y)$ with the eigenfunction $f_{jm}(y)$ along with continuity of velocity and pressure as in Eq. 6(a) across the vertical interface $x = 0, 0 < y < h$ to obtain

$$\begin{aligned} \langle \phi_j(x,y), f_{jm}(y)\rangle_{j=1} &= \int_0^h \phi_j(x,y) f_{jm}(y)dy \\ &= \int_0^{h_1} \phi_{j+1}(x,y) f_{jm}(y)dy + (s_1 + if_1)\int_{h_1}^h \phi_{j+2}(x,y) f_{jm}(y)dy \text{ for } m = 0,1,2,\ldots, \end{aligned} \tag{5.20a}$$

$$\begin{aligned} \langle \phi_{jx}(x,y), f_{jm}(y)\rangle_{j=1} &= \int_0^h \phi_{jx}(x,y) f_{jm}(y)dy \\ &= \int_0^{h_1} \phi_{(j+1)x}(x,y) f_{jm}(y)dy + \varepsilon_1\int_{h_1}^h \phi_{(j+2)x}(x,y) f_{jm}(y)dy \text{ for } m = 0,1,2,\ldots, \end{aligned} \tag{5.20b}$$

Further, the orthogonal mode coupling relation as in Eq. (5.19) is employed on $\phi_j(x,y)$ and $\phi_{jx}(x,y)$ with the eigenfunction $f_{jm}(y)$ along with continuity of velocity and pressure as in Eq. 5.6(b) across the vertical interface $x=-a_1, 0<y<h$ to obtain

$$\begin{aligned}\left\langle \phi_j(x,y), f_{jm}(y)\right\rangle_{j=4} &= \int_0^h \phi_j(x,y) f_{jm}(y)\,dy \\ &= \int_0^{h_1} \phi_{j-2}(x,y) f_{jm}(y)\,dy + (s_1+if_1)\int_{h_1}^h \phi_{j-1}(x,y) f_{jm}(y)\,dy \text{ for } m=0,1,2,...,\end{aligned} \tag{5.21a}$$

$$\begin{aligned}\left\langle \phi_{jx}(x,y), f_{jm}(y)\right\rangle_{j=4} &= \int_0^h \phi_{jx}(x,y) f_{jm}(y)\,dy \\ &= \int_0^{h_1} \phi_{(j-2)x}(x,y) f_{jm}(y)\,dy + \varepsilon_1\int_{h_1}^h \phi_{(j-1)x}(x,y) f_{jm}(y)\,dy \text{ for } m=0,1,2,...,\end{aligned} \tag{5.21b}$$

Now, due to the presence of the submerged floating plate, the orthogonal mode coupling relation as in Eq. (5.19) is employed on $\phi_j(x,y)$ and $\phi_{jx}(x,y)$ with the eigenfunction $f_{jm}(y)$ along with continuity of velocity and pressure as in Eq. 5.7(a) across the vertical interface $x=-a_2, 0<y<h$ to obtain

$$\begin{aligned}\left\langle \phi_j(x,y), f_{jm}(y)\right\rangle_{j=4} &= \int_0^h \phi_j(x,y) f_{jm}(y)\,dy \\ &= \int_0^{h_1} \phi_{j+1}(x,y) f_{jm}(y)\,dy + \int_{h_1}^h \phi_{j+2}(x,y) f_{jm}(y)\,dy \text{ for } m=0,1,2,...,\end{aligned} \tag{5.22a}$$

$$\begin{aligned}\left\langle \phi_{jx}(x,y), f_{jm}(y)\right\rangle_{j=4} &= \int_0^h \phi_{jx}(x,y) f_{jm}(y)\,dy \\ &= \int_0^{h_1} \phi_{(j+1)x}(x,y) f_{jm}(y)\,dy + \int_{h_1}^h \phi_{(j+2)x}(x,y) f_{jm}(y)\,dy \text{ for } m=0,1,2,...,\end{aligned} \tag{5.22b}$$

Further, the orthogonal mode coupling relation as in Eq. (5.19) is employed on $\phi_j(x,y)$ and $\phi_{jx}(x,y)$ with the eigenfunction $f_{jm}(y)$ along with continuity of velocity and pressure as in Eq. 5.7(b) across the vertical interface $x=-a_3, 0<y<h$ to obtain

$$\begin{aligned}\left\langle \phi_j(x,y), f_{jm}(y)\right\rangle_{j=7} &= \int_0^h \phi_j(x,y) f_{jm}(y)\,dy \\ &= \int_0^{h_1} \phi_{j-2}(x,y) f_{jm}(y)\,dy + \int_{h_1}^h \phi_{j-1}(x,y) f_{jm}(y)\,dy \text{ for } m=0,1,2,...,\end{aligned} \tag{5.23a}$$

$$\begin{aligned}\left\langle \phi_{jx}(x,y), f_{jm}(y)\right\rangle_{j=7} &= \int_0^h \phi_{jx}(x,y) f_{jm}(y)\,dy \\ &= \int_0^{h_1} \phi_{(j-2)x}(x,y) f_{jm}(y)\,dy + \int_{h_1}^h \phi_{(j-1)x}(x,y) f_{jm}(y)\,dy \text{ for } m = 0,1,2,...,\end{aligned} \tag{5.23b}$$

Again, due to the presence of fully-extended porous structure, the orthogonal mode coupling relation as in Eq. (5.19) is employed on $\phi_j(x,y)$ and $\phi_{jx}(x,y)$ with the eigenfunction $f_{jm}(y)$ along with continuity of velocity and pressure as in Eq. (5.8) across the vertical interface $x = -a_4, 0 < y < h$ for to obtain

$$\begin{aligned}\left\langle \phi_{j}(x,y), f_{jm}(y)\right\rangle_{j=7} &= \int_0^h \phi_{j}(x,y) f_{jm}(y)\,dy \\ &= \int_0^h \phi_{j+1}(x,y) f_{jm}(y)\,dy \text{ for } m = 0,1,2,...,\end{aligned} \tag{5.24a}$$

$$\begin{aligned}\left\langle \phi_{jx}(x,y), f_{jm}(y)\right\rangle_{j=7} &= \int_0^h \phi_{jx}(x,y) f_{jm}(y)\,dy \\ &= \int_0^h \phi_{(j+1)x}(x,y) f_{jm}(y)\,dy \text{ for } m = 0,1,2,...,\end{aligned} \tag{5.24b}$$

The infinite sums presented in the Eqs. (5.20a,b)-(5.24a,b) are truncated upto finite M terms to obtain a linear system of $10(M+1)$ algebraic equation for the determination of $10(M+1)$ unknowns and the wave reflection and transmission due to the combined bottom-standing porous structure, submerged plate and fully-extended porous structure are obtained as

$$K_r = \left|\frac{R_{10}}{I_{10}}\right| \quad \text{and} \quad K_t = \left|\frac{T_{90}}{I_{10}}\right|. \tag{5.25a}$$

Due the existence of composite structures the energy dissipation in the wave propagation through the composite structures as in Chwang and Chan (1998) is represented as

$$K_d = 1 - K_r^2 - K_t^2. \tag{5.25b}$$

5.3.1 Wave force on the porous structure and submerged plate

The wave force acting on the front and back of the bottom-standing porous structure can be represented as

$$K_{fs_1} = \frac{F_f}{2\rho g I_{10} h} \quad \text{and} \quad K_{fs_2} = \frac{F_b}{2\rho g I_{10} h} \tag{5.26a}$$

where $$F_f = i\rho\omega\int_{h_1}^{h}(\phi_3 - \phi_1)dy \quad \text{at} \quad x = 0 \tag{5.26b}$$

$$F_b = i\rho\omega\int_{h_1}^{h}(\phi_3 - \phi_4)dy \quad \text{at} \quad x = -a_1 \tag{5.26c}$$

The wave force acting on the horizontal porous plate is given by

$$K_{fp} = \frac{F_p}{2\rho g I_{10} h} \tag{5.27a}$$

where $$F_p = i\rho\omega\int_{-a_3}^{-a_2}(\phi_5 - \phi_6)dx \tag{5.27b}$$

The wave force acting on the fully-extended porous barrier can be represented as

$$K_{fb} = \frac{F_{barrier}}{2\rho g I_{10} h} \tag{5.28a}$$

where $$F_{barrier} = i\rho\omega\int_{0}^{h}(\phi_8 - \phi_7)dy \quad \text{at} \quad x = -a_4 \tag{5.28b}$$

5.3.2 Surface displacement

The surface defection $\eta_j(x, y)$ is given by

$$\eta_j(x, y) = \left(-\frac{1}{i\omega}\right)\phi_{jy}(x, y) \quad \text{on} \quad y = 0 \quad \text{for} \quad j = 1, 4, 7, 8. \tag{5.29}$$

5.4 RESULTS AND DISCUSSION

The combination of bottom-standing porous structure, submerged porous plate, and fully extended porous structure barrier is investigated numerically. The results are plotted to analyse the structural porosity, plate submergence depth, angle of incidence, and porous structure width on the wave energy dissipation. The reflection K_r, transmission K_t, and dissipation coefficients K_d are plotted and analysed. In addition, the wave force on the front $K^1_{fs_1}$ and back $K^1_{fs_2}$ of the bottom-standing porous structure, wave force on the plate K_{fp} and surface elevation are analysed. The density of the fluid $\rho = 1025\ kg/m^3$ and the acceleration due to gravity $g = 9.8\ m/s^2$ are kept constant throughout the numerical study.

5.4.1 Validation of Numerical Result

In order to study the efficiency of the submerged porous plate, a comparative study is performed between the present study and numerical results obtained by Cho and Kim (2013).

In Fig. 5.2, the comparative study of the numerical results for a single submerged horizontal porous plate and theoretical results developed by Cho and Kim (2013) is analysed. The reflection coefficient and transmission coefficients are plotted against the non-dimensional wave number $\gamma_{10}h$ for a submerged porous plate considering $d/h=0.2$, $\theta=0^0$ and $a_1/h=0.5$. The study shows the numerical result obtained using the present study exactly matches with the result obtained by Cho and Kim (2013) and the correlation with previous analytical solutions is acceptable.

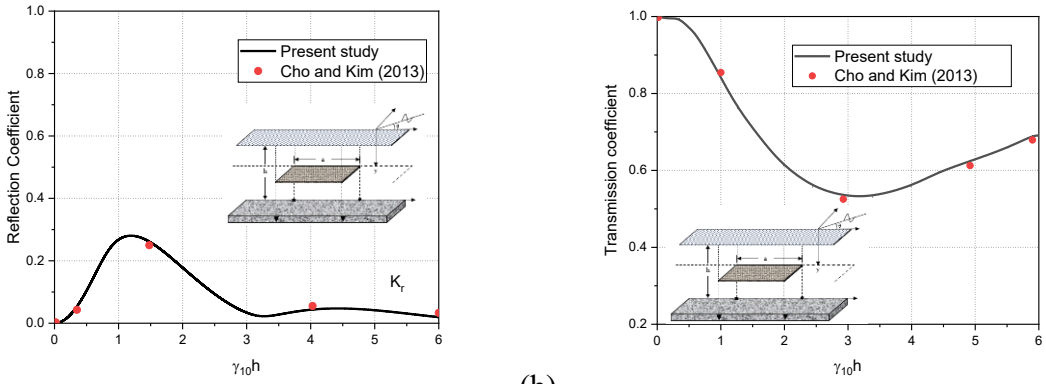

(a) (b)

Fig. 5.2: Comparative study between the present approach and Cho and Kim (2013) for (a) reflection coefficient and (b) transmission coefficient due to the submerged porous plate.

5.4.2 Reflection, Transmission and Dissipation Coefficients

The wave interaction due to the combination of submerged porous structure, submerged horizontal porous plate and vertical barrier is investigated. The wave reflection coefficient K_r, transmission coefficient K_t, energy loss coefficient K_d, wave force acting on the plate and barrier and surface deflection are analysed. The present study elaborates the importance of porosity, angle of wave incidence, length of the plate, friction factor, width between structure and plate. The numerical computations are carried out by considering $\rho_w=1025kg/m^3$, $g=9.81m/s^2$, $s_1=0.1$, $f_1=0.5$, $s_2=0.2$, $f_2=0.4$, $s_3=0.5$, and $f_3=0.5$.

5.4.2.1 Effect of porosity of plate

In Fig.5.3(a,b), the variation of K_r, K_t and K_d versus $\gamma_{10}h$ for different porosity of the plate of the composite breakwater is analysed for $\varepsilon_1=0.4$, $\varepsilon_3=0.1$, $h_1/h=0.25$, $a/h=1.0$, $L/h=1.0$ and $\theta=0^0$. The numerical results shows that the submerged plate with higher

porosity have lower reflection. This could be due to the fact that as porosity increases, more water may pass through, causing more wave dissipation. Further, as the non-dimensional wave number increases, there is a resonating trend in wave reflection, which is due to wave trapping between the structures. In Fig. 5.3(a), it is observed that transmission is found to be decreasing with increase in non-dimensional wave number. The transmission coefficient decreases to 42.6% when porosity waries within changes from $0.2 < \varepsilon_2 < 0.8$ at $\gamma_{10}h = 6$. The dissipation coefficient (Fig. 5.3b) is high for plates with lower porosity and as the porosity is increased within $0.2 < \varepsilon_2 < 0.8$ the wave dissipation increases to 30.6%. Thus , the porosity of the plate should be kept minimum to reduce transmission and increase wave dissipation.

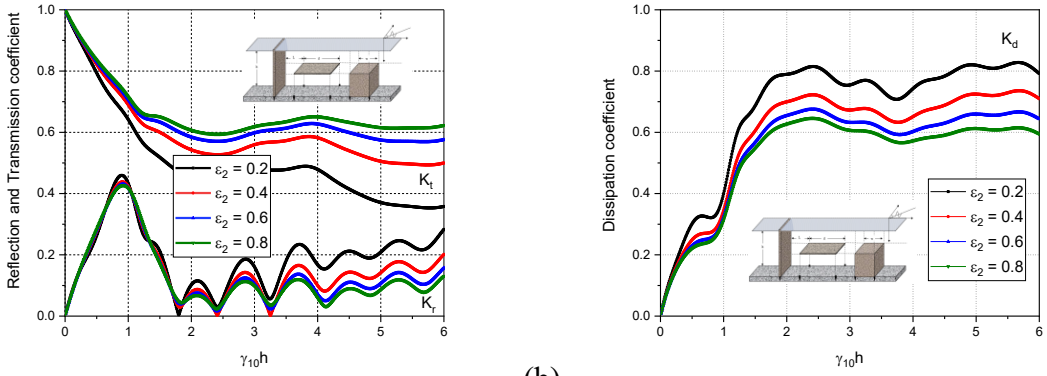

(a) (b)

Fig. 5.3: Variation of (a) K_r and K_t and (b) K_d versus $\gamma_{10}h$ for different porosity of plate considering $\varepsilon_1 = 0.4$, $\varepsilon_3 = 0.1$, $h_1 / h = 0.25$, $a/h = 1.0$, $L/h = 1.0$ and $\theta = 0^0$.

5.4.2.2 Effect of angle of incidence

In Fig. 5.4(a,b), the variation of K_r, K_t and K_d versus $\gamma_{10}h$ for different angle of wave incidence in the case of a composite breakwater is analysed for $\varepsilon_1 = 0.4$, $\varepsilon_2 = 0.2$, $h_1 / h = 0.25$, $a/h = 1.0$ and $L/h = 1.0$. The resonating trend is observed in the reflection coefficient (Fig. 5.4a) due to the wave trapping between the structure and submerged plate, and the wave reflection is found to be decreasing as angle of wave incidence increases to $\theta = 60^0$. The angle at which minimum reflection is observed is termed as critical angle and it is observed at $\theta = 60^0$ and $\gamma_{10}h = 4.1$. It is observed that wave transmission reduces when non-dimensional wave number increases and it reduces to $K_t = 0.2$ when wave angle of incidence is $\theta = 0^0$. The transmission coefficient decreases to 52.3% when wave angle of incidence changes from $\theta = 60^0$ to $\theta = 0^0$ at $\gamma_{10}h = 5$. The energy dissipation (Fig. 5.4b) is high when $0^0 < \theta < 30^0$. The

energy dissipation increases to 33.3% when angle of wave incidence decreases from $\theta = 60^0$ to $\theta = 0^0$ and at $\gamma_{10}h = 1.5$. An increment in wave transmission is observed with the increase of incident wave angle θ. The waves with shorter wavelengths are observed to transmit less energy than waves with longer wavelengths. Also, higher wave reflection is observed for $\theta = 0^0$, when the wave crests are parallel to the structure.

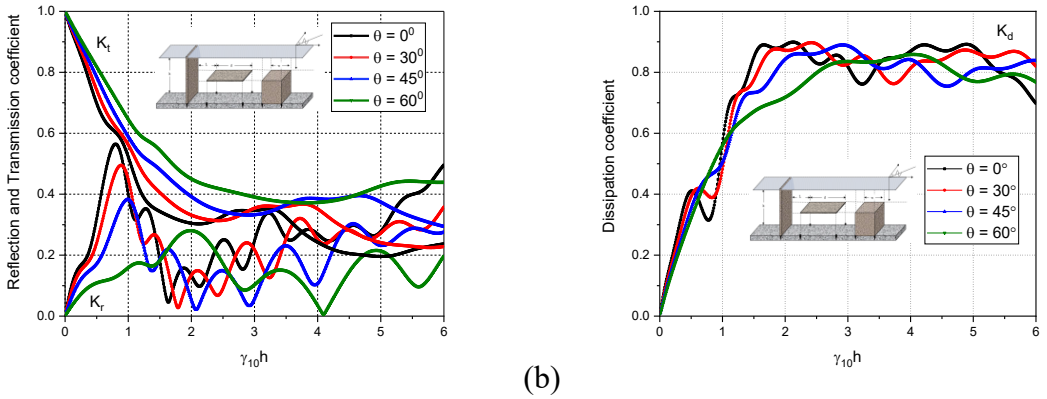

(a) (b)

Fig. 5.4: Variation of (a) K_r and K_t and (b) K_d versus $\gamma_{10}h$ for different angle of incidence considering $\varepsilon_1 = 0.4$, $\varepsilon_2 = 0.2$, $h_1 / h = 0.25$, $a / h = 1.0$ and $L / h = 1.0$.

5.4.2.3 Effect of submergence depth

The depth of submergence of porous plate an plays important role in wave transformation. In Fig. 5.5(a,b), the variation of K_r, K_t and K_d versus $\gamma_{10}h$ varying d / h for for $\varepsilon_1 = 0.4$, $\varepsilon_2 = 0.2$, $\varepsilon_3 = 0.1$, $a / h = 1.0$, $L / h = 1.0$ and $\theta = 0^0$ is analysed. The study shows that for $\gamma_{10}h < 1.5$, and for the plate on free surface, the reflection coefficient (Fig. 5.5a) is higher, which could be due to more constructive interference between incident and reflected waves. Further, as the plate submergence depth increases, the reflection is found to be decreasing up to $\gamma_{10}h < 1.5$ and as the non-dimensional wave number increases, the reflection coefficient increases when submergence depth increases. In the case of the plate at the free surface, the transmission coefficient decreases which could be due to wave blocking and maximum wave dissipation. In addition, the study shows that at $\gamma_{10}h = 6$, the wave dissipation increases to 95% as the submergence depth decreases from $h_1 / h = 0.5$ to free surface. The lowest wave energy (Fig. 5.5b) dissipation is observed when the porous plate is kept on water surface and within $1.0 < \gamma_{10}h < 1.5$.

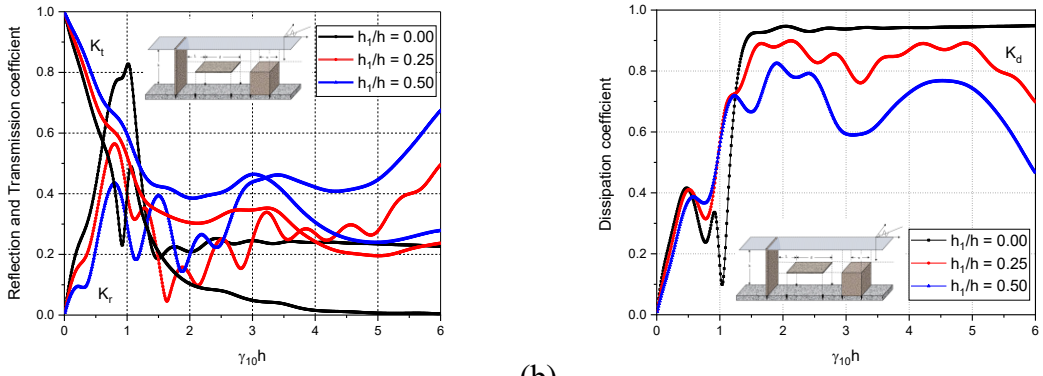

(a) (b)

Fig. 5.5: Variation of (a) K_r and K_t and (b) K_d versus $\gamma_{10}h$ for different submergence depth of plate considering $\varepsilon_1 = 0.4$, $\varepsilon_2 = 0.2$, $\varepsilon_3 = 0.1$, $a/h = 1.0$, $L/h = 1.0$ and $\theta = 0^0$.

5.4.2.4 Effect of porosity of structure

The wave reflection, transmission, and wave dissipation are affected by the porosity of submerged structures. Fig. 5.6(a,b) shows the variation of K_r, K_t and K_d versus $\gamma_{10}h$ for different porosity of the submerged structure of the composite breakwater for $\varepsilon_2 = 0.2$, $\varepsilon_3 = 0.1$, $h_1/h = 0.25$, $a/h = 1.0$, $L/h = 1.0$ and $\theta = 0^0$. The wave reflection coefficient (Fig. 5.5a) is observed to follow an oscillating pattern. The wave trapping between the structure, submerged plate, and the barrier could be due to the oscillation in wave reflection coeficient. Further, the reflection coefficient decreases as $\gamma_{10}h > 2$ and the porosity of the submerged structure increases. This could be due to the increased wave penetration between the fluid particles and the submerged porous structure, which improves wave dissipation.

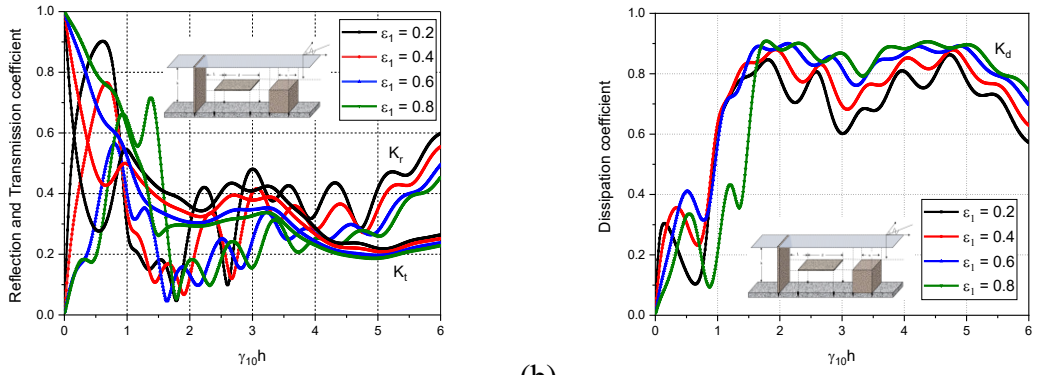

(a) (b)

Fig. 5.6: Variation of (a) K_r and K_t and (b) K_d versus $\gamma_{10}h$ for different porosity of submerged structure considering for $\varepsilon_2 = 0.2$, $\varepsilon_3 = 0.1$, $a/h = 1.0$, $L/h = 1.0$ and $\theta = 0^0$.

It is seen that at $\gamma_{10}h = 6,$ there is 42.8% reduction in wave reflection when porosity increases to 80%. Numerical results show that, for $\gamma_{10}h > 1.5$, the transmission coefficient decreases to $K_t = 0.2$ for porosity $\varepsilon_1 = 0.8.$ It is found that energy dissipation (Fig. 5.6b) increases when non-dimensional wave number increases. Thus, as the submerged structure is hit by waves with longer wavelengths $0.1 < \gamma_{10}h < 1.0$, the wave energy dissipation K_d is found to be less than 40% for all porosity values. Around 60%-80% wave energy dissipation is observed for higher porosity of submerged structure and higher wave number within $2.0 < \gamma_{10}h < 6.0$. The wave damping increases to $K_d = 0.9$, when porosity of structure increases to $\varepsilon_1 = 0.8$, which is due to more wave and structure interaction. In the case of the structural porosity $\varepsilon_1 = 0.2$, higher wave reflection is observed, which could be due to the fact that, for lower porosity of the structure, the void spaces is less for incident waves to penetrate, resulting in higher reflection.

5.4.2.5 Effect of spacing between structure and plate

The space between a porous block and a plate, or a porous barrier and a plate, acts as a captive region, capturing incident waves and damping the energy. In Fig 5.7(a), it is observed that when spacing between submerged porous structure and plate increases, the reflection coefficient decreases for moderate values of incident waves, which may be due to the decay of waves due to the trapping of waves between structure and plate.

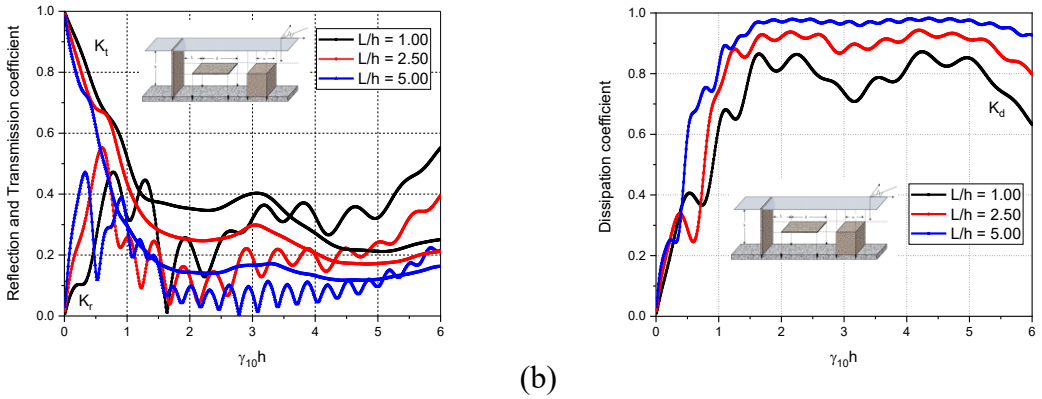

(a) (b)

Fig. 5.7: Variation of (a) K_r and K_t and (b) K_d versus $\gamma_{10}h$ for different spacing between the structure and submerged plate L/h considering $\varepsilon_1 = 0.4,\ \varepsilon_2 = 0.2,\ \varepsilon_3 = 0.1,\ a/h = 1.0,$ $h_1/h = 0.25$ and $\theta = 0^0.$

In the case of $\gamma_{10}h = 6$ and $L/h = 5$, there is a decrease in reflection coefficient to 61.8% when compared with $L/h = 1$. The transmission coefficient (Fig. 5.7a) decreases as the distance between the structure and the porous plate increases. This could be due to the fact that as the spacing widens, the waves travel a greater distance, dissipating more energy. Further, for $\gamma_{10}h = 6$ and $L/h = 5$, there is a decrease in transmission coefficient to 18% than for $L/h = 1$. The energy dissipation (Fig. 5.7b) increases as the spacing between the submerged porous structure and the submerged horizontal porous plate increases. The study shows that the energy dissipation for $L/h = 5$ is 46.7% higher than for $L/h = 1$.

5.4.2.6 Effect of inertia factor

In Fig. 5.8(a), it is evident that wave reflection is less for low inertia factors. The periodic change in the reflection coefficient is noted, which may be due to the resonance and wave trapping between structures. Fig. 5.8(a) shows that, higher inertia factors have low transmission coefficient for long incident waves, while low inertia factors have a lower transmission coefficient for moderate incident waves. Energy dissipation is also high for low inertia factors. Thus the study suggests that low inertia factor should be used in the design to reduce reflection and transmission. The periodic change in wave reflection could be due to the trapping of incident waves in the confined regions between plate and porous structures. The percentage change in wave reflection and transmission is observed to be less and negligible for all the values of inertia factors. More than 80% wave energy dissipation (Fig. 5.8b) is achieved by the composite structure for $1 < \gamma_{10}h < 2$ and $4 < \gamma_{10}h < 5$. For all the inertia factors, the wave energy dissipation achieved is very less and below 30% for $0.1 < \gamma_{10}h < 1.0$.

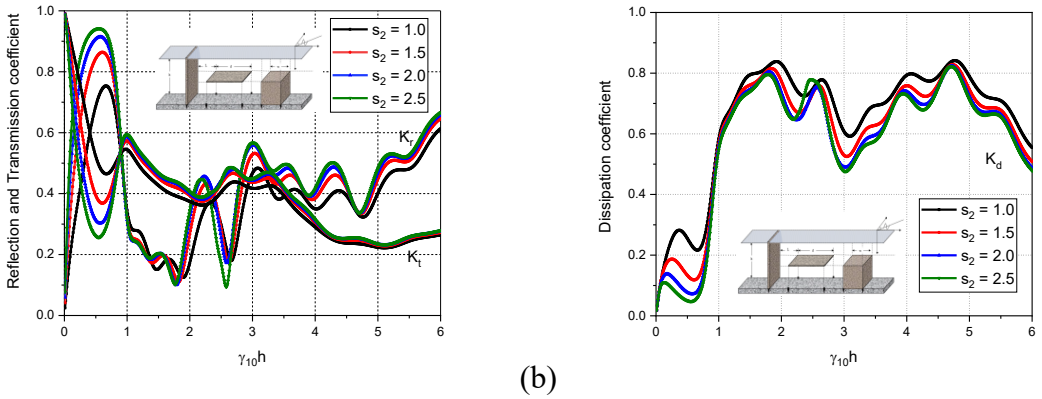

(a) (b)

Fig. 5.8: Variation of (a) K_r and K_t and (b) K_d versus for different inertia factors considering $\varepsilon_1 = 0.4$, $\varepsilon_2 = 0.2$, $\varepsilon_3 = 0.1$, $a/h = 1.0$, $L/h = 1.0$ $h_1/h = 0.25$ and $\theta = 0^0$.

5.4.3 Wave force on the structure, submerged plate and vertical barrier

The wave force on the bottom-standing porous structure, submerged plate and vertical barrier is analysed for different plate porosity and porous structure width to understand the effect of wave dissipation due to the composite breakwater system.

5.4.3.1 Effects of plate porosity

The porosity of the plate is observed to affect the wave reflection and transmission coefficients due to an improved wave-plate interaction, resulting in significant wave energy damping and thus affecting the impact of wave forces on the structure. Fig. 5.9(a,b), shows the variation of wave forces acting on the front side of the submerged porous structure, back side of the submerged porous structure, submerged plate and vertical barrier versus $\gamma_{10}h$ on varying the porosity of plate for the composite breakwater for considering $\varepsilon_1 = 0.4$, $\varepsilon_3 = 0.2$, $h_1 / h = 0$, $a / h = 1.0$, $L / h = 1.0$ and $\theta = 30^0$. It is observed that when porosity of the plate is increasing from 10% to 40%, the wave force acting on the structure (Fig. 5.9a) is found to be decreasing. There is a 90% reduction in wave forces in submerged porous structure when porosity of the submerged plate is 0.4. But when the porosity of plate increases, there is a 57.5% reduction in wave forces acting on the barrier (Fig. 5.9b). The wave force acting on porous block is comparatively greater than that acts on plate and barrier. The wave force acting on the porous structure is observed to be negligible when long waves are incident on the structure for $0.1 < \gamma_{10}h < 2$.

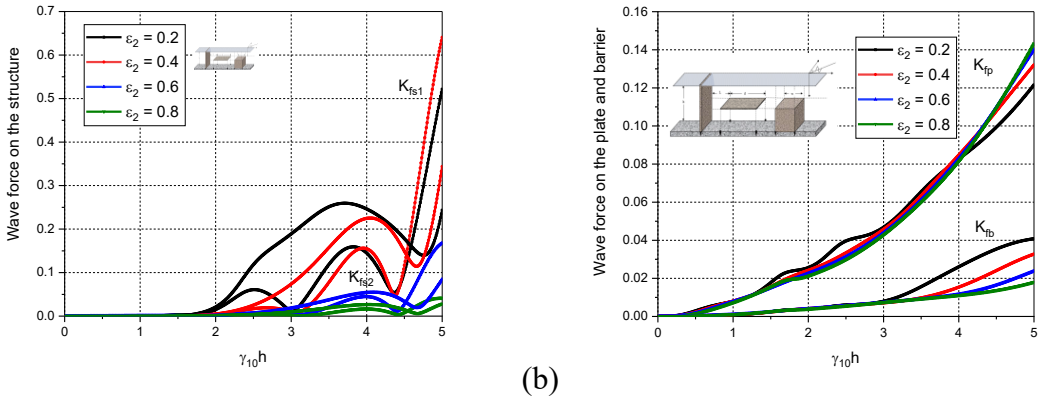

(a) (b)

Fig. 5.9: Variation of (a) K_{fs_1} and K_{fs_2} and (b) K_{fp} and K_{fb} versus $\gamma_{10}h$ for different values of porosity of plate considering $\varepsilon_1 = 0.4$, $\varepsilon_3 = 0.2$, $h_1 / h = 0$, $a / h = 1.0$, $L / h = 1.0$ and $\theta = 30^0$.

5.4.3.2 Effects of porous structure length

The wave force on the composite porous structure is investigated in Fig. 5.10(a,b) depicting the variation of wave forces acting on the front side, back side, submerged plate, and barrier versus $\gamma_{10}h$ varying the width of submerged porous structure considering $\varepsilon_1 = 0.4,\ \varepsilon_2 = 0.1,$ $\varepsilon_3 = 0.2,\ h_1/h = 0,\ a/h = 1.0,\ L/h = 1.0$ and $\theta = 30^0$.

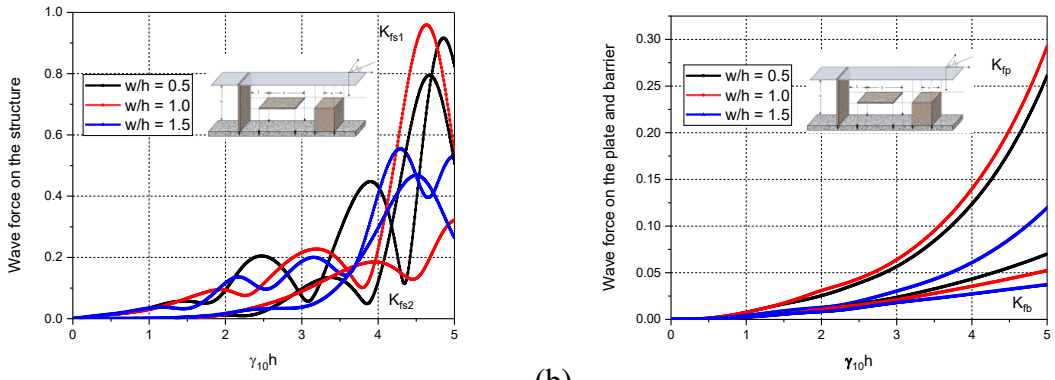

(a) (b)

Fig. 5.10: Variation of (a) K_{fs_1} and K_{fs_2} and (b) K_{fp} and K_{fb} versus $\gamma_{10}h$ for different values of width of submerged porous structure w/h considering $\varepsilon_1 = 0.4,\ \varepsilon_2 = 0.1,\ \varepsilon_3 = 0.2,$ $h_1/h = 0,\ a/h = 1.0,\ L/h = 1.0$ and $\theta = 30^0$.

It is observed that as the width of the submerged porous structure w/h increases, the wave force acting is found to be decreasing, which may be due to more wave structure interaction and wave dissipation. The numerical results shows that there is a 47% reduction in wave forces acting on the barrier when the width of the structure increases. In the case of width of porous block $w/h = 1$, the wave force acting on the submerged porous plate is found to be 143% greater than the force acting on the porous barrier. Also, for long waves, $0.1 < \gamma_{10}h < 0.5$, the wave force acting on porous structure is observed to be very negligible and it increases comparatively when short waves are incident on the structure.

5.4.4. Surface Deflection

The surface deflection in the incident and the transmitted region is analysed on varying the angle of incidence, submergence depth and non-dimensional wave number to understand the wave attenuating phenomenon due to the composite breakwater system.

5.4.4.1 Effects of angle of incidence

In Fig 5.11(a,b), the surface deflection in the incident region and transmitted region is plotted versus distance x for various values of angle of incidence θ considering $h_1/h=0$

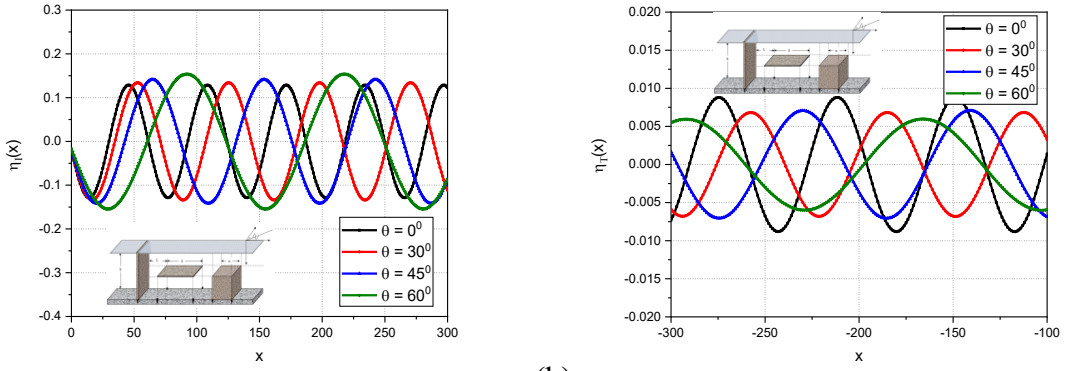

(a) (b)

Fig. 5.11: Variation of (a) $\eta_I(x)$ and (b) $\eta_T(x)$ versus x for different values of angle of incidence considering $\varepsilon_1=0.4,\ \varepsilon_2=0.2,\ \varepsilon_3=0.2,\ h_1/h=0,\ a/h=1.0$ and $L/h=1.0$.

The study shows that the surface elevation in the incident wave region increases with the increase in the angle of incidence and due to that the phase angle of the incident wave changes. In Fig. 5.11(b), it is observed that the surface deflection in the transmitted region is lower as compared to that of the incident region. It is also observed that the surface deflection in the transmitted region decreases as the wave angle of incidence decreases. The crest region of surface deflection in the transmitted region reduces to 96% when $\theta=60^0$. The surface deflection in the transmitted region is observed to be higher when the incident wave angle is $\theta=0^0$. Further, on comparing the surface deflection in the incident wave region, the transmitted region's surface deflection is reduced by 173%. A reduction in surface deflection is observed as the incident wave angle increases.

5.4.4.2 Effect of submergence depth

The surface deflections in the incident and transmitted regions are presented in Fig. 5.12(a,b) for varying submergence depth.. The study shows the surface deflection with change of submergence depth of plate h_1/h considering $\gamma_{10}h=2,\ \theta=30^0, \varepsilon_1=0.4,\ \varepsilon_2=0.2,\ \varepsilon_3=0.2,$ $a/h=1.0$ and $L/h=1.0$. It is observed that the surface deflection in the incident region (Fig. 5.12a) slightly decreases with increase in the submergence depth. In Fig. 5.12(b), the surface deflection in the transmitted region is plotted versus various values of submergence depth of

plate and it is found that the surface deflection in the transmitted region is less compared to that of the incident region. It is also seen that the surface deflection decreases when the submerged plate is on the free surface. The crest region of surface deflection in the transmitted region reduces to 92% when plate is on the free surface. The surface deflection in the incident region is found to be decreasing as the depth of submergence increases, while the surface deflection in the transmitted region is found to be increasing as the depth of submergence increases.

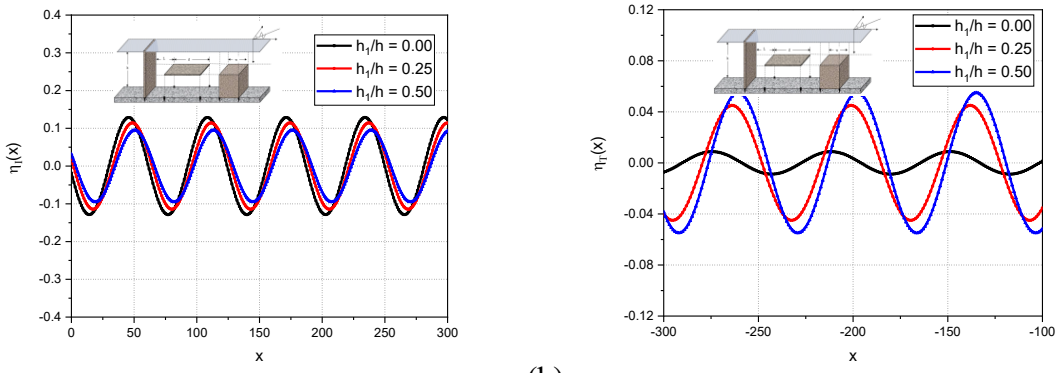

(a) (b)

Fig. 5.12: Variation of (a) $\eta_1(x)$ and (b) $\eta_T(x)$ versus x for different values of submergence depth of plate considering $\varepsilon_1 = 0.4,\ \varepsilon_2 = 0.2,\ \varepsilon_3 = 0.2,\ \theta = 30^0,\ a/h = 1.0$ and $L/h = 1.0$.

5.4.4.3 Effect of dimensionless wave number

In Fig. 5.13(a,b), the surface deflection in the incident and transmitted region is plotted versus distance x for various values of dimensionless wave number $\gamma_{10}h$ considering $h_1/h = 0$. It can be seen that the amplitude of the wave with least wave number in incident wave region turns out to be the wave of maximum amplitude on transmission. The phase lag also seems to be magnified after transmission takes place relative to that of the incident waves. In Fig. 5.13(a), it is observed that with the increase in the wave number the surface elevation in the incident wave region increases and the phase angle of the incident wave also changes. On the other hand, in Fig. 5.13(b), it is observed that the surface deflection in the transmitted region is less compared to that of the incident region for all values of non-dimensional wave number. Thus, as the wave number is increasing, it is found that surface elevation in the transmitted region is decreasing. The crest region of surface deflection in the transmitted region reduces to 96.4% when $\gamma_{10}h = 2.5$.

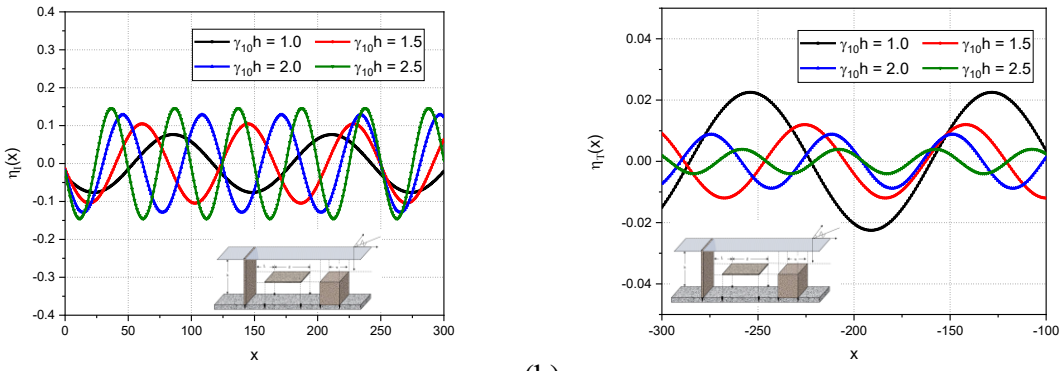

(a) (b)

Fig. 5.13: Variation of (a) $\eta_1(x)$ and (b) $\eta_T(x)$ versus x for different values of dimensionless wavenumber considering $\varepsilon_1 = 0.4$, $\varepsilon_2 = 0.2$, $\varepsilon_3 = 0.2$, $h_1/h = 0$, $\theta = 30^0$, $a/h = 1.0$ and $L/h = 1.0$.

5.5 CLOSURE

The interaction of oblique monochromatic incident waves with a composite breakwater consisting of a submerged porous structure, a submerged horizontal porous plate, and a fully-extended barrier is investigated using two-dimensional linear potential theory. The reflection, transmission, and dissipation coefficients, wave forces acting on the composite breakwater, and surface deflection corresponding to changes in the porosity of the structure, submergence depth of the plate, and spacing between the structures are analysed in the numerical study. The numerical results for the submerged porous plate breakwater are compared with the previous predictions of Cho and Kim (2013). The conclusions drawn from the study are as follows:

- The resonating trend in wave reflection is observed on varying the non-dimensional wave number and this may be due to the trapping of waves in the confined regions between plate and porous structure or barrier. The critical angle is found to be at $\theta = 60°$ and $\gamma_{10}h = 4.1$.

- The wave transmission decreases to 42.6% when porosity of the structure changes from $\varepsilon_1 = 0.8$ to $\varepsilon_1 = 0.2$ and when $\gamma_{10}h = 6$. Further, the transmission coefficient decreases as the distance between the structure and the porous plate increases. This could be because as the spacing widens, waves must travel a greater distance, dissipating more energy.

- The energy dissipation increases as the spacing between the submerged porous structure and the submerged horizontal porous plate increases. In addition, the wave damping increases to $K_d = 0.9$, when porosity of submerged structure increases to 80%, this could be due to the enhanced wave-structure interaction.
- The waves with higher wave numbers are observed to be exhibiting comparatively higher wave energy damping than long waves. Further, it is observed that higher inertia factors have a low transmission coefficient for long incident waves, while low inertia factors have a lower transmission coefficient for moderate incident waves.
- Around 90% reduction in wave forces is observed in submerged porous structure when porosity is 0.4 and the crest region of surface deflection in the transmitted region reduces to 92% when plate is on the free surface.

CHAPTER 6

STRATIFIED POROUS STRUCTURE WITH STEPPED SEABED

6.1 GENERAL INTRODUCTION

The wave interaction with stratified porous structure combined with a surface-piercing porous block in stepped seabed is analysed based on the small amplitude wave theory. The study is performed to analyse the effectiveness of partial porous structure in increasing the wave attenuation in the nearshore regions consisting of stratified porous structures of different configuration using eigenfunction expansion method and orthogonal mode-coupling relation. The hydrodynamic characteristics such as wave reflection coefficient, transmission coefficient, dissipation coefficient, wave force impact and surface elevation are investigated due to the presence of both horizontally and vertically stratified porous structures. The effect of varying porosity, structural width, angle of incidence, wavelength and length between the porous block and stratified structure are examined. The numerical results are validated with the results available in the literature. The present study demonstrates that the presence of stratified structure can decrease wave transmission thereby serving as an efficient wave attenuation mechanism. The wave force acting on stratified structure can be decreased if the structure is combined with wider surface-piercing porous blocks. Further, the presence of stratified porous structure combined with porous block helps in creating a tranquil zone in the leeside of the structure. The combination of vertical and horizontal stratified porous structure with surface-piercing porous block is intended to be an effective solution for protection of coastal facility.

6.2 MATHEMATICAL FORMULATION

The present study investigates the oblique wave interaction with stratified porous structure combined with a surface piercing porous block placed on stepped sea bottom using the small amplitude wave theory. The study is performed on both horizontally and vertically stratified porous structures consisting of two layers of different porosities and friction factors. The surface piercing porous block is on the seaward side of stratified porous structure. The

horizontally stratified porous structure is placed over the first rigid step whereas vertically stratified structure over first and second rigid steps such that each layer is over each step. The thickness of both the porous layers are kept equal throughout the study. The physical problem is analysed in the three-dimensional cartesian coordinate system with x and $z-$axis in horizontal directions and the $y-$axis is considered positive downward.

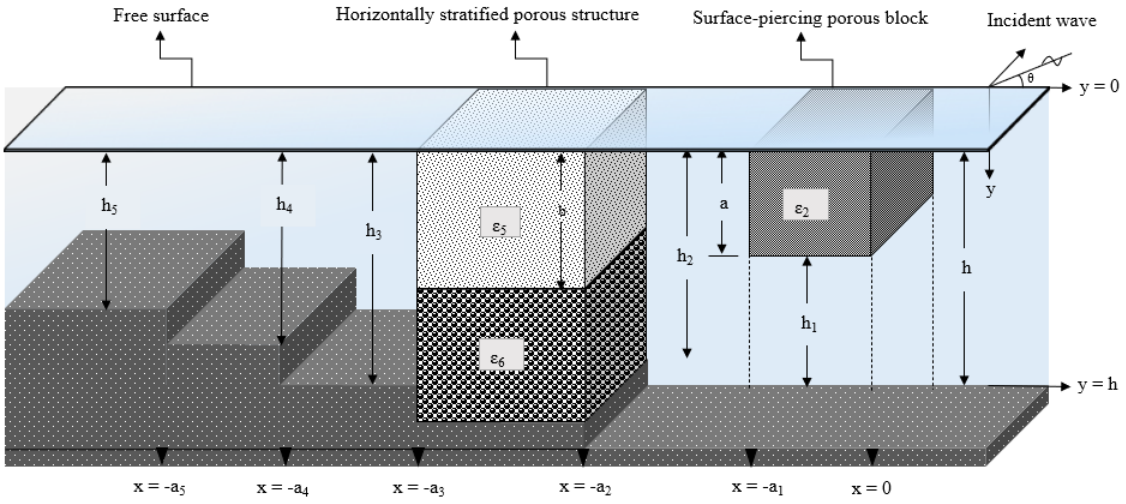

Fig. 6.1: Horizontally stratified porous structure with porous block in stepped seabed.

The seabed is assumed to be impervious such that no flow is possible in perpendicular direction. The porous structure is assumed to be fully extended and the height is considered equal to free surface. The fluid domain is divided into nine regions as shown in Fig. 6.1 and Fig. 6.2. In the case of horizontally stratified porous structure, the regions considered include the upstream open sea region $I_1 \equiv (0 \le x \le \infty, 0 \le y \le h)$, porous block region $I_2 \equiv (-a_1 \le x \le 0, 0 \le y \le a)$, region below porous block $I_3 \equiv (-a_1 \le x \le 0, a \le y \le h)$, open sea region between porous block and stratified porous block $I_4 \equiv (-a_2 \le x \le -a_1, 0 \le y \le h)$, surface porous region of stratified structure $I_5 \equiv (-a_3 \le x \le -a_2, 0 \le y \le b)$, bottom porous structure region $I_6 \equiv (-a_3 \le x \le -a_2, b \le y \le h)$, open sea region above second rigid step $I_7 \equiv (-a_4 \le x \le -a_3, 0 \le y \le h_3)$, open sea region above the third rigid step $I_8 \equiv (-a_5 \le x \le -a_4, 0 \le y \le h_4)$ and the downward open sea region $I_9 \equiv (-\infty \le x \le -a_5, 0 \le y \le h_5)$. In the case of vertically stratified porous structure, the regions include the upstream open sea region $I_1 \equiv (0 \le x \le \infty, 0 \le y \le h)$, porous block region $I_2 \equiv (-a_1 \le x \le 0, 0 \le y \le a)$, region below porous block $I_3 \equiv (-a_1 \le x \le 0, a \le y \le h)$, open sea

region between porous block and stratified porous block $I_4 \equiv (-a_2 \le x \le -a_1, 0 \le y \le h)$, seaward porous layer over first rigid step $I_5 \equiv (-a_3 \le x \le -a_2, 0 \le y \le h_2)$, leeward porous layer over second rigid step $I_6 \equiv (-a_4 \le x \le -a_3, 0 \le y \le h_3)$, open sea region above third rigid step $I_7 \equiv (-a_5 \le x \le -a_4, 0 \le y \le h_4)$, open sea region above the fourth rigid step $I_8 \equiv (-a_6 \le x \le -a_5, 0 \le y \le h_5)$ and the downward open sea region $I_9 \equiv (-\infty \le x \le -a_6, 0 \le y \le h_6)$.

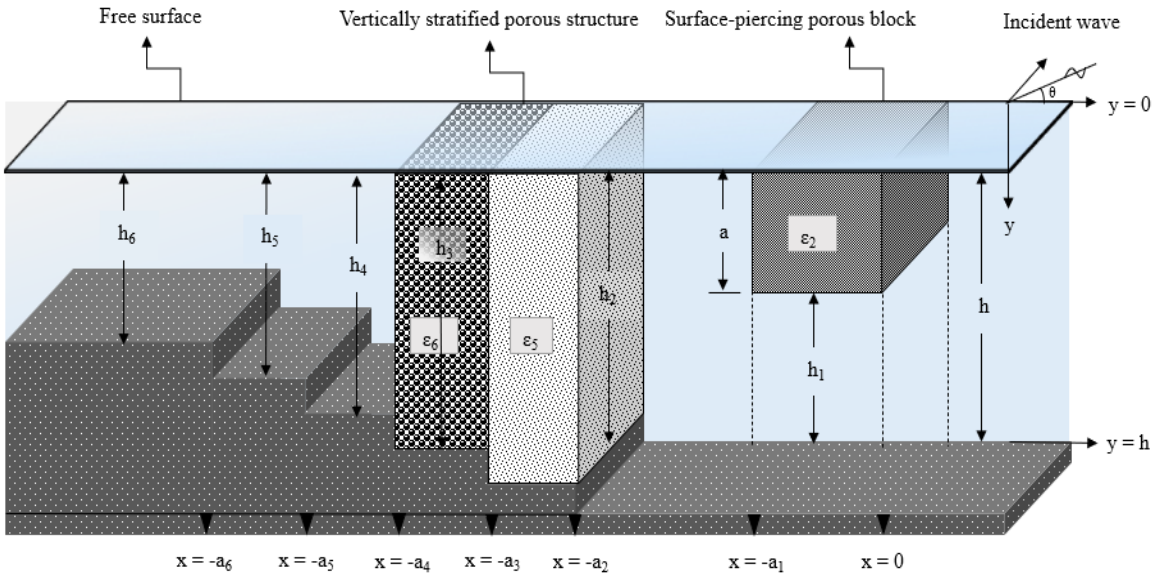

Fig. 6.2: Vertically stratified porous structure with porous block in stepped seabed.

The incident wave is considered to be obliquely propagating in $x-$direction with an angle θ. It is assumed that fluid is inviscid, incompressible, irrotational and time harmonic with angular frequency ω. The velocity potentials in the respective regions are represented in the form $\phi_j(x,y,z,t) = \mathrm{Re}\left[\phi_j(x,y)\,\mathrm{e}^{\mathrm{i}(lz-\omega t)}\right]$, where $l = \gamma_{10}\sin\theta$ and γ_{10} is the progressive wave number in open water region. The velocity potentials in the respective regions satisfy the Helmholtz equation given by

$$\frac{\partial^2\phi_j}{\partial x^2} + \frac{\partial^2\phi_j}{\partial y^2} - l^2\phi_j = 0, \text{ for } -\infty < x < \infty, 0 < y < h. \tag{6.1}$$

The linearized free surface boundary condition for the open water and porous structure region is of the form

$$\frac{\partial\phi_j}{\partial y} + K_j\phi_j = 0, \quad \text{on} \quad y = 0, \tag{6.2}$$

where $K_{j=1,4,5,6}=\dfrac{\omega^2}{g}$, and $K_{j=2,3}=\dfrac{\omega^2}{g}\left(S_j-if_j\right)$ for free surface and porous structure region, S_j and f_j are reactance and frictional coefficients of porous regions of breakwater and g is the acceleration due to gravity. The bottom boundary condition due to the presence of impermeable sea-bed is given by

$$\frac{\partial\phi_j}{\partial y}=0,\ \text{ on }\ y=h. \tag{6.3}$$

The wave propagating due to the presence of the porous structure suggest the continuity of fluid pressure and velocity across the seaward and leeward structural interfaces. The linearized resistance f_j and reactance coefficients S_j (Sollitt and Cross, 1972) offered by each of the porous layer is determined on solving the relation given by

$$S_j=1+C_m\left[\frac{1-\varepsilon_j}{\varepsilon_j}\right],\ \text{ on }\ j=2,3, \tag{6.4a}$$

$$f_j=\frac{1}{\omega}\left\{\frac{\int_V dV\int_t^{t+T}\varepsilon_j^2\left(\dfrac{\nu q^2}{\Lambda_p}+\dfrac{C_f\varepsilon_j}{\sqrt{\Lambda_p}}|q|^3\right)dt}{\int_V dV\int_t^{t+T}\varepsilon_j q^2 dt}\right\},\ \text{ on } j=2,3, \tag{6.4b}$$

where, C_m is coefficient of added mass considered to be very minimal/zero (Sollitt and Cross, 1972), thus $S_j=1$ is kept fixed throughout the study. The $\Lambda_p=$ intrinsic permeability, $q=$ instantaneous Eulerian velocity vector, $\nu=$ kinematic viscosity, $V=$ volume, $C_f=$ turbulent resistant coefficient and $T=$ wave period. The continuity of the velocity and pressure is satisfied for both surface piercing porous block and stratified porous structures. In the far-field region, the radiation conditions in the presence of porous structure is given by

$$\phi_{j=1,9}(x,y)=\begin{cases}\left(I_{10}e^{-i\gamma_{10}x}+R_{10}e^{i\gamma_{10}x}\right)f_{10}(y) & \text{as}\ \ x\to\ \infty,\\ \left(T_{90}e^{-i\gamma_{30}x}\ \right)f_{90}(y) & \text{as}\ \ x\to-\infty,\end{cases} \tag{6.5}$$

where, I_{10}, R_{10} and T_{90} are the complex amplitude of the incident, reflected and transmitted wave energies respectively. In the present study, the incident wave I_{10} is considered to be unity. The continuity of pressure and velocity due to the presence of surface piercing porous block at the edge $x=0,-a_1$ and $j=1,4$ are given by

$$\phi_j(x,y)\Big|_{j=1,4} = \begin{cases} (S_2 + if_2)\phi_2(x,y) & \text{for } 0 < y < a, \\ \phi_3(x,y) & \text{for } a < y < h, \end{cases} \tag{6.6a}$$

$$\frac{\partial \phi_j(x,y)}{\partial x}\Big|_{j=1,4} = \begin{cases} \varepsilon_2 \dfrac{\partial \phi_2(x,y)}{\partial x} & \text{for } 0 < y < a, \\ \dfrac{\partial \phi_3(x,y)}{\partial x} & \text{for } a < y < h. \end{cases} \tag{6.6b}$$

The wave number in surface piercing porous block region satisfies the dispersion relation for finite water depth given by

$$\omega^2 - g\gamma_{2n} \tanh \gamma_{2n} h - F_n \left[\omega^2 \tanh \gamma_{2n} h - g\gamma_{2n} \right] = 0 \quad \text{for} \quad n = 0, 1, 2, ... \tag{6.7a}$$

where,

$$F_n = \frac{\left((S_2 + if_2) - \varepsilon_2\right) \tanh \gamma_{2n} a}{\left((S_2 + if_2) - \varepsilon_2 \tanh^2 \gamma_{2n} a\right)} \tag{6.7b}$$

6.2.1 Horizontally Stratified Porous Structure

The horizontally stratified porous structure is assumed to be placed at $-a_3 < x < -a_2$ on the leeward side of porous block over a rigid step and the water depth $0 < y < h_2$. So, the continuity of pressure and velocity due to the presence of two layered porous structure at the edge $x = -a_2, -a_3$ and $j = 4, 7$ are given by

$$\phi_j(x,y)\Big|_{j=4,7} = \begin{cases} (S_5 + if_5)\phi_5(x,y) & \text{for } 0 < y < b, \\ (S_6 + if_6)\phi_6(x,y) & \text{for } b < y < h_2, \end{cases} \tag{6.8a}$$

$$\frac{\partial \phi_j(x,y)}{\partial x}\Big|_{j=4,7} = \begin{cases} \varepsilon_5 \dfrac{\partial \phi_5(x,y)}{\partial x} & \text{for } 0 < y < b, \\ \varepsilon_6 \dfrac{\partial \phi_6(x,y)}{\partial x} & \text{for } b < y < h_2. \end{cases} \tag{6.8b}$$

In addition, there exists a flow within the surface and bottom porous layers in the vertical direction for $-a_3 < x < -a_2$ and $y = b$ (Liu et al., 2007) is given by

$$(S_5 + if_5)\phi_5(x,y) = (S_6 + if_6)\phi_6(x,y), \tag{6.9a}$$

$$\varepsilon_5 \frac{\partial \phi_5(x,y)}{\partial y} = \varepsilon_6 \frac{\partial \phi_6(x,y)}{\partial y}. \tag{6.9b}$$

In the case of change in the bottom topography, the flow near rigid step at $x = -a_2, -a_3, -a_4, -a_5$ satisfies the zero-flow condition given by

$$\frac{\partial \phi_4(x,y)}{\partial x}=0 \text{, for } h_2<y<h \text{,} \quad \frac{\partial \phi_6(x,y)}{\partial x}=0 \text{, for } h_3<y<h_2 \tag{6.10a}$$

$$\frac{\partial \phi_7(x,y)}{\partial x}=0 \text{, for } h_4<y<h_3 \quad \text{and} \quad \frac{\partial \phi_8(x,y)}{\partial x}=0 \text{, for } h_5<y<h_4 \tag{6.10b}$$

The wave number in upstream/downstream free-water region γ_{j0} for $j=1,4,7,8,9$ and porous structure region γ_{20} satisfies the dispersion relation for finite water depth is given by

$$\omega^2=\begin{cases} g\gamma_{j0}\tanh\gamma_{j0}h_j & \text{for} \quad n=0 \\ -g\gamma_{jn}\tan\gamma_{jn}h_j & \text{for} \quad n=1,2,.... \end{cases} \text{ for } j=1,4,7,8,9 \tag{6.11a}$$

$$(S_5+if_5)\omega^2-g\gamma_{5n}\tanh\gamma_{5n}h_2=P_n\left[(S_5+if_5)\omega^2\tanh\gamma_{5n}h_2-g\gamma_{5n}\right] \text{for } j=5, n=0,1,2,.... \tag{16.11b}$$

where, $h_j=h$ for $j=1,4$, $h_j=h_3$ for $j=7$, $h_j=h_4$ for $j=8$ and $h_j=h_5$ for $j=9$ respectively with

$$P_n=\frac{\left(1-\dfrac{\varepsilon_6(S_5+if_5)}{\varepsilon_5(S_5+if_5)}\right)\tanh\gamma_{5n}b}{\left(1-\dfrac{\varepsilon_6(S_5+if_5)}{\varepsilon_5(S_6+if_6)}\tanh^2\gamma_{5n}b\right)} \tag{6.11c}$$

6.2.2 Vertically Stratified Porous Structure

The vertically stratified porous structure is assumed to be placed at $-a_4\le x\le -a_2$ over two rigid steps with water depths $0\le y\le h_2$ and $0<y<h_3$. So, the continuity of pressure and velocity due to the presence of two layered porous structure at the edges $x=-a_2,-a_3,-a_4$ are given by

$$\phi_4(x,y)=(S_5+if_5)\phi_5(x,y) \text{ and } \frac{\partial \phi_4(x,y)}{\partial x}=\varepsilon_5\frac{\partial \phi_5(x,y)}{\partial x} \text{ at } x=-a_2, \tag{6.12a}$$

$$(S_5+if_5)\phi_5(x,y)=(S_6+if_6)\phi_6(x,y) \text{ and } \varepsilon_5\frac{\partial \phi_5(x,y)}{\partial x}=\varepsilon_6\frac{\partial \phi_6(x,y)}{\partial x} \text{ at } x=-a_3 \tag{6.12b}$$

$$(S_6+if_6)\phi_6(x,y)=\phi_7(x,y) \text{ and } \varepsilon_6\frac{\partial \phi_6(x,y)}{\partial x}=\frac{\partial \phi_7(x,y)}{\partial x} \text{ at } x=-a_4 \tag{6.12c}$$

In the case of vertically stratified porous structure, zero flow condition exists at the interface of rigid steps $x=-a_2,-a_3,-a_4,-a_5,-a_6$ given by

$$\frac{\partial \phi_4(x,y)}{\partial x} = 0 \text{, for } h_2 < y < h \text{,} \quad \frac{\partial \phi_5(x,y)}{\partial x} = 0 \text{, for } h_3 < y < h_2 \tag{6.13a}$$

$$\frac{\partial \phi_6(x,y)}{\partial x} = 0 \text{, for } h_4 < y < h_3 \text{,} \quad \frac{\partial \phi_7(x,y)}{\partial x} = 0 \text{, for } h_5 < y < h_4 \quad \text{and} \tag{6.13b}$$

$$\frac{\partial \phi_8(x,y)}{\partial x} = 0 \text{, for } h_6 < y < h_5 \tag{6.13c}$$

The wave numbers in the upstream/downstream free-water regions are same as Eq. (6.9a) and the porous structure region satisfy the dispersion relation given by

$$\omega^2 (S_j + if_j) = g\gamma_{jn} \tanh \gamma_{jn} h_j \qquad \text{for} \qquad n = 0,1,2,.... \tag{6.14}$$

where $h_j = h_2, h_3$ for $j = 5,6$ respectively.

The dispersion relation of open water regions is solved using Newton-Raphson method while the dispersion relation for the porous structure region is solved using perturbation method as in Mendez and Losada (2004).

6.3 METHOD OF SOLUTION

The wave interaction with the stratified porous structures combined with porous block in the presence of elevated step is examined using the eigenfunction expansion method. In the present section, the solution approach for both horizontally and vertically stratified porous structure is presented in detail. The velocity potential in the incident open water region for both the horizontally and vertically stratified cases is given by

$$\phi_1(x,y) = \left(I_{10} e^{-ik_{10}x} + R_{10} e^{ik_{10}x} \right) f_{10}(y) + \sum_{n=1}^{\infty} R_{1n} e^{-ik_{1n}x} f_{1n}(y) \quad \text{for } 0 \le x \le \infty, 0 \le y \le h \tag{6.15}$$

where, I_{10} is the amplitude of the incident wave, R_{1n} for $n = 1,2,3,....$ are the unknown constants to be determined. The vertical eigenfunction for incident open water region is given by

$$f_{1n}(y) = \begin{cases} \dfrac{\cosh \gamma_{10}(h-y)}{\cosh \gamma_{10} h} & \text{for } n = 0, \\ \dfrac{\cos \gamma_{1n}(h-y)}{\cos \gamma_{1n} h} & \text{for } n = 1,2,.... \end{cases} \tag{6.16}$$

The velocity potential due to the presence of surface piercing porous block and leeward open water region are given by

$$\phi_2(x,y) = \sum_{n=0}^{\infty} \{ A_{2n} e^{-ik_{2n}x} + B_{2n} e^{ik_{2n}(x+a_1)} \} f_{2n}(y), \quad -a_1 \le x \le 0, \ 0 \le y \le a \tag{6.17a}$$

$$\phi_3(x,y)=\sum_{n=0}^{\infty}\{A_{2n}e^{-ik_{2n}x}+B_{2n}e^{ik_{2n}(x+a_1)}\}f_{3n}(y),\qquad -a_1\le x\le 0,\ a\le y\le h \tag{6.17b}$$

$$\phi_4(x,y)=\{A_{40}e^{-ik_{j0}(x+a_{j-3})}+B_{40}e^{ik_{j0}(x+a_{j-2})}\}f_{40}(y)+\sum_{n=1}^{\infty}\{A_{4n}e^{-ik_{jn}(x+a_{j-3})}+B_{4n}e^{ik_{jn}(x+a_{j-2})}\}f_{4n}(y), \tag{6.17c}$$
$$-a_2\le x\le -a_1,\ 0\le y\le h$$

where $A_{2n},B_{2n},A_{40},B_{40},A_{4n},B_{4n}$ for $n=0,1,2,....$ are the unknown constants to be determined, $w_1=a_1$ is the thickness of the porous block. The vertical eigenfunctions for the porous block and leeward open water regions are given by

$$f_{2n}(y)=\frac{\cosh\gamma_{2n}(h-y)-F_n\sinh\gamma_{2n}(h-y)}{\cosh\gamma_{2n}h-F_n\sinh\gamma_{2n}h} \tag{6.18a}$$

$$f_{3n}(y)=\frac{(1-F_n\tanh\gamma_{2n}a\cosh\gamma_{2n}(h-y)}{(S_2+if_2)(\cosh\gamma_{2n}h-F_n\sinh\gamma_{2n}h)},\ \text{for}\ \ n=0,1,2,.... \tag{6.18b}$$

$$f_{4n}(y)=\begin{cases}\dfrac{\cosh\gamma_{40}(h-y)}{\cosh\gamma_{40}h} & \text{for n=0,}\\[2ex] \dfrac{\cos\gamma_{4n}(h-y)}{\cos\gamma_{4n}h} & \text{for n=1,2,....}\end{cases} \tag{6.18c}$$

The eigenfunctions $f_{jn}(y)$ for $j=2,3$ satisfy the orthogonal mode-coupling relation of the form

$$\langle f_{jn},f_{jm}\rangle_{j=2,3}=\int_0^h f_{jn}(y)f_{jm}(y)dy=\int_0^a f_{2n}(y)f_{2m}(y)dy+\int_a^h f_{3n}(y)f_{3m}(y)dy \tag{6.19}$$

Using the continuity of pressure and velocity along with orthogonal mode-coupling relation at the interface $x=0,-a_1$, the equation given by

$$\begin{aligned}\langle\phi_j(x,y),f_{jm}(y)\rangle_{j=1,4}&=\int_0^h\phi_j(x,y)f_{jm}(y)dy=\left\{\int_0^a+\int_a^h\right\}\phi_j(x,y)f_{jm}(y)dy\\&=(S_2+if_2)\int_0^a\phi_2(x,y)f_{jm}(y)dy+\int_a^h\phi_3(x,y)f_{jm}(y)dy\ \text{for}\ m=0,1,2,....\end{aligned} \tag{6.20a}$$

$$\begin{aligned}\langle\phi_{jx}(x,y),f_{jm}(y)\rangle_{j=1,4}&=\int_0^h\phi_{jx}(x,y)f_{jm}(y)dy=\left\{\int_0^a+\int_a^h\right\}\phi_{jx}(x,y)f_{jm}(y)dy\\&=\varepsilon_2\int_0^a\phi_2(x,y)f_{jm}(y)dy+\int_a^h\phi_3(x,y)f_{jm}(y)dy\ \text{for}\ m=0,1,2,....\end{aligned} \tag{6.20b}$$

6.3.1 Horizontally Stratified Porous Structure

The velocity potentials due the presence of horizontally stratified porous structure and leeward open water regions are given by

$$\phi_j(x,y)\big|_{j=5,6} = \sum_{n=0}^{\infty}\{A_{jn}e^{-ik_{jn}(x+a_{j-3})} + B_{jn}e^{ik_{jn}(x+a_{j-2})}\}f_{jn}(y), \qquad 0\le y\le b \text{ if } j=5, b\le y\le h_2 \text{ if } j=6 \tag{6.21a}$$

$$\phi_j(x,y)\big|_{j=7,8} = \{A_{j0}e^{-ik_{j0}(x+a_{j-3})} + B_{j0}e^{ik_{j0}(x+a_{j-2})}\}f_{j0}(y) + \sum_{n=1}^{\infty}\{A_{jn}e^{-ik_{jn}(x+a_{j-3})} + B_{jn}e^{ik_{jn}(x+a_{j-2})}\}f_{jn}(y),\ 0\le y\le h_3 \text{ if } j=7, 0\le y\le h_4 \text{ if } j=8 \tag{6.21b}$$

$$\phi_9(x,y) = T_{90}e^{-ik_{90}(x+a_5)}f_{90}(y) + \sum_{n=1}^{\infty}T_{9n}e^{k_{9n}(x+a_5)}f_{9n}(y), \qquad -\infty\le x\le -a_5, 0\le y\le h_5 \tag{6.21c}$$

where T_{90} is the transmitted wave amplitude, A_{jn}, B_{jn} and T_{9n} for $n=0,1,2,....$ and $j=5,6,7,8$ are the unknown constants to be determined, $w_2=(a_3-a_2)$ is thickness of the porous structure. The vertical eigenfunctions for the porous structure and leeward open water regions are given by

$$f_{5n}(y) = \frac{\cosh\gamma_{5n}(h_2-y) - P_n\sinh\gamma_{5n}(h_2-y)}{\cosh\gamma_{5n}h_2 - P_n\sinh\gamma_{5n}h_2} \tag{6.22a}$$

$$f_{6n}(y) = \frac{(S_5+if_5)(1-P_n\tanh(\gamma_{5n}b)\cosh\gamma_{5n}(h_2-y)}{(S_6+if_6)(\cosh\gamma_{5n}h_2 - P_n\sinh\gamma_{5n}h_2)}, \quad \text{for} \quad n=0,1,2,.... \tag{6.22b}$$

$$f_{jn}(y) = \begin{cases} \dfrac{\cosh\gamma_{j0}(h'-y)}{\cosh\gamma_{j0}h'} & \text{for n=0,} \\ \dfrac{\cos\gamma_{jn}(h'-y)}{\cos\gamma_{jn}h'} & \text{for n=1,2,....} \end{cases} \tag{6.22c}$$

where, $h'=h_3,h_4,h_5$ for $j=7,8,9$ respectively. The eigenfunctions $f_{jn}(y)$ for $j=1,4,7,8,9$ satisfy the orthogonal mode-coupling relation of the form

$$\langle f_{jn}, f_{jm}\rangle_{j=1,4,7,8,9} = \begin{cases} 0 & \text{for} \quad m\ne n, \\ C'_{jn} & \text{for} \quad m=n, \end{cases} \tag{6.23a}$$

$$\langle f_{jn}, f_{jm}\rangle_{j=5,6} = \int_0^{h_2} f_{jn}(y)f_{jm}(y)dy = \int_0^{b} f_{5n}(y)f_{5m}(y)dy + \int_b^{h} f_{6n}(y)f_{6m}(y)dy \tag{6.23b}$$

where $C'_{jn}=\left\{\dfrac{2\gamma_{jn}h_j+\sinh 2\gamma_{jn}h_j}{4\gamma_{jn}\cosh^2\gamma_{jn}h_j}\right\}$, for $j=1,4,7,8,9,\ n=0$ respectively with $C'_{jn}\big|_{j=1,4,7,8,9}$ for $n=1,2,3,.....$ are obtained by substituting $\gamma_{jn}=i\gamma_{jn}$ in the case of open water region. Using the continuity of pressure and velocity along with orthogonal mode-coupling relation at the interface $x=-a_2,-a_3$, the equation given by

$$\begin{aligned}\left\langle\phi_j(x,y),f_{jm}(y)\right\rangle_{j=4,7}&=\int_0^{h_2}\phi_j(x,y)f_{jm}(y)dy\ =\left\{\int_0^b+\int_b^{h_2}\right\}\phi_j(x,y)f_{jm}(y)dy\\&=(S_5+if_5)\int_0^b\phi_5(x,y)f_{jm}(y)dy+(S_6+if_6)\int_b^{h_2}\phi_6(x,y)f_{jm}(y)dy\ \text{for } m=0,1,2,....\end{aligned}\tag{6.24a}$$

$$\begin{aligned}\left\langle\phi_{jx}(x,y),f_{jm}(y)\right\rangle_{j=4,7}&=\int_0^{h_2}\phi_{jx}(x,y)f_{jm}(y)dy=\left\{\int_0^b+\int_b^{h}\right\}\phi_{jx}(x,y)f_{jm}(y)dy\\&=\varepsilon_5\int_0^b\phi_5(x,y)f_{jm}(y)dy+\varepsilon_6\int_b^{h_2}\phi_6(x,y)f_{jm}(y)dy\ \text{for } m=0,1,2,....\end{aligned}\tag{6.24b}$$

Next, the continuity of pressure and velocity at the edge $x=-a_4$ along with orthogonal mode-coupling relation is utilized to obtain the equation given by

$$\begin{aligned}\left\langle\phi_j(x,y),f_{jm}(y)\right\rangle_{j=7}&=\int_0^{h_3}\phi_7(x,y)f_{jm}(y)dy\\&=\int_0^{h_4}\phi_8(x,y)f_{jm}(y)dy\ \ \text{for } x=-a_4,\ m=0,1,2,...\end{aligned}\tag{6.25a}$$

$$\begin{aligned}\left\langle\phi_{jx}(x,y),f_{jm}(y)\right\rangle_{j=7}&=\int_0^{h_3}\phi_{7x}(x,y)f_{jm}(y)dy\\&=\int_0^{h_4}\phi_{8x}(x,y)f_{jm}(y)dy\ \ \text{for } x=-a_4,\ m=0,1,2,...\end{aligned}\tag{6.25b}$$

Further, the continuity of pressure and velocity at the edge $x=-a_5$ along with orthogonal mode-coupling relation is utilized to obtain the equation given by

$$\begin{aligned}\left\langle\phi_j(x,y),f_{jm}(y)\right\rangle_{j=8}&=\int_0^{h_4}\phi_8(x,y)f_{jm}(y)dy\\&=\int_0^{h_5}\phi_9(x,y)f_{jm}(y)dy\ \ \text{for } x=-a_5,\ m=0,1,2,....\end{aligned}\tag{6.26a}$$

$$\left\langle \phi_{jx}(x,y), f_{jm}(y) \right\rangle_{j=8} = \int_0^{h_4} \phi_{8x}(x,y) f_{jm}(y) dy$$
$$= \int_0^{h_5} \phi_{9x}(x,y) f_{jm}(y) dy \text{ for } x = -a_5,\ m = 0,1,2,.... \tag{6.26b}$$

The infinite sums presented in the Eqs. 6.24(a,b), 6.25(a,b) and 6.26(a,b) obtained from the orthogonal mode-coupling relation are truncated upto finite M terms to obtain a linear system of $12(M+1)$ algebraic equations for the determination of $12(M+1)$ unknowns. The wave reflection and transmission due to the porous structure obtained as

$$K_r = \left| \frac{R_{10}}{I_{10}} \right| \quad \text{and} \quad K_t = \left| \frac{T_{90}}{I_{10}} \right|. \tag{6.27a}$$

Due the existence of porous structure the energy dissipation in the wave propagation is represented as

$$K_d = 1 - K_r^2 - \chi K_t^2. \tag{6.27b}$$

where $\chi = \left\{ \frac{k_{j0} \tanh \gamma_{j0} h_j}{k_{10} \tanh \gamma_{10} h} \right\} \left\{ \frac{\cosh^2 \gamma_{10} h}{\cosh^2 \gamma_{j0} h_j} \right\} \left\{ \frac{2\gamma_{j0} h_j + \sinh 2\gamma_{j0} h_j}{2\gamma_{10} h + \sinh 2\gamma_{10} h} \right\}$.

6.3.2 Vertically Stratified Porous Structure

The velocity potentials in the porous structure and leeward open water regions for the vertically stratified porous structure are given by

$$\phi_j(x,y)\big|_{j=5,6} = \sum_{n=0}^{\infty} \{ A_{jn} e^{-ik_{jn}(x+a_{j-3})} + B_{jn} e^{ik_{jn}(x+a_{j-2})} \} f_{jn}(y),$$
$$0 \le y \le h_2 \text{ if } j = 5, 0 \le y \le h_3 \text{ if } j = 6, \tag{6.28a}$$

$$\phi_j(x,y)\big|_{j=7,8} = \{ A_{j0} e^{-ik_{j0}(x+a_{j-3})} + B_{j0} e^{ik_{j0}(x+a_{j-2})} \} f_{40}(y) +$$
$$\sum_{n=1}^{\infty} \{ A_{jn} e^{-ik_{jn}(x+a_{j-3})} + B_{jn} e^{ik_{jn}(x+a_{j-2})} \} f_{jn}(y),\ \ 0 \le y \le h_4 \text{ if } j = 7, 0 \le y \le h_5 \text{ if } j = 8 \tag{6.28b}$$

$$\phi_9(x,y) = T_{90} e^{-ik_{90}(x+a_6)} f_{90}(y) + \sum_{n=1}^{\infty} T_{9n} e^{k_{9n}(x+a_6)} f_{9n}(y), \qquad \text{for} \quad -\infty \le x \le -a_6, 0 \le y \le h_6 \tag{6.28c}$$

where T_{90} is the transmitted wave amplitude, A_{jn}, B_{jn} and T_{9n} for $j = 5,6,7,8,\ n = 0,1,2,....$ and are the unknown constants to be determined, $w_2 = (a_4 - a_2)$ is thickness of the porous structure. The vertical eigenfunctions for the porous structure and leeward open water regions are given by

$$f_{jn}(y)=\frac{\cosh\gamma_{jn}(h-y)}{\cosh\gamma_{jn}h} \text{ for } j=5,6,\ n=0,1,2,....., \tag{6.29a}$$

$$f_{jn}(y)\big|_{j=7,8,9}=\begin{cases}\dfrac{\cosh\gamma_{j0}(h_j-y)}{\cosh\gamma_{j0}h_j} & \text{for } n=0,\\ \dfrac{\cos\gamma_{jn}(h_j-y)}{\cos\gamma_{jn}h_j} & \text{for } n=1,2,....\end{cases} \tag{6.29b}$$

where, $h_j=h_4$ for $j=7$, $h_j=h_5$ for $j=8$ and $h_j=h_6$ for $j=9$ respectively. The eigenfunctions $f_{jn}(y), j=1,4,7,8,9$ satisfy the orthogonality relation of the form

$$\langle f_{jn},f_{jm}\rangle_{j=1,4,7,8,9}=\begin{cases}0 & \text{for } m\neq n,\\ C'_{jn} & \text{for } m=n,\end{cases} \text{ and } \langle f_{jn},f_{jm}\rangle_{j=5,6}=\begin{cases}0 & \text{for } m\neq n,\\ C''_{jn} & \text{for } m=n,\end{cases} \tag{6.30}$$

where $C'_n|_{j=1,4,7,8,9}=\left\{\dfrac{2\gamma_{jn}h_j+\sinh 2\gamma_{jn}h_j}{4\gamma_{jn}\cosh^2\gamma_{jn}h_j}\right\}, n=0$, and $C''_n|_{j=5,6}=\left\{\dfrac{2\gamma_{jn}h+\sinh 2\gamma_{jn}h}{4\gamma_{jn}\cosh^2\gamma_{jn}h}\right\}$,

$n=0,1,2,...$ with $C'_n|_{j=1,4,7,8,9}$ for $n=1,2,3,.....$ are obtained by substituting $\gamma_{jn}=i\gamma_{jn}$ in the case of open water region.

The relations at interface $x=-a_2$, $0\le y\le h_2$ using the orthogonal mode-coupling relation we have

$$\langle\phi_4(x,y),f_{4m}(y)\rangle=\int_0^{h_2}\phi_4(x,y)f_{4m}(y)dy=(S_5+if_5)\int_0^{h_2}\phi_5(x,y)f_{4m}(y)dy \text{ for } m=0,1,2,... \tag{6.31a}$$

$$\langle\phi_{4x}(x,y),f_{4m}(y)\rangle=\int_0^{h_2}\phi_{4x}(x,y)f_{4m}(y)dy=\varepsilon_5\int_0^{h_2}\phi_{5x}(x,y)f_{4m}(y)dy \text{ for } m=0,1,2,... \tag{6.31b}$$

for $m=0,1,2,....$

Also, at the interface between the porous layers $x=-a_3$, $0\le y\le h_2$, continuity of pressure and the velocity along with the orthogonal relation gives

$$\langle\phi_5(x,y),f_{5m}(y)\rangle=\int_0^{h_2}\phi_5(x,y)f_{5m}(y)dy=\left\{\frac{S_6+if_6}{S_5+if_5}\right\}\int_0^{h_2}\phi_6(x,y)f_{5m}(y)dy \text{ for } m=0,1,2,... \tag{6.32a}$$

$$\langle\phi_{5x}(x,y),f_{5m}(y)\rangle=\int_0^{h_2}\phi_{5x}(x,y)f_{5m}(y)dy=\left\{\frac{\varepsilon_6}{\varepsilon_5}\right\}\int_0^{h_2}\phi_{6x}(x,y)f_{5m}(y)dy \text{ for } m=0,1,2,... \tag{6.32b}$$

The continuity of pressure and velocity at the edge $x=-a_4$ along with orthogonal mode-coupling relation is utilized to obtain the equation given by

$$\begin{aligned}\left\langle \phi_7(x,y), f_{7m}(y)\right\rangle &= \int_0^{h_4} \phi_7(x,y) f_{7m}(y)dy \\ &= (S_6+if_6)\int_0^{h_4} \phi_6(x,y) f_{7m}(y)dy \quad \text{for } x=-a_4,\ m=0,1,2,...\end{aligned} \tag{6.33a}$$

$$\begin{aligned}\left\langle \phi_{7x}(x,y), f_{7m}(y)\right\rangle &= \int_0^{h_4} \phi_{7x}(x,y) f_{7m}(y)dy \\ &= \varepsilon_6\int_0^{h_4} \phi_{6x}(x,y) f_{7m}(y)dy \quad \text{for } x=-a_4,\ m=0,1,2,...\end{aligned} \tag{6.33b}$$

Next, the continuity of pressure and velocity at the edge $x=-a_5$ along with orthogonal mode-coupling relation is utilized to obtain the equation given by

$$\begin{aligned}\left\langle \phi_j(x,y), f_{jm}(y)\right\rangle_{j=7} &= \int_0^{h_4} \phi_7(x,y) f_{jm}(y)dy \\ &= \int_0^{h_5} \phi_8(x,y) f_{jm}(y)dy \quad \text{for } x=-a_5,\ m=0,1,2,...\end{aligned} \tag{6.34a}$$

$$\begin{aligned}\left\langle \phi_{jx}(x,y), f_{jm}(y)\right\rangle_{j=7} &= \int_0^{h_4} \phi_{7x}(x,y) f_{jm}(y)dy \\ &= \int_0^{h_5} \phi_{8x}(x,y) f_{jm}(y)dy \quad \text{for } x=-a_5,\ m=0,1,2,...\end{aligned} \tag{6.34b}$$

Further, the continuity of pressure and velocity at the edge $x=-a_6$ along with orthogonal mode-coupling relation is utilized to obtain the equation given by

$$\left\langle \phi_j(x,y), f_{jm}(y)\right\rangle_{j=8} = \int_0^{h_5} \phi_8(x,y) f_{jm}(y)dy = \int_0^{h_6} \phi_9(x,y) f_{jm}(y)dy \quad \text{for } x=-a_6,\ m=0,1,2,.. \tag{6.35a}$$

$$\begin{aligned}\left\langle \phi_{jx}(x,y), f_{jm}(y)\right\rangle_{j=8} &= \int_0^{h_5} \phi_{8x}(x,y) f_{jm}(y)dy \\ &= \int_0^{h_6} \phi_{9x}(x,y) f_{jm}(y)dy \quad \text{for } x=-a_6,\ m=0,1,2,....\end{aligned} \tag{6.35b}$$

The infinite sums presented in the Eqs. 31(a,b)-35(a,b) obtained from the orthogonal mode-coupling in open water regions are truncated upto finite M terms to obtain a linear system of $14(M+1)$ algebraic equations for the determination of $14(M+1)$ unknowns. The wave

reflection, transmission and dissipation coefficients due to the presence of vertically stratified structure are same as in Eq. 6.27(a,b).

6.3.3 Wave force on the front face of porous block and stratified structure

The wave force impact acting on the front face of porous block, K_{fb1} and that of stratified structure, K_{fs1} are given by

$$K_{fb1} = \left| \frac{F_{fb1}}{2\rho g h I_{10}} \right| \text{ and } K_{fs1} = \left| \frac{F_{fs1}}{2\rho g h I_{10}} \right| \tag{6.36a}$$

and I_{10} is the amplitude of the incident wave potential considered to be unity. In the case of surface piercing porous block, F_{fb1} is given by

$$F_{fb1} = i\rho\omega \int_0^a \left\{ \phi_2(x,y) - \phi_1(x,y) \right\} dy \quad \text{at} \quad x = 0, \tag{6.36b}$$

In the case of horizontally stratified porous structure, F_{fs1} is given by

$$F_{fs1} = i\rho\omega \left\{ \int_0^b \phi_5(x,y)\, dy + \int_b^{h_2} \phi_6(x,y)\, dy - \int_0^h \phi_4(x,y)\, dy + \right\} \quad \text{at} \quad x = -a_2, \tag{6.37a}$$

In the case of vertically stratified porous structure, F_{fs1} is given by

$$F_{fs1} = i\rho\omega \int_0^{h_2} \left\{ \phi_5(x,y) - \phi_4(x,y) \right\} dy \quad \text{at} \quad x = -a_2. \tag{6.37b}$$

6.3.4 Surface Elevation

The free surface gravity wave elevation in the incident and transmitted wave regions are obtained from the relations

$$-i\omega\zeta_j = \phi_{jy} \quad \text{on} \quad y = 0, \quad j = 1, 9, \tag{6.38a}$$

which can be expressed in the form as

$$\zeta_j(x) = \frac{i}{\omega} \begin{cases} -\left(I_{10} e^{-ik_{10}x} + R_{10} e^{ik_{10}x} \right) \gamma_{10} \tanh \gamma_{10} h + \sum_{n=1}^{\infty} R_{1n} e^{-\kappa_{1n}x} \gamma_{1n} \tan \gamma_{1n} h & \text{for } 0 < x < \infty, \\ -T_{90} e^{-ik_{60}(x+a_j)} \gamma_{90} h_j + \sum_{n=1}^{\infty} T_{9n} e^{\kappa_{9n}(x+a_j)} \gamma_{9n} \tan \gamma_{9n} h_j & \text{for } -\infty < x < -a_j. \end{cases}$$

(6.38b)

where, $-a_j = -a_5, h_j = h_5$ for horizontally stratified structure and $-a_j = -a_6, h_j = h_6$ in the case of vertically stratified porous structure.

6.4 RESULTS AND DISCUSSION

The numerical investigation is performed to examine the wave interaction due to stratified porous structure combined with surface-piercing porous block in changing bottom topography considering various values of porosity ε, linearized friction factor f, angle of incidence θ, finite spacing between the structures and porous block L. The wave reflection K_r, transmission coefficient K_t, energy dissipation K_d, wave force impact on the front face of the porous block K_{fb1}, wave force impact on the front face of the stratified structure K_{fs1} and the surface deflection in the incident and transmitted region $\zeta_j(x)$ is plotted to understand the behaviour of porous structure with change in bottom topography for wave energy dissipation. The parameters that are kept constant are $\rho = 1000$ kg/m^3, $g = 9.81$ m/s^2 and $S = 1$ throughout the computation.

6.4.1 Validation of the numerical model

The numerical modelling of single layered and multi-layered porous structures for different configurations is performed by Dattatri et al. (1978), Dalrymple et al. (1991), Zhu and Chwang (2001) and Liu and Li (2013). The study conducted on a single layer porous structure is validated with results from the literature in order to assess the validity of the present numerical model based on the eigenfunction expansion method. Dalrymple et al. (1991) examined the reflection and transmission characteristics for oblique wave incidence on a vertical porous structure using plane wave approximation.

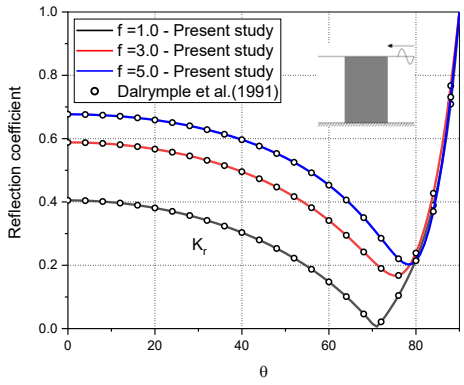

Fig. 6.3: Comparative study for the reflection coefficient in the case of single porous structure and Dalrymple et al. (1991) considering $B/h = 1$, $\omega^2 h/g = 0.2012$, $S = 1$ and $\varepsilon = 0.45$.

In Fig. 6.3, the comparative study between the present numerical model for single porous structure on wave reflection coefficient for varying angle of incidence is performed, and a good agreement with the result obtained by Dalrymple et al. (1991) is noted. The study reveals that, with the increase in the linearized friction factor, the minimum in the reflection coefficient is obtained for $65^0 < \theta < 75^0$. Liu and Li (2013) developed a new analytical solution for wave reflection and transmission by a surface-piercing porous breakwater without using the complex dispersion relation. The results obtained for the reflection and transmission coefficient (Fig. 6.4) based on the analytical solution of single layer porous structure as in Liu and Li (2013) is compared with that result obtained using the present numerical approach. The study shows a considerable agreement between the results using the present numerical approach and by Liu and Li (2013) for both reflection and transmission coefficients. Thereafter, the numerical investigation is extended for both horizontally and vertically stratified porous structure combined with porous block in varying seabed.

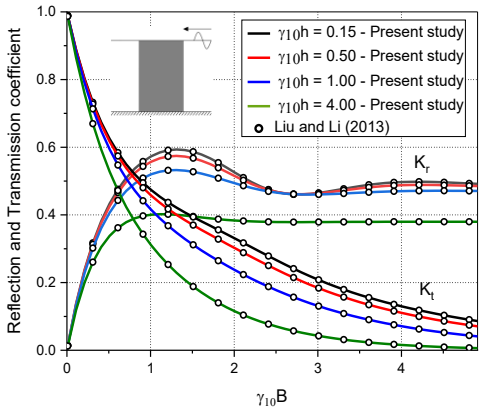

Fig. 6.4: Comparative study for K_r and K_t using the present analytical approach for single porous structure and Liu and Li (2013) considering $\varepsilon = 0.45$, $S = 1$ and $f = 1$.

6.4.2 Horizontally stratified porous structure with surface-piercing porous block

The wave transformation due to horizontally stratified porous structure combined with porous block in changing bottom topography is analyzed on studying the wave reflection coefficient K_r, transmission coefficient K_t, dissipation coefficient K_d, surface displacement $\zeta_j(x)$, wave force acting on the front face of porous block K_{fb1} and on the stratified structure K_{fs1}.

6.4.2.1 Reflection, transmission and dissipation coefficient

The wave reflection, transmission and dissipation coefficients are analysed for the change in the porosity, structural width, dimensionless wave number and angle of incidence.

6.4.2.1.1 Effect of multiple porosities

In order to analyze the effect of porosity on hydrodynamic coefficients, the behaviour of combinations of different porosity for top and bottom porous layer of stratified structure is studied in Fig. 6.5(a,b) for varying dimensionless width of structure. The stratified porous structure with uniform porosity of 50% is observed to have more wave reflection and intermediate transmission compared to the other combinations. Although wave reflection coefficient shows intermediate characteristics, the transmission coefficient is observed least for combination of $\varepsilon_5 = 0.7$ and $\varepsilon_6 = 0.3$. As a result, wave dissipation is higher for the porosity combination $\varepsilon_5 = 0.7$ and $\varepsilon_6 = 0.3$. A mono resonating behaviour is observed for K_r and maximum peak is observed when width of porous structure is same as the depth of incident open water region. Maximum wave reflection attributes to the constructive interference between incident and reflected waves caused by the porous structure. At this point, K_r for uniform porosity is 33.33% more than that of combination of $\varepsilon_5 = 0.9$ and $\varepsilon_6 = 0.1$. Most of the surface concentrated waves may be either attenuated or reflected by the surface-piercing porous block and hence only the remaining incoming wave energy need to be attenuated by the stratified structure.

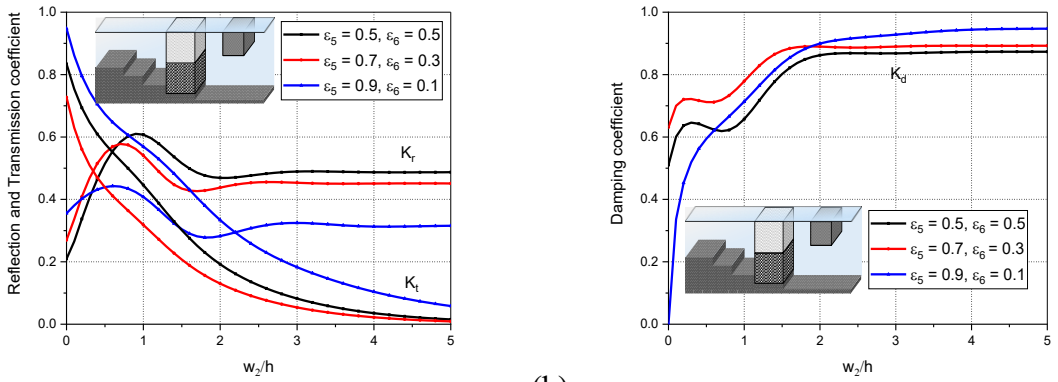

(a) (b)

Fig. 6.5: Variation of (a) K_r and K_t (b) K_d versus w_2/h for different combinations of porosities considering $\gamma_{10}h = 1.5$, $h_s/h = 0.10$, $w_1/h = 0.50$, $L/h = 0.25$, $\theta = 20°$, $S_2 = S_5 = S_6 = 1$, $\varepsilon_2 = 0.2$, $f_2 = 0.6$, $f_5 = 0.8$ and $f_6 = 0.5$.

In Fig. 6.5(a), it can be noted that K_r is decreasing as the porosity of surface layer is increasing which may be caused due to the easy penetration of waves through the pores of surface layer of stratified structure. This is evident from K_t in Fig. 6.5(a) with the maximum wave transmission being shown by the combination with highest porosity at the surface layer. Further, about 95% wave energy dissipation is achieved when width of stratified structure is more than 1.5 times the water depth as depicted in Fig. 6.5(b).

6.4.2.1.2 Effect of structural width of porous block and stratified structure

Fig. 6.6(a,b) illustrates the hydrodynamic coefficients versus θ for different structural width of the porous block varying from $0.5 < w_1 / h < 3.0$. The increase in the structural width w_1 / h shows an increase in wave reflection but a decrease in wave transmission. For direct wave attack, K_r for $w_1 / h = 3.0$ is observed to be twice of that of $w_1 / h = 0.5$. Also, a small mono resonating behaviour in K_r is prominent at $\theta = 22°$ as width of porous block increases. This can be due to the change in phase of the incident and reflected wave due to the increased width of the porous structure. For largely oblique waves, a steep increase in wave reflection is observed.

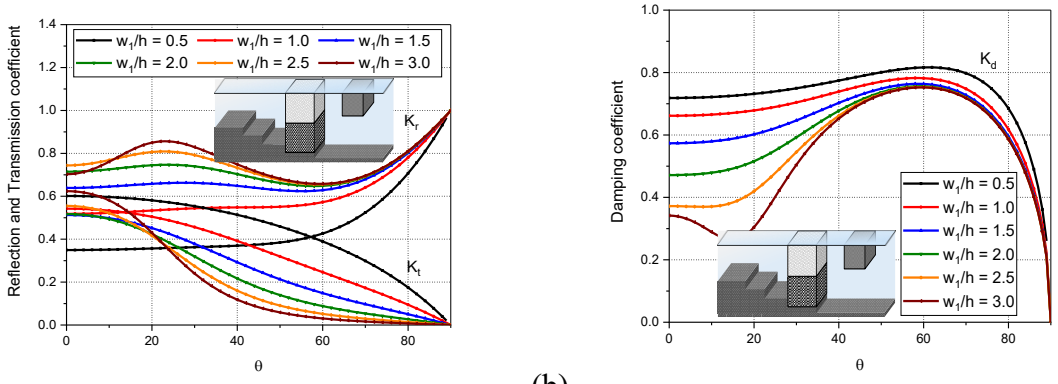

(a) (b)

Fig. 6.6: Variation of (a) K_r and K_t (b) K_d versus θ for different values of w_1 / h considering $\gamma_{10} h = 1.5$, $h_s / h = 0.10$, $a / h = 0.25$, $w_2 / h = 0.50$, $L / h = 0.25$, $S_2 = S_5 = S_6 = 1$, $\varepsilon_2 = 0.2$, $\varepsilon_5 = 0.7$, $\varepsilon_6 = 0.4$, $f_2 = 0.6$, $f_5 = 0.8$ and $f_6 = 0.5$.

As depicted in Fig. 6.6(b), wave energy dissipation decreases with increase in width of porous block, although larger variation is not there for oblique waves with angle of incidence greater than $\theta = 45°$. At $\theta = 15°$, K_d shows a decrease of 65.28% from $w_1 / h = 0.5$ to $w_1 / h = 3.0$. This decrease in wave energy dissipation is caused as most of the incoming waves are being

reflected by the porous block. A local minimum is observed in K_d for $w_1/h = 3.0$ due to the sudden increase in wave reflection as explained before. A steep decrease in K_d is observed for largely oblique waves which is an opposite trend to that of K_r. This may be due to the less effective wave trapping of these highly oblique waves as most of this incoming wave energy is being reflected by the porous structure.

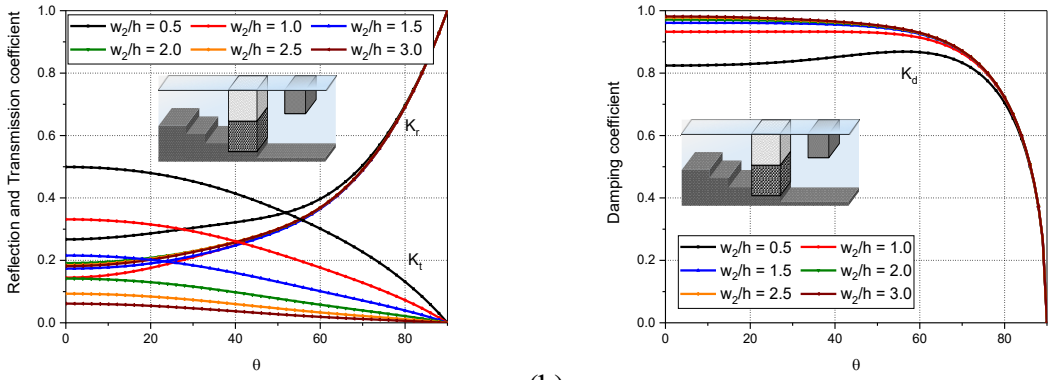

(a) (b)

Fig. 6.7: Variation of (a) K_r and K_t (b) K_d versus θ for different values of w_2/h considering $\gamma_{10}h = 1.5$, $h_s/h = 0.10$, $a/h = 0.25$, $w_1/h = 0.50$, $L/h = 0.25$, $S_2 = S_5 = S_6 = 1$, $\varepsilon_2 = 0.2$, $\varepsilon_5 = 0.7$, $\varepsilon_6 = 0.4$, $f_2 = 0.6$, $f_5 = 0.8$ and $f_6 = 0.5$.

The hydrodynamic behaviour of structure with respect to different structural width of stratified porous structure as well is analysed for varying angle of incidence. In Fig. 6.7(a) the variation in K_r is such that it increases with more oblique wave angle. Also wave reflection is more when width of structure is half of that of incident open water depth. In all other cases, no significant variation in K_r is observed. Wave transmission characteristics shown by $w_2/h = 0.5$ also suggests that this structural width is not suitable for stratified structure as K_t is more. This is due to the availability of shorter path through the stratified porous structure and hence lesser pore spaces for the wave energy to be dissipated. For $\theta = 0$, wave transmission decreases by around 82% when w_2/h is increased from 0.5 to 3.0. Wave damping efficiency for most cases, except for $w_2/h = 0.5$ is greater than 90% as noted in Fig. 6.7(b). Since, for all other cases, wave damping efficiency is almost the same, it is economical to construct stratified porous structure with intermediate structural width and to decrease wave transmission for this width of stratified structure, it is better to increase the width of surface-piercing porous

block. Thus, cost can be considerably reduced due to the combination of a fully extend structure with a partial porous structure.

6.4.2.1.3 Effect of dimensionless wavenumber

To examine the behaviour of waves in the presence of horizontal stratified structure combined with porous block in changing bottom topography the dimensionless wave number ranging from 0.75 to 1.75 is varied. In Fig. 6.8(a,b), the wave reflection, transmission and dissipation coefficients are analysed for varying length between stratified structure and porous block with the change in the non-dimensional wave number. Due to high wave oscillations in the confined region, resonating behaviour is observed for the hydrodynamic coefficients which allow us to determine the optimum length to be provided between stratified structure and porous block from the resonating troughs. The minimum value in wave reflection as observed in Fig. 6.8(a) corresponds to the destructive interference of the waves due to the presence of the porous block. It is observed that wave reflection for shorter waves is more compared to longer waves. Further, wave transmission for longer waves is more. This is due to the lesser interaction of longer waves compared to the length of the structure and vice versa for shorter waves. In addition, as represented in Fig. 6.8(b), wave damping efficiency for shorter waves is higher for the structure, although more prominent resonating behaviour is observed for such waves. However, the oscillating pattern diminishes for lesser value of $\gamma_{10}h$ and more uniform value is achieved due to the formation of the standing waves in the confined region formed by the porous block in seaward side and rigid steps in leeward side with the horizontally stratified structure.

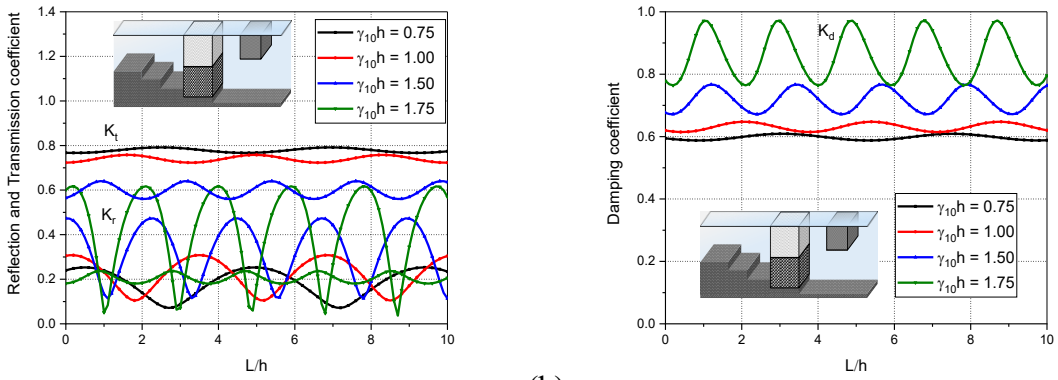

(a) (b)

Fig. 6.8: Variation of (a) K_r and K_t (b) K_d versus L/h for different values of $\gamma_{10}h$ considering $h_s/h = 0.10$, $a/h = 0.25$, $w_1/h = w_2/h = 0.50$, $\theta = 20°$, $S_2 = S_5 = S_6 = 1$, $\varepsilon_2 = 0.2$, $\varepsilon_5 = 0.7$, $\varepsilon_6 = 0.3$, $f_2 = 0.6$, $f_5 = 0.8$ and $f_6 = 0.5$.

In Fig. 6.9(a,b) the effect of dimensionless wavenumber is presented for varying dimensionless width of stratified structure. For shorter waves, wave reflection is more, and transmission is minimum compared to longer ones due to increased wave interaction with the structure as illustrated in Fig. 6.9(a). In addition, as the width of stratified structure is increased, K_r achieves more consistent value and hence any further increase in width of structure has less effect on characteristics of wave reflection. The local maxima observed in K_r for $0.5 < w_2 / h < 1.5$ may be due to the constructive interference between incoming and reflected waves. However, this local maximum value shifts towards left with the increase in $\gamma_{10}h$, which can be due to the change in phase of incident and reflected waves when the wavelength of incoming waves changes. Also, even for small structural width, wave dissipation behaviour for shorter waves is efficient as given in Fig. 6.9 (b). A local minima is observed in the case of $\gamma_{10}h = 1.75$ because of high wave reflection on account of standing wave formation. Hence, this structure is better economical for waves with shorter wavelength. If an increased width of stratified structure is feasible, longer waves can also be attenuated effectively by better interaction of wave with structure.

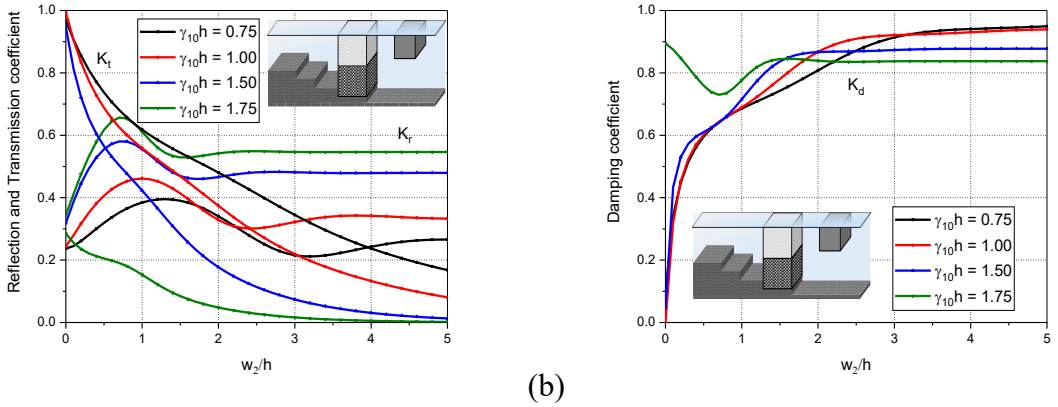

(a) (b)

Fig. 6.9: Variation of (a) K_r and K_t (b) K_d versus w_2 / h for different values of $\gamma_{10}h$ considering $h_s / h = 0.10$, $a / h = 0.25$, $w_1 / h = 0.50$, $L / h = 0.25$, $\theta = 20°$, $S_2 = S_5 = S_6 = 1$, $\varepsilon_2 = 0.2$, $\varepsilon_5 = 0.7$, $\varepsilon_6 = 0.3$, $f_2 = 0.6$, $f_5 = 0.8$ and $f_6 = 0.5$.

6.4.2.1.4 Effect of angle of incidence

The impact of angle of wave attack on the wave transformation is examined for the stratified porous structure combined with porous block in the presence of step topography. The hydrodynamic coefficients are studied by varying angle of incidence within $0 \le \theta \le 90°$ in Fig.

6.10(a,b) for different combinations of porosity of surface and bottom layers of stratified structure. It can be inferred from Fig. 6.10(a) that, for $\theta > 60°$, K_r increases considerably, whereas transmission decreases due to increased wave interaction with structure on account of obliquity of waves. Further, for large oblique waves as seen from Fig. 6.10(b) the wave dissipation by the structure is seen to decrease. This may be caused due to increased reflection, as a result of which only marginal number of waves would be passing through the porous structure and hence lesser wave energy attenuation of incoming waves.

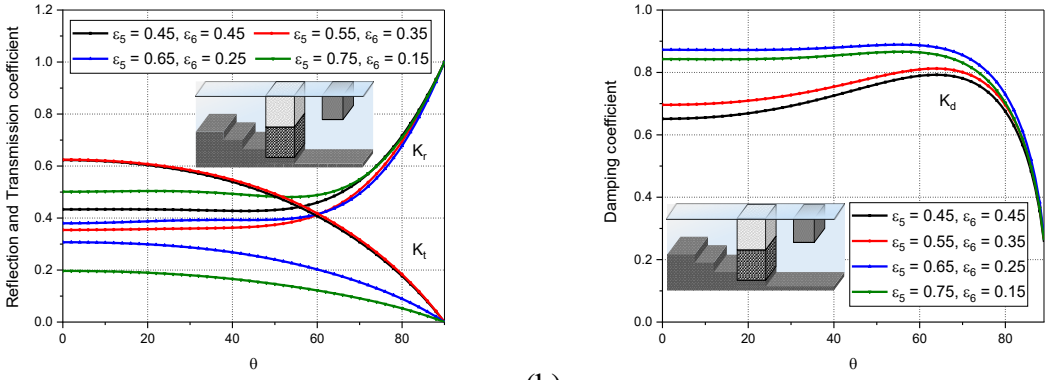

(a) (b)

Fig. 6.10: Variation of (a) K_r and K_t (b) K_d versus θ for different combinations of porosities considering $\gamma_{10}h = 1.5$, $h_s / h = 0.10$, $a / h = 0.25$, $w_1 / h = w_2 / h = 0.50$, $L / h = 0.25$, $S_2 = S_5 = S_6 = 1$, $\varepsilon_2 = 0.2$, $f_2 = 0.6$, $f_5 = 0.8$ and $f_6 = 0.5$.

6.4.2.1.5 Effect of length between porous block and stratified structure

The variation of hydrodynamic coefficients with the change in the length between porous block and the stratified structure for varying combination of porosity of surface and bottom porous layer is studied and presented in Fig. 6.11(a,b). An oscillating pattern is obtained for all the cases of combinations of porosity. This oscillation diminishes as the porosity of surface layer is increased and that of bottom layer is decreased. This may be due to the formation of standing waves in the confined region between surface-piercing porous block and stratified structure. In addition, the trough is observed for L / h having the value 1.0, 3.0, 4.0 and so on. The L / h vales are significant while designing the structure as we can achieve minimal wave reflection. In these cases, even zero wave reflection is observed in Fig. 6.11(a). This may be the case when incident and reflected waves are $180°$ out of phase and all the waves are absorbed within the confined region. Also, reflection coefficient decreases as the porosity of surface layer is increased and that of bottom layer is decreased. This is due to the availability of more pore

spaces in surface layer to allow more surface waves to pass through. Resonating peaks are also observed in the case of K_t, such that the value is increasing with increase in porosity of surface layer. However, wave damping efficiency is maximum shown for the combination with $\varepsilon_5 = 0.7$ and $\varepsilon_6 = 0.3$. Resonating crests for K_d as depicted in Fig. 6.11(b) are observed for L/h corresponding to negligible or fairly zero wave reflection due to the absorption of incoming wave energy as explained before.

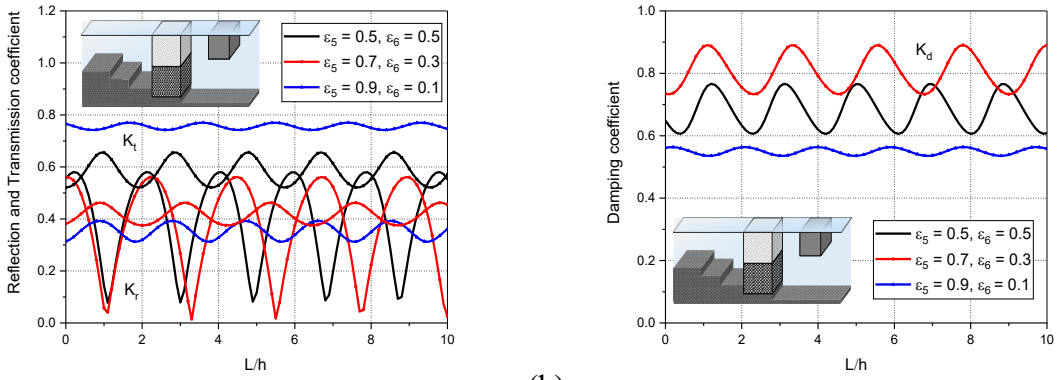

(a) (b)

Fig. 6.11: Variation of (a) K_r and K_t (b) K_d versus L/h for different combinations of porosities considering $\gamma_{10}h = 1.5$, $h_s/h = 0.10$, $a/h = 0.25$, $w_1/h = w_2/h = 0.50$, $\theta = 20°$, $S_2 = S_5 = S_6 = 1$, $\varepsilon_2 = 0.2$, $f_2 = 0.6$, $f_5 = 0.8$ and $f_6 = 0.5$.

6.4.2.2 Surface elevation

The surface elevation in the open water regions for various obliquity of gravity waves in the range $0 \le \theta \le 60°$ is analysed in Fig. 6.12.

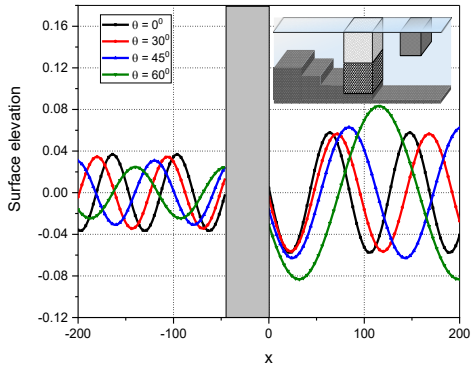

Fig. 6.12: Surface elevation versus x for different values of θ considering $\gamma_{10}h = 1.5$, $h_s/h = 0.10$, $a/h = 0.25$, $w_1/h = w_2/h = 0.50$, $L/h = 0.25$, $S_2 = S_5 = S_6 = 1$, $\varepsilon_2 = 0.2$, $\varepsilon_5 = 0.7$, $\varepsilon_6 = 0.3$, $f_2 = 0.6$, $f_5 = 0.8$ and $f_6 = 0.5$.

The maximum surface elevation is observed in the case of $\theta = 60°$ for the incident open water region. However, irrespective of incident wave angle, considerable reduction in surface elevation of transmitted region is achieved due to the presence of the structure. Most attenuation is achieved in the case of highly oblique wave itself due to considerably more interaction of oblique waves with the structure as discussed in previous sections. Phase change in the incoming waves is observed in Fig. 6.12 due to the presence of the structure. Thus, it is clear that a tranquil zone can be created in the leeward side by the combination of stratified structure with surface-piercing porous block.

6.4.2.3 Wave force on front face of porous block and stratified structure

Fig. 6.13(a,b) shows the force acting on front face of both horizontally stratified porous structure and the surface piercing porous block varying dimensionless wavenumber. It is observed that K_{fs1} is less when longer waves are incident as noted in Fig. 6.13(a). This is because longer waves have least interaction with structure and hence less reflection. The resonating behaviour gradually diminishes as the wavelength increases and tend to attain a more uniform value. In the case of same L/h, for $\gamma_{10}h = 1.75$ attains the peak value, K_{fs1} is 86% more compared to that of $\gamma_{10}h = 0.75$. The same trend is observed for K_{fb1}.

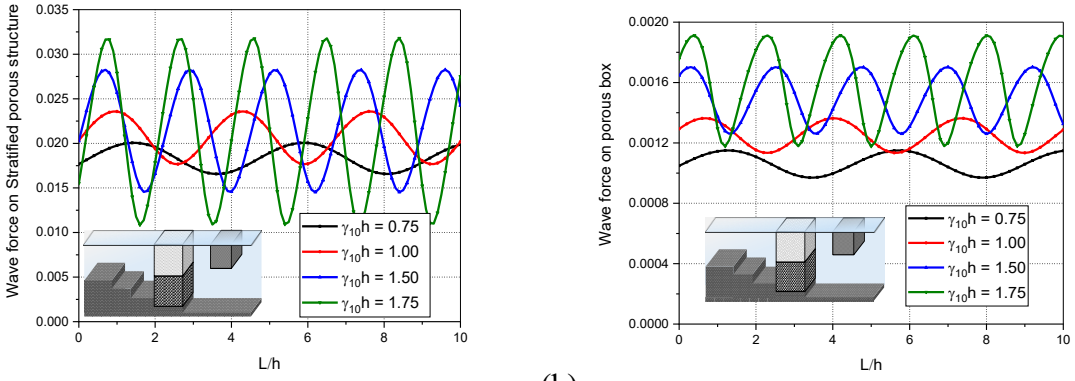

(a) (b)

Fig. 6.13: Variation of (a) K_{fs1} and (b) K_{fb1} versus L/h for different values of $\gamma_{10}h$ considering $h_s/h = 0.10$, $a/h = 0.25$, $w_1/h = w_2/h = 0.50$, $\theta = 20°$, $S_2 = S_5 = S_6 = 1$, $\varepsilon_2 = 0.2$, $\varepsilon_5 = 0.7$, $\varepsilon_6 = 0.3$, $f_2 = 0.6$, $f_5 = 0.8$ and $f_6 = 0.5$.

On varying angle of incidence of wave, the wave force on the front face of the stratified structure and porous block is studied for different dimensionless width of porous block as in Fig. 6.14(a,b). Both K_{fs1} and K_{fb1} is decreasing with increase in obliquity. For $w_1/h = 3.0$,

K_{fs1} is maximum for $\theta < 10°$ and minimum for $\theta \geq 20°$. From Fig. 6.14(a), it is clear that, as the structural width of porous block is increased, wave transmission to the confined region between porous block and stratified structure decreases and hence considerably less wave would be incident on the stratified structure. As a result, wave force acting on the stratified structure would be less. Thus, with the presence of surface-piercing partial structure in combination with a fully extended structure, wave force acting on our primary structure can be significantly reduced. As depicted in Fig. 6.14(b), wave force acting on the front face of the porous block increases with increase in width of porous block as most of the incident wave energy is being reflected by the surface-piercing structure.

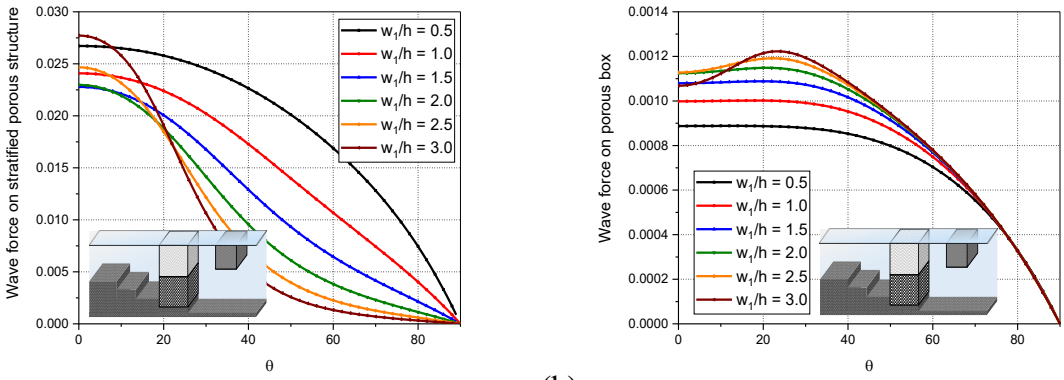

(a) (b)

Fig. 6.14: Variation of (a) K_{fs1} and (b) K_{fb1} versus θ for different values of w_1 / h considering $\gamma_{10}h = 1.5$, $h_s / h = 0.10$, $a / h = 0.25$, $w_2 / h = 0.50$, $L / h = 0.25$, $S_2 = S_5 = S_6 = 1$, $\varepsilon_2 = 0.2$, $\varepsilon_5 = 0.7$, $\varepsilon_6 = 0.4$, $f_2 = 0.6$, $f_5 = 0.8$ and $f_6 = 0.5$.

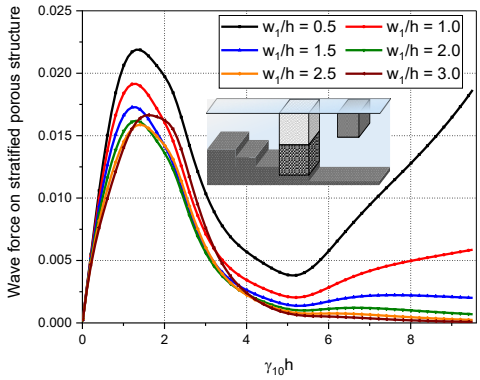

Fig. 6.15: Variation of K_{fs1} versus $\gamma_{10}h$ for different values of w_1 / h considering $h_s / h = 0.10$, $a / h = 0.25$, $L / h = 0.25$, $w_2 / h = 0.50$, $\theta = 20°$, $S_2 = S_5 = S_6 = 1$, $\varepsilon_2 = 0.2$, $\varepsilon_5 = 0.7$, $\varepsilon_6 = 0.4$, $f_2 = 0.6$, $f_5 = 0.8$ and $f_6 = 0.5$.

Further, to study the effect of structural width on wave transformation, w_1/h is varied from 0.5 to 3.0 against $\gamma_{10}h$. There is considerable variation in K_{fs1} for different w_1/h values and it is observed to have peak value at around $\gamma_{10}=1.5$ for any structural width, as in Fig. 6.15. The wave force on stratified structure is observed to be decreasing with the aid of wider surface-piercing porous blocks. Beyond $\gamma_{10}h=5$, for smaller structural widths, K_{fs1} again increases whereas for larger structural widths, K_{fs1} becomes constant.

6.4.3 Vertically stratified porous structure with surface-piercing porous block

The wave transformation due to the vertically stratified porous structure combined with porous block in changing bottom topography is analyzed on studying the wave reflection coefficient K_r, transmission coefficient K_t, dissipation coefficient K_d, surface displacement $\zeta_j(x)$, wave force acting on the front face of porous block K_{fb1} and on the stratified structure K_{fs1}.

6.4.3.1 Reflection, transmission and dissipation coefficient

The wave reflection, transmission and dissipation coefficients are analysed for the change in porosity, change in structural width, change in dimensionless wave number, change in the angle of incidence.

6.4.3.1.1 Effect of multiple porosities

In Fig. 6.16(a,b), the vertically stratified porous structure combined with porous block in the presence of stepped bottom topography is analyzed for hydrodynamic coefficients, varying the dimensionless width of porous block and for different combinations of porosities of seaward and leeward porous layers. A mono resonating behaviour is observed for K_r in Fig. 6.16(a) which becomes more prominent as porosity of seaward layer increases. Minimum K_r is observed for the combination of $\varepsilon_5=0.9$ and $\varepsilon_6=0.1$ when $w_2/h=0.75$. Thus, this structural width can be used while designing the structure to achieve minimum wave reflection. The reason for zero wave reflection may be that the incoming and reflected waves become 180° out of phase. The K_t value is also considerably reduced as porosity of seaward layer increases and that of leeward porous layer decreases. This can be due to more wave trapping while passing through the porous layers. Compared to horizontally stratified structure in combination with porous block, the combination of vertically stratified structure and porous block showed

less K_r and K_t, resulting in more wave energy dissipation as given in Fig. 6.16(b). This may be because, most of the surface concentrated waves are being reflected and dissipated by the surface-piercing porous block and the remaining incident waves on the stratified structure would be reflected and trapped effectively within the porous layers of vertically stratified structure. This effective trapping is possible when the difference between porosity of seaward and leeward porous layer become larger as observed in the combination of $\varepsilon_5 = 0.9$ and $\varepsilon_6 = 0.1$.

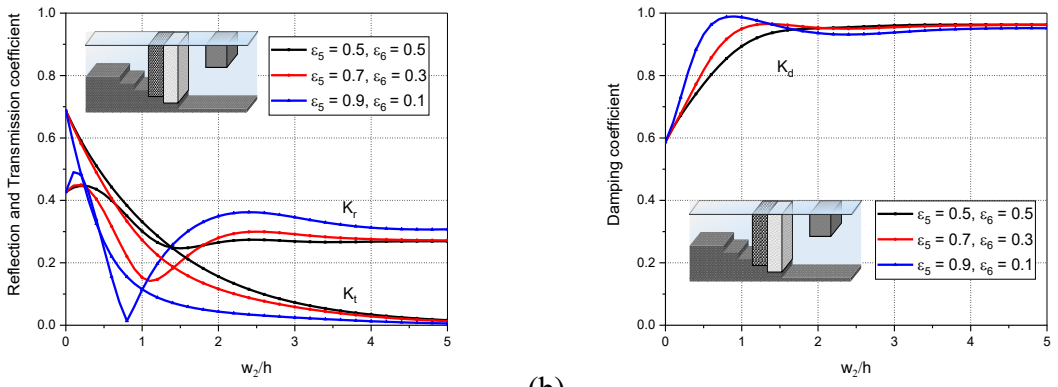

(a) (b)

Fig. 6.16: Variation of (a) K_r and K_t (b) K_d versus w_2/h for different combinations of porosities considering $\gamma_{10}h = 1.5$, $h_s/h = 0.10$, $w_1/h = 0.50$, $L/h = 0.25$, $\theta = 20°$, $S_2 = S_5 = S_6 = 1$, $\varepsilon_2 = 0.2$, $f_2 = 0.6$, $f_5 = 0.8$ and $f_6 = 0.5$.

The hydrodynamic characteristics of vertically stratified porous structure combined with porous block is again studied with various combinations of porosity varying dimensionless wavelength. In Fig. 6.17, it is observed that the reflection coefficient is same for all combinations of porosity except that the sudden drop of K_r shows different minimum value for different combinations. This sudden reduction in K_r may be due to the destructive interference. The critical wavelength for which reflection coefficient is minimal is observed to be near to $\lambda/h = 3.0$. This critical wavelength decreases as the porosity of seaward layer is increased and that of leeward layer is decreased. Further, for dimensionless wavelength beyond the critical wavelength, an increase in K_r is observed. In the case of wave transmission coefficient, a considerable decrease in K_t is observed for $\varepsilon_5 = 0.75$ and $\varepsilon_6 = 0.15$. Thus, this combination of porosity may be suitable while designing the vertically stratified structure to

achieve less reflection and transmission simultaneously and thereby more wave energy attenuation.

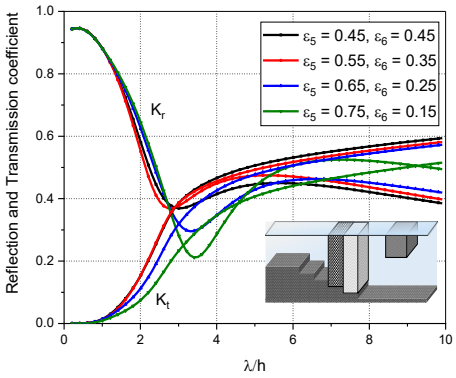

Fig. 6.17: Variation of K_r and K_t versus λ/h for different combinations of porosities considering $h_s/h=0.10$, $a/h=0.25$, $w_1/h=w_2/h=0.50$, $L/h=0.25$, $\theta=20°$, $S_2=S_5=S_6=1$, $\varepsilon_2=0.2$, $f_2=0.6$, $f_5=0.8$ and $f_6=0.5$.

6.4.3.1.2 Effect of structural width of porous block and stratified structure

To examine the dependence of hydrodynamic properties on structural width of the structure (Fig. 6.18a,b), the wave reflection, transmission, and dissipation coefficients versus λ/h is studied for $0.5<w_1/h<2.0$.

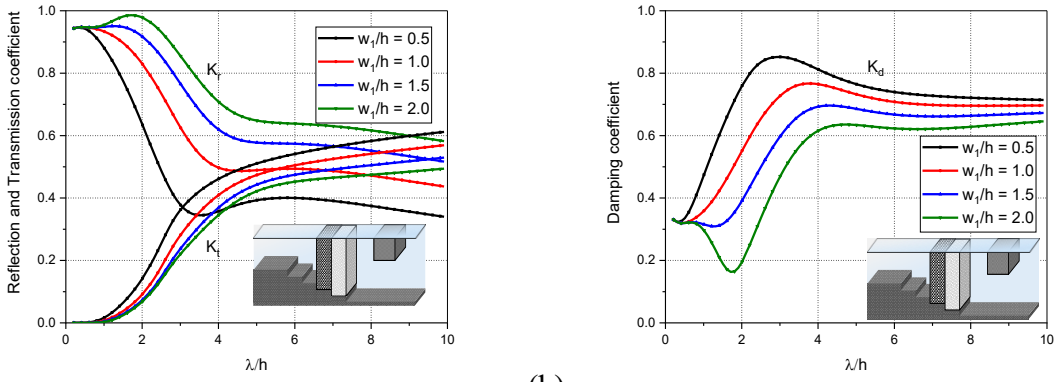

(a) (b)

Fig. 6.18: Variation of (a) K_r and K_t (b) K_d versus λ/h for different values of w_1/h considering $h_s/h=0.10$, $a/h=0.25$, $w_2/h=0.50$, $L/h=0.25$, $\theta=20°$, $S_2=S_5=S_6=1$, $\varepsilon_2=0.2$, $\varepsilon_5=0.7$, $\varepsilon_6=0.3$, $f_2=0.6$, $f_5=0.8$ and $f_6=0.5$.

It can be inferred from Fig. 6.18(a) that due to the presence of the structure, wave reflection first decreases up to a minimum value and then achieves a nearly stable value for $\lambda/h>4$.

Also, for wider structures, as observed in the case of horizontally stratified structure, reflection coefficient is more while the transmission coefficient is less. However, the decrease in K_r is more prominent than increase in K_t for less wider structures, which helps in improving the wave dissipation characteristics as observed in Fig. 6.18(b). For $\lambda/h=2$, a decrease in w_1/h from 2.0 to 0.5, increased K_d by four times. A sudden drop in K_d is observed for $w_1/h=2.0$ due to high wave reflection and less transmission of incoming wave energy.

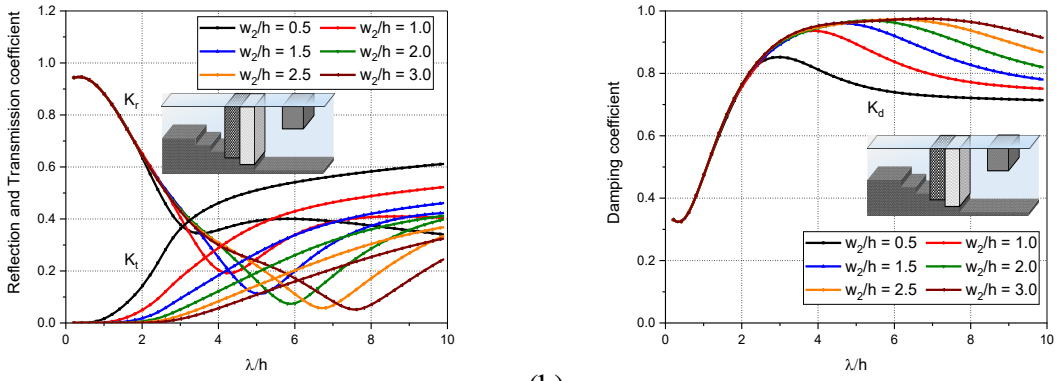

(a) (b)

Fig. 6.19: Variation of (a) K_r and K_t (b) K_d versus λ/h for different values of w_2/h considering $h_s/h=0.10$, $a/h=0.25$, $w_1/h=0.50$, $L/h=0.25$, $\theta=20°$, $S_2=S_5=S_6=1$, $\varepsilon_2=0.2$, $\varepsilon_5=0.7$, $\varepsilon_6=0.4$, $f_2=0.6$, $f_5=0.8$ and $f_6=0.5$.

Further, to understand the significance of width of stratified structure (Fig. 6.19a,b) in influencing hydrodynamic behaviour, different values of w_2/h in the range $0.5\le w_2/h\le 3.0$ are varied against dimensionless wavenumber. It can be inferred from Fig. 6.19(a) that, for shorter waves, K_r is nearly the same irrespective of the width of stratified structure. However, for further increase in λ/h, K_r sharply decreases to a critical value and then increases. These local minima shift towards right with increase in width of stratified structure, may be due to the phase shift when waves encounter more with wider structure. In addition, the wave transmission decreases with increase in structural width. For shorter waves, K_t is less but K_d remains same for any structural width. As observed in the case of horizontally stratified structure, longer waves require wider sections for effective wave attenuation. Thus, for these longer waves, wave dissipation of upto 97% can be achieved (Fig. 6.19b) by the design of wider structures.

6.4.3.1.3 Effect of angle of incidence

The impact of angle of incidence in wave transformation by vertically stratified porous structure (Fig. 6.20a,b) combined with porous block is studied for $0<\theta<90^{o}$ varying porosity of seaward and leeward porous layer. In the case of higher angle of incidence, the K_t seems to be considerably less while K_r steeply increases as observed in Fig. 6.20(a). In comparison to horizontally stratified structure, although wave reflection is nearly same but the transmission coefficient can be considerably reduced by the construction of vertically stratified structure of same structural width in combination with the partial porous structure. Wave damping efficiency for any angle of attack less than $60°$ has a constant value, beyond which K_d sharply decreases (Fig.6. 20b).

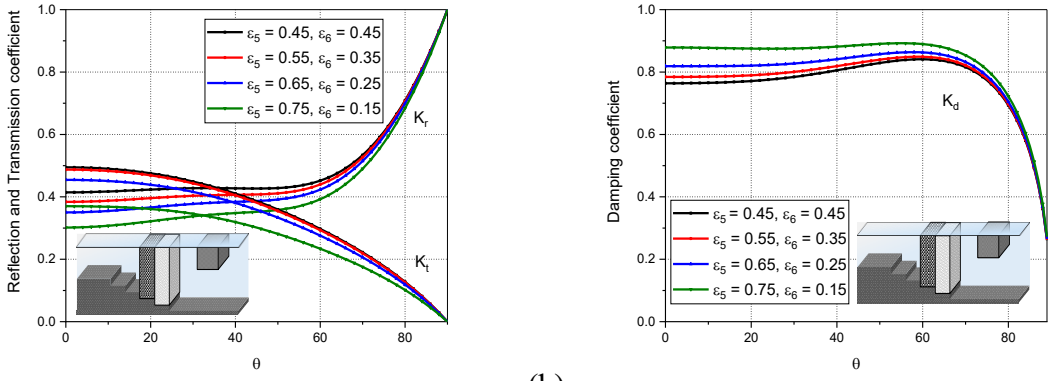

(a) (b)

Fig. 6.20: Variation of (a) K_r and K_t (b) K_d versus θ for different combinations of porosities considering $\gamma_{10}h=1.5$, $h_s/h=0.10$, $a/h=0.25$, $w_1/h=w_2/h=0.50$, $L/h=0.25$, $S_2=S_5=S_6=1$, $\varepsilon_2=0.2$, $f_2=0.6$, $f_5=0.8$ and $f_6=0.5$.

6.4.3.1.4 Effect of dimensionless wave number

In Fig. 6.21(a,b), the hydrodynamic coefficients for the vertically stratified structure combined with porous block in the presence of stepped bottom is analysed for $0.75<\gamma_{10}h<1.75$ varying dimensionless width of stratified structure, w_2/h. Slight resonating behaviour is observed for K_r with the minimum value being shifted towards right as the wavenumber decreases due to phase shift and destructive interference. The local maxima correspond to the situation when there is constructive interference between incoming and reflected waves. K_r again increases to achieve a fairly stable value, which increases with decrease in wavelength. Wave

transmission is on a slightly higher side for longer waves. Compared to the hydrodynamic behaviour of horizontally stratified structure in combination with the porous block, wave reflection and transmission for vertically stratified structure is significantly reduced as observed in previous sections. This is because of effective wave trapping by the vertical layers of stratified structure. For K_d, as shown in Fig. 6.21(b), variation is observed particularly for longer waves only, in the range of $0.5 < \gamma_{10}h < 3$. In contrast to horizontally stratified structure, wave damping was also efficient even for less wider structures.

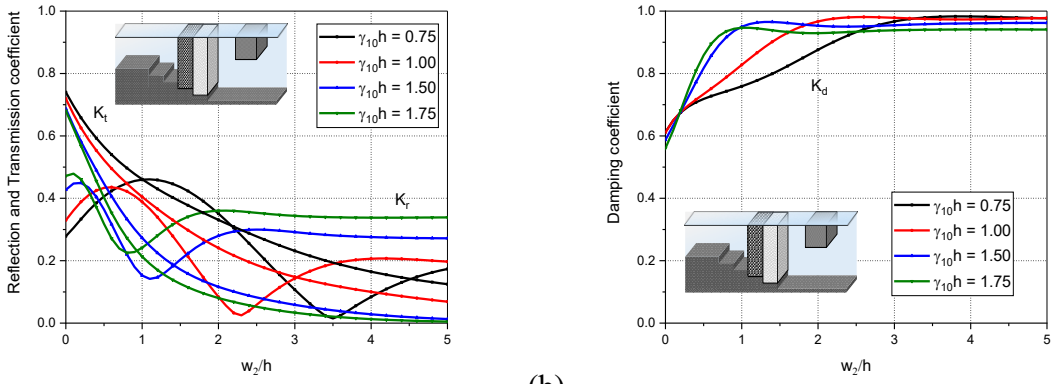

(a) (b)

Fig. 6.21: Variation of (a) K_r and K_t (b) K_d versus w_2/h for different values of $\gamma_{10}h$ considering $h_s/h = 0.10$, $a/h = 0.25$, $w_1/h = 0.50$, $L/h = 0.25$, $\theta = 20°$, $S_2 = S_5 = S_6 = 1$, $\varepsilon_2 = 0.2$, $\varepsilon_5 = 0.7$, $\varepsilon_6 = 0.3$, $f_2 = 0.6$, $f_5 = 0.8$ and $f_6 = 0.5$.

6.4.3.2 Surface elevation

In Fig. 6.22, the surface elevation in the incident and transmitted regions for various angle of incidence is observed.

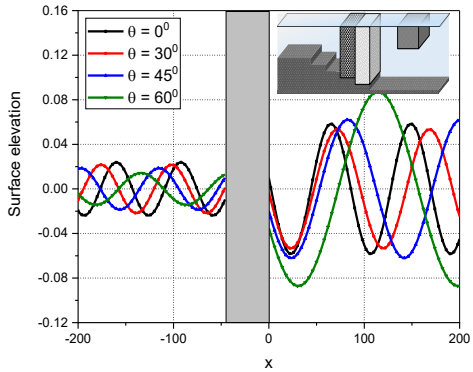

Fig. 6.22: Surface elevation versus x for different values of θ considering $\gamma_{10}h = 1.5$, $h_s/h = 0.10$, $a/h = 0.25$, $w_1/h = w_2/h = 0.50$, $L/h = 0.25$, $S_2 = S_5 = S_6 = 1$, $\varepsilon_2 = 0.2$, $\varepsilon_5 = 0.7$, $\varepsilon_6 = 0.3$, $f_2 = 0.6$, $f_5 = 0.8$ and $f_6 = 0.5$.

The maximum surface elevation is observed in the case of $\theta = 60^o$ in the incident open sea region, although there is no considerable variation for different angle of incidence. The reduction in surface elevation by vertically stratified structure is more efficient compared to that of horizontally stratified structure in combination with surface-piercing porous block. There is nearly 60% more decrease in surface elevation for vertically stratified structure. Thus, it is more advisable to construct a vertically stratified porous structure combined with porous block for more tranquil zone in the leeward side.

6.4.3.3 Wave force on front face of porous block and stratified structure

The wave force on the front face of the stratified structure and porous block is observed to show a resonating behaviour, for varying length between porous block and stratified structure and is plotted for different values of $\gamma_{10}h$ as shown in Fig. 6.23(a,b).

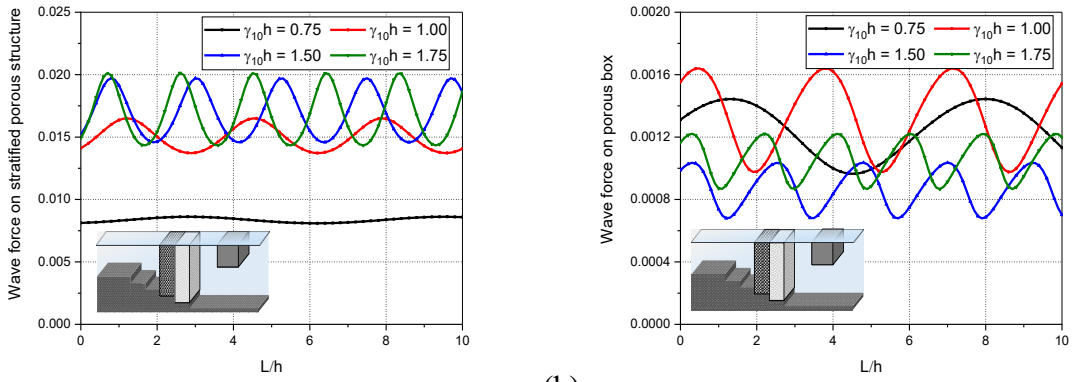

(a) (b)

Fig. 6.23: Variation of (a) K_{fs1} and (b) K_{fb1} versus L/h for different values of $\gamma_{10}h$ considering $h_s/h = 0.10$, $a/h = 0.25$, $w_1/h = w_2/h = 0.50$, $\theta = 20°$, $S_2 = S_5 = S_6 = 1$, $\varepsilon_2 = 0.2$, $\varepsilon_5 = 0.7$, $\varepsilon_6 = 0.3$, $f_2 = 0.6$, $f_5 = 0.8$ and $f_6 = 0.5$.

The wave force due to shorter wave is although more on porous block, it is significantly less when acting on the stratified structure. As observed in Fig. 6.23(b), harmonic crests and troughs tend to be increasing with increase in wavenumber due to more interaction of wave with porous block. Optimum length between porous block and stratified structure so as to have minimum wave force can be determined from the plot while designing the structure. In contrary to the wave force acting on horizontally stratified structure, vertically stratified structure combined with porous block is subjected to less impact of waves. This can be due to less wave reflection and more wave trapping within the structure.

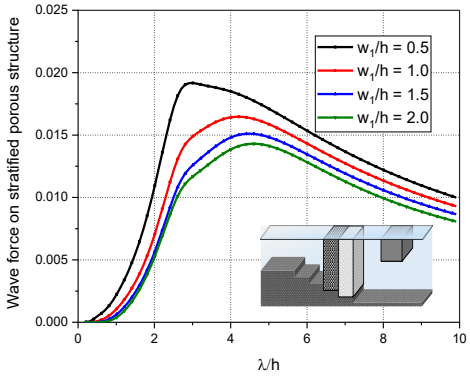

Fig. 6.24: Variation of K_{fs1} versus λ / h for different values of w_1 / h considering $h_s / h = 0.10$, $a / h = 0.25$, $w_2 / h = 0.50$, $L / h = 0.25$, $\theta = 20°$, $S_2 = S_5 = S_6 = 1$, $\varepsilon_2 = 0.2$, $\varepsilon_5 = 0.7$, $\varepsilon_6 = 0.4$, $f_2 = 0.6$, $f_5 = 0.8$ and $f_6 = 0.5$.

In order to study the wave force on the front face of vertically stratified structure K_{fs1}, different values of w_1 / h is considered for varying λ / h. Wave force seems to be increasing with wavelength to attain a peak value and then decreases with further increase in wavelength. This may be due to more reflection that is taking place from the structure for that particular wavelength as a result of constructive interference. Also, it is observed in Fig. 6.24 that wave force decreases with increase in structural width of porous block. This is because, a major part of incident wave energy would be reflected by the wider surface-piercing porous block creating less impact on the stratified structure. However, there are optimum widths of porous block for which wave force can be kept minimal which is discussed in next section.

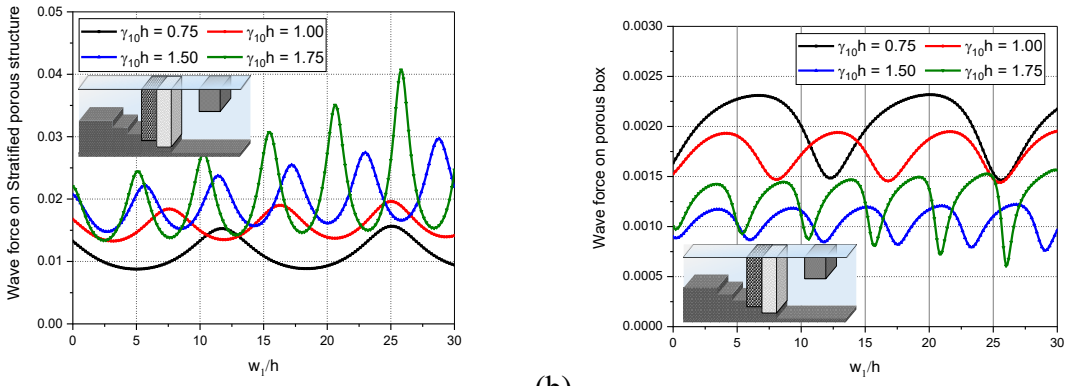

(a) (b)

Fig. 6.25: Variation of (a) K_{fs1} and (b) K_{fb1} versus w_1 / h for different values of $\gamma_{10} h$ considering $h_s / h = 0.10$, $a / h = 0.25$, $w_2 / h = 0.50$, $L / h = 0.25$, $\theta = 20°$, $S_2 = S_5 = S_6 = 1$, $\varepsilon_2 = 0.2$, $\varepsilon_5 = 0.7$, $\varepsilon_6 = 0.4$, $f_2 = 0.6$, $f_5 = 0.8$ and $f_6 = 0.5$.

In Fig. 6.25(a,b) the wave forces K_{fs1} and K_{fb1} versus w_1/h is analysed for values of $\gamma_{10}h$. Again, harmonic crests and troughs are observed for both K_{fs1} and K_{fb1} in such a way that harmonic peaking is increasing with increase in width of porous block. This is more visible in the case of shorter waves due to increased wave interaction with structure and hence more constructive interference takes place between the incident and reflected waves. The values of w_1/h for which wave force is minimum correspond to the optimum width of porous block. As observed in the previous case, K_{fb1} is considerably more for longer waves (Fig. 6.25b). Further, to understand the effect of wave force due to varying width of stratified structure, K_{fs1} and K_{fb1} are plotted for varying w_2/h for different values of $\gamma_{10}h$ in Fig. 6.26(a,b). For smaller structural width, mono resonating behaviour is observed in K_{fs1} such that shorter waves tend to show peaking at lesser widths of stratified structure due to constructive interference between incoming and reflected waves. The same is observed in the case of K_{fb1}. However, wave forces tend to attain a stable value for wider structures.

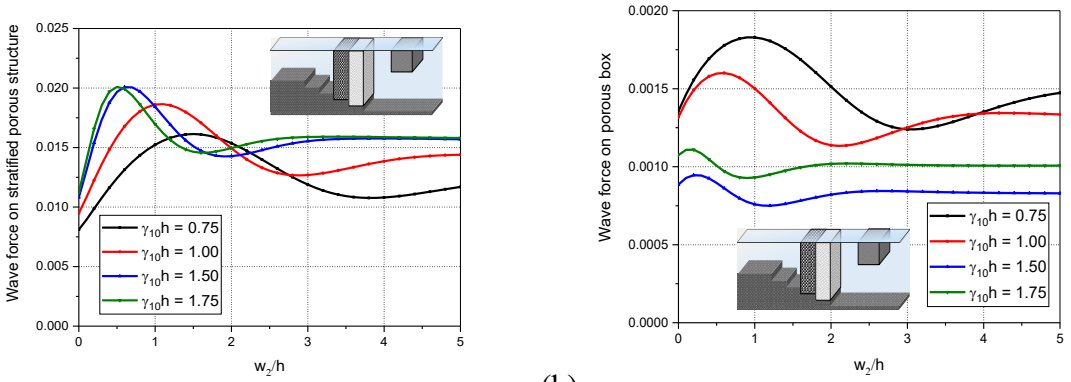

(a) (b)

Fig. 6.26: Variation of (a) K_{fs1} and (b) K_{fb1} versus w_2/h for different values of $\gamma_{10}h$ considering $h_s/h = 0.10$, $a/h = 0.25$, $w_1/h = 0.50$, $L/h = 0.25$, $\theta = 20°$, $S_2 = S_5 = S_6 = 1$, $\varepsilon_2 = 0.2$, $\varepsilon_5 = 0.7$, $\varepsilon_6 = 0.3$, $f_2 = 0.6$, $f_5 = 0.8$ and $f_6 = 0.5$.

6.5 CLOSURE

The wave transformation due to horizontally and vertically stratified porous structures combined with surface piercing porous block with stepped seabed is analyzed based on eigenfunction expansion method. The theoretical results presented are useful in design of such structures for wave energy dissipation. The conclusions drawn from the present study as follows:

- In the case of the horizontally stratified structure, least transmission can be achieved for combination of $\varepsilon_5 = 0.7$ and $\varepsilon_6 = 0.3$ along with 20% porosity for surface-piercing block. Wave damping was also efficient in this case.
- The wave energy dissipation decreases with increase in width of porous block. K_d shows a decrease of 65.28% from $w_1 / h = 0.5$ to $w_1 / h = 3.0$ in case of horizontally stratified structure combined with porous block.
- In the case of normal angle of incidence, wave transmission decreases by around 82% when width of horizontally stratified porous structure is increased from 0.5 to 3.0 times the incident open water depth.
- The wave reflection for shorter waves is more compared to longer waves. However, wave transmission is least and wave attenuation can be easily achieved due to the presence of the structure. Further, for longer waves, wave dissipation of upto 97% can be achieved by designing wider structures.
- The wave force acting on stratified structure can be decreased if the structure is combined with wider surface-piercing porous blocks.In the case of vertically stratified porous structure, minimum wave reflection can be achieved for the combination of $\varepsilon_5 = 0.9$ and $\varepsilon_6 = 0.1$ when width of the stratified structure is 0.75 times the incident open water depth.
- The vertically stratified structure combined with the surface-piercing porous block seems to be more efficient in terms of less wave reflection and transmission and thereby high wave energy dissipation compared to vertically stratified structure.

CHAPTER 7

CONCLUSIONS AND FUTURE WORK

7.1 SUMMARY OF RESEARCH WORK

The wave transformation due to composite porous structures of different configurations is analysed numerically based on small amplitude wave theory. The porous structures considered in the analysis consists of submerged vertical barriers associated with porous structures, pile-rock porous structures, multiple porous barriers associated with porous blocks, submerged horizontal porous plate associated with submerged porous barriers, submerged horizontal porous plate associated with submerged porous blocks, vertical porous barrier and porous structure, horizontally and horizontally stratified porous blocks associated with a stepped. The eigenfunction expansion method alongwith the matching edge conditions and mode-coupling relations are adopted to analyze composite breakwater system. The hydrodynamic coefficients, such as wave reflection coefficient, transmission coefficient, energy dissipation coefficient, wave force on the structures and barriers and free surface displacements are analysed and discussed. The effect of various parameters such as structural porosity, friction factor, width of the structure, spacing between the porous structures, angle of incidence and non-dimensional wave number on wave scattering is analysed. The analytical results of the present study are compared and validated with experimental and numerical results obtained from the literature. The summary of the research work performed in the present study is discussed briefly as follows:

7.1.1 Wave damping due to composite permeable porous structures and barrier

- The higher wave damping is evident for pile-rock porous structure with a barrier compared to that of single porous structure. The wave damping of around 35% for surface-piercing and bottom-standing barriers and 30.5% for fully-extended barriers is observed at normal angle of incidence.

- The transmission coefficient is observed minimum and dissipation coefficient is noted maximum for the porosity of the structure $\varepsilon_s = 0.8$, in the case of pile-rock structure. Thus the increased porosity can be considered efficient in wave energy dissipation.

- The wave decay due to dimensionless structural width $d/h = 3$ is evident for optimal wave damping in the case of pile-rock porous structure with barrier for all the cases of porosity within $0.2 \le \varepsilon_s \le 0.8$.

- In the case of composite porous structures, the oscillatory trend in the reflection coefficient K_r increases with the increase in the non-dimensional gap w/h between the porous structure and the barrier for all three configurations.

- The wave force acting on the structure decreases with an oscillatory trend for porous structure associated with a fully-extended barrier and surface-piecing barrier as the structural porosity and non-dimensional width increases, which may be due to the trapping of waves inside the gap between the barrier and the porous structure.

7.1.2 Wave scattering due to multiple porous structures and barrier

- In the analysis of wave transformation due to the submerged multiple porous structures associated with a vertical permeable barrier, it is found that the porous structure configurations with fully-extended barrier and surface-piercing barrier exhibit 100% wave energy damping for the non-dimensional width of the structure $d/L = 1.4$ and structural porosity $\varepsilon_r = 0.4$, whereas for $d/L = 1.4$ and $\varepsilon_r = 0.8$, the porous structure associated with the bottom-standing barrier exhibits complete wave energy dissipation.

- The wave forces acting on the structure are reduced with the decrease in the barrier porosity which result in a higher life period of the multiple porous structures associated with a vertical permeable barrier breakwater system. The energy damping is high for high angle of incidence, which may be due to the trapping of oblique waves inside the finite spacing between the barrier and the structure.

- The porous structure associated with the bottom-standing barrier exhibits less wave reflection for all the structural porosities ranging within $0.2 < \varepsilon_r < 0.8$, when compared

with the fully-extended and surface-piercing barriers. The wave force acting on the structure is found to be decreasing with a resonating trend for porous structure associated with fully-extended barrier and surface-piecing barrier as the structural porosity and non-dimensional width increase, which may be due to the trapping of waves inside the gap between the barrier and the porous structure.

7.1.3 Gravity wave dissipation due to submerged horizontal plate and porous structure

- In the case of a submerged porous plate backed by a bottom-standing porous structure, it is noted that the most effective wave dissipation is obtained when the porous plate is kept on the water surface level. The wave energy dissipation is noted higher, and the wave force on the structure is less for $h_1 / h = 0$.

- The hydrodynamic performance for the submerged plate with porous structure is noted better for higher plate lengths. However, it is observed that the wave force impact on the plate is higher for higher plate lengths, thus reduces the wave force impact on the submerged porous structure. The wave force impact on the structure and the surface displacement in the transmitted region is noted to decrease as the angle of incidence increases.

- In the case of a submerged porous plate backed by a surface-piercing porous structure, a 7.5% increase in energy damping is observed as the structural porosity increased from 0.2 to 0.8. It is noted that the wave force impact is minimal for higher structural porosity and the wave energy dissipation is higher for a lower angle of incidence. Further, the surface displacement in the transmitted region is lower for the higher angle of incidence.

7.1.4 Wave energy damping due to coupled porous structure and submerged plate

- The composite structure consists of a bottom-standing porous structure, a submerged horizontal porous plate, and a full- extended porous structure performs better when the plate is on the water surface, and the energy damping is maximum at plate submergence depth $d / h_1 = 0.111$.

- The transmission coefficient and energy damping in the case of coupled porous structure and submerged plate is observed low for higher plate lengths. Further, the

hydrodynamic coefficients shows an oscillating pattern as the distance between the porous structure varies. Thus, a suitable distance between the porous structure should be chosen where the transmission coefficient is low, and energy dissipation is higher.

- The wave transmission is reduced by 50% at $\gamma_{10}h_1 = 1$ for fully-extended porous structure porosity $\varepsilon_3 = 0.2$ when compared to $\varepsilon_3 = 0.8$ in the case of coupled porous structure and submerged porous plate.

7.1.5 Wave attenuation due to submerged porous structure, plate and barrier

- The resonating trend in wave reflection is observed against the non-dimensional wave number for the composite breakwater consisting of submerged porous structure, submerged horizontal porous plate and vertical porous barrier. This may be due to the trapping of waves in the confined regions between the plate and porous structure or barrier. Also, the transmission coefficient decreases as the distance between the structure and the porous plate increases.
- In the case of composite breakwater consisting of a submerged porous structure, submerged horizontal porous plate and vertical porous barrier, the higher inertia factors have a low transmission coefficient for long incident waves, while low inertia factors have a lower transmission coefficient for moderate incident waves.
- The study noted that, as the length of the submerged porous structure increases, the wave force impact decreases, possibly due to enhanced wave energy dissipation. Also, the waves with higher wave numbers exhibit comparatively higher wave energy damping than long waves.

7.1.6 Wave transformation due to stratified porous structure with stepped seabed

- The wave transformation caused by horizontally and vertically stratified porous structures associated with a stepped seabed suggests that 20% increase in leeward step height decreases transmission coefficient by 17% for the normal angle of incidence. In contrast, for the angle of incidence $\theta = 57^0$, the transmission coefficient is decreased by 31% in the case of the vertically stratified porous structure.

- In the case of horizontally stratified porous structure, with a 20% decrease in step height, the reflection coefficient is observed to decrease by 95% for $\theta = 46^0$. Also, the

horizontally stratified porous structure performs well when the step heights vary between 10% and 40%.

- The friction factor plays a dominant role in the variation in the hydrodynamic properties. The friction factor, $f = 2$ with average structure porosity of 0.35 for vertically stratified porous structures, is observed to have less reflection and transmission coefficient and helps in achieving 95-98% wave damping for $0 < \theta < 68^{o}$.

- The wave energy dissipation is observed to be more for horizontally stratified structures, whereas a vertically stratified structure effectively damps shorter waves.

7.2 SIGNIFICANT CONTRIBUTION FROM THE RESEARCH WORK

The present analytical study on the composite breakwater system is concentrated on the wave scattering and wave trapping performance of different combination of breakwaters that have recently aroused the interest of coastal engineers. The wave reflection and transmission coefficients by various porous structures are analysed and compared and validated with the experimental results available in the literature. The significant contributions of the present research study is as follows:

- The present study primarily focused on the wave scattering and trapping performance of different types of composite breakwaters. The generalised eigenfunction expansion method along with the orthogonal mode-coupling relation is adopted to solve the wave interaction with composite breakwater.
- The hydrodynamic coefficients such as wave reflection, transmission, and energy dissipation are computed by ensuring the energy balance equation is satisfied. The hydrodynamic coefficients, such as wave reflection, transmission, energy dissipation, and wave forces acting on various porous configurations that include composite porous structures are reported.
- The wave transformation due to composite permeable porous structures associated with a vertical permeable barrier of different configurations is examined. The porous structure is often analysed for wave transformation studies. In contrast, the porous block with an outer periphery of closely spaced piles that protects the porous block is introduced, and a pile-

rock structure associated with different vertical barriers such as a fully-extended barrier, bottom-standing barrier, and surface-piercing barrier is analysed.

- The porous structure associated with different configurations of vertical porous barriers such as fully-extended, bottom-standing, and surface-piercing barriers, have been analysed and the efficiency of the configurations are compared.
- The wave decay due to dimensionless structural width $d/h = 3$ is evident for optimal wave damping by pile-rock porous structure with barrier for all the cases of porosity within $0.2 \le \varepsilon_s \le 0.8$.
- The presence of vertical porous barriers such as fully-extended barrier, surface-piercing barrier and bottom standing barrier are found to cause less wave force impact on the associated porous structure which would further result in the long life of the porous structures.
- The presence of fully-extended barrier and surface-piercing barrier is observed to exhibit almost similar results for wave energy dissipation when it is subjected to multiple porous structure. So, the selection of vertical barrier can be adopted depending on the economic conditions.
- The surface-piercing barrier is more effective in wave energy damping when compared to the bottom-standing barrier.
- The multiple chambers present in the composite breakwater system is observed to be causing a resonating trend on wave reflection which could be due to the trapping of waves in the chamber/confined regions in the composite porous breakwater systems.
- The horizontal porous plate is effective in wave energy damping. The wave force impact on the plate is higher for higher plate lengths, thus reducing the impact on the backed submerged porous structure. The higher porosity of horizontal submerged plates is found to exhibit enhanced wave-structure interaction.
- The non-dimensional spacing between the plate and barrier is found to effectively affect the wave force impact on the structure in the case of submerged horizontal porous plate associated with vertical barrier.
- The higher inertia factor is observed to have a low transmission coefficient for long incident waves for submerged composite breakwater consisting of the porous block, porous plate

and vertical barrier. In contrast, low inertia factors have lower transmission coefficient for moderate incident waves.

- The wave energy dissipation in the case of long waves is observed to be more for horizontally stratified structures. On the other hand, the vertically stratified structure effectively damps shorter waves.
- The stepped seabed in the transmitted region helps in producing a tranquil sea environment by dissipating the energy that has entered the stratified porous structure, resulting in a calm shoreline side.
- The relative step height is observed to play a major role in dissipating wave energy in the case of stepped seabed. The increase in relative step height of stepped seabed is observed to cause increased wave energy dissipation when it is associated with stratified porous structures.

7.3 FUTURE SCOPE OF RESEARCH

The possible extension of the present study are as follows:

- The present study can be extended for the wave interaction with multiple porous structures considering undulating bottom topography condition in both single and two-layer fluid.
- The stratified porous structures considered in the study consist of only two layers for both horizontal and vertical stratified porous structures. The number of layers can be increased/varied and the analysis can be performed.
- The seabed considered in the present research is rigid. The composite breakwater configurations can be extended and analysed for permeable seabed conditions.
- The porous structures analysed in the present research are rectangular in shape. The study can be extended for various shapes of the porous structure.
- The porous plate considered in various breakwater configurations are in submerged conditions. The study can be extended for floating plate moored at the bottom.
- The study performed on the composite breakwater system can be extended for non-linear wave-structure interaction.

REFERENCES

Barman, K.K. and Bora, S.N. (2021). Linear water wave interaction with a composite porous structure in a two-layer fluid flowing over a step-like seabed. *Geophysical & Astrophysical Fluid Dynamics,* 115(5-6), 577-611.

Behera, H., Sahoo, T. and Ng, C.O. (2016). Wave scattering by a partial flexible porous barrier in the presence of step-type bottom topography. Coastal Engineering Journal, 58(3), 1650008 (1-26).

Burke, J.E. (1964). Scattering of surface waves on an infinitely deep fluid. *Journal of Mathematical Physics*, *5*(6), 805-819.

Chwang A.T. (1983). A porous-wavemaker theory. *Journal of Fluid Mechanics*, 132, 395–406.

Chwang, A.T. and Chan, A.T. (1998). Interaction between porous media and wave motion. *Annual Review of Fluid Mechanics*, 30(1), 53–84.

Chang, H.S. and Liou, J.C. (2007). Long wave reflection from submerged trapezoidal breakwaters. *Ocean Engineering,* 34,185-191.

Cho, I.H. and Kim, M.H. (2008). Wave absorbing system using inclined perforated plates. *Journal of Fluid Mechanics,* 608, 1-20.

Cho, I.H. and Kim, M.H. (2013). Transmission of oblique incident waves by a submerged horizontal porous plate. *Ocean Engineering,* 61, 56–65.

Cho, I.H., Koh, H.J., Kim, J.R. and Kim, M.H. (2013). Wave scattering by dual submerged horizontal porous plates. *Ocean Engineering, 73,* 149–158.

Das, S. and Bora, S.N. (2014). Reflection of oblique ocean water waves by a vertical porous structure placed on a multi-step impermeable bottom. *Applied Ocean Research*, *47*, 373-385.

Dalrymple, R.A., Losada, M.A. and Martin, P.A. (1991). Reflection and transmission from porous structures under oblique wave attack. *Journal of Fluid Mechanics*, *224*, 625-644.

Dattatri, J., Shankar, N.J., Raman, H. (1978). Performance characteristics of submerged breakwaters. *Coastal Engineering,* 130, 2153-2171.

Dick, T.M. and Brebner, A. (1968). Solid and permeable submerged breakwaters. *Coastal Engineering,* 72, 1141-1158.

Evans, D.V. (1976). A note on the waves produced by the small oscillations of a partially immersed vertical plate. *IMA Journal of Applied Mathematics*, 17(2), 135-140.

Fugazza, M. and Natale, L. (1992). Hydraulic design of perforated breakwaters. *Journal of Waterway, Port, Coastal and Ocean Engineering*, *118*(1), 1-14.

Gayathri, R., Kar, P., Behera, H. and Sahoo, T. (2021). Oblique wave scattering by a floating bridge in the presence of a vertical permeable flexible barrier. *Journal of Offshore Mechanics and Arctic Engineering*, 143(2), 021701-1-17.

Gayathri, R., Khan, M.B.M. and Behera, H. (2022). Attenuation of wave force on a floating dock by multiple porous breakwaters. *Engineering Analysis with Boundary Elements*, 143, 170-189.

Goda, Y. and Suzuki, Y. (1976). Estimation of incident and reflected waves in random wave experiments. P*roceedings of 15th Costal Engineering Conference (ASCE)*, Honolulu, pp. 828 – 845.

Grilli, S.T., Losada, M.A. and Martin, F. (1994). Characteristics of solitary wave breaking induced by breakwaters. *Journal of Waterway, Port, Coastal and Ocean Engineering*, 120(1), 74-92.

Hayashi, T., Hattori, M., Kano, T. and Shirai, M. (1966). Hydraulic research on the closely spaced pile breakwater. *Coastal Engineering Journal*, 9(1), 107-117.

Herbich, J.B. and Douglas, B. (1988). Wave transmission through a double-row pile breakwater. *Proceedings of 21st Coastal Engineering Conference*, Costa del Sol Malaga, Spain, 20-25 June 1988, pp. 2229–2241.

He, F. and Huang, Z. (2014). Hydrodynamic performance of pile-supported OWC-type structures as breakwaters: an experimental study. *Ocean Engineering*, *88*, 618-626.

He, K., Huang, T. and Ye, J. (2018). Stability analysis of a composite breakwater at Yantai port, China: An application of FSSI-CAS-2D, *Ocean Engineering*, 168, 95-107.

Hu, J., Zhao, Y. and Liu, P.L.F. (2019). A model for obliquely incident wave interacting with a multi-layered object. *Applied Ocean Research, 87*, 211–222.

Hur, D.S. and Mizutani, N., (2003). Numerical estimation of the wave forces acting on a three-dimensional body on the submerged breakwater. *Coastal Engineering*, 47(3), 329-345.

Huang, Z. (2007). An experimental study of wave scattering by a vertical slotted barrier in the presence of a current. *Ocean Engineering*, *34*(5-6), 717-723.

Huang, L.H. and Chao, H.I. (1992). Reflection and transmission of water wave by porous breakwater. *Journal of Waterway, Port, Coastal and Ocean Engineering,* 118, 437-452.

Isaacson, M. (1991). Measurement of regular wave reflection. *Journal of Waterway, Port, Coastal, Ocean Engineering*, 117, 553-569.

Isaacson, M., Baldwin, J., Allyn, N. and Cowdell, S. (2000). Wave interactions with perforated breakwater. *Journal of Waterway, Port, Coastal and Ocean Engineering*, 126(5), 229-235.

Johnson, H.K., (2006). Wave modelling in the vicinity of submerged breakwaters. *Coastal Engineering*, 53, 39-48.

Kaligatla, R.B., Sharma, M. and Sahoo, T. (2021). Wave interaction with a pair of submerged floating tunnels in the presence of an array of submerged porous breakwaters. *Journal of Offshore Mechanics and Arctic Engineering*, 143(2), 021402-1-14.

Karmakar, D. and Sahoo, T. (2008). Gravity wave interaction with floating membrane due to change in water depth, *Ocean Engineering*, 35(7), 598-615.

Karmakar, D. and Guedes Soares, C. (2014). Wave transformation due to multiple bottom-standing porous barriers. *Ocean Engineering*, 80, 50-63.

Karmakar, D. and Guedes Soares, C. (2015). Propagation of gravity waves past multiple bottom-standing barriers. *Journal of Offshore Mechanics and Arctic Engineering*, 137, 011101, 1-10.

Karmakar, D. and Guedes Soares, C. (2018). Wave motion control over submerged horizontal plates. *Journal of Offshore Mechanics and Arctic Engineering,* 140, (031101)1-10.

Kakuno, S. and Liu, P.L.F. (1993). Scattering of water waves by vertical cylinders. *Journal of Waterway, Port, Coastal and Ocean Engineering*, 119(3), 302 – 322.

Kaligatla, R. B., Tabssum, S., and Sahoo, T. (2018). Effect of bottom topography on wave scattering by multiple porous barriers. *Meccanica*, 53(4-5), 887-903.

Kirkgöz, M.S. (1991). Impact pressure of breaking waves on vertical and sloping walls. *Ocean Engineering*, *18*(1-2), 45-59.

Kobayashi, N. and Wurjanto, A. (1989). Wave transmission over submerged breakwaters. *Journal of Waterway, Port, Coastal and Ocean Engineering,* 115:662-680.

Koley, S., Behera, H. and Sahoo, T. (2015). Oblique wave trapping by porous structures near a wall. *Journal of Engineering Mechanics,* 141(3), 04014122.

Koley, S., Sarkar, A. and Sahoo, T. (2015). Interaction of gravity waves with bottom-standing submerged structures having perforated outer-layer placed on a sloping bed. *Applied Ocean Research*, *52*, 245-260.

Kriebel, D.L. (1993). Vertical wave barriers: wave transmission and wave forces. In *Coastal Engineering,* 1313-1326.

Krishna, K.R.A., Venkateswarlu, V. and Karmakar, D. (2019). Wave transformation due to a submerged porous block associated with a vertical barrier, *Proceedings of 10th International Conference on Asian and Pacific Coasts (Springer Nature)*, 717-724.

Liu, P.L.F. and Iskandarani, M. (1991). Scattering of short-wave groups by submerged horizontal plate. *Journal of Waterway, Port, Coastal, and Ocean Engineering*, *117*(3), 235-246.

Liu, Y., Li, Y.C. and Teng, B. (2007). Wave interaction with a perforated wall breakwater with a submerged horizontal porous plate. *Ocean Engineering,* 34(17–18), 2364–2373.

Liu, Y., Li, Y.C., Teng, B. and Dong, S. (2008). Wave motion over a submerged breakwater with an upper horizontal porous plate and a lower horizontal solid plate. *Ocean Engineering,* 35, 1588-1596.

Liu, Y. and Li, Y.C. (2011). An alternative analytical solution for water-wave motion over a submerged horizontal porous plate. *Journal of Engineering Mathematics,* 69, 385-400.

Liu, Y., Li, H.J. and Li, Y.C. (2012). A new analytical solution for wave scattering by a submerged horizontal porous plate with finite thickness. *Ocean Engineering*, 42, 83-92.

Liu, Y. and Li, H.J. (2013). Analysis of oblique wave interaction with a submerged perforated semi-circular breakwater. *Journal of Engineering Mathematics*, 83(1), 23-36.

Liu, Y. and Li, H.J. (2013). Wave reflection and transmission by porous breakwaters: A new analytical solution. *Coastal Engineering*, *78*, 46-52.

Liu, Y. and Li, H.J. (2013). Hydrodynamic performance of a composite breakwater with an upper horizontal porous plate and a lower rubble mound. *Ocean Systems Engineering*, *3*(1), 55-70.

Liu, Y. and Li, H.J. (2014). Analysis of wave performance through pile-rock breakwaters. *Proceedings of the Institution of Mechanical Engineers, Part M: Journal of Engineering for the Maritime Environment*, 228(3), 284-292.

Li, A.J., Li, H.J. and Liu, Y. (2017). Analytical study of oblique wave scattering by a submerged pile–rock breakwater, *Proceedings of the Institution of Mechanical Engineers, Part M: Journal of Engineering for the Maritime Environment*, 227(3) 295–308.

Losada, I.J., Dalrymple, R.A. and Losada, M.A. (1991). Water waves on crown breakwaters. *Journal of Waterway, Port, Coastal and Ocean Engineering,* 119(4), 367-380.

Losada, I.J., Losada, M.A. and Roldán, A.J. (1992). Propagation of oblique incident waves past rigid vertical thin barriers. *Applied Ocean Research*, *14*(3), 191-199.

Losada, I.J., Losada, M.A. and Martin, F.L. (1995). Experimental study of wave induced flow in a porous structure. *Coastal Engineering*, 26, 77-98.

Losada, I.J., Silva, R. and Losada, M.A. (1996). 3-D non-breaking regular wave interaction with submerged breakwaters. *Coastal Engineering,* 28, 229-248.

Losada, I.J., Silva, R. and Losada, M.A. (1996). 3-D non-breaking regular wave interaction with submerged breakwaters. *Coastal Engineering,* 28, 229-248.

Madsen, O.S. (1974). Wave transmission through porous structures. *Journal of the Waterways, Harbors and Coastal Engineering Division*, 100(3), 169-188.

Madsen, P.A. (1983). Wave reflection from a vertical permeable wave absorber. *Coastal Engineering*, 7(4), 381-396.

Macaskill, C. (1979). Reflexion of water waves by a permeable barrier. *Journal of Fluid Mechanics*, *95*(1), 141-157.

Mallayachari, V. and Sundar, V. (1994). Reflection characteristics of permeable seawalls. *Coastal Engineering*, 23(1-2), 135-150.

Mani, J.S., and Jayakumar, S. (1995). Wave transmission by suspended pipe breakwater, *Journal of Waterway, Port, Coastal and Ocean Engineering*, 121, 335-338.

Mei, C.C. and Black, J.L. (1969). Scattering of surface waves by rectangular obstacles in waters of finite depth. *Journal of Fluid Mechanics*, *38*(3), 499-511.

Mei, C.C. (1966). Radiation and scattering of transient gravity waves by vertical plates. *The Quarterly Journal of Mechanics and Applied Mathematics*, *19*(4), 417-440.

Mendez, F.J. and Losada, I.J. (2004). A perturbation method to solve dispersion equations for water waves over dissipative media. *Coastal Engineering, 51*(1), 81-89.

Milgram, J.H. (1970). Active water-wave absorbers. *Journal of Fluid Mechanics,* 42, 845-859.

Mohapatra, S.C., Sahoo, T. and Guedes Soares, C. (2018). Surface gravity wave interaction with a submerged horizontal flexible porous plate. *Applied Ocean Research,* 78, 61-74.

Ming, D. and Chiew, Y.M. (2000). Shoreline changes behind the detached breakwater. *Journal of Waterway, Port, Coastal, and Ocean Engineering*, 126(2), 63-70.

Neelamani, S. and Gayathri, T. (2006). Wave interaction with twin plate wave barrier. *Ocean Engineering*, 33(3–4), 495–516.

Neelamani, S. and Reddy, M.S. (1992). Wave transmission and reflection characteristics of a rigid surface and submerged horizontal plate. *Ocean Engineering,* 19(4), 327–341.

Patarapanich, M., (1984). Maximum and zero reflection from submerged plate. *Journal of Waterway, Port, Coastal and Ocean Engineering*, *110*(2), 171-181.

Patarapanich, M. and Cheong, H.F. (1989). Reflection and transmission characteristics of regular and random waves from a submerged horizontal plate. *Coastal Engineering*, 13(2), 161–182.

Porter, D. (1974). The radiation and scattering of surface waves by vertical barriers. *Journal of Fluid Mechanics*, *63*(4), 625-634.

Rambabu, A.C. and Mani, J.S. (2005). Numerical prediction of performance of submerged breakwaters. *Ocean Engineering,* 32, 1235-1246.

Rojanakamthorn, S., Isobe, M. and Watanabe, A. (1990). Modelling of Wave Transformation on submerged breakwaters. *Coastal Engineering,* 80, 1060-1073.

Sahoo, T., Lee, M.M. and Chwang, A.T. (2000). Trapping and generation of waves by vertical porous structures. *Journal of Engineering Mechanics*, *126*(10), 1074-1082.

Sollitt, C.K. and Cross, R.H. (1972). Wave transmission through permeable breakwaters. In *Coastal Engineering,* 1827-1846.

Suh, K.D., Kim, Y.W. and Ji, C.H. (2011). An empirical formula for friction coefficient of a perforated wall with vertical slits. *Coastal Engineering*, 58(1), 85-93.

Sulisz, W. (1985). Wave reflection and transmission at permeable breakwaters of arbitrary cross-section. *Coastal Engineering*, *9*(4), 371-386.

Tabssum, S., Kaligatla, R.B. and Sahoo, T. (2020). Gravity wave interaction with a porous breakwater in a two-layer ocean of varying depth. *Ocean Engineering*, 196, 106816.

Ting, C.L., Lin, M.C. and Cheng, C.Y. (2004). Porosity effects on non-breaking surface waves over permeable submerged breakwaters. *Coastal Engineering,* 50, 213–224.

Tsai, C.P., Yu, C.H., Chen, H.B. and Chen, H.Y. (2012). Wave height transformation and set-up between a submerged permeable breakwater and a seawall. *China Ocean Engineering*, *26*(1), 167-176.

Tsoukala, V.K., Katsardi, V., Hadjibiros, K. and Moutzouris, C.I., (2015). Beach erosion and consequential impacts due to the presence of harbours in sandy beaches in Greece and Cyprus. *Environmental Processes*, *2*(1), 55-71.

Tuck, E.O. (1971). Transmission of water waves through small apertures. *Journal of Fluid Mechanics*, *49*(1), 65-74.

Twu, S.W. and Chieu, C.C. (2000). A highly wave dissipation offshore breakwater. *Ocean Engineering*, 27(3), 315-330.

Twu, S.W., Liu, C.C. and Hsu, W.H. (2001). Wave damping characteristics of deeply submerged breakwaters. *Journal of Waterway, Port, Coastal and Ocean Engineering,* 127, 97-105.

Twu, S.W., Liu, C.C. and Twu, C.W. (2002). Wave damping characteristics of vertically stratified porous structures under oblique wave action. *Ocean Engineering*, *29*(11), 1295-1311.

Urashima, S., Ishizuka, K. and Kondo, H. (1986). Energy dissipation and wave force at slotted wall. In *Coastal Engineering,* 2344-2352.

Usha, R. and Gayathri, T. (2005). Wave Motion over a twin-plate breakwater. *Ocean Engineering*, 32(8-9), 1054–1072.

Venkateswarlu, V. and Karmakar, D. (2019). Wave scattering by vertical porous block placed over flat and elevated seabed. *Marine Systems and Ocean Technology*, *14*(2-3), 85-109.

Venkateswarlu, V. and Karmakar, D. (2020a). Significance of seabed characteristics on wave transformation in the presence of stratified porous block. *Coastal Engineering Journal*, 62(1), 1-22.

Venkateswarlu, V. and Karmakar, D. (2020b). Wave transformation due to barrier-rock porous structure placed on step-bottom. *Ships and Offshore Structures*, 15(8), 895-909.

Venkateswarlu, V. And Karmakar, D. (2020c), Wave motion over stratified porous absorber combined with seaward vertical barrier, *Journal of Engineering for Maritime Environment-Part-M*, 234(4), 830-845.

Venkateswarlu, V. and Karmakar, D. (2020d). Gravity wave trapping by series of horizontally stratified wave absorbers away from seawall. *Journal of Offshore Mechanics and Arctic Engineering, 142*(6), 061201, 1-13.

Venkateswarlu, V. and Karmakar, D. (2020e). Influence of impermeable elevated bottom on the wave scattering due to multiple porous structures. *Journal of Applied Fluid Mechanics, 13*(1), 371-385.

Venkateswarlu, V., Praveen, K.M. and Karmakar, D. (202f). Surface gravity wave scattering by multiple energy absorbing structures of variable horizontal porosity. *Coastal Engineering Journal*, *62*(4), 504-526.

Venkateswarlu, V. and Karmakar, D. (2021). Numerical investigation on the wave dissipating performance due to multiple porous structures. *ISH Journal of Hydraulic Engineering*, 27(S1), 202-219.

Wang, K.H. and Shen, Q. (1999). Wave motion over a group of submerged horizontal plates. *International Journal of Engineering Science,* 37, 703-715.

Wang, Y., Wang, G. and Li, G. (2006). Experimental study on the performance of the multiple-layer breakwater. *Ocean Engineering,* 33, 1829-1839.

Yip, T.L. and Chwang, A.T. (1997). Water wave control by a pitching plate. *Journal of Engineering Mechanics,* 123, 800-807.

Yip, T.L. and Chwang, A.T. (2000). Perforated wall breakwater with internal horizontal plate. *Journal of Engineering Mechanics*, 126(5), 533-538.

Yu, X. and Chwang, A.T. (1994). Wave motion through porous structures. *Journal of Engineering Mechanics*, 120(5), 989-1008.

Yueh, C.Y. and Kuo, Y.Y. (1993a). The nonlinear wave effects by a submerged horizontal plate to the vertical wall. *Journal of Hydraulic Research,* 31(5), 651-664.

Yueh, C.Y. and Kuo, Y.Y. (1993b). The study of wave pressure and uplift force on a submerged plate. *Ocean Engineering,* 20, 263-280.

Zhu, S. and Chwang, A.T. (2001). Analytical study of porous wave absorber. *Journal of Engineering Mechanics*, 127(4), 326-332.

AUTHOR'S RESUME

K.R. Athul Krishna
Ph.D. Research Scholar
Department of Water Resources and Ocean Engineering
National Institute of Technology Karnataka, Surathkal
Mangalore – 57502, Karnataka
Contact No: +91-7560973459
Email ID: athulkrishna202@gmail.com

The author was born on 14th February 1994 in Ernakulam District, Kerala, India. Having passed the Board of Secondary Education from Hidayathul Islam Higher Secondary School (H.I.H.S.S.), Ernakulam, Kerala, in 2009 and thereafter completed Intermediate from H.I.H.S.S. in 2011. He graduated with Bachelor in Civil Engineering from the Federal Institute of Science and Technology (FISAT), Mahatma Gandhi University, Kottayam, in 2015. Thereafter, he obtained Master in Coastal and Harbour Engineering from Kerala University of Fisheries and Ocean Studies (KUFOS), Panangad, Kochi, in 2017. After completing his Master's degree, he joined the Doctoral research program in the Department of Water Resources and Ocean Engineering, National Institute of Technology, Karnataka, Surathkal, in 2017. The author's interest lies in the problems related to wave dissipation due to composite breakwater system. He communicated and published his work in reputed international Journals and Conference proceedings during his research. The detailed list of publications are presented below:

(a) List of publications in Journals:

1. Sreebhadra, M.N., **K.R. Athul Krishna** & D. Karmakar, (2022). Wave trapping due to composite pile-rock structure coupled with vertical barrier. Proceedings of the Institution of Mechanical Engineers, Part M: Journal of Engineering for the Maritime Environment, (Scopus indexed Journal), DOI: 10.1177/147509022211127.

2. **K.R. Athul Krishna**, Abhishek G. Karaseeri & D. Karmakar, (2022). Oblique wave propagation through composite permeable porous structures, Marine Systems and Ocean Technology, (Scopus indexed Journal), DOI: 10.1007/s40868-022-00122-1.

3. **K.R. Athul Krishna**, Khansa Abdullah & D. Karmakar, (2023). Dissipation of gravity waves due to submerged porous plate coupled with porous structures, Journal of Offshore Mechanics & Arctic Engineering, 145, 011201-1-13, (Scopus indexed Journal), DOI: 10.1115/1.4055702.

4. **K.R. Athul Krishna**, Khansa Abdullah & D. Karmakar, (2023). Wave energy damping due to coupled porous structure and submerged porous plate, Journal of Marine Science and Application, (Scopus indexed Journal), (Accepted).

5. Ashna Varghese, **K.R. Athul Krishna** and D. Karmakar, (2022). Wave transformation due to stratified porous structure in the presence of stepped obstacle, Marine Systems and Ocean Technology, (Under Review).

(b) List of publications in Book Chapters:

6. **K.R. Athul Krishna**, V. Venkateshwarlu & D. Karmakar, (2019). Wave transformation due to a submerged porous block associated with a vertical barrier, Proceedings of 10th International Conference on Asian and Pacific Coasts (Springer Nature), 717-724.

(c) List of publications in Conference Proceedings:

7. V. Venkateswarlu, **K.R. Athul Krishna** and D. Karmakar, (2018). Wave force control on seawall using seaside porous blocks. Conference on Next Frontiers in Civil Engineering (NFiCE), IIT Bombay, 30th Nov – 1st December 2018.

8. **K.R. Athul Krishna**, V. Venkateswarlu & D. Karmakar, (2018). Wave reflection and transmission characteristics due to a piston type porous wave energy converter, Conference on Next Frontiers in Civil Engineering (NFiCE), IIT Bombay, 30th November – 1st December, 2018, 108-109.

9. **K.R. Athul Krishna** & D. Karmakar, (2019). Wave dissipation due to multiple submerged porous blocks associated with vertical barrier, 24th International Conference on Hydraulics, Water Resource and Coastal Engineering (HYDRO), 18th – 20th December, 2019, University College of Engineering, Osmania University, Hyderabad, India.

10. **K.R. Athul Krishna** & D. Karmakar, (2021). Gravity wave dissipation due to multiple porous structures, 25th International Conference on Hydraulics, Water Resources and Coastal Engineering (HYDRO), March 26-28, 2021, NIT Rourkella, Odisha, India.

11. Abhishek G. Karaseeri, **K.R. Athul Krishna** & D. Karmakar, (2021). Wave transformation due to stratified porous structure and vertical barrier, 2nd International Conference on Recent Advances in Fluid and Thermal Sciences (iCRAFT), 19th -21st March 2021, Birla Institute of Technology, Dubai.